Theoretical study of weakly bound vibrational states of the sodium trimer: numerical methods; prospects for the formation of Na$_3$ in an ultracold gas

Kai Willner

geboren am 17. Januar 1975 in Freiburg im Breisgau

2006

Université Paris-Sud XI
Faculté des Sciences d'Orsay

Universität Hannover
Fakultät für Mathematik und Physik

Theoretical study of weakly bound vibrational states of the sodium trimer: numerical methods; prospects for the formation of Na$_3$ in an ultracold gas

Thèse

presentée par

Kai Willner

pour obtenir le grade de

Docteur en Sciences
Doktor der Naturwissenschaften Dr. rer. nat.

de l'Université Paris-Sud XI et de l'Université Hannover

Soutenue le 27 septembre 2005 à Orsay devant la commission d'examen

M. François Aguillon	Président
M. Enrico Bodo	
M. Joachim Großer	Rapporteur
M. Georges Jolicard	Rapporteur
M. Jean-Michel Launay	
Mme Françoise Masnou-Seeuws	Directrice de thèse
M. Eberhard Tiemann	Directeur de thèse

Remerciements

Ce mémoire de thèse représente l'aboutissement de mes recherches effectuées principalement au Laboratoire Aimé Cotton à Orsay entre octobre 2001 et janvier 2005. Ce travail n'aurait pas été possible sans l'appui d'un grand nombre de personnes, auxquelles je tiens à exprimer ma sincère gratitude.

Je souhaite tout d'abord remercier M. Jacques Bauche de m'avoir accueilli dans l'école doctorale "Ondes et Matière".

Je remercie également MM. Christian Colliex et Pierre Pillet de m'avoir accueilli au laboratoire et de m'avoir permis de réaliser mon travail dans les meilleures conditions.

Je remercie sincèrement ma directrice de thèse, Mme Françoise Masnou-Seeuws, pour m'avoir confié un sujet très riche. Mes premiers pas dans l'étude des systèmes triatomiques ont été difficiles, mais Mme Masnou m'a toujours soutenu, tout en me laissant une entière liberté dans l'organisation de mon travail.

Je remercie chaleureusement M. Eberhard Tiemann de m'avoir accueilli comme visiteur à l'Institut d'Optique Quantique à l'Université de Hanovre.

Je tiens à remercier les membres du jury MM. François Aguillon et Enrico Bodo, et particulièrement les rapporteurs MM. Joachim Grosser et Georges Jolicard, d'avoir accepté la charge de juger ce travail.

Je remercie vivement M. Jean-Michel Launay pour avoir mis à ma disposition ses méthodes numériques sophistiquées et pour m'avoir fait bénéficier de son savoir et de son savoir-faire. Travailler avec lui fut une expérience à la fois enrichissante et stimulante.

Merci à l'Institut du Développement et des Ressources en Informatique Scientifique (IDRIS) d'Orsay et au Pôle de Calcul Intensif de l'Ouest (PCIO) de Rennes, qui ont mis à ma disposition les ressources en calcul numérique dont j'avais besoin.

Merci au Centre National de Recherche Scientifique (CNRS) pour le soutien financier dont j'ai bénéficié en tant que doctorant au laboratoire: matériel de bureau, frais de transport, frais de participation aux conférences.

Merci à l'ensemble du personnel technique et administratif du Laboratoire Aimé Cotton. Je remercie tout particulièrement Jocelyne Sinzelle

Contents

Chapter 1

Introduction

The present thesis has been motivated by the rapid development of the field of cold molecules during the last decade. Before 1998 the coldest molecules in the laboratory were at temperatures of about $T \approx 1$ Kelvin, either in supersonic beams or in helium nanodroplets. This is colder than in the interstellar medium, where the lowest temperature for molecules is controlled by the blackbody radiation at $T \approx 2.7$ K. Spectacular progress has produced samples of cold ($T \ll 1$K) and ultracold ($T < 1$ mK) molecules. Three main routes are presently being developed:

- Sympathetic cooling by cryogenic helium has made it possible to cool CaH down to ≈ 400 mkin: the method is being further developed in the group of John Doyle at Harvard, [273] and by Achim Peters in Berlin. An essential requirement for the applicability of the method is that the cross sections for elastic collisions must be much larger than for inelastic collisions. A strong theoretical effort has been devoted to the calculation of such cross sections [239, 33]

- Gerard Meijer and his group, first in Utrecht, and now in Berlin, have developed a technique of Stark deceleration for polar molecules such as CO, ND_3, OH, using inhomogeneous time-dependent electric fields [29, 28, 30]. Several laboratories are presently developing similar experiments : deceleration of SO_2 in Hannover (Prof. Tiemann's group in Hannover) aims at producing cold SO and O by predissociation; deceleration of YbF at Imperial College, London (Hind's group) [113, 255] aims at measuring an upper limit for the electron dipole moment as a test of the standard model. Further developments concern the deceleration of Rydberg molecules with a high dipole moment (work of Merkt in Zurich and Softley in Oxford [218, 268], project in Pillet's group at Orsay [265])

- Since direct laser cooling is very efficient for atoms but not for molecules,

another route forms ultracold molecules starting from ultracold atoms. The photoassociation reaction, where two colliding atoms absorb a photon, creates a molecule in an excited electronic state, in a highly excited vibrational level. The excited molecule may be stabilized by spontaneous emission, populating bound levels of the electronic ground state. The method was implemented first in Orsay for Cs_2 [83], then at Storrs for K_2 [200, 199], in Pisa for Rb_2 [91], at NIST (Gaithersburg) for Na_2 [80], yielding homonuclear diatomic molecules at $T \sim$ 2-50 μK , in samples of typical densities 10^{11} cm^{-3}. Recent progress concerns the formation of ultracold heteronuclear dimers: RbCs at Yale (2003) [129, 128], KRb at Storrs and in Sao Paulo (2004) [271, 270, 181]. The densities in the mixed atomic traps are higher, typically 10^{12} cm^{-3}.

- Several groups have been capable to trap the ultracold molecules, in magnetic traps for triplet molecules [266, 270], or in dipole traps using CO_2 lasers [84], for singlet or triplet molecules. Here the molecular densities typically reach 10^8 cm^{-3}.

- Since 2004, a wealth of new experimental results has been published concerning the formation of molecules in a degenerate gas. The molecules are formed either in an atomic Bose-Einstein condensate (BEC) [65, 51, 97, 280, 68] or in an atomic Fermi gas [225, 289, 253, 58, 120, 119, 224]. Most groups are using magnetic Feshbach resonances (D. Jin at JIlA, R. Grimm in Innsbruck, W. Ketterle, MIT, C. Salomon, ENS, ...). The molecules are formed in highly excited vibrational levels, which makes them very sensitive to collisions. Recent results from the Innsbruck group seem to indicate the presence of Cs_4 molecules in the condensates.

- Many groups are working at schemes to transfer the ultracold molecules from excited vibrational levels to the ground level v=0 [231].

The experimental progress has been accompanied by a strong theoretical effort. In particular, accurate methods have been developed to evaluate elastic and inelastic atom-atom cross-sections, for collision energies where long-range potentials play a key role. The cross-sections are either computed by *ab initio* methods or fitted to observed data.

The theoretical work presented in this thesis can be considered as a continuation of the work by V. Kokoouline *et al.* [135, 137, 136] on the mapped Fourier grid method, by A. Crubellier *et al.* [57] on the determination of atom-atom scattering lengths using spectroscopic information on the last bound vibrational levels of the dimer, and by J.-M. Launay *et al.* [248] on

the determination of an atom-diatom scattering length and inelastic cross sections at ultra-low temperatures.

Indeed, atom-diatom collisions at ultra-low temperatures have become an important and challenging research subject. Dense samples containing both ultracold atoms and ultracold diatomic molecules are now available, and their dynamics are controlled by the cross sections for elastic and inelastic atom-diatom collisions. The stability of molecular condensates will depend on atom-diatom scattering lengths, and on cross-sections for vibrational quenching collisions. This necessitates an important theoretical effort, the dynamics of atom-molecule collisions being much more complex compared to atom-atom collisions. A bottleneck is the accurate determination of the potential surface, with an accuracy adapted to the very low kinetic energy of the colliding partners.

Finally, the formation of ultracold triatomic molecules via atom-diatom photoassociation would be a major breakthrough, opening the way to ultracold chemistry.

The aim of the present thesis is to contribute to the understanding of atom-molecule collisions at ultra-low kinetic energy. We have focussed on two problems:

1. Improvement of the Mapped Fourier Grid method.

2. Computation of the last bound vibrational levels of an alkali trimer.

This thesis is organized as follows.
The Mapped Fourier Grid method is discussed in Chapter 2.
Essential facts about three-body systems are summarized in Chapter 3.
The potential energy surface of the lowest quartet electronic state of the sodium trimer Na_3 is described in Chapter 4.
Numerical results concerning the highest, most weakly bound vibrational levels of Na_3 are presented in Chapter 5.
The possibility of forming a trimer through photoassociation of its atomic constituents is briefly discussed in Chapter 6.
Chapter 7 is the conclusion.

Chapter 2

Mapped Fourier Grid

2.1 Grid methods

Grid methods are widely used to compute wavefunctions of molecular systems [142]. Any grid method is based on a *collocation* scheme [39, 170], also called Lagrange mesh [26]. In such a scheme, an arbitrary wavefunction φ is approximated by its projection $\hat{P}\varphi$, a linear combination of interpolation functions, such that φ and $\hat{P}\varphi$ have the same values in the collocation points. The wavefunction φ is thus represented by its values at the collocation points. The Hamiltonian is represented by a matrix, which can be used to compute bound and continuum states or to simulate the temporal evolution of a wavepacket. Quasibound states can be calculated using complex absorbing potentials [203]. Spectral and collocation methods are discussed in a famous monograph by D. Gottlieb and S. Orszag [94]. In atomic and molecular physics, collocation methods have been used to study a great variety of systems, using various sets of interpolation functions [191, 36, 161, 35, 67, 37]. Multidimensional grids have been implemented to study systems with more than one degree of freedom [127].

2.2 The Mapped Fourier Grid

V. Kokoouline *et al.* [135] implemented a Mapped Fourier Grid in order to interpret data obtained in photoassociation experiments performed in the group "Atomes et Molécules Froids" at Laboratoire Aimé-Cotton (Orsay). In such an experiment, electronically excited diatomic molecules are formed in an ultracold cloud of atoms when two colliding ground state atoms absorb a photon emitted from a laser source [83, 215]. The electronically excited molecules are generally formed in highly excited vibrational states, at energies very close to the atom-atom dissociation limit. In order to represent their radial (vibrational) wavefunctions on a grid, the grid step must be adapted

to the great variation of the local de Broglie wavelength from short to large internuclear distances [135].

During a three-month's practical in 2001 ("stage de D.E.A"), I used V. Kokoouline's Mapped Fourier Grid [135] to calculate very weakly bound vibrational levels of Rb_2 and Cs_2. By diagonalizing the Hamiltonian matrix in the Fourier grid representation I obtained correct values for vibrational energies and radial wavefunctions. However, the method did not only yield physical solutions: the computed eigenvalues generally included a small number of unphysical, spurious levels, at energies lying between the physical energies. We may sometimes call the spurious levels *ghosts* (this seems to be an established expression, see for example [272]). The origin of the spurious solutions was unclear. Although they did not affect the accuracy of the computed physical levels in our time-independent calculations, we were afraid that they might be inconvenient in wavepacket propagation schemes, which were being planned at the time in our group and which have been implemented since [175, 176, 131, 130]. For this reason we decided to investigate the "ghosts" in greater detail. We found that they are inherent to the Fourier transform algorithm itself and not due to any specific numerical or programming error. We observed [276] that the spurious solutions do not arise if the standard discrete Fourier transform described in Ref. [135] is replaced by Borisov's [35] sine-cosine transform algorithm.

This Chapter contains many results and equations which were already given in our article [276]. However, we shall point out a few additional details, and we shall address the non-trivial question of how to interpolate the wavefunction between the grid points.

2.2.1 Adaptive coordinate

In the adiabatic or Born-Oppenheimer approximation, the relative motion of two atoms is governed by the Hamiltonian $\hat{H}$ defined as follows:

$$\hat{H}\,\varphi(R) \;=\; -\frac{\hbar^2}{2\mu}\frac{d^2\varphi}{dR^2}(R) + V(R)\,\varphi(R) \tag{2.1}$$

Here $\varphi(R)$ is the radial wavefunction, $R \in [0,\infty)$ is the internuclear distance, μ is the reduced mass of the two nuclei, and $V(R)$ is the molecular potential energy, which may include a centrifugal barrier

$$\frac{\hbar^2 l(l+1)}{2\mu R^2} \;.$$

The equilibrium distance of the potential is denoted R_e.

The stationary Schrödinger equation is

$$\hat{H}\varphi \;=\; E\varphi \tag{2.2}$$

where E is the energy associated with an eigenfunction $\varphi(R)$.

Our aim is to solve (2.2) for energies up to a maximum energy E_{max} using an *equidistant* collocation scheme.

The local de Broglie wavelength

$$\lambda(R) \;=\; \frac{h}{\sqrt{2\mu[E_{\text{max}} - V(R)]}} \tag{2.3}$$

for the maximum energy E_{max} is generally far larger at large distances R than at short distances ($R \approx R_{\text{e}}$). Therefore it is useful to introduce a new coordinate x adapted to the variation of the local de Broglie wavelength $\lambda(R)$.

Since $\lambda(R)$ diverges at classical turning points, we replace the true potential $V(R)$ in Eq. (2.3) by a reference potential $V_{\text{ref}}(R)$ in order to define the

$$R \leftrightarrow x$$

coordinate transformation, following V. Kokoouline *et al.* [135]. The reference potential must be a smooth function of the internuclear distance, and it must lie below both E_{max} and $V(R)$:

$$V_{\text{ref}}(R) \;\leq\; E_{\text{max}} \,, \qquad V_{\text{ref}}(R) \;\leq\; V(R) \,. \tag{2.4}$$

In calculations involving a single potential curve $V(R)$, the reference potential V_{ref} was taken constant at distances smaller than the equilibrium distance, and identical to the true potential $V(R)$ at distances larger than the equilibrium distance (see Refs. [135, 276]):

$$V_{\text{ref}}(R) \;=\; \begin{cases} V(R_{\text{e}}) \,, & R \;\leq\; R_{\text{e}} \\ V(R) \,, & R \;\geq\; R_{\text{e}} \end{cases} \,. \tag{2.5}$$

The local de Broglie reference wavelength is given by

$$\lambda_{\text{ref}}(x) \;=\; \frac{h}{\sqrt{2\mu[E_{\text{max}} - V_{\text{ref}}(R)]}} \;; \tag{2.6}$$

it is used to define the Jacobian

$$J(x) \;=\; \frac{dR}{dx} \;=\; \frac{\beta\,\lambda_{\text{ref}}(x)}{2} \tag{2.7}$$

of the $R \leftrightarrow x$ coordinate transformation. The parameter β in the above definition was introduced by V. Kokoouline *et al.* [135] as a means of controlling the density of grid points on the R-axis. A grid step $\Delta x = 1$ on the x-axis corresponds to the step

$$\Delta R \;=\; J(x)\Delta x \;=\; \frac{\beta\,\lambda_{\text{ref}}(x)}{2} \tag{2.8}$$

on the R-axis.

The coordinate R as a function of x is found by integration, starting at a point $x = a$:

$$R(x) = R(a) + \int_a^x J(x') \, dx' . \qquad (2.9)$$

For the choice $\beta = 1$, the grid step ΔR measures roughly the distance between two neighbouring nodes of a semi-classical oscillatory wavefunction $\varphi(R)$ at energy $E_{\max}$. By reducing the parameter β, it is possible to improve the numerical accuracy until the results may be considered converged. β is typically chosen between 0.5 and 0.8, depending on the potential.

We note that the $R \to x$ coordinate mapping can be related to a classical canonical coordinate transformation, in which the classically allowed region in phase space is transformed into a rectangle [81, 276].

Using the coordinate x, Eq. (2.1) for the Hamiltonian takes the form

$$\hat{H} \, \varphi(x) = -\frac{\hbar^2}{2\mu} \frac{1}{J(x)} \frac{d}{dx} \frac{1}{J(x)} \frac{d}{dx} \varphi(x) + V(x) \, \varphi(x) \qquad (2.10)$$

where $\varphi(x)$ and $V(x)$ are short-hand notations for $\varphi[R(x)]$ and $V[R(x)]$, respectively. The kinetic energy operator[1]

$$\hat{T} = -\frac{\hbar^2}{2\mu} \frac{1}{J(x)} \frac{d}{dx} \frac{1}{J(x)} \frac{d}{dx} \qquad (2.11)$$

can be rewritten as

$$\hat{T} = -\frac{\hbar^2}{4\mu} \left[J^{-\frac{5}{2}} \frac{d^2}{dx^2} J^{\frac{1}{2}} + J^{-\frac{1}{2}} \frac{d^2}{dx^2} J^{-\frac{3}{2}} - \frac{7}{2} J'^2 J^{-4} + J^{-3} J'' \right] \qquad (2.12)$$

or as

$$\hat{T} = -\frac{\hbar^2}{4\mu} \left[2 \, J^{-\frac{3}{2}} \frac{d^2}{dx^2} J^{-\frac{1}{2}} - \frac{3}{2} J^{-4} J'^2 + J^{-3} J'' \right] . \qquad (2.13)$$

The symmetric expression for the kinetic energy operator given in Ref. [135] is obtained by multiplying Eq. (2.12) on the left by $J^{+\frac{1}{2}}(x)$ and on the right by $J^{-\frac{1}{2}}(x)$.

In Ref. [276], we explained that a numerical evaluation of the derivatives $J'(x)$ and $J''(x)$ can be an important source of error, and that it is preferable to calculate the kinetic operator directly from Eq. (2.11), unless $J(x)$ and its derivatives are known analytically.

As discussed in References [135] and [276], the stationary radial Schrödinger equation

$$-\frac{\hbar^2}{2\mu} \frac{1}{J(x)} \frac{d}{dx} \frac{1}{J(x)} \frac{d}{dx} \varphi(x) + V(x) \, \varphi(x) = E \, \varphi(x) \qquad (2.14)$$

---

[1]In this and in the other expressions for $\hat{T}$, terms of the form $\frac{d}{dx} f(x)$ are *operators*, not numbers. The operator $\frac{d}{dx} f(x)$ can be rewritten as $\frac{df}{dx} + f(x) \frac{d}{dx}$.

can be solved very accurately and efficiently by expanding the wavefunction $\varphi(x)$ in a set of N interpolation functions, using a set of N equidistant collocation points on the x-axis. In Ref. [276], we compared three different collocation schemes, using the following sets of basis functions:

1. trigonometric functions obeying periodic boundary conditions

2. trigonometric functions obeying strict boundary conditions

3. cardinal sine functions (Hardy functions).

The important conclusion was that the trigonometric functions obeying strict boundary conditions, i.e. particle-in-a-box functions, seemed preferable compared to the two other basis sets, since only they did not lead to the appearance of ghost levels.

The two different trigonometric interpolation schemes, the periodic one and the non-periodic one, are discussed in the following.

2.2.2 Discrete Fourier transform

We shall briefly review the standard Fourier transform algorithm, using the same notations as in Ref. [276].

We define a set of N grid points

$$x_i \; = \; i\Delta x \qquad (i = 1, \ldots, N) \tag{2.15}$$

covering the interval $[0, L]$ on the x-axis, along with N periodic Fourier interpolation functions $\tilde{u}_j(x)$ such that

$$\tilde{u}_j(x_i) \; = \; \delta_{ij} \qquad (i, j = 1, \ldots, N) \; . \tag{2.16}$$

We now choose as grid step $\Delta x = 1$, so that $x_i = i$ and $L = N$. This does not imply any restriction but allows to simplify a few formulas.

The interpolation functions are constructed from travelling plane waves such that $\tilde{u}_j(x)$ is centered on the j-th grid point x_j:

$$\tilde{u}_j(x) \; = \; \sum_{k=-\nu}^{\nu} u_k(x)\, F_{kj}^{\dagger} \tag{2.17}$$

where

$$u_k(x) \; = \; \frac{e^{\mathrm{i}k\frac{2\pi}{N}x}}{\sqrt{N}} \tag{2.18}$$

and

$$F_{jk} \; = \; \frac{e^{\mathrm{i}k\frac{2\pi}{N}j}}{\sqrt{N}} \; . \tag{2.19}$$

The interpolation functions $\tilde{u}_j(x)$ are explicitly given by

$$\tilde{u}_j(x) = \begin{cases} 1 & (x = j) \\ \frac{\sin[\pi(x-j)]}{N \sin\left[\frac{\pi}{N}(x-j)\right]} & (x \neq j) \end{cases} ; \tag{2.20}$$

they were already discussed by R. Meyer [191] (our function $\tilde{u}_j$ is the same as Meyer's function δ_j).

We define the collocation operator $\hat{P}^{\mathcal{F}}$ by the relation

$$\hat{P}^{\mathcal{F}}\varphi(x) = \sum_{j=1}^{N} \tilde{u}_j(x)\,\varphi(x_j) \tag{2.21}$$

where $\varphi(x)$ is an arbitrary wavefunction. $\hat{P}^{\mathcal{F}}$ is a non-orthogonal projection operator: in Eq. (2.21), it is used to project φ on the space spanned by the plance waves u_k. Using Eq. (2.16), one sees that φ and its projection $\hat{P}^{\mathcal{F}}\varphi$ match in the grid points x_i $(i = 1, \ldots, N)$:

$$\left[\hat{P}^{\mathcal{F}}\varphi\right](x_i) = \varphi(x_i) . \tag{2.22}$$

We emphasize that $\hat{P}^{\mathcal{F}}\varphi$ is a "skew" projection with respect to the L^2-scalar product.

In Ref. [276] we showed how $\hat{T}\varphi$ ("the action of the kinetic energy operator on the wavefunction") can be evaluated numerically using the collocation operator $\hat{P}^{\mathcal{F}}$, given the values of φ at the grid points. The method has also been discussed by M. Nest and P. Saalfrank [196].

It is interesting to compare the projection by collocation and the orthogonal projection based on the L^2 scalar product. The L^2-projection of φ on the space spanned by the N plane waves u_k is given by

$$\hat{P}_{\perp}\varphi(x) = \sum_{k=1}^{N} u_k(x)\frac{\langle u_k|\varphi\rangle}{\langle u_k|u_k\rangle} = \sum_{j=1}^{N} \tilde{u}_j(x)\frac{\langle \tilde{u}_j|\varphi\rangle}{\langle \tilde{u}_j|\tilde{u}_j\rangle} \tag{2.23}$$

where $\hat{P}_{\perp}$ is the L^2-projection operator and $\langle\cdot|\cdot\rangle$ denotes the L^2 scalar product

$$\langle\varphi_1|\varphi_2\rangle = \int_0^L J(x)\,\varphi_1^*(x)\,\varphi_2(x)\,dx . \tag{2.24}$$

The functions (2.21) and (2.23) are generally different, except if φ lies in the space spanned by the plane waves u_k.

Fourier interpolation and cardinal sine functions

We have found a simple formal relation between the Fourier interpolation functions $\tilde{u}_j(x)$ and cardinal sine functions: using the Eisenstein series [227]

$$\frac{\pi}{\sin(\pi z)} = \sum_{m=-\infty}^{\infty} \frac{(-1)^m}{z+m} \tag{2.25}$$

we may express (2.20) as a "periodic superposition" of cardinal sine functions:

$$\tilde{u}_j(x) = \sum_{m=-\infty}^{\infty} \text{sinc}[\pi(x-j-mN)] . \tag{2.26}$$

This expression shows that $\tilde{u}_j(x)$ is well approximated by the cardinal sine function

$$\text{sinc}[\pi(x-j)]$$

provided that

$$1 \ << \ j \ << \ N .$$

The function $\tilde{u}_N(x)$, on the other hand, can be written as

$$\tilde{u}_N(x) = \sum_{m=-\infty}^{\infty} \text{sinc}[\pi(x-mN)]$$

$$\approx \text{sinc}(\pi x) + \text{sinc}[\pi(x-N)] . \tag{2.27}$$

The peak of this function appears at both ends of the grid, which reflects the fact that the basis functions

$$u_k(x) \qquad (k=1,\ldots,N)$$

obey periodic boundary conditions.[2]

2.2.3 Discrete sine and cosine transforms

D. Lemoine [161] and A. G. Borisov [35] both presented a mapped sine grid method. We adopted Borisov's method, since it allows to compute the kinetic energy operator without using the derivatives of the Jacobian $J(x)$.

---

[2] I would like to thank Prof. David Tannor for the comments he made on a poster I presented at Gif-sur-Yvette in 2001. Prof. Tannor remarked that the Fourier interpolation functions peaked near the right border ($x = N$) of the grid must also be "visible" at the left border ($x = 0$), due to the periodicity of the basis set. Following this hint, I formed the infinite sum (2.26), in an attempt to define a simple alternative set of periodic interpolation functions. Afterward I realized that the sum (2.26) and the Fourier interpolation function (2.17) are the same.

In the following we present Borisov's method from our own perspective, using explicit continuous interpolation functions $\tilde{s}_i(x)$ and $\tilde{c}_i(x)$. These functions are analogous to the Fourier interpolation functions $\tilde{u}_i(x)$ described above.

Grid points

We define the following set of equidistant grid points x_i covering the interval $[0, L]$ on the x-axis:

$$x_i = i\Delta x , \qquad \Delta x = \frac{L}{N} \qquad (i = 0, \ldots, N) \tag{2.28}$$

Basis functions

The basis functions

$$s_k(x) = \sqrt{\frac{2}{N}} \sin\left(k\frac{\pi}{L}x\right) \qquad (k = 1, \ldots, N-1) \tag{2.29}$$

$$c_k(x) = \sqrt{\frac{2}{N}} \cos\left(k\frac{\pi}{L}x\right) \qquad (k = 0, \ldots, N) \tag{2.30}$$

are orthogonal in the following sense:

$$\int_0^L dx\, s_k^*(x)\, s_l(x) = \delta_{kl}\, \Delta x \tag{2.31}$$

$$\int_0^L dx\, c_k^*(x)\, c_l(x) = \begin{cases} 2\,\Delta x & (k = l = 0) \\ \delta_{kl}\,\Delta x & \text{otherwise} \end{cases} \tag{2.32}$$

Discrete sine and cosine transformation

The discrete sine and cosine transformations of the first type [217] are given by:

$$S_{ik} = s_k(x_i) = \sqrt{\frac{2}{N}} \sin\left(k\frac{\pi}{N}i\right) \tag{2.33}$$
$$(i, k = 1, \ldots, N-1)$$

$$C_{ik} = \alpha_k\, c_k(x_i)\, \alpha_i = \sqrt{\frac{2}{N}}\, \alpha_k \cos\left(k\frac{\pi}{N}i\right) \alpha_i \tag{2.34}$$
$$(i, k = 0, \ldots, N)$$

where

$$\alpha_k = \begin{cases} \sqrt{\frac{1}{2}} & (k = 0, \ k = N) \\ 1 & (k = 1, \ldots, N-1) \end{cases} . \tag{2.35}$$

24

S and **C** are unitary matrices of dimensions $N - 1$ and $N + 1$, respectively:

$$(\mathbf{SS}^\dagger)_{ij} = \sum_{k=1}^{N-1} S_{ik} S^\dagger_{kj} = \delta_{ij} \tag{2.36}$$

$$(\mathbf{CC}^\dagger)_{ij} = \sum_{k=0}^{N} C_{ik} C^\dagger_{kj} = \delta_{ij} \tag{2.37}$$

Interpolation functions

The sine and cosine interpolation functions

$$\tilde{s}_j(x) = \sum_{k=1}^{N-1} s_k(x) S^\dagger_{kj} \tag{2.38}$$

$$\tilde{c}_j(x) = \sum_{k=0}^{N} c_k(x) \alpha_k C^\dagger_{kj} \alpha_j \tag{2.39}$$

are such that

$$\tilde{s}_j(x_i) = \delta_{ij} \tag{2.40}$$

$$\tilde{c}_j(x_i) = \delta_{ij} . \tag{2.41}$$

Note that the transformation (2.39) relating $\tilde{c}_j(x)$ and $c_k(x)$ is only approximately unitary, due to the coefficients α_k and α_j.

Explicit expressions for the interpolation functions $\tilde{s}_j(x)$ and $\tilde{c}_j(x)$ are obtained by evaluating the sums in Eqs. (2.38) and (2.39):

$$\tilde{s}_j(x) = \frac{1}{2N} \left\{ \frac{\sin\left[(2N-1)\frac{\pi}{2L}(x - x_j)\right]}{\sin\left[\frac{\pi}{2L}(x - x_j)\right]} - \frac{\sin\left[(2N-1)\frac{\pi}{2L}(x + x_j)\right]}{\sin\left[\frac{\pi}{2L}(x + x_j)\right]} \right\}$$

$$(x \neq x_j)$$

$$\tilde{s}_j(x_j) = 1 \tag{2.42}$$

$$\tilde{c}_j(x) = \frac{\alpha_j^2}{2N} \left\{ \frac{\sin\left[(2N-1)\frac{\pi}{2L}(x - x_j)\right]}{\sin\left[\frac{\pi}{2L}(x - x_j)\right]} + \cos\left[N\frac{\pi}{L}(x - x_j)\right] \right.$$

$$\left. + \frac{\sin\left[(2N-1)\frac{\pi}{2L}(x + x_j)\right]}{\sin\left[\frac{\pi}{2L}(x + x_j)\right]} + \cos\left[N\frac{\pi}{L}(x + x_j)\right] \right\}$$

$$(x \neq x_j)$$

$$\tilde{c}_j(x_j) = 1 \tag{2.43}$$

Eqs. (2.42) is needed for the interpolation of the wavefunction $\varphi(x)$.
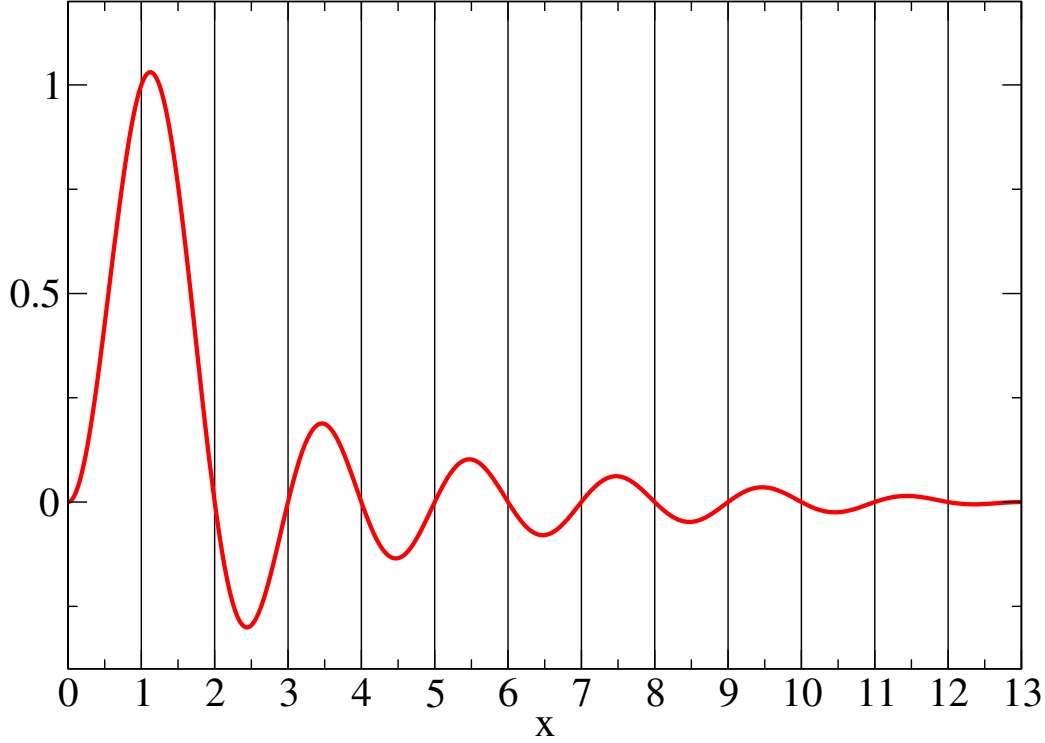
Figure 2.1: Cosine interpolation function $\tilde{c}_1(x)$ for $L = 13$, $N = 13$. The function vanishes in all grid points $x_i = i$ $(i = 0, \ldots, 13)$ except in $x_1 = 1$.

We note that the denominators in Eq. (2.42) can be rewritten as Eisenstein series using Eq. (2.25). The sine-interpolation function $\tilde{s}_i(x)$ can thus be expressed as a linear combination of cardinal sine functions, similar to Eq. (2.26).

Fig. 2.1 shows the interpolation function $\tilde{c}_1(x)$ for the case $N = 13$. Plots of other interpolation functions are given in our article [276]. See also the article by F. J. Lin and J. T. Muckerman [170], who refer to the interpolation functions as "discrete coordinate eigenfunctions".

Collocation operators

We define the collocation operators $\hat{P}^{\mathcal{S}}$ and $\hat{P}^{\mathcal{C}}$ associated with the sine and the cosine basis such that

$$\hat{P}^{\mathcal{S}} \varphi(x) = \sum_{i=1}^{N-1} \tilde{s}_i(x) \, \varphi(x_i) \tag{2.44}$$

$$\hat{P}^{\mathcal{C}} \varphi(x) = \sum_{i=0}^{N} \tilde{c}_i(x) \, \varphi(x_i) \, . \tag{2.45}$$

$\hat{P}^{\mathcal{S}}$ and $\hat{P}^{\mathcal{C}}$ are used to project an arbitrary function $\varphi(x)$ onto the space spanned respectively by the sine functions (2.29) and by the cosine functions (2.30) such that $\varphi(x)$ and its projections match in the grid points:

$$\varphi(x_i) = \hat{P}^{\mathcal{S}}\varphi(x)\Big|_{x=x_i} \qquad (i = 1, \ldots, N-1) \qquad (2.46)$$

$$\varphi(x_i) = \hat{P}^{\mathcal{C}}\varphi(x)\Big|_{x=x_i} \qquad (i = 0, \ldots, N) \qquad (2.47)$$

We may express $\hat{P}^{\mathcal{S}}\varphi$ and $\hat{P}^{\mathcal{C}}\varphi$ in terms of the sine and cosine functions (2.29) and (2.30) as follows:

$$\hat{P}^{\mathcal{S}}\varphi(x) = \sum_{k=1}^{N-1} s_k(x)\, \varphi_k^{\mathcal{S}} \qquad (2.48)$$

$$\hat{P}^{\mathcal{C}}\varphi(x) = \sum_{k=0}^{N} c_k(x)\, \varphi_k^{\mathcal{C}} \,. \qquad (2.49)$$

The expansion coefficients $\varphi_k^{\mathcal{S}}$ and $\varphi_k^{\mathcal{C}}$ thus defined are related to the values $\varphi(x_i)$ of the wavefunction on the grid by a discrete sine and a discrete cosine transformation, respectively:

$$\varphi_k^{\mathcal{S}} = \sum_{i=1}^{N-1} S^{\dagger}{}_{ki}\, \varphi(x_i) \qquad (2.50)$$

$$\varphi(x_i) = \sum_{k=1}^{N-1} S_{ik}\, \varphi_k^{\mathcal{S}} \qquad (2.51)$$

$$\varphi_k^{\mathcal{C}} = \sum_{i=0}^{N} \alpha_k C^{\dagger}{}_{ki} \alpha_i\, \varphi(x_i) \qquad (2.52)$$

$$\varphi(x_i) = \sum_{k=0}^{N} \frac{1}{\alpha_i} C_{ik} \frac{1}{\alpha_k} \varphi_k^{\mathcal{C}} \,. \qquad (2.53)$$

Evaluation of the scalar product

Assuming that $\varphi_1(x)$ and $\varphi_2(x)$ can be expanded in the sine basis (2.29), their scalar product (2.24) can be approximated as follows:

$$\langle \varphi_1 | \varphi_2 \rangle = \sum_{i,j=1}^{N-1} \int_0^L dx\, J(x)\, [\tilde{s}_i(x)\, \varphi_1(x_i)]^*\, \tilde{s}_j(x)\, \varphi_2(x_j)$$

$$\approx \sum_{i,j=1}^{N-1} J(x_j)\, \varphi_1(x_i)^*\, \varphi_2(x_j) \int_0^L dx\, \tilde{s}_i^*(x)\, \tilde{s}_j(x)$$

27

$$= \sum_{i=1}^{N-1} J(x_i)\, \varphi_1(x_i)^* \, \varphi_2(x_i)\, \Delta x \; . \tag{2.54}$$

In this derivation we have used the fact that the product of a function $f(x)$ and an interpolation function $\tilde{s}_i(x)$ can generally be approximated as follows:

$$f(x)\tilde{s}_i(x) \;\approx\; \hat{P}^{\mathcal{S}} f(x)\tilde{s}_i(x) \;=\; \sum_{j=1}^{N-1} \tilde{s}_j(x)\, f(x_j)\tilde{s}_i(x_j) \;=\; f(x_i)\tilde{s}_i(x) \; . \tag{2.55}$$

Grid representation of the differential operator d/dx

The derivatives of s_k and c_k are

$$\frac{ds_k}{dx}(x) \;=\; k\frac{\pi}{L}\, c_k(x) \tag{2.56}$$

$$\frac{dc_k}{dx}(x) \;=\; -k\frac{\pi}{L}\, s_k(x) \; . \tag{2.57}$$

The derivatives of $\tilde{s}_j$ and $\tilde{c}_j$ at the grid point x_i are accordingly given by

$$
\begin{aligned}
\frac{d\tilde{s}_j}{dx}(x_i) \;&=\; \sum_{k=1}^{N-1} \frac{ds_k}{dx}(x_i)\, S^\dagger_{kj} \\[2mm]
&=\; \sum_{k=1}^{N-1} k\frac{\pi}{L}\, c_k(x_i)\, S^\dagger_{kj} \\[2mm]
&=\; \frac{1}{\alpha_i}\frac{\pi}{L} \sum_{k=1}^{N-1} C_{ik}\, k\, S^\dagger_{kj} \\[2mm]
&=\; \frac{1}{\alpha_i}\frac{\pi}{L}\, D_{ij} \\
&\qquad (j = 1,\ldots,N-1; \qquad i = 0,\ldots,N)
\end{aligned}
\tag{2.58}
$$

$$
\begin{aligned}
\frac{d\tilde{c}_j}{dx}(x_i) \;&=\; \sum_{k=0}^{N} \frac{dc_k}{dx}(x_i)\, \alpha_k\, C^\dagger_{kj}\, \alpha_j \\[2mm]
&=\; -\sum_{k=0}^{N} k\frac{\pi}{L}\, s_k(x_i)\, \alpha_k\, C^\dagger_{kj}\, \alpha_j \\[2mm]
&=\; -\alpha_j \frac{\pi}{L} \sum_{k=1}^{N-1} S_{ik}\, k\, C^\dagger_{kj} \\[2mm]
&=\; -\alpha_j \frac{\pi}{L}\, D^\dagger_{ij} \\
&\qquad (j = 0,\ldots,N; \qquad i = 1,\ldots,N-1)
\end{aligned}
\tag{2.59}
$$

28

In Eqs. (2.58) and (2.59) we have introduced a rectangular matrix $\mathbf{D}$

$$D_{ij} = \sum_{k=1}^{N-1} C_{ik}\, k\, S^{\dagger}_{kj} \tag{2.60}$$

where $i = 0, \ldots, N$ and $j = 1, \ldots, N-1$. The sum in Eq. (2.60) can be calculated analytically (see the Appendix B). The result is

$$D_{ij} = \begin{cases} -\alpha_i \frac{1}{2} (-1)^{i+j} \left[\cot\left(\pi \frac{i+j}{2N}\right) - \cot\left(\pi \frac{i-j}{2N}\right) \right] & (i \neq j) \\ -\alpha_i \frac{1}{2} \cot\left(\pi \frac{i}{N}\right) & (i = j) \end{cases} . \tag{2.61}$$

Potential energy operator

The grid representation of the potential energy operator is found by evaluating $V(x)\varphi(x)$ at the grid points x_i:

$$V(x)\varphi(x)|_{x=x_i} = \sum_{j=1}^{N-1} V_{ij}\, \varphi(x_j) \qquad (i = 1, \ldots, N-1) \tag{2.62}$$

where
$$V_{ij} = V(x_i)\, \delta_{ij} \qquad (i, j = 1, \ldots, N-1) . \tag{2.63}$$

As in any grid method, the potential energy operator is represented by a diagonal matrix $\mathbf{V}$.

Kinetic energy operator

A grid representation of the kinetic energy operator is found by estimating the value of $\hat{T}\varphi(x)$ at the grid points x_i, using the projection operators (2.44) and (2.45):

$$\begin{aligned} \hat{T}\,\varphi(x)\Big|_{x=x_i} &= -\frac{\hbar^2}{2\mu} J^{-1}(x) \frac{d}{dx} J^{-1}(x) \frac{d}{dx}\, \varphi(x)\Big|_{x=x_i} \\ &\approx -\frac{\hbar^2}{2\mu} J^{-1}(x) \frac{d}{dx} \hat{P}^{\mathcal{C}} J^{-1}(x) \frac{d}{dx} \hat{P}^{\mathcal{S}}\, \varphi(x)\Big|_{x=x_i} \\ &= -\frac{\hbar^2}{2\mu} \sum_{j=1}^{N-1} J^{-1}(x) \frac{d}{dx} \hat{P}^{\mathcal{C}} J^{-1}(x) \frac{d}{dx} \tilde{s}_j(x)\, \varphi(x_j)\Big|_{x=x_i} \\ &= -\frac{\hbar^2}{2\mu} \sum_{j=1}^{N-1} \sum_{k=0}^{N} J^{-1}(x) \frac{d}{dx} \tilde{c}_k(x) J(x_k)^{-1} \frac{d\tilde{s}_j}{dx}(x_k)\, \varphi(x_j)\Big|_{x=x_i} \\ &= -\frac{\hbar^2}{2\mu} \sum_{j=1}^{N-1} \sum_{k=0}^{N} J(x_i)^{-1} \frac{d\tilde{c}_k}{dx}(x_i) J(x_k)^{-1} \frac{d\tilde{s}_j}{dx}(x_k)\, \varphi(x_j) \end{aligned}$$

29

$$= \quad +\frac{\hbar^2}{2\mu} \frac{\pi^2}{L^2} \sum_{k=0}^{N} J(x_i)^{-1} \alpha_k D^{\dagger}_{ik} J(x_k)^{-1} \frac{1}{\alpha_k} D_{kj} \varphi(x_j)$$

$$= \quad \frac{\hbar^2}{2\mu} \frac{\pi^2}{L^2} \sum_{k=0}^{N} J(x_i)^{-1} D^{\dagger}_{ik} J(x_k)^{-1} D_{kj} \varphi(x_j) \ . \tag{2.64}$$

We have thus derived the following grid representation of the kinetic energy operator:

$$T_{ij} \quad = \quad \frac{\hbar^2}{2\mu} \frac{\pi^2}{L^2} \sum_{k=0}^{N} J(x_i)^{-1} D^{\dagger}_{ik} J(x_k)^{-1} D_{kj} \tag{2.65}$$

$$(i, j \ = \ 0, \ldots, N-1)$$

The matrix $\mathbf{T}$ defined by the above equation is not symmetric but can easily be converted into a symmetric matrix $\bar{\mathbf{T}}$ (see Sec. 2.2.4).

$\mathbf{T}$ can be calculated numerically from Eq. (2.65) using the values $J(x_i)$ of the Jacobian at the grid points and the matrix elements D_{ij} given explicitly in Eq. (2.61). This method is convenient if numerical speed is not a priority: it is simple to implement, and the number of grid points N can be chosen freely. However, if N is very large, the computation of the $(N \times N)$-matrix $\mathbf{T}$ becomes very time-consuming: for each of its

$$\frac{N(N+1)}{2}$$

different elements, $N + 1$ terms must be summed, which means that the numerical effort scales as N^3.

A more efficient method is to compute $\mathbf{T}$ directly from the formula

$$T_{ij} \quad = \quad \frac{\hbar^2}{2\mu} \frac{\pi^2}{L^2} \sum_{k=0}^{N} \sum_{l,m=1}^{N-1} J(x_i)^{-1} S_{il} \, l \, C^{\dagger}_{lk} J(x_k)^{-1} C_{km} \, m \, S^{\dagger}_{mj} \tag{2.66}$$

using the fast sine and cosine transform algorithms, following A. G. Borisov [35]. The computational effort for each of the N^2 matrix elements then grows only logarithmically with N, compared to linearly if the summation in Eq. (2.65) is carried out explicitly. It should be noted that the fast routines imply certain restrictions on the number of grid points. The simplest routines only work if N is an integer power of 2 [39]. Eq. (2.66) is the basis of the wavepacket propagation schemes implemented by E. Luc-Koenig *et al.* [175, 176] and by Ch. P. Koch *et al.* [131, 130].

A variant of the Fourier sine-cosine technique

Before A. G. Borisov's article [35] came to our attention, we had combined the discrete sine transform of the *first* type (2.33) with the discrete cosine

transform of the *second* type [217, 35] in order to evaluate $\hat{T}\varphi$. We had found the discrete cosine transform of the second type more appealing, because it is slightly simpler. However, the collocation points for the transforms of the first and of the second type are not the same. The collocation points for the discrete sine and cosine transforms of the second type are

$$y_i \;=\; \frac{x_i - x_{i-1}}{2} \;=\; \left(i - \frac{1}{2}\right)\Delta x \qquad (i = 1, \ldots, N)$$

where x_i are the equidistant grid points defined in Eq. (2.28). The method yields the following matrix representation of the kinetic energy operator, which is analogous to Eq. (2.65):

$$T_{ij} \;=\; \frac{1}{2\mu}\frac{\pi^2}{L^2}\sum_{k=1}^{N} J(x_i)^{-1}\,\bar{D}^{\dagger}_{ik}\,J(y_k)^{-1}\,\bar{D}_{kj} \qquad (2.67)$$

$$(i, j \;=\; 0, \ldots, N-1)$$

Here $\bar{\mathbf{D}}$ is a matrix similar to the matrix $\mathbf{D}$ defined in Eq. (2.60). The method based on Eq. (2.67) gave correct numerical results (vibrational energies and wavefunctions), without spurious solutions. However, we found the computed eigenvalues to be about two digits less accurate compared to the eigenvalues derived from Eq. (2.65). Furthermore, the computed eigenvalues were often *smaller* than the exact values. This loss in accuracy may have been due to a programming error, but it could also be linked to the fact that the collocation points x_i and y_i are not the same. We did not investigate these aspects any further, because the method based on formula (2.65) proved to be entirely satisfactory.

2.2.4   Diagonalization of the Hamiltonian matrix

Evaluating both sides of the radial Schrödinger equation

$$\hat{H}\varphi(x) \;=\; E\,\varphi(x) \qquad (2.68)$$

at the collocation points x_i $(i = 1, \ldots, N-1)$ yields the following linear system:

$$\sum_{j=1}^{N-1} H_{ij}\varphi(x_j) \;=\; E\,\varphi(x_i)\ . \qquad (2.69)$$

Here H_{ij} are the elements of the *asymmetric* Hamiltonian matrix

$$\mathbf{H} \;=\; \mathbf{T} + \mathbf{V}\ , \qquad (2.70)$$

related to a *symmetric* matrix

$$\bar{\mathbf{H}} \;=\; \bar{\mathbf{T}} + \bar{\mathbf{V}} \tag{2.71}$$

by the transformation

$$\bar{H}_{ij} \;=\; J(x_i)^{1/2}\, H_{ij}\, J(x_j)^{-1/2} \;, \tag{2.72}$$

corresponding to a rescaling of the wavefunction $\varphi(x)$. The scaled function $\bar{\varphi}(x)$ and the unscaled functions $\varphi(x)$ are related as

$$\bar{\varphi}(x) \;=\; \varphi(x)\sqrt{J(x)} \;. \tag{2.73}$$

The linear system (2.69) is thus transformed into the following linear system for the values of the *scaled* wavefunction at the collocation points:

$$\sum_{j=1}^{N-1} \bar{H}_{ij}\bar{\varphi}(x_j) \;=\; E\,\bar{\varphi}(x_i) \;. \tag{2.74}$$

The symmetric matrix $\bar{\mathbf{H}}$ can be diagonalized efficiently using standard numerical methods. The procedure yields the eigenvalues E and, for each eigenvalue E, the values of the rescaled wavefunction $\bar{\varphi}(x)$ at the grid points x_i ($i = 1, \ldots, N-1$).

It should be mentioned that the matrix elements $\bar{H}_{ij}$ obtained by the collocation method can be regarded as *approximations* to the integrals

$$\int_0^L \tilde{s}_i(x)\,\hat{H}\tilde{s}_j(x)\,dx$$

$$= \int_0^L \tilde{s}_i(x)\left[-\frac{\hbar^2}{2\mu}\frac{1}{\sqrt{J(x)}}\frac{d}{dx}\frac{1}{J(x)}\frac{d}{dx}\frac{1}{\sqrt{J(x)}}\,\tilde{s}_j(x) + V(x)\,\tilde{s}_j(x) \right]dx \tag{2.75}$$

which occur in the variational method (see the Appendix C). The validity of such an approximation has been discussed by R. Meyer [191], for the related case of trigonometric interpolation using a periodic basis set (the set of function $\tilde{u}_i(x)$ in our notation).

2.2.5   How to interpolate the wavefunction

Given the values of the wavefunction $\varphi(x)$ at the grid points x_i, one needs an interpolation formula in order to compute $\varphi(x)$ at distances *between* the grid points.

A linear interpolation must be ruled out, because the grid step may measure almost half the local de Broglie wavelength.

The obvious alternative is to use the trigonometric interpolation functions $\tilde{s}_i(x)$ introduced above. The remaining question is whether these functions should be used to interpolate $\varphi(x)$ or its scaled equivalent $\bar{\varphi}(x)$.

In order to give an answer, we shall first consider the Hilbert space of *rescaled* wavefunctions $\bar{\varphi}(x)$ defined on the interval $[0, L]$ covered by the grid. The scalar product of two arbitrary rescaled wavefunctions is defined as

$$\langle \bar{\varphi}_1 | \bar{\varphi}_2 \rangle \;=\; \int_0^L \bar{\varphi}_1^*(x)\, \bar{\varphi}_2(x)\, dx \; . \tag{2.76}$$

Eq. (2.31) shows that the sine interpolation functions $\tilde{s}_j(x)$ form an *orthogonal* basis set with respect to this scalar product. It therefore seems natural to expand the rescaled wavefunction in the sine basis, in other words, to interpolate it as follows:

$$\bar{\varphi}(x) \;=\; \sum_{i=1}^{N-1} \tilde{s}_i(x)\, \bar{\varphi}(x_i) \; . \tag{2.77}$$

The corresponding unscaled wavefunction is

$$\varphi(x) \;=\; \frac{1}{\sqrt{J(x)}} \sum_{i=1}^{N-1} \tilde{s}_i(x) \bar{\varphi}(x_i) \; . \tag{2.78}$$

However, numerically we found that the interpolation formula (2.77) can yield very poor results for $\varphi(x)$ at short distances if $\varphi(x)$ belongs to a highly excited vibrational level in a long-range $1/R^6$ or $1/R^3$ potential. In fact, the factor $J(x)$ in Eq. (2.73) can cause the amplitude of the rescaled wavefunction $\bar{\varphi}(x)$ to be orders of magnitudes larger at large distances than at short distances. Thus, if x_i is a grid point in the outer region, $\bar{\varphi}(x_i)$ can be very large, and the term

$$\tilde{s}_i(x)\bar{\varphi}(x_i)$$

in Eq. (2.77) can have a noticible amplitude even at short distances. We recall that the interpolation function $\tilde{s}_i(x)$ resembles a cardinal sine function centered on x_i, which means that its amplitude falls off very slowly, roughly as $1/|x - x_i|$. It seems that only a few terms in Eq. (2.77), belonging to grid points at large distances, can make the dominant contribution to the waveamplitude at short distances and thus spoil the wavefunction there.

This problem does not arise if the *unscaled* wavefunction $\varphi(x)$ is expanded in the basis functions $\tilde{s}_i(x)$:

$$\varphi(x) \;=\; \sum_{i=1}^{N-1} \tilde{s}_i(x)\varphi(x_i) \;=\; \sum_{i=1}^{N-1} \tilde{s}_i(x)\frac{\bar{\varphi}(x_i)}{\sqrt{J(x_i)}} \; . \tag{2.79}$$

33

The above formula is very similar to the expansion in cardinal sine functions proposed by V. Kokoouline *et al.* [135]. We found that Eq. (2.79) always gave excellent results. Therefore we believe that it should replace Eq. (2.78).

The interpolation formula (2.79) is furthermore consistent with the approximation we made in order to derive the grid representation (2.65) of the kinetic energy operator: it is the wavefunction $\varphi(x)$, not its scaled equivalent $\bar{\varphi}(x)$, that is approximated as $\hat{P}^{\mathcal{S}} \varphi(x)$ in Eq. (2.64), that is, as a linear combination of the sine functions $s_k(x)$.

It must be noted, however, that the basis functions $s_k(x)$ ($k = 1, \ldots, N - 1$), now considered as vectors in the Hilbert space of *unscaled* functions $\varphi(x)$ with L^2 scalar product (2.24), are not strictly orthogonal. Their scaled counterparts $\sqrt{J(x)}\, s_k(x)$ in the Hilbert space of scaled functions $\bar{\varphi}(x)$ are not orthogonal either, which follows immediately from the fact that the scaling

$$\varphi(x) \ \leftrightarrow \ \bar{\varphi}(x)$$

does not affect the scalar product $\langle \varphi_1 | \varphi_2 \rangle$ of two states φ_1 and φ_2. At this point it does not matter which set of basis functions is used in the collocation scheme: the questions related to the orthogonality of the basis functions are fundamentally the same for the periodic basis set $\{u_k\}$ as for the sine basis set $\{s_k\}$.

2.2.6 Ghost levels

In Ref. [276] we discussed the appearance of spurious solutions in calculations of weakly bound vibrational levels of diatomic molecules. Spurious solutions arising in pseudo-spectral methods were also reported by J. P. Boyd *et al.* [37].

We observed spurious solutions only if we constructed the Hamiltonian matrix using the periodic Fourier basis $\{u_k\}$. We found no spurious solutions when we constructed it using the sine basis $\{s_k\}$, provided that the grid step was chosen reasonably small. It did not matter in this respect whether Eq. (2.67) or Eq. (2.65) was used to compute the kinetic energy operator in the sine basis.

In some calculations using the periodic Fourier basis $\{u_k\}$, we found a spurious solution at an energy *below* the energy of the physical ground state. This can only be explained if the Hamiltonian matrix obtained by the collocation method is *not* equivalent to the Hamiltonian matrix

$$H_{kk'} \ = \ \frac{\langle u_k | \hat{H} | u_{k'} \rangle}{\langle u_k | u_{k'} \rangle} \ = \ \frac{\int_0^L J(x)\, u_k^*(x) \hat{H} u_{k'}(x)\, dx}{\int_0^L J(x)\, u_k^*(x)\, u_{k'}(x)\, dx} \tag{2.80}$$

used in the Ritz-Rayleigh variational method (see the Appendix C): the Ritz variational principle guarantees that the lowest eigenvalue of the above ma-

trix (the elements of which are true *integrals*, not sums) is an *upper* estimate for the true ground state energy.

In the previous paragraph, we suggested that the underlying basis set of the Mapped Fourier grid is not strictly orthogonal. It would be interesting to find out whether the phenomenon of spurious solutions is related to this "loss of orthogonality" caused by the change of coordinate $R \to x$. In Ref. [276] we showed that the periodic Fourier basis

$$\tilde{u}_i(x) \qquad (i = 1, \ldots, N)$$

differs from the non-periodic sine basis

$$\tilde{s}_i(x) \qquad (i = 1, \ldots, N-1)$$

significantly only in that it comprises the function $\tilde{u}_N(x)$, which is peaked exactly on the borders of the grid, $x = 0$ and $x = L$. The sine basis does not have a similar member. It could be worth examining the orthogonality of this particular basis function, $\tilde{u}_N(x)$, with respect to the other interpolation functions $\tilde{u}_i(x)$ using the scalar product (2.24). For this purpose, the interpolation functions $\tilde{u}_i(x)$ should first be normalized to unity with respect to the scalar product (2.24); next one could compute numerically some integrals $\langle \tilde{u}_i | \tilde{u}_j \rangle$, in particular $\langle \tilde{u}_{N-1} | \tilde{u}_N \rangle$ and $\langle \tilde{u}_N | \tilde{u}_1 \rangle$, in order to find out how much they differ from zero. Perhaps this could also be done analytically, using an analytical Jacobian function $J(x)$.

Of course it might be possible that there is no simple explanation for the appearance of spurious solutions in the Fourier grid method: in fact we do not see any reason why the method should yield *only* physical solutions.

2.2.7 Mapped Fourier Grid for a multi-channel system

The collocation method is easily generalized to the case of several coupled channels, involving more than one electronic state of the diatomic molecule or the colliding atoms.

In the case of p coupled states, the radial wavefunction $\varphi(x)$ can be represented by a vector

$$\varphi(x) = \begin{pmatrix} \varphi_1(x) \\ \vdots \\ \varphi_p(x) \end{pmatrix} \tag{2.81}$$

such that each entry $\varphi_k(x)$ describes the relative motion of the nuclei in the k-th channel ($k = 1, ..., p$).

The grid-representation $\mathbf{H}$ of the multi-channel Hamiltonian $\hat{H}$ is obtained by expanding $\varphi_k(x)$ as

$$\varphi_k(x) = \sum_{i=1}^{N-1} \tilde{s}_i(x) \, \varphi_k(x_i) \qquad (k = 1, ..., p) \tag{2.82}$$

and evaluating $\hat{H}\varphi(x)$ at the grid points x_i $(i = 1, \ldots, N)$, in the same manner as in the single-channel case. The matrix $\mathbf{H}$ is of dimension $(pN \times pN)$.

Mapping and radial interaction

I. Tuvi and Y. B. Band [262] showed how to formulate non-adiabatic radial couplings such that their grid-representation is a Hermitian matrix.

Their method remains applicable for a mapped grid. If the scaled coordinate x is used instead of the radial coordinate R, the differential operator

$$\frac{d}{dR}$$

in Tuvi's and Band's equations must be replaced by

$$\frac{1}{J(x)} \frac{d}{dx}$$

for the space of unscaled functions $\varphi(x)$ and by

$$\frac{1}{\sqrt{J(x)}} \frac{d}{dx} \frac{1}{\sqrt{J(x)}}$$

for the space of scaled functions $\bar{\varphi}(x)$.

2.3 Conclusion

We have described an efficient way for solving the single-channel or the multichannel radial Schrödinger equation numerically.

We found that Borisov's sine-cosine transform technique [35] yields a very accurate Hamiltonian matrix without spurious eigenvalues.

At present we do not see any default of the method or any simple possibility of improving it. Of course this does not exclude that other numerical methods such as Wavelet or B-spline techniques could have certain advantages compared to the Mapped Fourier Grid.

In 2002, we used the Mapped Fourier Sine Grid to compute loosely bound vibrational and scattering states of Rb_2, Cs_2 and RbCs, for each diatomic system using a model of two coupled electronic states. The work was aimed at interpreting photoassociation spectra of Rb_2, Cs_2 and RbCs, as an extension of my "stage de D.E.A." and of the studies by V. Kokoouline *et al.* [137, 202, 134]. It was done in cooperation with M. Raoult, who computed an energy-dependent "short-range reactance matrix" summarizing the effects of non-adiabatic couplings. Using the Mapped Fourier Sine Grid, we computed

bound and discretized continuum levels to which we fitted the short-range reactance matrix. The numerical values for the short-range reactance matrix deduced from the fit agree very well with the accurate values computed by M. Raoult. The work has not been published yet, and it is not described in this thesis.

Within the framework of this thesis, we used the Mapped Fourier Sine Grid only to solve the adiabatic hyperradial Schrödinger equation of the sodium trimer Na_3 (see Chapter 5).

However, the sine-cosine transform technique has become the basis for time-dependent wavepacket calculations developed in the group "Atomes et molécules froids" at Laboratoire Aimé-Cotton [175, 176, 131].

Recently, M. Leduc *et al.* [160] used the Mapped Fourier Sine Grid to compute bound vibrational states of giant helium dimers, in relation to photoassociation experiments [163, 162].

2.4   Article "Mapped grid methods for long-range molecules and cold collisions"

A copy of the article

Mapped grid methods for long-range molecules and cold collisions
K. Willner, O. Dulieu, and F. Masnou-Seeuws
Journal of Chemical Physics **120** (2004) 548
©2004 American Institute of Physics

is included as part of this thesis with kind permission of the American
Institute of Physics.

Mapped grid methods for long-range molecules and cold collisions

K. Willner, O. Dulieu, and F. Masnou-Seeuws[a)]
Laboratoire Aimé Cotton, CNRS, Bât. 505, Campus d'Orsay, 91405 Orsay Cedex, France

The paper discusses ways of improving the accuracy of numerical calculations for vibrational levels of diatomic molecules close to the dissociation limit or for ultracold collisions, in the framework of a grid representation. In order to avoid the implementation of very large grids, Kokoouline *et al.* [J. Chem. Phys. **110**, 9865 (1999)] have proposed a mapping procedure through introduction of an adaptive coordinate x subjected to the variation of the local de Broglie wavelength as a function of the internuclear distance R. Some unphysical levels ("ghosts") then appear in the vibrational series computed via a mapped Fourier grid representation. In the present work the choice of the basis set is reexamined, and two alternative expansions are discussed: Sine functions and Hardy functions. It is shown that use of a basis set with fixed nodes at both grid ends is efficient to eliminate "ghost" solutions. It is further shown that the Hamiltonian matrix in the sine basis can be calculated very accurately by using an auxiliary basis of cosine functions, overcoming the problems arising from numerical calculation of the Jacobian $J(x)$ of the $R \rightarrow x$ coordinate transformation. © *2004 American Institute of Physics.* [DOI: 10.1063/1.1630031]

I. INTRODUCTION

Due to rapid progress in experiments with cold atom samples, and more recently with cold molecule samples, there is an important need for modeling and theoretical interpretation. Numerical tools should be constantly refined for treatment of atomic collisions at very low energy and for determination of the bound vibrational levels of diatomic molecules (mostly alkali dimers at present) close to the dissociation limit. Among the many applications, we may emphasize:

(i)   interpretation of photoassociation experiments, calculation of formation rates for ultracold molecules;
(ii)   determination of the scattering lengths and of collision cross sections at low energies;
(iii)   calculation of the coupling parameters between an atomic and a molecular condensate.

The Fourier grid Hamiltonian representation (FGHR), described in detail in several papers,[1–6] now widely used to solve the time-independent radial Schrödinger equation, is an efficient tool for the problems mentioned above. Once a grid of N equidistant points is defined, the energies and wave functions of bound levels of a p-closed-channels problem are obtained through diagonalization of a $pN \times pN$ Hamiltonian matrix. Inclusion of open channels is made possible through optical potentials.[5] From the computed wave functions, accurate evaluation of the dipole transition moments or overlap integrals becomes straightforward through numerical quadrature.[7]

However, when applied to the present class of problems, the FGHR implemented with a constant grid step becomes cumbersome, since the local de Broglie wavelength may vary by several orders of magnitude from the short-range to the long-range region. Kokoouline *et al.* have overcome this difficulty by defining a working grid in a coordinate adapted to the variation of the local de Broglie wavelength.[8] Their work generalizes the mapped Fourier grid method, originally proposed for Coulomb potentials by Fattal *et al.*,[9] to potentials with R^{-n} asymptotes ($n \geqslant 2$). In the latter, the adaptive coordinate was defined through optimization of the use of the phase space. A similar procedure was introduced by Tiesinga *et al.*[10] for the calculation of bound vibrational states of alkali dimers by a filter method.

The definition of the adaptive coordinate x could follow an analytical procedure, considering the asymptotic form of the potential and a lower limit of the local de Broglie wavelength. However, Kokoouline *et al.*[8] have shown that a better optimization of the occupancy of the phase space was achieved with a numerical change of variable, following strictly the R-variation of the local de Broglie wavelength as $[E - V(R)]^{-1/2}$, where $V(R)$ is the actual potential. The latter is generally defined by interpolation of results of *ab initio* calculations at a set of R values, matched to analytical expressions in the asymptotic region. The numerical method then involves calculations of the Jacobian $J(x)$ of the transformation $R \rightarrow x$, and of its first and second derivatives $J'(x)$ and $J''(x)$. The method has already given accurate results for calculations of photoassociation spectra[8,11–13] and of predissociation widths.[14]

In the present work, we propose ways of improving the method by overcoming two problems frequently encountered in calculations dealing with long-range molecules or cold collisions. Indeed

(i)   numerical errors may arise in the calculation of the derivatives of the Jacobian, reducing the final accuracy;
(ii)   besides, unphysical levels ("ghosts") are found when the mapped Hamiltonian is diagonalized in a periodic

---
[a)]Electronic mail: francoise.masnou@lac.u-psud.fr

      548

plane wave (Fourier) basis. Their elimination is cumbersome, and they may lead to errors in problems involving several coupled channels, due to a possible coupling between spurious and physical levels. The "ghosts" may also affect solutions of the time-dependent Schrödinger equation.

For that purpose, the present paper checks the efficiency of numerical methods where the plane waves are replaced by alternative basis sets. The discussion is focussed on the determination of vibrational levels of diatomic molecules close to the dissociation limit. The first alternative choice is a set of mapped sine functions, already introduced by Lemoine[15] and Borisov[16] in the framework of different applications, namely thermal collisions between atoms and surfaces. The second choice is a mapped version of the Hardy (cardinal sine) function representation proposed by Colbert and Miller[4,17] for collinear reactive scattering.

We show that use of a sine basis and in some cases of a Hardy basis seems sufficient to suppress the "ghost" levels. We present a new way to calculate the Hamiltonian matrix using a combination of a sine and a cosine basis set which avoids the numerical evaluation of the derivatives of the Jacobian. We show on three examples that the mapped sine grid method permits an accurate determination of energies and wave functions for levels very close to the dissociation limit.

The problem of "ghost" levels has been previously addressed by Hua Wei[18] in the context of discrete variable representation (DVR) of orthogonal polynomials. The appearance of "ghost" levels was explained by the errors stemming from the quadrature of the potential, especially for small and medium-sized basis sets. A "near variational" DVR was implemented to improve the accuracy of the quadrature and to eliminate the "ghost" solutions. Errors coming from the quadrature of potentials in DVR are also addressed in various articles such as Ref. 19. We shall see below that the "ghost" levels in our problem seem to have a different origin, being linked to the behavior of the basis functions at the boundaries and also to the mapping procedure.

The paper is organized as follows: Section II recalls the principles of the mapped representation with introduction of an adaptive coordinate x, while Sec. III summarizes the collocation method. Section IV recalls the Fourier grid method and shows examples of calculations where "ghost" levels appear among the computed physical levels in vibrational series of long-range molecules. Section V proposes two alternative choices for an expansion of the wave function. The efficiency of the various basis sets is discussed in Sec. VI through analysis of a few examples typical of the present class of problems. Section VII is the conclusion.

II. MAPPING PROCEDURE

We recall below the main steps of the mapping procedure extensively described elsewhere,[8,9] using slightly modified notations for clarity sake. The main purpose is a change of coordinate which transforms a given radial wave function into a new wave function with regular oscillations.

Let us consider the radial Schrödinger equation for the relative motion of two atoms with reduced mass μ in a potential $V(R)$ with R^{-n} asymptotic behavior ($n=3,5,6$), typical of studies on photoassociation or cold collisions

$$(\hat{T}+\hat{V})\psi(R)=\left(-\frac{1}{2\mu}\frac{d^2}{dR^2}+V(R)\right)\psi(R)=E\psi(R). \quad (2.1)$$

The standard Fourier grid method uses N equidistant points on the R axis in order to represent the radial wave functions $\psi(R)$ for bound or continuum levels up to a maximum energy $E_{\max}$. A constant grid step ΔR is determined by the maximum value $P_R^{\max}$ of the classical momentum $P_R=\mu\dot{R}$

$$P_R^{\max}=\sqrt{2\mu(E_{\max}+V_{\min})}, \quad (2.2)$$

where $-V_{\min}$ is the minimum value of the potential $V(R)$. As discussed by Fattal et al.[9] and Kokoouline et al.,[8] this grid corresponds to a rectangle of length L_R and height $2P_R^{\max}$ in the (R,P_R) phase space.

The need for a change of the grid step becomes obvious in the case of weakly bound molecules or slowly colliding atoms, where the local Broglie wavelength

$$\Lambda(E,R)=\frac{h}{\sqrt{2\mu[E-V(R)]}}=\frac{2\pi\hbar}{P_R}, \quad (2.3)$$

may vary by several orders in magnitude from the inner to the outer region. For these systems the classically allowed region $\mathcal{S}$ occupies only a small fraction of the rectangle in phase space,[8] due to a great variation of the classical momentum P_R from short to long distances. In order to optimize the occupancy of phase space, we consider an adaptive coordinate x and its conjugated momentum p_x. The change of variable from R to x will be defined by the condition that the classically allowed region in the (x,p_x) phase space be as close as possible to a rectangle.[8,9] It is then straightforward to set up an equidistant Fourier grid on the x axis so that its associated rectangle in (x,p_x) phase space matches the classically allowed region.

We shall now consider the change of coordinate in detail. The conjugated momentum p_x, obtained by derivation of the classical Lagrangian, $\mathcal{L}(x,\dot{x})$, verifies $p_x=\partial\mathcal{L}(x,\dot{x})/\partial\dot{x}=\mu J(x)^2\dot{x}=J(x)\ P_R$, where

$$J(x)=\frac{dR}{dx}, \quad (2.4)$$

is the Jacobian of the transformation $R\rightarrow x$. The canonical transformation $(R,P_R)\rightarrow(x,p_x)$ conserves the area in classical phase space since

$$\begin{vmatrix} \dfrac{\partial R}{\partial x} & \dfrac{\partial R}{\partial p_x} \\[2mm] \dfrac{\partial P_R}{\partial x} & \dfrac{\partial p_R}{\partial p_x} \end{vmatrix} = \begin{vmatrix} J(x) & 0 \\[2mm] -(p_x J'(x))/J(x)^2 & \dfrac{1}{J(x)} \end{vmatrix} = 1, \quad (2.5)$$

so that $dR\ dp_R=dx\ dp_x$. For a given maximum energy $E_{\max}$, the classically allowed region $\mathcal{S}$ in phase space is defined by

$$\mathcal{H}(x,p_x)\leqslant E_{\max}\Leftrightarrow(x,p_x)\in\mathcal{S}, \quad (2.6)$$

where $\mathcal{H}(x,p_x)$ is the classical Hamiltonian. This region $\mathcal{S}$ is a rectangle of length L and height $2p_{max}$ if the maximum allowed value of the momentum $|p_x|$ is the same for all x

$$\forall x: \quad \mathcal{H}(x,p_{max}) = \frac{p_{max}^2}{2\mu J(x)^2} + V(x) = E_{max}, \quad (2.7)$$

which shows that the Jacobian has to be chosen as

$$J(x) = \frac{p_{max}}{\sqrt{2\mu[E_{max}-V(R)]}} = p_{max}\frac{\Lambda(E_{max},R)}{h}. \quad (2.8)$$

Thus the Jacobian $J(x)$ needs to be proportional to the local de Broglie wavelength $\Lambda(E,R)$ at energy $E=E_{max}$ [see Eq. (2.3)]. The adaptive coordinate x is obtained by integration

$$x(R) = \int_{R_{in}}^{R} \frac{dR'}{J(R')} = \frac{\sqrt{2\mu}}{p_{max}} \int_{R_{in}}^{R} dR' \sqrt{E_{max}-V(R')}, \quad (2.9)$$

where R_{in} is the inner turning point at energy E_{max}. For the maximum energy $E=E_{max}$, the classical momentum takes on the values $-p_{max}$ and $+p_{max}$, which are now independent of the distance x, making the classical shell $\mathcal{S}$ a rectangle of area $2p_{max} \times L$, where the length L of the grid is defined from the classical turning points. This justifies grid calculations with a constant stepsize in x.[2] The minimum number of grid points is fixed by dividing the rectangle in elementary cells of area h and putting one grid point per cell, so that the stepsize becomes

$$\Delta x = h/2p_{max} = \pi\hbar/p_{max}. \quad (2.10)$$

In practice a more flexible definition of the Jacobian $J(x)$ is needed: First, the Jacobian defined by Eq. (2.8) becomes infinite at classical turning points. More importantly, the derivation of Eqs. (2.8) and (2.10) relies on classical arguments. Since we must treat quantal tunneling effects, we need a higher density of grid points in order to represent the nonclassical parts of the wave functions. Finally, for multichannel calculations, it is convenient to consider a common enveloping potential $V_{env}(R)$ located below all the potential curves. Therefore, the usual choice[8] is

$$x(R) = \int_{R_0}^{R} \frac{dR'}{J_{env}(R')} = \beta\frac{\sqrt{2\mu}}{p_{max}} \int_{R_0}^{R} dR' \sqrt{E_{max}-V_{env}(R')}. \quad (2.11)$$

In Eq. (2.11), the distance R_0 is slightly smaller than the position of the repulsive wall in the potential, while the parameter $\beta \leq 1$ must be adjusted to improve the description of the evanescent part of the wave function. The enveloping potential V_{env} is equal or deeper than the true potential V: For instance one may choose an asymptotic potential $V_{env} = -C_n/R^n$ to derive analytical formulas for x.

In the new coordinate x, in order to eliminate the Jacobian from the scalar product of two wave functions $\phi(R)$ and $\psi(R)$, it is convenient to introduce rescaled wave functions $\bar{\phi}(x) = \sqrt{J(x)}\phi(R)$ and $\bar{\psi}(x) = \sqrt{J(x)}\psi(R)$. The scalar product then reads

$$\int_0^\infty dR\,\phi^*(R)\psi(R) = \int_0^L dx J(x)\phi^*(R(x))\psi(R(x))$$

$$= \int_0^L dx\,\bar{\phi}^*(x)\bar{\psi}(x). \quad (2.12)$$

Let A be an operator acting on the wave function $\psi(R)$. We define a transformed operator $\bar{A}$ that acts on $\bar{\psi}(x)$

$$\bar{A}\bar{\psi}(x) \equiv \overline{A\psi}(x) = \sqrt{J(x)}(A\psi)(x). \quad (2.13)$$

We apply this rule to transform the differential operator $d/dR = [1/J(x)](d/dx)$

$$\frac{\bar{d}}{dR} = \frac{1}{\sqrt{J(x)}} \frac{d}{dx} \frac{1}{\sqrt{J(x)}}. \quad (2.14)$$

The kinetic and potential energy operators become

$$\bar{T} = -\frac{\hbar^2}{2\mu} \frac{1}{\sqrt{J(x)}} \frac{d}{dx} \frac{1}{J(x)} \frac{d}{dx} \frac{1}{\sqrt{J(x)}}, \quad (2.15)$$

$$\bar{V} = V(x). \quad (2.16)$$

As discussed in Ref. 8, the kinetic-energy operator (2.15) can be rewritten as

$$\bar{T} = -\frac{1}{4\mu}\left[\frac{1}{J(x)^2}\frac{d^2}{dx^2} + \frac{d^2}{dx^2}\frac{1}{J(x)^2} - \frac{7}{2}\frac{J'(x)^2}{J(x)^4} + \frac{J''(x)}{J(x)^3}\right]. \quad (2.17)$$

This alternative expression is useful for numerical applications in the case where the Jacobian and its derivatives can be computed through analytical formulas. But in calculations where the potential is defined by a set of points with interpolation procedure, numerical errors frequently arise from use of Eq. (2.17), due to the presence of the local term

$$T_{loc} = -\frac{7}{2}\frac{J'(x)^2}{J(x)^4} + \frac{J''(x)}{J(x)^3}. \quad (2.18)$$

This is illustrated in Fig. 1 in case of calculations involving the Cs_2 0_u^+ $(6s+6p_{1/2})$ electronic state.[11–13] The adiabatic potential is represented on the top figure. As in many situations, the potential is calculated by two different methods, *ab initio* calculations at short range[20] and multipole expansion in the asymptotic region.[21] In the border region, a matching of the potential value and first derivative does not guarantee a matching of the second derivative. Also represented is the enveloping potential $V_{env}(x)$ that was used to define the Jacobian: It is identical to the physical potential at distances beyond the equilibrium distance R_{eq} and chosen constant for $R \leq R_{eq}$ in order to avoid divergence of the Jacobian at the inner turning point. In the bottom figure, we may identify three regions where rapid variations of the Jacobian derivatives result into strong variations of T_{loc} that may create computational problems. Small oscillations occur at $x \approx 380$, where *ab initio* data for the potential are matched to asymptotic expansion. At $x \approx 170$, there is an avoided crossing of $V(R)$ with the 0_u^+ $(6s+6p_{3/2})$ potential curve. Finally, for $x = 100$, brute matching to a constant potential in-
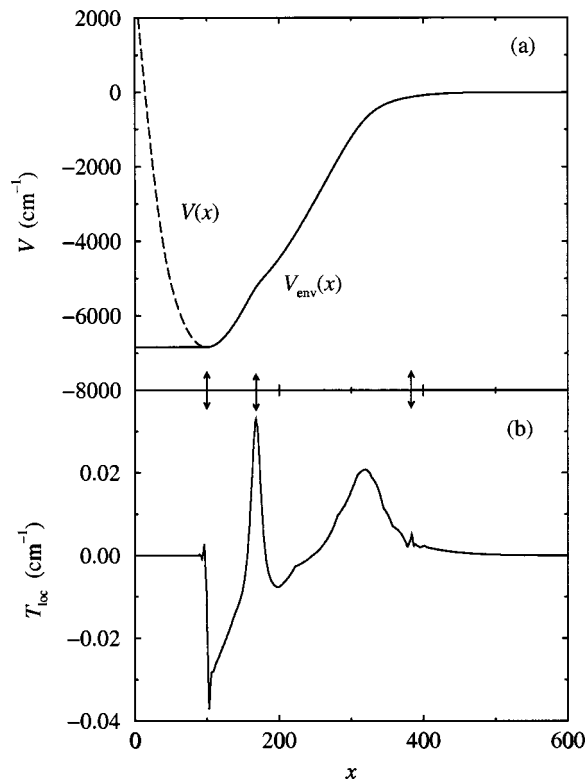
FIG. 1. Example of a mapping based on a numerical potential, where the Jacobian $J(x)$ and its derivatives are calculated numerically. (a) Variation, as a function of the working coordinate x, of the adiabatic potential curve $V(x)$ for the 0_u^+ ($6s+6p_{1/2}$) state of Cs_2 (dashed line) and the enveloping potential $V_{env}(x)$ (full line) used to define the Jacobian. (b) The local kinetic-energy term $T_{loc}(x)$ defined in Eq. (2.18) varies rapidly at the distances indicated by the marks on the x axis (see text).

troduces an angular point. The latter effect could, of course, be suppressed: for a given potential, a smoother variation of the enveloping potential could be implemented; alternatively, the improvement of the mapped Fourier method near the classical turning point has been discussed recently,[22] defining a procedure well-suited to calculations in a restricted energy range. However, such refinements are not implemented in the present paper, since we aim at defining a general method that can easily yield accurate values for a large number of vibrational levels up to a maximum energy, in a variety of physical situations. Although the variations in T_{loc} in Fig. 1 remain small in comparison with the potential energy, and can be discarded in most applications, the high accuracy required in problems involving cold molecules demands to suppress them by computing the kinetic operator directly from Eq. (2.15). This procedure, already discussed by Nest and Saalfrank[23] and by Borisov[16] in view of different applications, requires a precise evaluation of the d/dx operator and will be discussed below.

III. COLLOCATION METHOD: DEFINITION OF A REPRESENTATION, INTERPOLATION FUNCTIONS

Our goal is now to define a representation for the wave functions and the Hamiltonian in the coordinate x. An arbitrary function $\bar{\psi}$ is approximated by an expansion on a set of N functions u_k ($k=1,...N$),

$$\bar{\psi}(x) \approx \hat{P}\bar{\psi}(x) = \sum_{k=1}^{N} u_k(x)\bar{\psi}_k, \tag{3.1}$$

where $\hat{P}$ is a projection operator such that $\hat{P}\bar{\psi}$ is a projection of $\bar{\psi}$ on the subspace spanned by the u_k functions. It is convenient to choose an orthonormal basis set

$$\langle u_k | u_l \rangle = \int_0^L dx\, u_k^*(x) u_l(x) = \delta_{kl}\Delta x, \tag{3.2}$$

where Δx is the constant stepsize on the grid. We define $\hat{P}$ by the *collocation principle*: $\bar{\psi}$ and $\hat{P}\bar{\psi}$ match at N grid points x_i ($i=1,...,N$), assumed here to be equidistant:

$$\bar{\psi}(x) = \hat{P}\bar{\psi}(x)\big|_{x=x_i} \quad (x_i = x_0 + i\Delta x, \; i=1,...,N). \tag{3.3}$$

The collocation method[24,25] has been used many times for applications in quantum-mechanics.[2,7,26,27] An isomorphism can be established between the set of N basis functions, and a set of N interpolation functions $\tilde{u}_i$ ($i=1,...,N$), verifying $\tilde{u}_i(x_j) = \delta_{ij}$, so that the ith interpolation function vanishes at every grid point but the ith. In general a function $\tilde{u}_i$ is a sharply peaked function centered on the ith grid point (an "approximate Dirac peak"). The projection of $\bar{\psi}$ can be expressed as

$$\hat{P}\bar{\psi}(x) = \sum_{i=1}^{N} \tilde{u}_i(x)\bar{\psi}(x_i), \tag{3.4}$$

where the values of the function $\bar{\psi}$ at the grid points appear as the coefficients of the expansion onto the interpolation functions $\tilde{u}_i(x)$. Moreover, Eq. (3.4) yields an interpolation of $\bar{\psi}$ at any position between the grid points.

We recently found that an expansion over the interpolation functions $\tilde{u}_i(x)$ generally yields better results when applied to the wave functions $\psi(x)$ instead of the rescaled functions $\bar{\psi}(x) = \sqrt{J(x)}\psi(x)$. For levels very close to the dissociation limit, the interpolation according to Eq. (3.4), starting from known values $\bar{\psi}(x_i)$, may indeed produce spurious oscillations of the wave function at short distances, due to a great variation in amplitude of the rescaled wave function $\bar{\psi}(x)$. We found it generally preferable to write $\psi(x) \approx \sum_{i=1}^{N} \tilde{u}_i(x)\psi(x_i)$ instead of $\bar{\psi}(x) \approx \sum_{i=1}^{N} \tilde{u}_i(x)\bar{\psi}(x_i)$. However, this is a subtle issue, involving the orthogonality of the basis sets, and we postpone its discussion to a forthcoming article.

A simple expression for the scalar product in the approximate space can also be derived

$$\int_0^L \hat{P}\bar{\phi}^*(x)\hat{P}\bar{\psi}(x)dx = \sum_{i=1}^{N} \bar{\phi}^*(x_i)\bar{\psi}(x_i)\Delta x, \tag{3.5}$$

in which the collocation points appear as the quadrature points. The Hamiltonian operator (like any operator) is represented in the interpolation basis by a $N \times N$ matrix,[28] as will be described in Secs. IV and V. Since the potential operator is diagonal, the numerical effort lies on the evaluation of the kinetic-energy operator and the diagonalization.

Several interpolation functions $\tilde{u}_i$, constructed from basis sets u_k, can be chosen, and we describe three possibilities
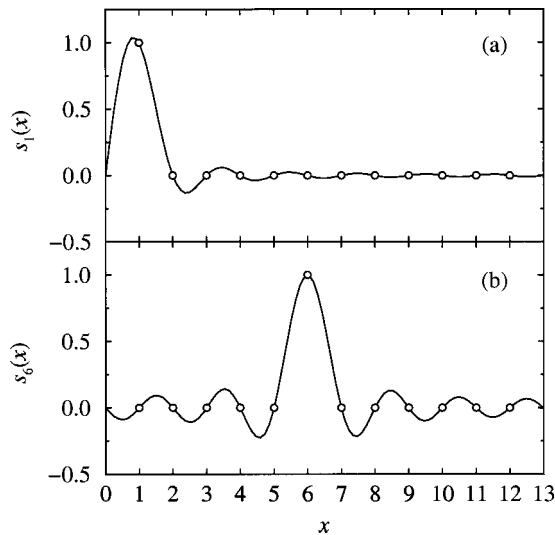
FIG. 2. Sine interpolation for $N=13$, $\Delta x=1$. The positions of the collocation points are indicated by the circles. (a) The interpolation function $\tilde{s}_1(x)$ (upper panel) vanishes at all the grid points x_i ($i=0,...,13$) except x_1, where it takes the value $\tilde{s}_1(x_1)=1$. Note that $\tilde{s}_1$ has its maximum not at the grid point $x_1=1$ itself but slightly to the left, at $x \approx 0.84$. (b) the interpolation function $\tilde{s}_6(x)$ (lower panel) vanishes at all the grid points except x_6 and closely resembles a cardinal sine function.

FIG. 3. Fourier interpolation for $N=13$, $\Delta x=1$. The positions of the collocation points are indicated by the circles. (a) The interpolation function $\tilde{u}_1(x)$ has to be compared to the sine interpolation function $\tilde{s}_1$ in Fig. 2(a). (b) The interpolation function $\tilde{u}_6$, to be compared with $\tilde{s}_6$ in Fig. 2(b). (c) Due to the periodicity of the basis set, the peak of the interpolation function $\tilde{u}_{13}$ is visible at both ends of the grid. In the sine basis, there is no analogous function.

in the following sections: (i) Fourier interpolation (ii) sine (or particle-in-a-box) interpolation, and (iii) cardinal sine (or Hardy) interpolation. These schemes mostly differ from each other by the boundary conditions on the interpolation functions at the edge of the grid. A comparison was already proposed by Muckerman,[7] who introduced "coordinate eigenfunctions" labeled here "interpolation functions" using both a periodic (Fourier) and a fixed node (sine) basis set. We show in Figs. 2 and 3 examples of the sine interpolation functions $\tilde{s}_i$, and the corresponding Fourier interpolation functions $\tilde{u}_i$ on a grid where $i=1$, 13 with stepsize $\Delta x=1$, so that the collocation points are located at $x=1,...,13$. For $i=1$, 12, the $\tilde{s}_i$ and $\tilde{u}_i$ look qualitatively similar, exhibiting a sharp peak in the vicinity of the collocation point $x=i$, and being close to zero elsewhere. However, some differences are visible: for $x=1$, the Fourier function $\tilde{u}_1$ has a vanishing derivative, whereas the derivative of $\tilde{s}_1$ is negative. In the interval $2<x<13$ both the Fourier function $\tilde{u}_1$ and the sine function $\tilde{s}_1$ display small oscillations, but their amplitude is much larger for $\tilde{u}_1$. The two functions $\tilde{u}_6$ and $\tilde{s}_6$ are similar. Finally, whereas the sine basis comprises only 12 interpolation functions, there is a Fourier interpolation function $\tilde{u}_{13}$, which is also nonzero at $x=0$, although the latter point is not a collocation point. We discuss below whether the problem of "ghost" levels in case of a periodic representation is partly linked to this behavior at the edges of the grid.

IV. MAPPED FOURIER GRID METHOD AND THE PROBLEM OF "GHOST" LEVELS

We recall here the main features of the plane wave expansion, or Fourier expansion, that was used in previous papers[8,11–13,28] in combination with the mapping procedure. We present the relevant equations with some details in order

to make the comparison with the other basis expansions easier. We also address the issue of the "ghost" levels.

A. Fourier expansion

Let us consider the operator $\hat{P}^{\mathcal{F}}$, defined in Eq. (3.3) in the general case, which describes the projection onto the subspace spanned by the N basis functions

$$u_k(x) = \frac{e^{ik(2\pi/L)x}}{\sqrt{N}}, \quad k=-\nu,...,\nu, \tag{4.1}$$

assuming an odd number $N=2\nu+1$ of grid points. The functions $u_k(x)$ are orthonormal according to the definition of Eq. (3.2), and they are periodic in the interval $[0,L]$. The discrete Fourier transform, involving a unitary matrix F with matrix elements

$$F_{jk} = \frac{e^{ik(2\pi/N)j}}{\sqrt{N}}, \quad k=-\nu,...,\nu, \quad j=1,...,N, \tag{4.2}$$

allows the definition of interpolation functions

$$\tilde{u}_j(x) = \sum_{k=-\nu}^{\nu} u_k(x) F_{kj}^{\dagger} \quad j=1,...,N, \tag{4.3}$$

$$= \frac{1}{N} \left[1 + 2 \sum_{k=-\nu}^{\nu} \cos\left(k \frac{2\pi}{N} \left(\frac{x}{\Delta x} - j \right) \right) \right], \tag{4.4}$$

J. Chem. Phys., Vol. 120, No. 2, 8 January 2004

Mapped grid methods for cold collisions   553

$$
= \begin{cases} 1 & (x=j\Delta x) \\ \dfrac{1}{N} \dfrac{\sin \pi \left(\dfrac{x}{\Delta x} - j \right)}{\sin \dfrac{\pi}{N} \left(\dfrac{x}{\Delta x} - j \right)} & \text{otherwise.} \end{cases}
\tag{4.5}
$$

An example of three interpolation functions was already given in Fig. 3 in the case of a grid with $N=13$ points. The values of an arbitrary function $\bar{\psi}$ at the grid points are related to the expansion coefficients $\bar{\psi}_k$ on the u_k basis by the discrete Fourier transform (4.2)

$$
\bar{\psi}(x_j) = \sum_{k=-\nu}^{\nu} F_{jk} \bar{\psi}_k = \sum_{k=-\nu}^{\nu} \frac{e^{ik(2\pi/N)j}}{\sqrt{N}} \bar{\psi}_k .
\tag{4.6}
$$

The evaluation of the derivatives of the interpolation functions is required for the representation of the Hamiltonian. We have

$$
\frac{d\bar{u}_j}{dx}(x_k) = i \frac{2\pi}{L} \sum_{l=1}^{N} F_{kl} l F_{lj}^{\dagger},
\tag{4.7}
$$

$$
= \frac{\pi}{L} D_{kj},
\tag{4.8}
$$

where the elements of the anti-symmetric square matrix D can be calculated analytically[4,28]

$$
D_{kj} = 2i \sum_{l=-\nu}^{\nu} F_{kl} l F_{lj}^{\dagger},
\tag{4.9}
$$

$$
= -\frac{4}{N} \sum_{l=1}^{\nu} l \sin\left[l \frac{2\pi}{N}(k-j) \right],
\tag{4.10}
$$

$$
= +\frac{4}{N} \frac{\partial}{\partial \alpha} \sum_{l=1}^{\nu} \cos(l\alpha) \quad \text{where} \quad \alpha = \frac{2\pi}{N}(k-j),
\tag{4.11}
$$

$$
= +\frac{2}{N} \frac{\partial}{\partial \alpha} \frac{\sin[(\nu + \frac{1}{2})\alpha]}{\sin\left(\dfrac{\alpha}{2}\right)},
\tag{4.12}
$$

$$
= \begin{cases} \dfrac{(-1)^{k-j}}{\sin\left[\dfrac{\pi}{N}(k-j) \right]} & (k \neq j) \\ 0 & (k=j). \end{cases}
\tag{4.13}
$$

The potential energy operator is represented by a diagonal matrix [see Eq. (2.16)], while a symmetric representation $\bar{T}$ of the kinetic-energy operator [Eq. (2.15)] is obtained using the projection operator $\hat{P}^{\mathcal{F}}$
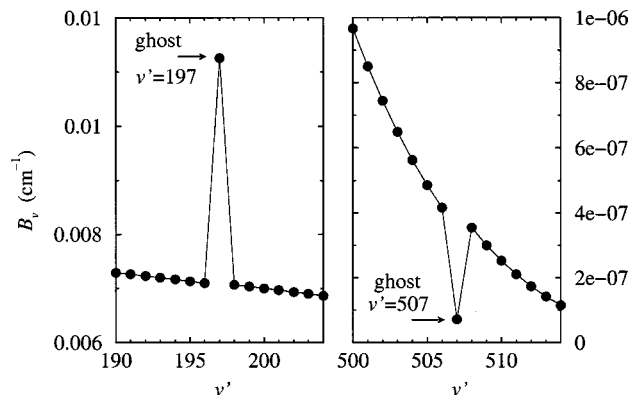
FIG. 4. The rotational constants for some calculated vibrational levels v' of the Cs$_2$ 0_u^+ $(6s+6p_{1/2})$ potential. The spurious levels are easily identified by their anomalous rotational constants.

$$
\bar{T}\bar{\psi}(x)\big|_{x=x_i}
$$

$$
\approx -\frac{1}{2\mu} J(x)^{-1/2} \frac{d}{dx} \hat{P}^{\mathcal{F}} J(x)^{-1} \frac{d}{dx} \hat{P}^{\mathcal{F}} J(x)^{-1/2} \bar{\psi}(x) \bigg|_{x=x_i},
$$

$$
= -\frac{1}{2\mu} \frac{\pi^2}{L^2}
$$

$$
\times \sum_{j,k=1}^{N} J(x_i)^{-1/2} D_{ik} J(x_k)^{-1} D_{kj} J(x_j)^{-1/2} \bar{\psi}(x_j),
$$

$$
= \bar{T}_{ij} \bar{\psi}(x_j).
\tag{4.14}
$$

B. "Ghost" levels

By diagonalization of the Hamiltonian matrix, eigenvalues and eigenvectors can be obtained with arbitrarily good accuracy, provided that the grid step is chosen small enough and the β parameter optimized. However, some spurious levels (hereafter referred to as "ghost" levels) usually occur. They are easily identified by irregularities in the vibrational progression and in the rotational constants. This is illustrated in Fig. 4 where we have represented the numerical results for the vibrational levels in the 0_u^+ $(6s+6p_{1/2})$ potential of the Cs$_2$ molecule. Two spurious levels were found when the kinetic-energy matrix was calculated from Eq. (2.15) using the discrete Fourier transform, one at $v'=197$ (between the physical levels $v=196$ and $v=197$) and another at $v'=507$ (between the physical levels $v=505$ and $v=506$). (We are using the index v' to number all the levels found in the calculations, and v to number the physical levels, so that $v \leq v'$.) The wave functions of the "ghost" levels are characterized by their unphysical rapid oscillations and nonvanishing amplitude in the classically forbidden region. This is illustrated in Figs. 5 and 6, where we have drawn as a function of R the wave functions for the physical level $v=196$ and for the "ghost" level just above it: At distances smaller than the inner turning point, the latter wave function does not manifest the expected exponential decrease but keeps on oscillating. This behavior can further be checked by considering for both wave functions the coefficients a_k and b_k of the Fourier expansion, as illustrated in Figs. 7 and 8. In the projection of a function ψ on the periodic Fourier basis:
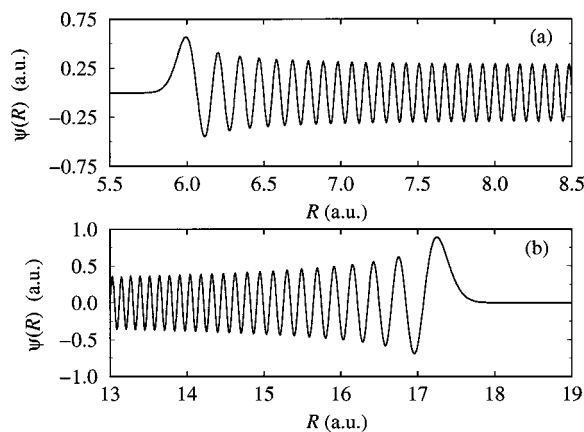
FIG. 5. The wave function $\psi(R)$ of the vibrational level $v=196$ for the potential 0_u^+ $(6s+6p_{1/2})$ of Cs_2 represented in the vicinity of (a) the inner (b) the outer classical turning point. This wave function shows the expected Wentzel–Kramers–Brillouin-type (WKB) behavior. The accuracy of the solution is unaffected by the presence of the spurious level $v'=197$ (see Fig. 6). Whereas the grid covers the range 5.3 a.u.$<R<10^6$ a.u., only the inner region $R<19$ a.u., where the wave function has a noticeable amplitude, is shown here.

$$\psi(x) \approx \hat{P}^{\mathcal{F}} \psi(x) = \frac{a_0}{\sqrt{N}} + \sqrt{\frac{2}{N}} \sum_{k=1}^{\nu} a_k \cos\left(k \frac{2\pi}{L} x \right)$$
$$+ b_k \sin\left(k \frac{2\pi}{L} x \right), \tag{4.15}$$

the a_k and b_k coefficients are calculated as

$$a_0 = \psi_0 = \sqrt{\frac{1}{N}} \sum_{j=1}^{N} \psi(x_j), \tag{4.16}$$

$$a_k = \sqrt{\frac{2}{N}} \sum_{j=1}^{N} \cos\left(k \frac{2\pi}{N} j \right) \quad (k=1,...,\nu), \tag{4.17}$$

$$b_k = \sqrt{\frac{2}{N}} \sum_{j=N}^{N} \sin\left(k \frac{2\pi}{N} j \right) \quad (k=1,...,\nu). \tag{4.18}$$
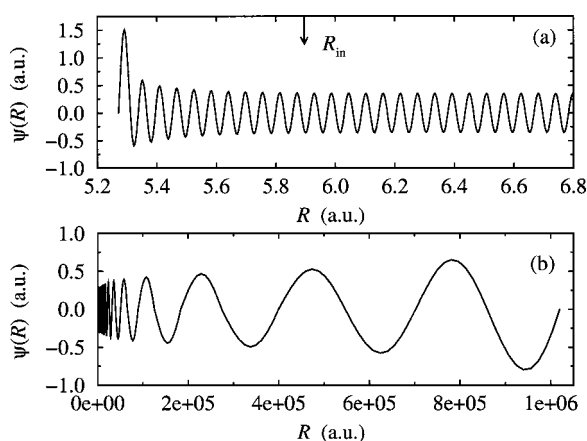
FIG. 6. Same as Fig. 5 for the spurious level $v'=197$ (binding energy: $D-E_{v'}=1179$ cm^{-1}) found between the physical levels $v=196$ and $v=197$ of the Cs_2 0_u^+ $(6s+6p_{1/2})$ potential. (a) The inner classical turning point R_{in} is indicated by the arrow. The outer turning point (not indicated) is at $R_{out}=17.4$ a$_0$. (b) The wave function extends over the entire grid and has a non-WKB behavior, displaying rapid oscillations in the classically forbidden region.
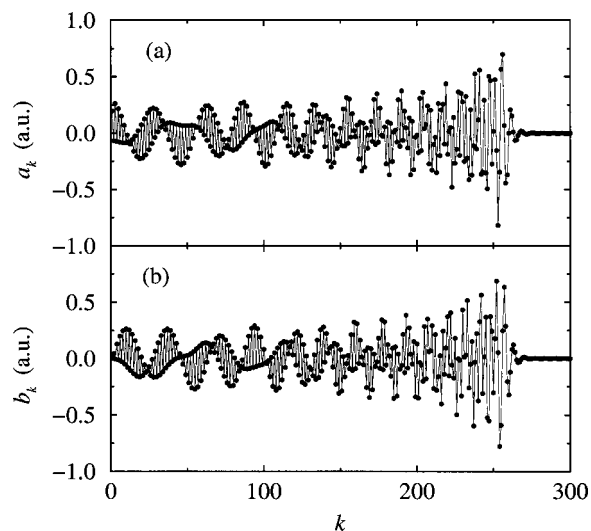
FIG. 7. The Fourier expansion coefficients (a) a_k and (b) b_k, defined in Eqs. (4.17) and (4.18) in the text, for the wave function $\psi(x)$ of the vibrational level $v=196$ in the Cs_2 0_u^+ $(6s+6p_{1/2})$ potential. The wave function is seen to be band-limited: For $k>280$, its Fourier coefficients are negligible.

Whereas the physical level has a broad spectrum, displayed in Fig. 7, the unphysical level, analyzed in Fig. 8, has no low frequency component and a few high frequency components.

Trying to eliminate the "ghost" levels is a crucial issue for future applications: Although they are easily identified in the present single-channel time-independent treatment, they induce numerical errors in a time-dependent approach, when a wavepacket is written as a superposition of stationary states. Besides, in any multichannel problem involving coupling between bound and continuum levels, the "ghost" levels may induce spurious resonances and modify the dynamics.

We have not found a satisfactory mathematical explanation for the occurence of the "ghost" levels, as they are found to be influenced by several features of the chosen representation:
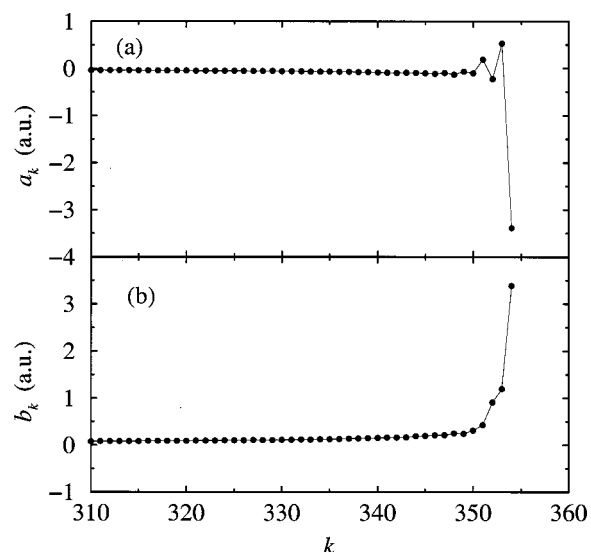
FIG. 8. The Fourier expansion coefficients (a) a_k and (b) b_k [see Eqs. (4.17) and (4.18) in text] for the wave function $\psi(x)$ of the spurious level $v'=197$ in the Cs_2 0_u^+ $(6s+6p_{1/2})$ potential. The wave function has very high momentum components and is not band-limited.
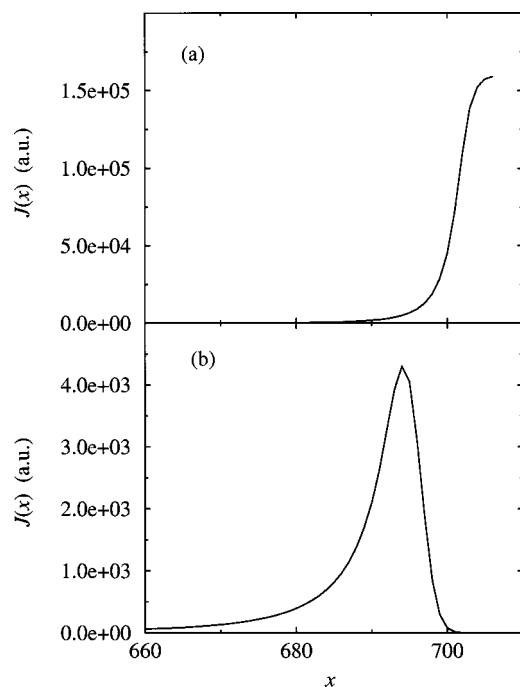
FIG. 9. Variation of the Jacobian $J(x)$ of the transformation $R \to x$ at the end of the grid. (a) The Jacobian is defined via the local de Broglie wavelength [see Eq. (2.8) in text]. (b) The Jacobian has been made periodic.

(i)   When we used a constant grid step, no spurious solutions at all were observed. However, the grid did not extend to very large distances, as this would have required a huge number of grid points;

(ii)   the number of "ghost" levels and their positions in the energy spectrum depends on the shape of the mapping function $J(x)$. Fewer "ghosts" are found when the Jacobian is calculated from a numerical enveloping potential, close to the physical one, than when the enveloping potential is defined by a C_n/R^n analytic function with rapid variation at short distance. This is why use of a constant, or at least slowly varying, enveloping potential at short distances is recommended;

(iii)   the accuracy in the determination of the Jacobian and its derivatives seems very important. We have calculated them by interpolating the function $R(x)$ between the grid points making use of a cubic spline procedure, i.e., interpolation polynomia of order 3. This was not sufficient to eliminate unphysical levels. Trigonometric interpolation can improve the accuracy, as discussed below;

(iv)   the "ghost" levels are also linked to the periodic boundary conditions of the basis functions, contrasting with the nonperiodic Jacobian function. We experimented with a periodic Jacobian satisfying

$$J(0) \approx J(L), \quad J'(0) \approx J'(L), \tag{4.19}$$

as suggested by Kokoouline.[8] We added a few extra points at the end of the grid $(x=L)$ and made the Jacobian decrease smoothly from $J(L)$ to its initial value $J(0)=0$, as illustrated in Fig. 9. In a calculation involving two coupled channels [Cs$_2$ 0_u^+ ($6s$ $+6p_{1/2,3/2}$)][11,13], this periodic condition did suppress

some "ghost" levels but was not sufficient to eliminate them all. Nevertheless, when combined with a trigonometric interpolation of $R(x)$ instead of the polynomial one, it proved to be successful. Unfortunately, the success was limited to this particular case, suggesting to explore another route;

(v)   in all cases, the number of "ghost" levels is significantly reduced when the kinetic-energy matrix is calculated from Eq. (2.15) instead of Eq. (2.17), avoiding numerical calculations of the derivatives of the Jacobian. In such a situation, changing from a nonperiodic to a periodic Jacobian in a mapped Fourier representation only shifts the positions of the "ghosts" in the spectrum, without eliminating them.

We have, therefore, chosen to change the basis set, in order to explore whether the presence of "ghost" levels is due to correlations between contiguous periods in the Fourier basis set. We have considered two representations where all basis functions $u_k(x)$ have nodes at the boundaries of the grid, with the hope that this condition would solve the problem of "ghost" levels.

V. FIXED-NODE REPRESENTATION

We have considered two basis sets of dimension $N-1$ such that all basis functions verify

$$u_k(0)=u_k(L)=0, \quad k=1,...,N-1. \tag{5.1}$$

A. Sine or particle-in-a-box representation

A particle in a box is described by a wave function which strictly vanishes at the boundaries of the grid, i.e., $\varphi(0)=\varphi(L)=0$, which corresponds to an infinite potential at the grid edges. Several authors[7,15,16] have already discussed the implementation of such a basis, and we present here our approach in combination with the mapping procedure.

We define the basis $s_k(x)$ of sine functions

$$s_k(x) = \sqrt{\frac{2}{N}} \sin\left(k \frac{\pi}{L} x \right) \quad (k=1,...,N-1), \tag{5.2}$$

together with the associated cosine basis

$$c_k(x) = \sqrt{\frac{2}{N}} \cos\left(k \frac{\pi}{L} x \right) \quad (k=0,...,N), \tag{5.3}$$

which both satisfy the orthonormal condition of Eq. (3.2), with the particular case $\langle c_0|c_0\rangle = 2\Delta x$. As in the previous section, the discrete sine transform and discrete cosine transform, represented by the unitary matrices S and C

$$S_{ik} = s_k(x_i) = \sqrt{\frac{2}{N}} \sin\left(k \frac{\pi}{N} i \right) \quad (i,k=1,...,N-1), \tag{5.4}$$

$$C_{ik} = \alpha_k c_k(x_i) \alpha_i = \sqrt{\frac{2}{N}} \alpha_k \cos\left(k \frac{\pi}{N} i \right) \alpha_i \quad (i,k=0,...,N),$$
$$\tag{5.5}$$

where $\alpha_k = 1/\sqrt{2}$ for $k=0$, N, and $\alpha_k = 1$ otherwise, provide the interpolation functions $\tilde{s}_j(x)$ and $\tilde{c}_j(x)$, which behave as approximate Dirac peaks (see Fig. 2)

$$\tilde{s}_j(x) = \sum_{k=1}^{N-1} s_k(x) S_{kj}^\dagger, \tag{5.6}$$

$$\tilde{c}_j(x) = \sum_{k=0}^{N} c_k(x) \alpha_k C_{kj}^\dagger \alpha_j. \tag{5.7}$$

The interpolation functions $\tilde{s}_j(x)$ are related to the basis functions $s_k(x)$ via the unitary transformation (5.4), while the transformation between $\tilde{c}_j(x)$ and $c_k(x)$ is only approximately unitary because of the coefficients α_k and α_j in Eq. (5.7).

The sums in Eqs. (5.6) and (5.7) can be evaluated analytically, giving the interpolation functions in an explicit form:

$$\tilde{s}_j(x) = \frac{1}{2N} \left\{ \frac{\sin\left[(2N-1)\frac{\pi}{2L}(x-x_j)\right]}{\sin\left[\frac{\pi}{2L}(x-x_j)\right]} \right.$$
$$\left. - \frac{\sin\left[(2N-1)\frac{\pi}{2L}(x+x_j)\right]}{\sin\left[\frac{\pi}{2L}(x+x_j)\right]} \right\} \quad (x \neq x_j), \tag{5.8}$$

$$\tilde{s}_j(x_j) = 1, \tag{5.9}$$

$$\tilde{c}_j(x) = \frac{\alpha_j^2}{2N} \left\{ \frac{\sin\left[(2N-1)\frac{\pi}{2L}(x-x_j)\right]}{\sin\left[\frac{\pi}{2L}(x-x_j)\right]} \right.$$
$$+ \cos\left[N\frac{\pi}{L}(x-x_j)\right] + \frac{\sin\left[(2N-1)\frac{\pi}{2L}(x+x_j)\right]}{\sin\left[\frac{\pi}{2L}(x+x_j)\right]}$$
$$\left. + \cos\left[N\frac{\pi}{L}(x+x_j)\right] \right\} \quad (x \neq x_j), \tag{5.10}$$

$$\tilde{c}_j(x_j) = 1. \tag{5.11}$$

The projection operators $\hat{P}^{\mathcal{S}}$ and $\hat{P}^{\mathcal{C}}$, defined as $\hat{P}^{\mathcal{S}}\bar{\psi}(x) = \Sigma_{i=1}^{N-1}\tilde{s}_i(x)\bar{\psi}(x_i)$ and $\hat{P}^{\mathcal{C}}\bar{\psi}(x) = \Sigma_{i=0}^{N}\tilde{c}_i(x)\bar{\psi}(x_i)$, are used to project the wave function on the sine functions and on the cosine functions, respectively.

The derivatives of the basis functions show the advantage of considering simultaneously the sine and cosine basis, as they transform into each other

$$\frac{d}{dx} s_k(x) = k\frac{\pi}{L} c_k(x), \tag{5.12}$$

$$\frac{d}{dx} c_k(x) = -k\frac{\pi}{L} s_k(x). \tag{5.13}$$

In contrast, the space of the periodic Fourier functions (4.1) is invariant under differentiation.

The derivatives of the interpolation functions can be obtained easily

$$\frac{d\tilde{s}_j}{dx}(x_i) = \frac{1}{\alpha_i}\frac{\pi}{L}D_{ij}, \tag{5.14}$$

$$\frac{d\tilde{c}_j}{dx}(x_i) = -\alpha_j\frac{\pi}{L}D_{ij}^\dagger, \tag{5.15}$$

where we have introduced a rectangular matrix D

$$D_{ij} = \sum_{k=1}^{N-1} C_{ik} k S_{kj}^\dagger, \tag{5.16}$$

where $i = 0,...,N$ and $j = 1,...,N-1$. The sum in Eq. (5.16) can be calculated analytically

$$D_{ij} = \begin{cases} -\alpha_i\frac{1}{2}(-1)^{i+j}\left[\cot\left(\pi\frac{i+j}{2N}\right) - \cot\left(\pi\frac{i-j}{2N}\right)\right] & (i \neq j) \\ -\alpha_i\frac{1}{2}\cot\left(\pi\frac{i}{N}\right) & (i = j). \end{cases} \tag{5.17}$$

The matrix of the potential energy is again diagonal while the kinetic-energy operator is derived as previously in Eq. (4.14), now using instead of $P^{\mathcal{F}}$ the projection operators $P^{\mathcal{S}}$ and $P^{\mathcal{C}}$

$$\bar{T}\bar{\psi}(x)|_{x=x_i}$$

$$\approx -\frac{1}{2\mu}J(x)^{-1/2}\frac{d}{dx}\hat{P}^C J(x)^{-1}\frac{d}{dx}\hat{P}^S J(x)^{-1/2}\bar{\psi}(x)\Big|_{x=x_i}$$

$$=\frac{1}{2\mu}\frac{\pi^2}{L^2}\sum_{k=0}^{N}J(x_i)^{-1/2}D_{ik}^{\dagger}J(x_k)^{-1}D_{kj}J(x_j)^{-1/2}\bar{\psi}(x_j)$$

$$=\bar{T}_{ij}\bar{\psi}(x_j), \tag{5.18}$$

where $\bar{T}$ is a symmetric matrix representation of the kinetic energy

$$\bar{T}_{ij}=\frac{1}{2\mu}\frac{\pi^2}{L^2}\sum_{k=0}^{N}J(x_i)^{-1/2}D_{ik}^{\dagger}J(x_k)^{-1}D_{kj}J(x_j)^{-1/2} \tag{5.19}$$

$$=\frac{1}{2\mu}\frac{\pi^2}{L^2}\sum_{k=0}^{N}\sum_{l,m=1}^{N-1}J(x_i)^{-1/2}S_{il}C_{lk}^{\dagger}J(x_k)^{-1}$$

$$\times C_{km}S_{mj}^{\dagger}J(x_j)^{-1/2}. \tag{5.20}$$

Since the matrix D is known analytically from Eqs. (5.16) and (5.17), the matrix $\bar{T}$ may be calculated directly from Eq. (5.19) by a numerical computation of the sum over k, which for a large basis can be time-consuming ($\propto N^3$). An alternative procedure[16] starts from Eq. (5.20), making use of fast sine and cosine transform algorithms, which yield exactly the same matrix $\bar{T}$, with a strongly reduced computational effort ($\propto N^2 \ln N$). The fast sine and fast cosine transform algorithm should also be used when one has to multiply some initial wave function repeatedly by the Hamiltonian matrix, for example in wave packet propagation schemes. The fast algorithm has been implemented for a time-dependent treatment of photoassociation of cold atoms,[29] and has proved very efficient. However, if one is only interested in solving the stationary Schrödinger equation, the slower procedure using Eq. (5.19) is useful: The corresponding numerical routine is implemented very easily, and there is no restriction on the number N of grid points. The fast routines only work if the number of grid points is a product of powers of a few small prime numbers, such as $2^5 3^2$.

B. Hardy representation

The Hardy functions, or cardinal sine functions, have also been used as a DVR basis by Colbert and Miller[4] and Groenenboom and Colbert[17]

$$\tilde{h}_j(x)=\text{sinc}\left[\frac{\pi}{\Delta x}(x-x_j)\right] \quad (j=1,...,N-1). \tag{5.21}$$

The Hardy functions verify $\tilde{h}_j(x_i)=\delta_{ij}$, so they can be used as interpolation functions. The Fourier transforms of the Hardy functions are orthogonal plane waves on the interval $[-p_x,p_x]$ in momentum space ($p_x=\pi/\Delta x$):

$$\tilde{h}_j(x)=\text{sinc}[p_x(x-x_j)]=\frac{1}{2p_x}\int_{-p_x}^{p_x}dp\,e^{-ipx_j}e^{ipx}. \tag{5.22}$$

The Hardy functions are functions with limited bandwidth: Their Fourier transforms are nonzero only on the interval $[-p_x,p_x]$ in momentum space. Their orthonormal properties result from those of their Fourier transforms:

$$\int_{-\infty}^{\infty}dx\,\tilde{h}_j^*(x)\tilde{h}_k(x)$$

$$=\int_{-\infty}^{\infty}dx\left(\frac{1}{2p_x}\int_{-p_x}^{p_x}dp\,e^{-ipx_j}e^{ipx}\right)^*$$

$$\times\left(\frac{1}{2p_x}\int_{-p_x}^{p_x}dp'\,e^{-ip'x_k}e^{ip'x}\right)$$

$$=\frac{1}{4p_x^2}\int_{-p_x}^{p_x}dp\,e^{ipx_j}\int_{-p_x}^{p_x}dp'\,e^{-ip'x_k}\int_{-\infty}^{\infty}dx\,e^{-ipx}e^{ip'x}$$

$$=\frac{\pi}{2p_x^2}\int_{-p_x}^{p_x}dp\,e^{ip(x_j-x_k)}=\frac{\pi}{p_x}\text{sinc}[p_x(x_j-x_k)]=\delta_{ik}\Delta x.$$

Their derivatives at the grid points are easily obtained

$$\frac{d\tilde{h}_j}{dx}(x_k)=\frac{d}{dx}\text{sinc}[P(x-x_j)]\Big|_{x=x_k}$$

$$=\begin{cases}\dfrac{1}{\Delta x}\dfrac{(-1)^{j-k}}{(j-k)} & (j\neq k)\\ 0 & (j=k).\end{cases} \tag{5.23}$$

The symmetric representation of the kinetic-energy operator is again obtained by using the associated projection operator $\hat{P}^{\mathcal{H}}$

$$\bar{T}\bar{\psi}(x)|_{x=x_i}$$

$$\approx -\frac{1}{2\mu}J(x)^{-1/2}\frac{d}{dx}\hat{P}^{\mathcal{H}}J(x)^{-1}\frac{d}{dx}\hat{P}^{\mathcal{H}}J(x)^{-1/2}\bar{\psi}(x)\Big|_{x=x_i}$$

$$=-\frac{1}{2\mu}\sum_{j,k=1}^{N-1}J(x_i)^{-1/2}\frac{d\tilde{h}_k}{dx}(x_i)J(x_k)^{-1}$$

$$\times\frac{d\tilde{h}_j}{dx}(x_k)J(x_j)^{-1/2}\bar{\psi}(x_j)=\bar{T}_{ij}\bar{\psi}(x_j). \tag{5.24}$$

C. Alternative representations

We also mention two other representations, not considered in the present work, which have proved useful in different applications. Schwartz interpolation functions and Lobatto shape functions are also characterized by the Kronecker property $u_i(x_j)=\delta_{ij}$. Dunseath et al.[30] have used Schwartz interpolation for problems involving the Coulomb potential, while Manolopoulos and Wyatt[31] have used Lobatto shape functions as radial basis functions in their work on the $H+H_2$ reaction.

VI. RESULTS

We have checked the performances of the different methods to compute vibrational levels of long-range alkali dimer molecules, relevant to experiments with cold molecules. In a first step, we used a Morse potential, in order to compare with analytical solutions, then we used realistic nu-

TABLE I. Comparison of the numerical accuracy for the levels of the Morse oscillator described in the text. A mapped grid of 276 points was used for each of the three interpolation schemes "sine," "Fourier," "Hardy." The kinetic energy was evaluated using expression (2.15). The analytical values E_v and the errors ΔE_v on the calculated values are in cm^{-1}. The error on the last level was reduced by using a wider grid, with 400 points, extending to 500 a$_0$.

Level	E_v^{ana}	ΔE_v sine	ΔE_v Fourier	ΔE_v Hardy
0	$-0.362\,785\times10^4$	$0.110\,50\times10^{-6}$	$0.110\,48\times10^{-6}$	$0.110\,48\times10^{-6}$
1	$-0.358\,532\times10^4$	$0.386\,70\times10^{-6}$	$0.386\,69\times10^{-6}$	$0.386\,69\times10^{-6}$
2	$-0.354\,304\times10^4$	$0.647\,46\times10^{-6}$	$0.647\,48\times10^{-6}$	$0.647\,47\times10^{-6}$
⋮	⋮	⋮	⋮	⋮
165	$-0.326\,122\times10^1$	$0.103\,56\times10^{-3}$	$0.103\,56\times10^{-3}$	$0.103\,56\times10^{-3}$
166	$-0.210\,770\times10^1$	$0.130\,45\times10^{-3}$	$0.130\,47\times10^{-3}$	$0.130\,46\times10^{-3}$
167	$-0.120\,493\times10^1$	$0.158\,19\times10^{-3}$	$0.158\,22\times10^{-3}$	$0.158\,21\times10^{-3}$
168	$-0.552\,941$	$0.175\,95\times10^{-3}$	$0.176\,54\times10^{-3}$	$0.176\,35\times10^{-3}$
169	$-0.151\,714$	$0.172\,80\times10^{-3}$	$0.173\,23\times10^{-3}$	$0.173\,04\times10^{-3}$
170	$-0.125\,383\times10^{-2}$	$0.165\,41\times10^{-3}$	$0.262\,67\times10^{-3}$	$0.132\,86\times10^{-3}$
Wider grid:				
170	$-0.125\,383\times10^{-2}$	$-0.111\,281\times10^{-4}$	$-0.111\,07\times10^{-4}$	$-0.110\,54\times10^{-4}$

merical potentials for the Cs$_2$ $X\,^1\Sigma_g^+$ $(6s+6s)$ ground state and for the Cs$_2$ 0_u^+ $(6s+6p_{1/2})$ excited state.

A. Accuracy check using a Morse potential

Considering the analytical model potential designed by Morse to reproduce the experimental vibrational energies of a diatomic molecule[32]

$$V(R)=V_0 e^{-2a(R-R_0)}-2V_0 e^{-a(R-R_0)}, \tag{6.1}$$

we have chosen the equilibrium distance $R_0=8.77$ a$_0$, the well depth $V_0=0.016\,627$ a.u., and the width parameter $a=0.372\,031\,199$ a.u. to make $V(R)$ as close as possible to the Cs$_2$ $X\,^1\Sigma_g^+$ $(6s+6s)$ ground-state potential. In fact, this similarity is restricted to the region of the well depth, since at large distances the Morse potential decays exponentially, whereas the real potential displays an $1/R^6$ asymptotic behavior. The advantage of the Morse potential is the analytical law linking the energies of the bound levels to the vibrational quantum number v

$$E_v=-\frac{a^2\hbar^2}{2\mu}(v_D-v)^2 \quad (v=0,1,...,v_{\max}\leqslant v_D), \tag{6.2}$$

$$v_D=\frac{\sqrt{2\mu V_0}}{a\hbar}-\frac{1}{2}, \tag{6.3}$$

where μ is the reduced mass of the nuclei. Choosing $\mu=121\,135.904\,213\,218\,88$ a.u. for the reduced mass of ^{133}Cs$_2$ we obtain $v_D=170.1$, which means that the highest bound level is $v_{\max}=170$. The vibrational energies E_v^{ana}, computed from the analytical formula (6.2), are then compared with results of numerical calculations using the various basis sets. Considering a grid with $N=277$ points, extending from $R=6.4$ a$_0$ to $R=80$ a$_0$, and defining an adaptive coordinate from Eq. (2.11), with $V_{\text{env}}(R)=V(R)$ for $R>R_0$, we have compared the convergence of the various calculations by varying the β parameter from 1 to 0.2. For the optimal choice $\beta=0.7$, we have performed calculations with two choices for the evaluation of the matrix elements of the kinetic-energy operator $\hat{T}$:

(i) When $\bar{T}$ is evaluated from expression (2.15), which uses only the Jacobian and not its derivatives, we give in Table I the three lowest and the six highest bound levels. The error $\Delta E_v=E_v-E_v^{\text{ana}}$ is always found positive, due to the fact that the method is "almost variational," as discussed in Ref. 28. The absolute error is very similar for the three methods, and remains small except for the very last levels. In contrast, no "ghost" level is found with the sine basis, while one is found for each of the two other ones. For the Fourier basis calculations, the "ghost" level is located between the levels $v=161$ and $v=162$, and for the Hardy basis, it is located between the levels $v=119$ and $v=120$. Finally, the error on the last level, for which the wave function extends far into the forbidden region, can be reduced to 10^{-5} by using a grid with 401 points extending from 6.4 to 500 a$_0$, for the value $\beta=0.6$.

(ii) When $\bar{T}$ is computed from expression (2.17), which explicitly contains the derivatives $J'(x)$ and $J''(x)$, we report in Table II the values of the bound level energies, choosing only the physical levels when "ghost" levels are found in the calculations. It is clear that a loss in accuracy of more than one digit results when the kinetic energy is evaluated according to Eq. (2.17) instead of Eq. (2.15). Moreover, some of the calculated eigenvalues are found *lower* than the true eigenvalues. These large errors should be attributed to numerical errors in the derivatives $J'(x)$ and $J''(x)$ of the Jacobian, making the additional kinetic term T_{loc} described in Eq. (2.18) inaccurate. The amplitude of the numerical noise is about 100 times larger than the errors of the lowest few calculated eigenvalues. The choice of the basis set (sine, Fourier, or Hardy) does not influence the magnitude of the error in the eigenvalue, except for the last level where a much larger grid is required. No "ghost" levels are found with the sine basis or the Hardy basis. In contrast, calculations with the Fourier basis provide two "ghost" levels, one

TABLE II. Same as Table I, but evaluating the kinetic energy from expression (2.17) containing the derivatives of the Jacobian.

Level	E_v	ΔE_v sine	ΔE_v Fourier	ΔE_v Hardy
0	$-0.362\,785\times10^4$	$-0.624\,74\times10^{-3}$	$-0.624\,74\times10^{-3}$	$-0.624\,74\times10^{-3}$
1	$-0.358\,532\times10^4$	$-0.623\,32\times10^{-3}$	$-0.623\,32\times10^{-3}$	$-0.623\,32\times10^{-3}$
⋮	⋮	⋮	⋮	⋮
168	$-0.552\,941$	$-0.426\,86\times10^{-2}$	$-0.426\,83\times10^{-2}$	$-0.426\,86\times10^{-2}$
169	$-0.151\,714$	$-0.249\,30\times10^{-2}$	$-0.249\,30\times10^{-2}$	$-0.249\,30\times10^{-2}$
170	$-0.125\,383\times10^{-2}$	$0.490\,37\times10^{-3}$	$0.688\,56\times10^{-3}$	$0.505\,78\times10^{-3}$

located between the levels $v=142$ and $v=143$, and one between the levels $v=169$ and $v=170$.

The qualitative conclusion of this check for a Morse potential is that the numerical accuracy is the same for all three interpolation methods, but the sine–cosine method seems preferable since it does not produce "ghost" levels. As we shall see below, this conclusion is still valid for potentials with $1/R^6$ or $1/R^3$ long-range behavior, and might be a general one.

For calculations involving a mapping procedure, expression (2.15) for the kinetic energy gives results with significantly better accuracy than expression (2.17), when the derivatives of the Jacobian are calculated numerically.

B. Calculations of vibrational levels for a potential with $1/R^6$ long-range behavior

We have used the three grid methods to compute vibrational levels for the ground state of the Cs_2 molecule, in a model where hyperfine structure effects are neglected in order to perform single channel calculations. The potential had been used previously for the interpretation of photoassociation experiments.[13] A grid extending from 6.1 to 400 a_0 with $N=323$ points is used. The adaptive coordinate is chosen from Eq. (2.11), with $\beta=0.6$, $E_{max}=D+1\times10^{-7}$ a.u., where D is the dissociation limit, and an enveloping potential identical to $V(R)$ for distances $R\geqslant8.8$ a_0, larger than the posi-

tion of the minimum, and constant below. The kinetic-energy operator is evaluated via Eq. (2.15). The accuracy of the calculations can be checked by verifying, for the upper levels, the validity of the asymptotic Le Roy–Bernstein law[33]

$$E_v=D-[H_6(v_D-v)]^3, \qquad (6.4)$$

linking the dissociation energy of a level, $D-E_v$, to its vibrational quantum number v. In Eq. (6.4), v_D is a noninteger parameter equal to the accumulated phase at threshold divided by π, while the parameter H_6 depends upon C_6 and the reduced mass μ, and should be $H_6=2.2785\times10^{-3}$ for $C_6=6600$ and the value of μ given above in Sec. VI A. The law is indeed verified for the last levels, as represented in Fig. 10. Fitting the energies of the levels $v=149$ to $v=154$, we find $H_6^{fit}=(2.321\pm0.003)\times10^{-3}$ and $v_D^{fit}=155.9\pm0.4$, so that the last level is either $v=155$ or $v=156$. The agreement with analytical results is satisfactory, but due to the presence of higher order terms of the multipole expansion in the asymptotic potential, the law is verified only approximately. The last computed level $v=155$ is found at $E=9.7\times10^{-9}$ a.u.$=2.1\times10^{-3}$ cm^{-1}, its wave function is drawn in Fig. 11. An accurate determination of such wave functions is important in multichannel calculations involving hyperfine structure in order to determine the scattering length, or to investigate Feshbach resonances. Again, no "ghost" level was found with the sine calculations while the Fourier and the Hardy calculations both yielded a "ghost" level, respectively, located between the physical levels $v=141-142$ and $v=132-133$.
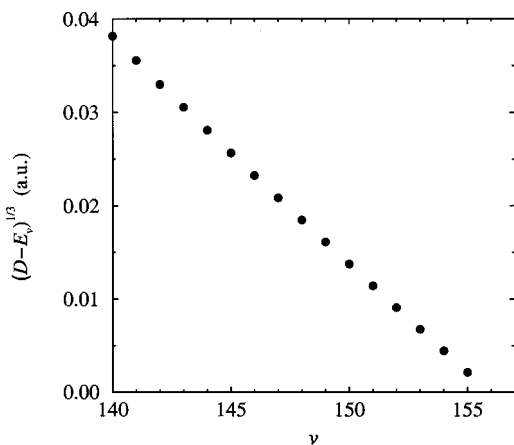
FIG. 10. Verification of the Le Roy–Bernstein law (see text) for the binding energies $(D-E_v)$ of the upper vibrational levels v of the $^{133}Cs_2$ $X\,^1\Sigma_g^+$ $(6s+6s)$ potential. One hundred fifty-six levels have been computed. The plot shows the quantities $(D-E_v)^{1/3}$ as a function of the vibrational index v: The linear variation is in perfect agreement with the Le Roy–Bernstein law for a potential with asymptotic $-C_6/R^6$ behavior.
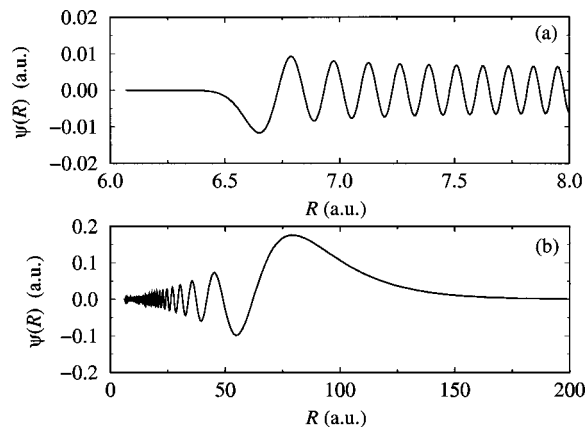
FIG. 11. The wave function $\psi(R)$ of the last computed vibrational level $v=155$ of the Cs_2 ground state. The calculated binding energy is $D-E_v=9.7\times10^{-9}$ a.u.$=2.1\times10^{-3}$ cm^{-1}, and the outer turning point is located about $R=94$ a_0. Note that such calculations were performed with a mapped sine–cosine grid method using only 322 grid points.
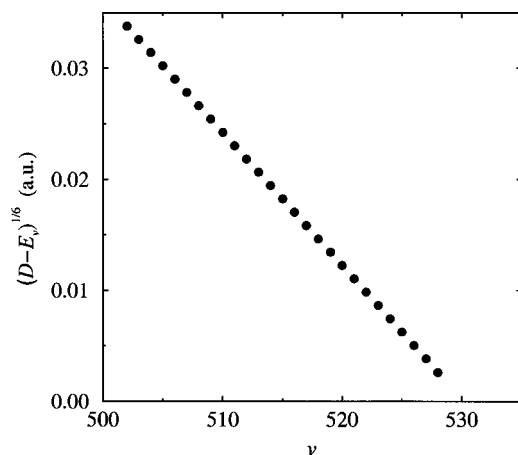
FIG. 12. Verification of the Le Roy–Bernstein law (see text) for the binding energies $(D-E_v)$ of the upper vibrational levels v of the $^{133}Cs_2$ 0_u^+ $(6s+6p_{1/2})$ potential. Levels up to $v=528$ could be computed (see Fig. 13), so that the missing levels are at most two. The plot shows the quantities $(D-E_v)^{1/6}$ as a function of the vibrational index v: The linear variation is in perfect agreement with the Le Roy–Bernstein's law for a potential with asymptotic $-C_3/R^3$ behavior.

FIG. 13. The wave function $\psi(R)$ of the vibrational level $v=528$ of $^{133}Cs_2$ in the 0_u^+ $(6s+6p_{1/2})$ state. The calculated binding energy is $D-E_v=9.4 \times 10^{-11}$ cm^{-1}, and the outer turning point is located about $R_{out}=2.7 \times 10^5$ a_0, that is 14 μm. This function has been computed with a mapped sine-cosine grid method using only $N=706$ points.

C. Calculations of vibrational levels for a potential with R^{-3} long-range behavior

We have next considered the Cs$_2$ $X\,^1\Sigma_u^+$ $(6s+6p_{1/2})$ potential, represented in Fig. 1. Calculations were performed with a grid of $N=707$ points, extending in the R coordinate from $R=5.3$ to $R=8\times10^5$. The adaptive coordinate was defined from Eq. (2.11), using the enveloping potential V_{env} represented in Fig. 1(a), and for the parameters the values $\beta=0.8$, $E_{max}=D+10^{-15}$ a.u., where D is the dissociation limit. Due to the C_3/R^3 long-range asymptotic behavior of the potential, the energies of vibrational levels close to the dissociation limit should verify the analytical Le Roy–Bernstein formula[33]

$$E_v = D - [H_3(v_D - v)]^6. \qquad (6.5)$$

The parameters H_3 and v_D can be fitted to the numerical results, making it possible to estimate the total number of bound levels. Such a fit is illustrated in Fig. 12, for calculations performed with the sine basis. The Le Roy–Bernstein law is verified up to the highest computed levels, yielding $v_D=530.2\pm0.1$. Thus the last bound level is $v=530$, but the highest level we have been able to compute is $v=528$, with a binding energy as small as $D-E_{v=528}=4.3\times10^{-16}$ a.u. $=9.4\times10^{-11}$ cm^{-1}. In such calculations, we no longer find "ghost" levels, in contrast with the results obtained with plane wave expansion and already described in Sec. IV B. The accuracy of the calculations can be estimated by comparing the value $H_3^{fit}=1.1974\times10^{-3}\pm2\times10^{-7}$ a.u. fitted on the numerical results for levels from $v=509$ to $v=526$, to the analytical value $H_3=1.1986\times10^{-3}$ a.u. corresponding to $C_3=13.467$. This yields a relative error of 10^{-3}, which should be considered as an upper bound, since the asymptotic C_3/R^3 behavior is reached only at very large distances. We also note that the upper levels are very close, the spacing between the levels $v=526$ and $v=527$ being only 1.3×10^{-14} a.u., that is only 2.8×10^{-9} cm^{-1}, yielding
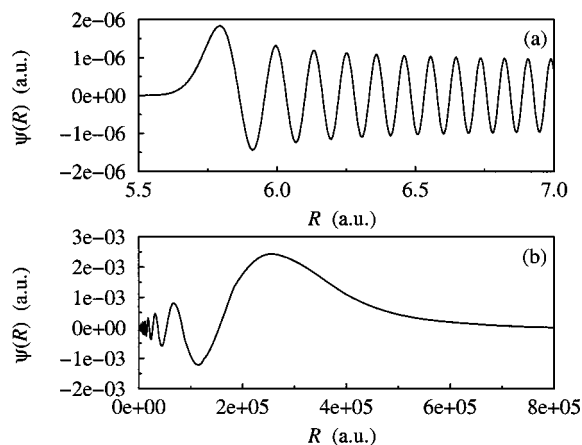
another estimation of the absolute accuracy of the calculations. The wave function for the last computed level, $v=528$, is represented in Fig. 13; the vibrational motion extends to several 100 000 a.u., i.e., a few tens of microns. It is remarkable that due to the mapping procedure, this wave function with 528 nodes is computed with a grid of only 706 points.

VII. CONCLUSION

In this paper we have discussed various ways of implementing mapped grid methods for cold molecules, when levels close to the dissociation limit have to be investigated, in calculations requiring high accuracy. In the framework of the mapping procedure previously implemented for problems where the dynamics at long-range markedly differs from the short-range dynamics,[8,9,15,16,22] we define an adaptive coordinate x scaled on the local de Broglie wavelength, and we introduce a discrete variable representation in x, considering Fourier, sine–cosine and Hardy basis sets. In the second case, we use both a sine basis set and an auxiliary cosine basis set, very convenient to evaluate first-order derivatives.

In each case, we have recalled the interpolation functions, and their derivatives. For a grid of N points, the energies and wave functions of the bound levels in a p-channel-problem are then obtained by diagonalization of a $pN\times pN$ matrix computed through analytical formulas. The paper explicitly gives those formulas in the three cases, unifying results that were separately presented in many earlier papers.[3–7,15,16] For clarity sake, although the main interest of the method is multichannel calculations, we have only given examples for single channel problems. Three main conclusions can be drawn:

(i)   When the adaptive coordinate is defined through a numerical potential, and even for analytical potentials, numerical errors arise in the evaluation of the derivatives of the Jacobian $J(x)$ for the coordinate transformation. It is preferable to write the kinetic-energy operator with products of the d/dx operator, which can

easily be evaluated via the interpolation functions and their derivatives. The three methods then provide results with equivalent accuracy;

(ii)　the presence of "ghost" levels can create problems in multichannel calculations or in time-dependent calculations. In the examples considered, it seems that the sine–cosine method is efficient to suppress them. The fast sine and cosine transform algorithms make the computing times comparable with the Fourier grid method;

(iii)　since it is very easy to switch from one method to another, it is recommended to use in parallel at least two of the three methods, to cross-check the results.

We have shown that accurate results can be obtained for vibrational levels very close to the dissociation limit. More details on the interpolation procedure will be given in a forthcoming paper.

In contrast to Wei's work,[18] we have not examined the accuracy of Gaussian quadratures, because our Hamiltonian matrices are derived using the collocation method, which does not require the evaluation of integrals. However, it is well-known that an orthogonal collocation scheme leads to Hamiltonian matrix elements which may be regarded as approximations to the integrals of the spectral (variational) method.[28] Therefore, it should be interesting to compare the Hamiltonian matrices of the collocation method with those of the spectral method, for all three basis sets.

Future work should address the problem of loosely bound triatomic molecules, or collisions between cold atoms and diatoms. Applications for triatomic molecules may require multi-dimensional mapping, involving many more vibrational levels: A combination of the present method with filtering methods should then be considered.

ACKNOWLEDGMENTS

[1] R. Kosloff, J. Phys. Chem. **92**, 2087 (1988).
[2] R. Kosloff, in *Dynamics of Molecules and Chemical Reactions*, edited by R. H. Wyatt and J. Z. H. Zhang (Dekker, New York, 1996), p. 185.
[3] C. C. Marston and G. Balint-Kurti, J. Chem. Phys. **91**, 3571 (1989).
[4] D. T. Colbert and W. H. Miller, J. Chem. Phys. **96**, 1982 (1992).
[5] M. Monnerville and J. M. Robbe, J. Chem. Phys. **101–112**, 7580 (1994).
[6] O. Dulieu and P. S. Julienne, J. Chem. Phys. **103**, 60 (1995).
[7] J. T. Muckerman, Chem. Phys. Lett. **173**, 200 (1990).
[8] V. Kokoouline, O. Dulieu, R. Kosloff, and F. Masnou-Seeuws, J. Chem. Phys. **110**, 9865 (1999).
[9] E. Fattal, R. Baer, and R. Kosloff, Phys. Rev. E **53**, 1217 (1996).
[10] E. Tiesinga, C. J. Williams, and P. S. Julienne, Phys. Rev. A **57**, 4257 (1998).
[11] V. Kokoouline, O. Dulieu, and F. Masnou-Seeuws, Phys. Rev. A **62**, 022504 (2000).
[12] V. Kokoouline, O. Dulieu, R. Kosloff, and F. Masnou-Seeuws, Phys. Rev. A **62**, 032716 (2000).
[13] C. M. Dion, C. Drag, O. Dulieu, B. Laburthe Tolra, F. Masnou-Seeuws, and P. Pillet, Phys. Rev. Lett. **86**, 2253 (2001).
[14] Ph. Pellegrini, O. Dulieu, and F. Masnou-Seeuws, Eur. Phys. J. D **20**, 77 (2002).
[15] D. Lemoine, Chem. Phys. Lett. **210**, 492 (2000).
[16] A. G. Borisov, J. Chem. Phys. **114**(18), 7770 (2001).
[17] G. C. Groenenboom and D. T. Colbert, J. Chem. Phys. **99**, 9681 (1993).
[18] H. Wei, J. Chem. Phys. **106**, 6885 (1997).
[19] T.-S. Ho and H. Rabitz, J. Chem. Phys. **104**, 2584 (1995).
[20] N. Spies, Ph.d thesis, Fachbereich Chemie, Universität Kaiserslautern (1989).
[21] M. Marinescu and A. Dalgarno, Phys. Rev. A **52**, 311 (1995).
[22] M. Nest and H.-D. Meyer, Chem. Phys. Lett. **352**, 486 (2002).
[23] M. Nest and P. Saalfrank, J. Chem. Phys. **113**, 8753 (2000).
[24] D. Gottlieb and S. A. Orszag, *Numerical Analysis of Spectral Methods: Theory and Applications*, Vol. 26 (Society for Industrial and Applied Mathematics, Philadelphia, Pa., 1977).
[25] D. Tannor, *Introduction to Quantum Mechanics: A Time Dependent Perspective* (University Science Books, Sausalito, 2003).
[26] J. V. Lill, G. A. Parker, and J. C. Light, Chem. Phys. Lett. **89**, 483 (1982).
[27] J. C. Light, in *Time Dependent Quantum Molecular Dynamics, NATO ASI Series*, edited by J. Broeckove and L. Lathouwers (Plenum, New York, 1992), p. 185.
[28] R. Meyer, J. Chem. Phys. **52**, 2053 (1970).
[29] E. Luc-Koenig, private communication (2002).
[30] K. M. Dunseath, J.-M. Launay, M. Terao-Dunseath, and L. Mouret, J. Phys. B **35**, 3539 (2002).
[31] D. E. Manolopoulos and R. E. Wyatt, Chem. Phys. Lett. **152**, 23 (1988).
[32] P. M. Morse, Phys. Rev. **34**, 57 (1929).
[33] R. J. Le Roy and R. B. Bernstein, J. Chem. Phys. **52**, 3869 (1970).

Chapter 3

Quantum dynamics of a triatomic system

We introduce the general notion of Jacobi vectors for many-body systems. The Jacobi coordinates for three particles are related to equivalent coordinates: bond, Euclidean, and hyperspherical coordinates.

An overview on existing computational techniques is given at the end of this Chapter.

3.1 Coordinates and Hamiltonian of a many-body system

A set of $f = 3N$ coordinates is needed to specify the positions of N particles. If the interactions between the particles are weak, it is natural to assign a three-component Cartesian position vector to each particle.

If the interactions are strong, however, it is more convenient to introduce the centre of mass, three Euler angles, and $3N - 6$ internal or vibrational coordinates describing the relative positions of the particles. The Euler angles indicate the orientation of the system with respect to the laboratory frame: they are defined as the angles that rotate a *body-fixed* Cartesian coordinate system, for example the principal axis of inertia, into a non-rotating *space-fixed* coordinate system.

The Euler angles remain useful in the intermediate case where the particles interact strongly but do not form a rigid body; in this case Coriolis coupling effects need to be taken into account.

It is in general impossible to distinguish between rotations and deformations: a closed sequence of changes in shape can in fact produce a net rotation of the system. At the end of the sequence, the system has reassumed its initial shape but is rotated. This is known as the "falling cat" phenomenon: a falling cat, after being dropped with its feet pointing upward, can turn in the

air and land on its feet [172]! The cat achieves the net rotation of 180° solely through changes of its shape, since its total orbital angular momentum must remain zero.

The kinetic energy operator of a many-body system can be written as [172])

$$\hat{T} \;=\; \hat{T}_{\mathrm{CM}} + \hat{T}_{\mathrm{rot}} + \hat{T}_{\mathrm{vib}} + \hat{T}_{\mathrm{cor}} \tag{3.1}$$

where $\hat{T}_{\mathrm{CM}}$, $\hat{T}_{\mathrm{rot}}$, $\hat{T}_{\mathrm{cor}}$ and $\hat{T}_{\mathrm{vib}}$ are the kinetic energy operators associated respectively with translations of the system as a whole (the centre-of-mass motion), with rotations, with vibrations, and with the Coriolis interaction. The operators $\hat{T}_{\mathrm{CM}}$, $\hat{T}_{\mathrm{rot}}$, and $\hat{T}_{\mathrm{vib}}$ can be expressed as differential operators in the coordinates of the centre-of-mass, the Euler angles, and the vibrational coordinates, respectively, whereas $\hat{T}_{\mathrm{cor}}$ is an operator in the vibrational *and* in the rotational coordinates. The problem of distinguishing between rotations and vibrations is discussed in a review article by R. G. Littlejohn and M. Reinsch [172] (see also Ref. [281, 190]).

3.1.1 Jacobi coordinates

In a Cartesian coordinate system, the spatial positions of N particles can be described by N position vectors $\mathbf{s}_i$ $(i = 1, ..., N)$ joining the centre of mass of each particle to the origin O. An equivalent set of coordinates consists of N space-fixed Jacobi vectors $\mathbf{r}_i$ defined as follows. Vector $\mathbf{r}_1$ runs from the centre of mass to the origin, and the vectors $\mathbf{r}_2, ..., \mathbf{r}_N$ are obtained recursively. In the first step, the system is divided into two subsystems, and the vector joining their centres of mass is called $\mathbf{r}_2$. Each of two subsystems may in turn be divided (unless it consists of only one particle) and its two fragments can be linked by a Jacobi vector. The process is repeated until each particle is reached by a Jacobi vector. This is illustrated in Fig. 3.1 for the case of $N = 4$ particles.

The Jacobi vectors $\mathbf{r}_k$ are related to the position vectors $\mathbf{s}_i$ by a matrix U such that

$$\mathbf{r}_i \;=\; \sum_{k=1}^{N} U_{ik}\mathbf{s}_k \;. \tag{3.2}$$

U is orthogonal in the following sense:

$$U_{ik}^{T}\mu_k U_{kj} \;=\; m_i\delta_{ij} \;. \tag{3.3}$$

Here m_k is the mass of the kth particle, and μ_i is the reduced mass for the two fragments joined by the vector $\mathbf{r}_i$. The total mass of the system, μ_1, may formally be regarded as a reduced mass by assuming that the origin O has an infinite mass. Because of the orthogonality relation (3.3), various physical quantities such as the total kinetic energy, the total angular momentum, and
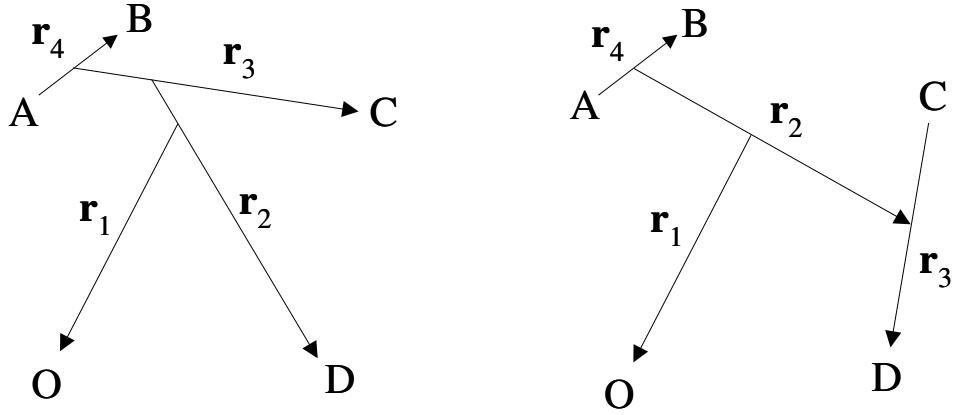
Figure 3.1: Two different sets of Jacobi vectors for a system of four particles A, B, C and D. In both cases, the vector $\mathbf{r}_1$ runs from the centre of mass of the complex $ABCD$ to the origin O.

the tensor of inertia are easily expressed in Jacobi coordinates. The components I_{ij} $(i,j = 1,2,3)$ of the inertia tensor $\mathbf{I}$ with respect to orthonormalized basis vectors $(\mathbf{e}_1, \mathbf{e}_2, \mathbf{e}_3)$ are given by [1]

$$I_{ij} = \sum_{k=1}^{N} \mu_k (\mathbf{e}_i \times \mathbf{r}_k) \cdot (\mathbf{e}_j \times \mathbf{r}_k) \ , \tag{3.4}$$

and the kinetic energy and angular momentum operators are:

$$\hat{T} = -\sum_{k=1}^{N} \frac{\hbar^2}{2\mu_k} \Delta_k \ , \qquad \hat{\mathbf{J}} = -\mathrm{i}\hbar \sum_{k=1}^{N} \mathbf{r}_k \times \nabla_k \ , \tag{3.5}$$

where Δ_i and ∇_i denote the Laplacian and the gradient operators for the variable $\mathbf{r}_i$. Analagous expressions hold for the corresponding classical quantities.

Kinematic rotations

For a system of more than two particles, there are several equivalent sets of Jacobi vectors (see again Fig. 3.1). Whenever it is necessary to distinguish between different sets, we shall label them using Greek indices (α, β, γ, ...)

---

[1]Eq. (3.4) can be rewritten using the vector identity

$$(\mathbf{a} \times \mathbf{b}) \cdot (\mathbf{c} \times \mathbf{d}) = (\mathbf{a} \cdot \mathbf{c})(\mathbf{b} \cdot \mathbf{d}) - (\mathbf{a} \cdot \mathbf{d})(\mathbf{b} \cdot \mathbf{c})$$

.

The transformation between two sets of Jacobi vectors is called a *kinematic rotation*:

$$\mathbf{r}_j^{(\beta)} = \sum_{i=1}^{N} K_{ij}^{(\beta\alpha)} \mathbf{r}_i^{(\alpha)} \;. \tag{3.6}$$

The non-orthogonal matrix $K^{(\beta\alpha)}$ is given by

$$K_{ij}^{(\beta\alpha)} = \sum_{k=N}^{N} U_{ik}^{(\beta)} \frac{1}{m_k} U_{kj}^{(\alpha)T} \;. \tag{3.7}$$

The matrices $U^{(\alpha)}$ and $U^{(\beta)}$, relating the Jacobi vectors $\mathbf{r}_i^{(\alpha)}$ and $\mathbf{r}_i^{(\beta)}$ to the position vectors $\mathbf{s}_i$, are defined as in Eq. (3.2).

Mass-scaled Jacobi vectors

The formulas (3.4) and (3.5) can be cumbersome, because they involve different reduced masses, $\mu_1, ..., \mu_N$. It can be more convenient to use *mass-scaled* Jacobi coordinates $\bar{\mathbf{r}}_i$ so that a single reduced mass μ appears in the calculations [207]. The scaled vector $\bar{\mathbf{r}}_i$ and the unscaled vector $\mathbf{r}_i$ are related according to:

$$\bar{\mathbf{r}}_i \sqrt{\mu} = \mathbf{r}_i \sqrt{\mu_i} \;. \tag{3.8}$$

The many-body reduced mass μ can in principal be chosen arbitrarily. A specific choice will be made for the case of three-body systems [see Eq. (3.21)]. The tensor of inertia becomes:

$$I_{ij} = \mu \sum_{k=1}^{N} (\mathbf{e}_i \times \bar{\mathbf{r}}_k) \cdot (\mathbf{e}_j \times \bar{\mathbf{r}}_k) \;. \tag{3.9}$$

The kinetic energy and angular momentum operators become

$$\hat{T} = -\frac{\hbar^2}{2\mu} \sum_{k=1}^{N} \bar{\Delta}_k \;, \tag{3.10}$$

$$\hat{\mathbf{J}} = -\mathrm{i}\hbar \sum_{k=1}^{N} \bar{\mathbf{r}}_k \times \bar{\nabla}_k \;, \tag{3.11}$$

where $\bar{\Delta}_k$ and $\bar{\nabla}_k$ are the Laplacian and gradient operators for the mass-scaled Jacobi vector $\bar{\mathbf{r}}_k$. The kinematic rotation between two sets of mass-scaled Jacobi vectors can now be written as

$$\bar{\mathbf{r}}_j^{(\beta)} = \sum_{i=1}^{N} \bar{K}_{ij}^{(\beta\alpha)} \bar{\mathbf{r}}_i^{(\alpha)} \;, \tag{3.12}$$

with the orthogonal matrix $\bar{K}^{(\beta\alpha)}$ given by:

$$\bar{K}_{ij}^{(\beta\alpha)} = \sqrt{\mu^{(\beta)}}) U_{ik}^{(\beta)} \frac{1}{m_k} U_{kj}^{(\alpha)T} \frac{1}{\sqrt{\mu^{(\alpha)}}} \;. \tag{3.13}$$

3.1.2 Hyperspherical coordinates

The *hyperradius* of a many-body system is defined as

$$\rho = \sqrt{\bar{r}_1^2 + \bar{r}_2^2 + \ldots + \bar{r}_N^2} \ , \tag{3.14}$$

where $\bar{r}_i$ is the length of the ith mass-scaled Jacobi vector $\mathbf{r}_i$. Its value is the same for all sets of Jacobi vectors, and it measures the overall size of the system (in the case where the centre-of-mass vector $\bar{r}_1$ is zero). Hyperspherical coordinates consist of the hyperradius ρ and $3N - 1$ dimensionless angles. They have been widely used in the description of three-body systems ($N = 3$, see Sec. 3.2). More recently, there have been attempts to use them for studies of Bose-Einstein condensates ($N > 3$) (see [34] and [249] and references therein).

3.1.3 Symmetries

The Hamiltonian $\hat{H}$ of a system of N particles in a field-free space commutes with the following symmetry operations:

- Translations.

- Rotations about an arbitrary axis.

- Inversion $\hat{I}$ of all the particles' coordinates.

- Permutations of identical particles.

The translational invariance implies that the velocity of the centre-of-mass is a constant. Therefore the centre-of-mass frame is used for computations, and the motion of the centre of mass does not need to be considered. Taking into account the other symmetries (rotations, inversion, permutations), one may seek the eigenfunctions of the Hamiltonian $\hat{H}$ in the form of partial waves $\varphi^{JM\epsilon_I\sigma}(\mathbf{r}_1, ..., \mathbf{r}_N)$ characterized by quantum numbers J, M, ϵ_I and σ defined as follows. The quantum numbers J and M indicate the eigenvalues of $\hat{\mathbf{J}}^2$ and $\hat{J}_z$, where $\hat{\mathbf{J}} = -i\hbar \sum_{k=1}^{N} \mathbf{r}_k \times \nabla_k$ is the total orbital angular momentum operator and $\hat{J}_z$ is its projection on the space-fixed z-axis:

$$\hat{\mathbf{J}}^2 \varphi^{JM\epsilon_I\sigma} = \hbar^2 J(J+1) \, , \varphi^{JM\epsilon_I\sigma} \tag{3.15}$$

$$\hat{J}_z \varphi^{JM\epsilon_I\sigma} = \hbar M \varphi^{JM\epsilon_I\sigma} \, . \tag{3.16}$$

The quantum number ϵ_I is the eigenvalue associated with the inversion operator $\hat{I}$,

$$\hat{I}\varphi^{JM\epsilon_I\sigma} = \epsilon_I \varphi^{JM\epsilon_I\sigma} \, , \tag{3.17}$$

and the index σ labels the irreducible representations of the permutation group of N particles.

For the case of three-body systems ($N = 3$), the permutational symmetry is known to have important consequences on the dynamics, see, for example, Ref. [208].

3.2 Three-body systems

The configuration space of three particles can usually be divided into the following regions:

- Potential wells where the three particles lie close together. At low energies, normal coordinates may be well-adapted in order to describe the three-body bound states. At higher energies, hyperspherical coordinates might be easier to handle.

- Three regions where two particles are bound closely together and the third particle is far away. These regions correspond to the three asymptotic atom-diatom arrangements, conveniently described in Jacobi coordinates.

- A region where the three particles are all at great distances from each other. This region lies energetically above the threshold for break-up into three bodies and is important, for example, in all studies concerning the recombination of three atoms to form a diatomic molecule and an atom (three-body recombination) or its inverse process, the fragmentation of a diatomic molecule due to a collision with an atom (collision-induced dissociation)

Many different coordinate systems have been developed over the years, but they all serve the same purpose: indicate the positions of the three particles A, B and C in space.

3.2.1 Jacobi coordinates

The geometry in which the distance between particle C and the centre of mass of AB is large compared to the distance between A and B is called the γ-arrangement. In this geometry, the system ABC is described most naturally using the Jacobi vectors $\mathbf{r}_\gamma = \overrightarrow{AB}$ and $\mathbf{R}_\gamma = \overrightarrow{(AB)C}$. The first vector, $\mathbf{r}_\gamma$, joins B to A and the second vector, $\mathbf{R}_\gamma$, joins C to the centre of mass of the fragment AB.

The other two asymptotic geometries, in which either A or B is situated far from the remaining two other particles, are respectively called the α- and the β-arrangements.
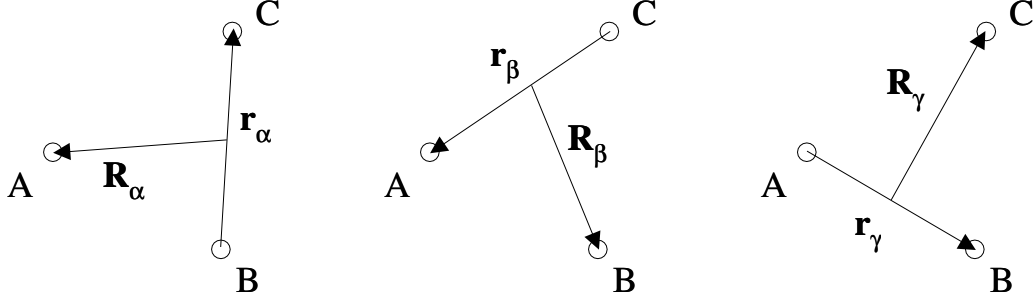
Figure 3.2: Jacobi vectors of the α-, β-, and γ-arrangements.

The three sets of Jacobi vectors, $(\mathbf{r}_\alpha, \mathbf{R}_\alpha)$, $(\mathbf{r}_\beta, \mathbf{R}_\beta)$, and $(\mathbf{r}_\gamma, \mathbf{R}_\gamma)$, are sketched in Fig. 3.2.

If the choice of arrangement is irrelevant and if there is no risk of confusion, we may sometimes omit the arrangement index in the formulas, and write, for example, $\mathbf{r}$ and $\mathbf{R}$ instead of $\mathbf{r}_\gamma$ and $\mathbf{R}_\gamma$.

Let now $(\mathbf{s}_A, \mathbf{s}_B, \mathbf{s}_C)$ be the positions vectors, and $(\mathbf{S}, \mathbf{R}, \mathbf{r})$ the centre-of-mass and Jacobi vectors. The total mass of the system is denoted M:

$$M = m_A + m_B + m_C \qquad (3.18)$$

where m_A, m_B and m_C are the masses of A, B, and C, respectively. The transformation (3.2) between position and Jacobi vectors now takes the form:

$$\begin{pmatrix} \mathbf{S} \\ \mathbf{R} \\ \mathbf{r} \end{pmatrix} = U \begin{pmatrix} \mathbf{s}_A \\ \mathbf{s}_B \\ \mathbf{s}_C \end{pmatrix}, \qquad U = \begin{pmatrix} \frac{m_A}{M} & \frac{m_B}{M} & \frac{m_C}{M} \\ 1 & -\frac{m_B}{m_B+m_C} & -\frac{m_C}{m_B+m_C} \\ 0 & -1 & 1 \end{pmatrix} \qquad (3.19)$$

The inverse matrix U^{-1} is given by:

$$U^{-1} = \begin{pmatrix} 1 & \frac{m_B+m_c}{M} & 0 \\ 1 & -\frac{m_a}{M} & -\frac{m_c}{m_B+m_c} \\ 1 & -\frac{m_a}{M} & \frac{m_B}{m_B+m_c} \end{pmatrix} . \qquad (3.20)$$

The mass-scaled vectors are denoted $\bar{\mathbf{r}}_\lambda$ and $\bar{\mathbf{R}}_\lambda$ ($\lambda = \alpha, \beta, \gamma$). The three-body reduced mass μ introduced in Eq. (3.8) can be chosen such that products of the Cartesian components of $\mathbf{r}_\lambda$ and $\mathbf{R}_\lambda$, like $R_{\lambda x} r_{\lambda y}$, are not affected by the scaling:

$$\mu = \sqrt{\mu_{A-BC}\,\mu_{BC}} = \sqrt{\frac{m_A\, m_B\, m_C}{m_A + m_B + m_C}} . \qquad (3.21)$$

59

The above definition implies $R_{\lambda x} r_{\lambda y} = \bar{R}_{\lambda x} \bar{r}_{\lambda y}$. As a consequence, the parallelogram spanned by the scaled vectors $\bar{\mathbf{r}}_\lambda$ and $\bar{\mathbf{R}}_\lambda$ has the same area as the one spanned by the unscaled vectors.

Note that the three-body reduced mass (3.21) is the same for all Jacobi arrangements.

The mass-scaled vectors of the α-arrangement are given by

$$\bar{\mathbf{R}}_\alpha = \sqrt{\frac{\mu_{A-BC}}{\mu}}\, \mathbf{R}_\alpha \tag{3.22}$$

$$\bar{\mathbf{r}}_\alpha = \sqrt{\frac{\mu_{BC}}{\mu}}\, \mathbf{r}_\alpha \,. \tag{3.23}$$

The kinematic rotation between the α- and the β-sets can be written as

$$\begin{pmatrix} \bar{\mathbf{R}}_\beta \\ \bar{\mathbf{r}}_\beta \end{pmatrix} = \begin{pmatrix} \cos \Phi_{\alpha\beta} & \sin \Phi_{\alpha\beta} \\ -\sin \Phi_{\alpha\beta} & \cos \Phi_{\alpha\beta} \end{pmatrix} \begin{pmatrix} \bar{\mathbf{R}}_\alpha \\ \bar{\mathbf{r}}_\alpha \end{pmatrix} \tag{3.24}$$

with an angle $\Phi_{\alpha\beta}$ given by

$$\tan \Phi_{\alpha\beta} = \frac{m_C}{\mu} \,, \qquad \Phi_{\alpha\beta} \in [\pi, 3\pi/2] \,. \tag{3.25}$$

The inverse rotation uses the angle $\Phi_{\beta\alpha} = -\Phi_{\alpha\beta}$. By considering the closed sequence of kinematic rotations $\alpha \to \beta \to \gamma \to \alpha$ and knowing that each of the angles $\Phi_{\alpha\beta}$, $\Phi_{\beta\gamma}$ and $\Phi_{\gamma\alpha}$ must lie between 0 and $3\pi/2$, one concludes that

$$\Phi_{\alpha\beta} + \Phi_{\beta\gamma} + \Phi_{\gamma\alpha} = 4\pi \,. \tag{3.26}$$

Case of three equal masses

If the three masses are equal, the lengths of the scaled and the unscaled Jacobi vectors are related as follows:

$$\frac{\bar{r}}{r} = \left(\frac{3}{4}\right)^{1/4} \approx 0.931 \,,$$

$$\frac{\bar{R}}{R} = \left(\frac{4}{3}\right)^{1/4} \approx 1.075 \,. \tag{3.27}$$

The kinematic rotation angles are:

$$\Phi_{\alpha\beta} = \Phi_{\beta\gamma} = \Phi_{\gamma\alpha} = \frac{4\pi}{3} \,. \tag{3.28}$$

Internal Jacobi coordinates

The shape and the size of the ABC triangle depend only on the lengths R and r of the two Jacobi vectors and on the angle η ($0 \le \eta \le \pi$) between them. These quantities are called *internal* Jacobi coordinates [see also Eq. (3.59)]:

$$R = |\mathbf{R}| \,, \qquad r = |\mathbf{r}| \,, \qquad \eta = \arccos\left(\frac{\mathbf{R.r}}{R\,r}\right) \,. \qquad (3.29)$$

The potential interaction energy of the three-body system depends only on the internal Jacobi coordinates and can be written $V(R, r, \eta)$.

The vibrational kinetic energy operator in internal Jacobi coordinates has the form: [2]

$$\hat{T}_{\mathrm{vib}} = -\frac{\hbar^2}{2\mu}\left[\frac{1}{R}\frac{\partial^2}{\partial R^2}R + \frac{1}{r}\frac{\partial^2}{\partial r^2}r + \left(\frac{1}{R^2} + \frac{1}{r^2}\right)\frac{1}{\sin\eta}\frac{\partial}{\partial\eta}\sin\eta\frac{\partial}{\partial\eta}\right] \,. \qquad (3.30)$$

The volume element is

$$d(R, r, \eta) = dR\,dr\,\sin\eta\,d\eta \,. \qquad (3.31)$$

We note that the singularities in $\eta = 0$ and $\eta = \pi$ can be avoided by replacing η with the variable $c = \cos\eta$ [47].

We have not made use of Eq. (3.30), but it is interesting to compare it to the kinetic energy operator in Smith-Whitten coordinates, Eq. (3.30)

Schrödinger equation

Whatever the choice of Jacobi arrangement, the kinetic energy operator (including the rotational and Coriolis coupling terms) has the form of a Laplacian in six dimensions. Eq. (3.10) takes the form

$$\hat{T} = -\frac{\hbar^2}{2\mu}[\Delta_{\bar{\mathbf{r}}} + \Delta_{\bar{\mathbf{R}}}] \,, \qquad (3.32)$$

or, more explicitly,

$$\hat{T} = -\frac{\hbar^2}{2\mu}\left[\frac{\partial^2}{\partial\bar{r}_x^2} + \frac{\partial^2}{\partial\bar{r}_y^2} + \frac{\partial^2}{\partial\bar{r}_z^2} + \frac{\partial^2}{\partial\bar{R}_x^2} + \frac{\partial^2}{\partial\bar{R}_y^2} + \frac{\partial^2}{\partial\bar{R}_z^2}\right] \,. \qquad (3.33)$$

The Hamiltonian operator $\hat{H}$ of the three-body system is obtained from (3.32) by adding the potential energy term:

$$\hat{H} = -\frac{\hbar^2}{2\mu}[\Delta_{\bar{\mathbf{r}}} + \Delta_{\bar{\mathbf{R}}}] + V(\bar{R}, \bar{r}, \eta). \qquad (3.34)$$

---

[2]Expression (3.30) can be derived from (3.33) using the partitioned matrix method outlined in the Appendix F and omitting the rotational degrees of freedom.

A wavefunction $\varphi(\bar{\mathbf{r}}, \bar{\mathbf{R}})$ describing a stationary state of the three-body system must satisfy the time-independent Schrödinger equation

$$\hat{H}\,\varphi \;=\; E\,\varphi\,. \tag{3.35}$$

3.2.2 Fock hyperspherical coordinates

Fock coordinates [86] are closely related to Jacobi coordinates. They are obtained by expressing the lengths $\bar{R}$ and $\bar{r}$ of the mass-scaled Jacobi vectors $\bar{\mathbf{R}}$ and $\bar{\mathbf{r}}$ in cylindrical coordinates ρ and ω:

$$\bar{R} = \rho \cos\omega\,, \qquad\qquad \bar{r} = \rho \sin\omega\,. \tag{3.36}$$

The hyperradius ρ measures the size of the three-body system, the other variables being angles: ω is a hyperradial correlation angle [157] which depends on the choice of Jacobi set (we have omitted the arrangement index λ).

Space-fixed Fock coordinates

The orientations of the vectors $\bar{\mathbf{R}}$ and $\bar{\mathbf{r}}$ may be indicated by polar and azimuthal angles (θ_R, ϕ_R) and (θ_r, ϕ_r), respectively. This leads to the definition of *space-fixed* Fock coordinates $(\rho, \omega, \theta_R, \phi_R, \theta_r, \phi_r)$:

$$
\begin{aligned}
\bar{R}_x &= \rho \cos\omega \sin\theta_R \cos\phi_R \\
\bar{R}_y &= \rho \cos\omega \sin\theta_R \sin\phi_R \\
\bar{R}_z &= \rho \cos\omega \cos\theta_R \\
\bar{r}_x &= \rho \sin\omega \sin\theta_r \cos\phi_r \\
\bar{r}_y &= \rho \sin\omega \sin\theta_r \sin\phi_r \\
\bar{r}_z &= \rho \sin\omega \cos\theta_r\,.
\end{aligned} \tag{3.37}
$$

The metric tensor (g_{ij}) $(i, j = 1, \ldots, 6)$ for space-fixed Fock coordinates is given by:

$$
\begin{pmatrix}
1 & 0 & 0 & 0 & 0 & 0 \\
0 & \rho^2 & 0 & 0 & 0 & 0 \\
0 & 0 & \rho^2 \cos^2(\omega) & 0 & 0 & 0 \\
0 & 0 & 0 & \rho^2 \cos^2(\omega) \sin^2(\theta_R) & 0 & 0 \\
0 & 0 & 0 & 0 & \rho^2 \sin^2(\omega) & 0 \\
0 & 0 & 0 & 0 & 0 & \rho^2 \sin^2(\omega) \sin^2(\theta_r)
\end{pmatrix}
\tag{3.38}
$$

Its determinant (related to the volume element) is

$$|g| \;=\; \frac{\rho^{10}}{16}\sin^4(2\omega)\sin^2(\theta_r)\sin^2(\theta_R)\,. \tag{3.39}$$

The kinetic energy operator is easily found from Eq. (3.33) using (3.38) and Podolsky's formula [see Eq. (F.10)]:

$$\hat{T} = -\frac{\hbar^2}{2\mu}\left[\frac{1}{\rho^5}\frac{\partial}{\partial\rho}\rho^5\frac{\partial}{\partial\rho} + \frac{1}{\rho^2\sin^2(2\omega)}\frac{\partial}{\partial\omega}\sin^2(2\omega)\frac{\partial}{\partial\omega} + \frac{1}{\rho^2}\left(\frac{\mathbf{l}}{\mathrm{i}\hbar}\right)^2 + \frac{1}{\rho^2}\left(\frac{\mathbf{L}}{\mathrm{i}\hbar}\right)^2\right],$$

$$\tag{3.40}$$

where $\hat{\mathbf{L}}$ and $\hat{\mathbf{l}}$ are the angular momentum operators associated with the mass-scaled Jacobi vectors $\bar{\mathbf{R}}$ and $\bar{\mathbf{r}}$:

$$\hat{\mathbf{L}} = -\mathrm{i}\hbar\bar{\mathbf{R}}\times\bar{\nabla}_R, \qquad \hat{\mathbf{l}} = -\mathrm{i}\bar{\mathbf{r}}\times\bar{\nabla}_r. \tag{3.41}$$

Body-fixed Fock coordinates

Body-fixed Fock coordinates are $(\rho,\omega,\eta,\alpha,\beta,\gamma)$, where (α,β,γ) are three Euler angles and η is the angle between the two Jacobi vectors, as in Eq. (3.29) [see also Eq. (3.67)].

In the geometry where two atoms AB are close together and atom C is far away, the Jacobi length $R = \overline{(AB)C}$ is large compared to $r = \overline{BC}$ and the hyperradial correlation angle ω is small. In this geometry, the hyperradius is essentially the same as the mass-scaled atom-molecule distance $\bar{R}$:

$$\bar{R}\sim\rho, \qquad \bar{r}\sim\rho\omega \qquad (\omega\to 0). \tag{3.42}$$

This geometry is illustrated in Fig. 3.3 for a fixed angle η between the two Jacobi vectors $\mathbf{r}$ and $\mathbf{R}$.

3.2.3 Hyperspherical harmonics

The Fock coordinates defined in Eq. (3.37) are but one of many hyperspherical coordinate systems which all have the hyperradius ρ in common and differ from each other in the definition of the five hyperangles.

For every hyperspherical coordinate system, the total kinetic energy operator has the form

$$\hat{T} = -\frac{\hbar^2}{2\mu}\frac{1}{\rho^5}\frac{\partial}{\partial\rho}\rho^5\frac{\partial}{\partial\rho} + \hat{T}_{\mathrm{ang}} \tag{3.43}$$

where $\hat{T}_{\mathrm{ang}}$ is a second-order differential operator in the five hyperangles. $\hat{T}_{\mathrm{ang}}$ corresponds to the kinetic energy associated with the hyperangular motion. It is often written as

$$\hat{T}_{\mathrm{ang}} = \frac{1}{2\mu}\hat{\Lambda}^2 \tag{3.44}$$

where $\hat{\Lambda}^2$ is the square of the grand angular momentum operator; its eigenvalues are $K(K+4)$ $(K = 1, 2, 3, ...)$ [188].
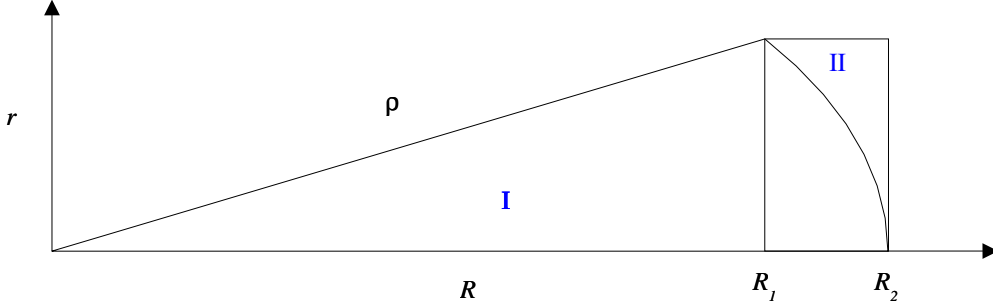
Figure 3.3: Illustration of Fock's hyperspherical coordinates (ρ, ω) and mass-scaled Jacobi lengths $(\bar{r}, \bar{R})$ for a fixed angle η between the two Jacobi vectors **r** and **R**. The Jacobi coordinates do not join smoothly onto the hyperspherical coordinates. The mass-scaled Jacobi lengths $\bar{r}$ and $\bar{R}$ needed to describe the classically allowed region $0 \leq \omega < \omega_{\mathrm{max}}$ at a constant hyperradius $\rho = \mathrm{const}$ lie respectively in the intervals $[0, \bar{r}_{\mathrm{max}}]$ and $[\bar{R}_1, \bar{R}_2]$. The larger ρ, the smaller the interval $[\bar{R}_1, \bar{R}_1]$ needed for a change from hyperspherical to Jacobi coordinates.

The eigenfunctions of $\hat{\Lambda}^2$ are called *hyperspherical harmonics*. Since they form a complete basis set in the space of hyperangular functions, they can be used to expand the three-body wavefunction for every fixed value of the hyperradius [89, 114].

3.2.4   Smith-Whitten hyperspherical coordinates

Smith-Whitten hyperspherical coordinates treat the three particles on an equal footing, and they naturally single out the principal axis of inertia [205, 207, 122, 123, 124, 157]. These two properties make Smith-Whitten coordinates very convenient.

They consist of the hyperradius $\rho \in [0, \infty)$, two hyperangles: $\Theta \in [0, \pi/4]$ and $\Phi \in [0, 2\pi)$, and three Euler angles: (α, β, γ). F. T. Smith and R. C. Whitten [246, 274] have defined Θ and Φ implicitly by specifying the projections of the mass-scaled Jacobi vectors $\bar{\mathbf{R}}$ and $\bar{\mathbf{r}}$ on the body-fixed xyz-coordinate axis:

$$
\begin{aligned}
\bar{r}_x &= \rho \cos \Theta \cos \Phi \, , \\
\bar{r}_y &= -\rho \sin \Theta \sin \Phi \, , \\
\bar{r}_z &= 0 \, , \\
\bar{R}_x &= \rho \cos \Theta \sin \Phi \, ,
\end{aligned}
$$

$$\bar{R}_y = \rho \sin \Theta \cos \Phi \, ,$$
$$\bar{R}_z = 0 \, . \tag{3.45}$$

The hyperradius ρ and the hyperangle Θ do not depend on the choice of arrangement, whereas the hyperangles Φ_α, Φ_β, and Φ_γ are related as follows:

$$\Phi_\beta = \Phi_\alpha - \Phi_{\alpha\beta} \, , \qquad \Phi_\gamma = \Phi_\alpha - \Phi_{\alpha\gamma} \, . \tag{3.46}$$

The identities in Eq. (3.46) are obtained by assuming that the Jacobi vectors in Eq. (3.45) are those of the α-arrangement ($\Phi \equiv \Phi_\alpha$). The Jacobi vectors of the β- and γ-arrangements are then calculated using kinematic rotations following Eq. (3.24). One sees that the vectors $(\mathbf{R}_\beta, \mathbf{r}_\beta)$ and $(\mathbf{R}_\gamma, \mathbf{r}_\gamma)$ can be written in the form of Eq. (3.45) with Φ replaced by Φ_β and Φ_γ given in Eq. (3.46). Thus the Smith-Whitten coordinates are essentially the same for all three arrangements.

In the body-fixed Cartesian coordinate system, the products of inertia vanish, which can be infered from the identities

$$\bar{r}_x \bar{r}_y + \bar{R}_x \bar{R}_y = 0 \, , \qquad \bar{r}_z = 0 \, , \qquad \bar{R}_z = 0 \, . \tag{3.47}$$

The xyz axis thus coincide with the principal axis of inertia. The principal moments of inertia are [3]

$$I_x = \mu \rho^2 \sin^2 \Theta \, ,$$
$$I_y = \mu \rho^2 \cos^2 \Theta \, ,$$
$$I_z = \mu \rho^2 \, . \tag{3.48}$$

$\Theta = 0$ corresponds to linear and $\Theta = \pi/4$ to perpendicular geometries.

The fact that the out-of-plane principal moment I_z is the sum of the other two is a property of all *planar* many-body systems.[4]

---

[3]Using the angles (θ, ϕ) defined in Eq. (F.28), we have

$$I_x = \mu \rho^2 \frac{1 - \sin \theta}{2} \, , \qquad I_y = \mu \rho^2 \frac{1 + \sin \theta}{2} \, , \qquad I_z = \mu \rho^2 .$$

[4]The diagonal elements of the inertia tensor of an N-particle system are

$$I_x = \sum_{i=1}^{N} m_i (y_i + z_i)^2 \, ,$$
$$I_y = \sum_{i=1}^{N} m_i (z_i + x_i)^2 \, ,$$
$$I_z = \sum_{i=1}^{N} m_i (x_i + y_i)^2$$

where m_i is the mass of the i-th particle and (x_i, y_i, z_i) are its Cartesian coordinates. If all particles lie in the xy-plane, the z-components z_i vanish, so that $I_x + I_y = I_z$.

Smith-Whitten coordinates cover the configuration space *twice.* When the angle Φ is increased gradually from 0 to 2π, the points A, B and C move on an ellipse in the body-fixed x-y-plane [154]. When $\Phi = \pi$, the ABC triangle has reassumed its initial shape but is rotated by π around the body-fixed z-axis with respect to its initial orientation. Only when $\Phi = 2\pi$, the triangle has regained both its initial shape and orientation.

Conversion into bond lengths

The Smith-Whitten coordinates defined in (3.45) are converted into mass-scaled bond lengths $\bar{r}_\lambda$ using:

$$
\bar{r}_\lambda \;=\; \rho \left[\frac{1 - \cos(2\Theta) \cos(2\Phi_\lambda)}{2} \right]^{1/2} \qquad (\lambda = \alpha, \beta, \gamma) . \tag{3.49}
$$

Symmetry operations

The symmetry operations for a system of N particles have been listed in Sec. 3.1.3. We now show how these operations (rotations, inversion, permutations) are performed for a system of three particles using Smith-Whitten coordinates.

Rotations can be realised through changes in the Euler angles (α, β, γ).

The inversion $\hat{I}$ can be performed in two ways, either by a transformation $\Phi \to \Phi + \pi$ or by a rotation of π around the body-fixed z-axis perpendicular to the ABC plane.

A permutation of two identical particles joined by the Jacobi vector $\mathbf{r}$ affects neither the centre of mass nor the principal axis of inertia of the three-body system. The permutation is therefore equivalent to the transformation

$$
\bar{\mathbf{r}} \to -\bar{\mathbf{r}} , \qquad \bar{\mathbf{R}} \to \bar{\mathbf{R}} .
$$

It can be expressed as the product of a transformation $\Phi \to -\Phi$ and a rotation of π around the body-fixed y-axis:

$$
\begin{pmatrix} \bar{r}_x \\ \bar{r}_y \\ \bar{R}_x \\ \bar{R}_y \end{pmatrix} \xrightarrow[\;\longrightarrow\;]{(\Phi \to -\Phi)} \begin{pmatrix} \bar{r}_x \\ -\bar{r}_y \\ -\bar{R}_x \\ \bar{R}_y \end{pmatrix} \xrightarrow[\;\longrightarrow\;]{\hat{D}_y(\pi)} \begin{pmatrix} -\bar{r}_x \\ -\bar{r}_y \\ \bar{R}_x \\ \bar{R}_y \end{pmatrix} . \tag{3.50}
$$

Here $\bar{r}_x$, $\bar{r}_y$, $\bar{R}_x$ and $\bar{R}_y$ are the projections of the two mass-scaled Jacobi vectors $\bar{\mathbf{r}}$ and $\bar{\mathbf{R}}$ on the *original* body-fixed x- and y-axis. The rotation $\hat{D}_y(\pi)$ is achieved through changes in the Euler angles (α, β, γ) and leads to a *new* body-fixed coordinate system BF′ whose z- and x- axis are reversed with respect to the original system. The projections of the *new* mass-scaled

Jacobi vectors $-\bar{\mathbf{r}}$ and $\bar{\mathbf{R}}$ on the *new* body-fixed x- and y-axis are therefore given by

$$\begin{pmatrix} \bar{r}_x \\ -\bar{r}_y \\ -\bar{R}_x \\ \bar{R}_y \end{pmatrix} . \tag{3.51}$$

Alternatively, the permutation can be written as the product of a transformation $\Phi \to \pi - \Phi$ and a rotation of π around the body-fixed x-axis:

$$\begin{pmatrix} \bar{r}_x \\ \bar{r}_y \\ \bar{R}_x \\ \bar{R}_y \end{pmatrix} \xrightarrow{(\Phi \to \pi - \Phi)} \begin{pmatrix} -\bar{r}_x \\ \bar{r}_y \\ \bar{R}_x \\ -\bar{R}_y \end{pmatrix} \xrightarrow{\hat{D}_x(\pi)} \begin{pmatrix} -\bar{r}_x \\ -\bar{r}_y \\ \bar{R}_x \\ \bar{R}_y \end{pmatrix} . \tag{3.52}$$

Classical motion

The expression for the classical kinetic energy in Smith-Whitten coordinates has been derived by B. R. Johnson [123] (we have verified the calculation):

$$T = \frac{\mu}{2} \left[\dot{\rho}^2 + \rho^2 (\dot{\Theta}^2 + \dot{\Phi}^2 - 4\dot{\Phi}\omega_z \cos\Theta \sin\Theta + \omega_z^2 + \omega_x^2 \sin^2\Theta + \omega_y^2 \cos^2\Theta) \right] . \tag{3.53}$$

From Eq. (3.53), we obtain the projections of the angular momentum on the body-fixed xyz-axis:

$$\begin{aligned} J_x &= \partial T/\partial\omega_x = I_x\omega_x , \\ J_y &= \partial T/\partial\omega_y = I_y\omega_y , \\ J_z &= \partial T/\partial\omega_z = I_z[\omega_z - \sin(2\Theta)\dot{\Phi}] . \end{aligned} \tag{3.54}$$

J_x and J_y are the familiar expressions for the angular momentum of a rigid rotor [150], whereas J_z contains an extra contribution involving the time derivative of the hyperangle Φ due to Coriolis coupling between the Euler angles and the vibrational coordinates.

We briefly consider the case of vanishing total angular momentum, $J_x = J_y = J_z = 0$. The classical motion is planar [123] in this case, and the space-fixed z'-axis can be chosen so that it coincides with the body-fixed z-axis. In this case only one Euler angle γ is needed: it describes the orientation of the body-fixed x- and y-axis with respect to the space-fixed x'- and y'-axis. Since J_z is assumed zero, one might believe that the body-fixed x- and y-axis will not rotate. However, this is generally *wrong*. In fact Eq. (3.54) shows that for $J_z = 0$, the angular velocity ω_z equals $\sin(2\Theta)\dot{\Phi}$, which is generally non-zero. A change in the shape coordinate Φ thus leads to a rotation of the principal axis of inertia with respect to the space-fixed frame, and therefore the Euler angle γ is not constant.

Kinetic energy operator in Smith-Whitten coordinates

The kinetic energy operator in Smith-Whitten coordinates is derived in the Appendix F, following Johnson's procedure [123, 124]. The result is a sum of a vibrational, a rotational and a Coriolis coupling term:

$$\hat{T} = \hat{T}_{\text{vib}} + \hat{T}_{\text{rot}} + \hat{T}_{\text{cor}} , \tag{3.55}$$

where the vibrational energy term $\hat{T}_{\text{vib}}$ is given by

$$\hat{T}_{\text{vib}} = -\frac{\hbar^2}{2\mu} \left[\frac{1}{\rho^5} \frac{\partial}{\partial \rho} \rho^5 \frac{\partial}{\partial \rho} + \frac{4}{\rho^2} \frac{1}{\sin(2\theta)} \frac{\partial}{\partial \theta} \sin(2\theta) \frac{\partial}{\partial \theta} + \frac{4}{\rho^2} \frac{1}{\cos^2(\theta)} \frac{\partial^2}{\partial \phi^2} \right] , \tag{3.56}$$

the rotational energy term $\hat{T}_{\text{rot}}$ has the form

$$\hat{T}_{\text{rot}} = \frac{1}{2} \left[\frac{\hat{J}_x^2}{I_x} + \frac{\hat{J}_y^2}{I_y} + \frac{\hat{J}_z^2}{I_z \sin \theta} \right] , \tag{3.57}$$

and the Coriolis coupling term $\hat{T}_{\text{cor}}$ can be written as

$$\hat{T}_{\text{cor}} = 2 \frac{i\hbar}{\mu \rho^2} \frac{\cos \theta}{\sin^2 \theta} \hat{J}_z \frac{\partial}{\partial \phi} . \tag{3.58}$$

3.2.5 Modified Smith-Whitten coordinates

In order to describe reactive collisions between atoms and diatomic molecules, J.-M. Launay [157] as well as R. T. Pack and G. A. Parker [207] use hypersperical coordinates that are essentially the same as the Smith-Whitten coordinates given in Eq. (3.45). Pack and Parker [207] have called their coordinates the Adiabatically Adjusting Principal Axis Hyperspherical (APH) coordinates.

The only important difference between the original Smith-Whitten coordinates and their modified versions lies in the labelling of the body-fixed coordinate axis, in other words, in the definition of the three Euler angles. J.-M. Launay and R. T. Pack *et al.* have defined the body-fixed coordinate system such that the body-fixed z-axis aligns with the internuclear axis when the molecule becomes linear. Thus the body-fixed z-axis is the axis of least inertia, and the y-axis is perpendicular to the molecular plane. This choice allows to minimize rotational coupling in linear geometries if the three-body wavefunction is expanded in symmetric top eigenfunctions [157].[5] It should be noted that the three moments of inertia are of the same order of magnitude in equilateral geometries ($I_z = I_x \approx I_y$) but not in linear ones ($I_z = 0$,

---

[5]The symmetric top functions $D_{mk}^{(J)}(\alpha, \beta, \gamma)$ are discussed in the Appendix G.

$I_x = I_y \neq 0$). Therefore, if both linear and equilateral geometries are energetically accessible, it is preferable to choose the axis of *least* inertia as the quantization axis (the body-fixed z-axis).

The Hamiltonian given by J.-M. Launay and M. Le Dourneuf in Ref. [157] is obtained from Eq. (F.39) in the Appendix by substituting $\theta \to \frac{\pi}{2} - \theta$ and $\phi \to \frac{\phi}{2}$ and by relabelling the principal axis of inertia ($xyz \to zxy$).

3.2.6 Internal Cartesian coordinates

R. T. Pack [206] has shown that the shape and size of the ABC-triangle can be described by a set of Cartesian-like coordinates (u, v, w) such that the kinetic energy operator for the vibrational motion resembles the kinetic energy operator of one particle. We have not used these coordinates in any computations, but they are interesting for a number of reasons:

- (u, v, w) are useful for plotting potential surfaces [122]. One uses as axis $(u/\rho, v/\rho, w/\rho)$, where ρ is the hyperradius.

- They provide a unified view on other coordinate systems [172].

- They are convenient for the Fourier Grid method [206].

The (u, v, w)-coordinates are defined as follows:

$$
\begin{aligned}
u &\in (-\infty, +\infty): & u &= \bar{\mathbf{R}}^2 - \bar{\mathbf{r}}^2 &= \bar{R}^2 - \bar{r}^2 \\
v &\in (-\infty, +\infty): & v &= 2\,\bar{\mathbf{R}} \cdot \bar{\mathbf{r}} &= 2\,\bar{R}\bar{r}\cos\eta \\
w &\in [0, +\infty) \quad : & w &= 2\,|\bar{\mathbf{R}} \times \bar{\mathbf{r}}| &= 2\,\bar{R}\bar{r}\sin\eta\ .
\end{aligned}
\tag{3.59}
$$

Here $\bar{\mathbf{R}}$ and $\bar{\mathbf{r}}$ are the mass-scaled Jacobi vectors, and η, $(0 \leq \eta \leq \pi)$ is the angle between them. The coordinate w is invariant under kinematic rotations: w is four times the area of the triangle ABC. The value $w = 0$ corresponds to linear configurations. The hyperradius ρ is

$$
\rho = (\bar{R}^2 + \bar{r}^2)^{1/2} = (u^2 + v^2 + w^2)^{1/4}\ .
\tag{3.60}
$$

The volume element in (u, v, w)-space is

$$
d(u, v, w) = \frac{w}{16\rho}\, du\, dv\, dw\ ,
\tag{3.61}
$$

and the kinetic energy operator for the internal motion has the simple form [206]:

$$
\hat{T}_{\text{vib}} = -\frac{\hbar^2}{2\mu}\, 4\rho^2 \left[\frac{\partial^2}{\partial u^2} + \frac{\partial^2}{\partial v^2} + \frac{\partial^2}{\partial w^2} + \frac{1}{w}\frac{\partial}{\partial w} \right]\ .
\tag{3.62}
$$

69

The first-derivative term in the kinetic energy operator can be eliminated by introducing a rescaled wavefunction $\psi^{\text{scaled}} = w^{\frac{1}{2}}\psi$. The volume element then becomes

$$d^{\text{scaled}}(u, v, w) = \frac{1}{16\rho} du\, dv\, dw\,, \tag{3.63}$$

and the kinetic energy operator takes the form

$$\hat{T}_{\text{vib}}^{\text{scaled}} = w^{\frac{1}{2}} \hat{T}_{\text{vib}}\, w^{-\frac{1}{2}} = -\frac{\hbar^2}{2\mu} 4\rho^2 \left(\frac{\partial^2}{\partial u^2} + \frac{\partial^2}{\partial v^2} + \frac{\partial^2}{\partial w^2} + \frac{1}{4w^2} \right)\,. \tag{3.64}$$

This simple form of the kinetic energy operator could make the (u, v, w)-coordinates particularly convenient for the Fourier grid method [206, 127].

The coordinates (u_β, v_β, w) of the β-arrangement are obtained from those of the α-arrangement by a rotation around the w-axis:

$$\begin{pmatrix} u_\beta \\ v_\beta \\ w \end{pmatrix} = \begin{pmatrix} \cos 2\Phi_{\alpha\beta} & \sin 2\Phi_{\alpha\beta} & 0 \\ -\sin 2\Phi_{\alpha\beta} & \cos 2\Phi_{\alpha\beta} & 0 \\ 0 & 0 & 1 \end{pmatrix} \begin{pmatrix} u_\alpha \\ v_\alpha \\ w \end{pmatrix} \tag{3.65}$$

with $\Phi_{\alpha\beta}$ given by Eq. (3.25). By introducing cylindrical or spherical coordinates in (u, v, w)-space, and choosing the w-axis as the principal axis, one thus obtains coordinates which describe the three particles equivalently.

The internal Cartesian coordinates are related to some other coordinate systems as follows:

- The mass-scaled Jacobi coordinates $(\bar{R}, \bar{r}, \eta)$ are *parabolical* coordinates with respect to the (u, v, w)-system. This follows directly from the definition (3.59).

- The Smith-Whitten coordinates (ρ, Θ, Φ) defined in Sec. 3.2.4 are *spherical* coordinates in the (u, v, w)-system :

$$\begin{aligned} u &= -\rho^2 \cos(2\Theta) \cos(2\Phi) \\ v &= \rho^2 \cos(2\Theta) \sin(2\Phi) \\ w &= \rho^2 \sin(2\Theta)\,. \end{aligned} \tag{3.66}$$

- The Fock hyperspherical coordinates (ρ, ω, η) defined in Sec. 3.2.2 are *spherical* coordinates in the (v, w, u)-system (note that the principal axis is u, not w):

$$\begin{aligned} v &= \rho^2 \sin(2\omega) \cos(\eta) \\ w &= \rho^2 \sin(2\omega) \sin(\eta) \\ u &= \rho^2 \cos(2\omega)\,. \end{aligned} \tag{3.67}$$

3.2.7 Bond coordinates

Bond coordinates (a, b, c) consist of the three distances between the particles,

$$a = \overline{BC} \ , \qquad b = \overline{CA} \ , \qquad c = \overline{CA} \ , \tag{3.68}$$

and they describe the three particles equivalently. Nevertheless they are inconvient for numerical calculations because their range is restricted by the triangular inequality:

$$a + b \leq c \ . \tag{3.69}$$

The triangular inequality can be avoided by using *perimetric* coordinates rather than bond lengths. Perimetric coordinates [127] are closely related to bond coordinates but their allowed range is not complicated in such a manner.

The unscaled Jacobi coordinates (R, r, η) are converted into bond lengths (a, b, c) using

$$
\begin{aligned}
a &= \sqrt{R^2 + \left(\frac{m_A}{m_A + m_B} r \right)^2 - 2R \frac{m_A}{m_A + m_B} r \cos \eta} \ , \\
b &= \sqrt{R^2 + \left(\frac{m_B}{m_A + m_B} r \right)^2 + 2R \frac{m_B}{m_A + m_B} r \cos \eta} \ , \\
c &= r \ .
\end{aligned}
\tag{3.70}
$$

The inverse relation is given by

$$
\begin{aligned}
R &= \sqrt{ \frac{m_B a^2 + m_A b^2}{m_A + m_B} - \left(\frac{m_A m_B}{m_A + m_B} \right)^2 c^2 } \ , \\
\cos \eta &= \frac{b^2 - a^2 + (m_A - m_B) c^2}{2 R c} \ , \\
r &= c \ .
\end{aligned}
\tag{3.71}
$$

3.3 Computational methods

A large variety of numerical methods for computing bound and scattering states of triatomic systems have been developed since the 1960s.

Pioneering work on reactive scattering was done by G. Schatz and A. Kuppermann [148, 235, 147], who performed quantum mechanical calculations for the linear, planar, and three-dimensional H + H_2 exchange reaction using a coupled-channels propagation technique.

3.3.1 Time-independent methods

The time-independent methods are the more traditional ones. They are still widely used, in particular for the analysis of resonances and threshold effects, and for the investigation of collisions at very low energies ("cold collisions").

Coupled-channels method for non-reactive scattering

Non-reactive collisions between atoms and a diatomic molecules are easier to study than reactive ones. Examples of non-reactive collisions are those between a chemically inert rare-gas atom and a stable diatomic molecule, such as Ar + H_2 [221, 263], He + H_2 [20], He + CO [152, 19], or He + I_2 [239].

These collisions can be modelized using a coupled-channels formalism based on the Jacobi vectors of one single arrangement: for every fixed atom-molecule distance R, the wavefunction is expanded in eigenfunctions of the atom and the diatomic molecule, leading to a system of coupled differential equations for the relative motion of the atom and the dimer. Such equations were first derived by A. M. Arthurs and A. Dalgarno [14] for the scattering of a structureless particle by a rigid rotator. The approach has become known as the Arthurs-Dalgarno expansion. It has been generalized since [204, 152, 261].

The coupled-channel method for non-reactive atom-molecule scattering is implemented in the MOLSCAT computer package developed by Jeremy M. Hutson and Sheldon Green[6] and in the Molcol package developed by D. R. Flower *et al.* [85] [7]

Hyperspherical propagation methods

In a hyperspherical propagation method, the six coordinates are separated into five "fast" hyperangles and the "slow" hyperradius. This separation allows to solve the Schrödinger equation in two steps. In the first step, the angular Schrödinger equation is solved, leading to a system of coupled hyperradial differential equations. In the second step, the coupled equations are solved by propagating a solution, or a set of solutions, along the hyperradius. The scattering matrix can be obtained by matching these solutions to wavefunctions of the three Jacobi regions.

Hyperspherical propagation methods have been used in molecular physics for over twenty years, starting with linear models, in which the three atoms are restricted to move on a straight line (see Refs. [156, 165, 166] and references therein).

J. G. Frey and B. J. Howard [89] extended the hyperspherical formalism to three spatial dimensions in order to compute the ground state energy of the weakly bound van-der-Waals trimers $(H_2)_3$, $(D_2)_3$ and Ne_3. They expanded the wavefunction in hyperspherical harmonics and used the resulting set of coupled hyperradial equations to propagate the wavefunction's logarithmic

---

[6]MOLSCAT is available on the internet at `http://www.dl.ac.uk/CCP/CCP6/molscat/` or `http://www.giss.nasa.gov/tools/molscat/`.

[7]Molcol is avalaible at `http://ccp7.dur.ac.uk/molcol.html`.

derivative matrix along the hyperradius, for a fixed energy E. Bound state energies were found iteratively using a bound-state matching condition (see the Appendix H). The same method was adopted by J. M. Hutson and co-workers to compute binding energies for H_3^+, $(H_2)_3$, Ne_3 and Ar_3 [114, 56].

Unfortunately, the hyperspherical harmonics are not well suited as basis functions for highly excited or scattering states. We recall that they are the eigenfunctions of the angular kinetic energy operator of three *free* particles. Clearly, they span the *entire* configuration space, including regions which are energetically forbidden in the presence of a potential. A large number of hyperspherical harmonics is therefore needed to expand a wavefunction that is localized mainly in the classically allowed region.

J.-M. Launay *et al.* [157] and R. T. Pack *et al.* [207] have overcome this problem by using potential-adapted basis functions which have a large amplitude only in the energetically allowed regions of configuration space. The potential-adapted basis functions are obtained through diagonalization of a ρ-dependent angular reference Hamiltonian that includes the potential energy. By expanding the wavefunction in potential-adapted basis functions rather than in hyperspherical harmonics, the necessary number of coupled differential equations is greatly reduced, and it becomes possible to study reactive atom-diatom collisions of the type

$$A + BC \qquad \leftrightarrow \qquad AB + C \ .$$
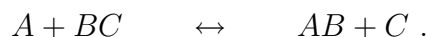
J.-M. Launay's method is described in detail in Sec. 5.1 of Chapter 5.

Recently, R. T. Pack *et al.* [54, 208] extended the hyperspherical method to energies above the three-body threshold and obtained converged results for the

$$Ne_2 + H \qquad \leftrightarrow \qquad Ne + Ne + Ne$$

recombination and collision-induced dissociation reactions.

Although the potential-adapted angular basis set can be much smaller than the basis set of hyperspherical harmonics, it usually remains fairly large in the case of alkali trimers. In order to study $K + K_2$ collisions, G. Quémener *et al.* [220] haved solved systems of more than 1000 coupled differential equations!

The situation is different for rare gas systems such as He_3, Ne_3, and Ar_3. B. D. Esry *et al.* [75, 31] have studied these systems in the adiabatic approximation, using a single ρ-dependent adiabatic angular basis function.

V. Kokoouline and C. H. Greene have adopted an adiabatic hyperspherical approach in their unified theoretical treatment of dissociative recombination of the H_3^+ and D_3^+ ions [139, 138]

The ABC quantum reactive scattering programme[8] developed by D. Skouteris, J. F. Castillo and D. E. Manolopoulos [243] is closely related to Launay's and Parker's methods. The essential difference is the way in which the angular basis functions are defined. For each hyperradial distance ρ, Skouteris *et al.* compute an orthogonal angular basis set from a non-orthogonal, multi-arrangement basis set of vibrational-rotational diatomic eigenfunctions of each arrangement. While the primitive basis of pseudo - hyperspherical harmonics used by Launay *et al.* to compute the potential-adapted set is *complete* (any function of the five hyperangles can be expanded in this basis set), it seems that the primitive multi-arrangement basis set used in ABC is incomplete, because the primitive basis functions fill the three arrangement valleys but not the strongly forbidden regions. In particular it is not clear whether we could have used the ABC programme for $Na + Na_2$ on the lowest quartet surface $^4A'_2$: the classically allowed region of this surface is noticibly enlarged by the strong three-body interaction (see Chapter 4). In the ABC programme, the three-body interaction is ignored in the definition of the angular basis set. Therefore it may be possible that the angular basis functions do not cover the entire classically allowed region. This would need to be tested numerically.

Algebraic methods

In an algebraic method, the wavefunction is approximated by a linear combination of basis functions which must cover the energetically accessible regions of configuration space. The resulting eigenvalue problem is solved numerically. Algebraic methods have been used to compute bound vibrational levels of triatomic molecules [143, 24, 25, 256, 257, 232] as well as scattering states for reactive encounters between atoms and diatomic molecules [55, 285, 286, 287, 284]. Various coordinate systems have been used: Jacobi coordinates of one arrangement, Jacobi coordinates of all three arragangements, and hyperspherical coordinates.

W. H. Miller [193] has rewritten the Schrödinger equation in the form of coupled integro-differential equations using basis functions of all three Jacobi arrangements. These equations can only be solved algebraically due to the non-local integral coupling terms.

J. Tennyson *et al.* [257] have developed the DVR3D suite of programmes for the computation of vibrational-rotational levels of triatomic molecules.[9] The method is based on a Discrete Variable Representation (DVR) using orthogonal polynomials. We have not used DVR3D, because the package

---

[8]ABC is available on the internet via the Computer Physics Communications Program library (`http://www.cpc.cs.qub.ac.uk/cpc/`).

[9]DVR3D is available via the Computer Physics Communications Program Library on the internet (`http://www.cpc.cs.qub.ac.uk/`).

is not designed for extremely weakly bound or low-energy scattering states (very weakly bound states are discussed in Chapter 5).

3.3.2   Time-dependent methods

In a time-dependent method, the temporal evolution of a wavepacket is simulated by solving the time-dependent Schrödinger equation numerically. Compared to the stationary methods, the time-dependent approach has the advantage of providing a time-dependent wavefunction, and it may be instructive to follow the temporal evolution of a wavepacket. A time-dependent description *must* be used if the three particles are placed in a time-dependent external field.

A discussion of the existing time-dependent methods is beyond the scope of the present work, but we wish to mention the works by John Z. H. Zhang *et al.* [213, 288], Stuart C. Althorpe *et al.* [10, 6, 7, 125, 8, 9], R. Kosloff *et al.* [2, 141, 142], and many others [241, 229, 238]. Time-dependent methods have also been adapted to compute bound [127] and quasi-bound states [242, 180, 209].

For the calculation of chemical reaction dynamics, John Z. H. Zhang's group has developed "Dynasol", a software package with graphical user interface.[10]

3.4   Summary

A particular coordinate system must be chosen if one wishes to describe a system of three particles numerically. There is no coordinate system which is superior to all the others in all respects. The decision which coordinates to choose will depend on the properties of the specific system to be studied, in particular on whether the system is reactive or not.

Non-reactive collisions between an atom and a tightly bound diatomic molecule can be treated using "standard" methods, based on space-fixed or body-fixed Jacobi coordinates. The MOLSCAT and Molcol computer packages have been designed for such collisions.

The modelization of reactive systems is much more demanding, since the initial and final arrangement of particles may differ. In this case more than one set of Jacobi vectors are needed for a complete analysis of the scattering state.

---

[10]Dynasol is available on the internet at
`http://p150.chem.nyu.edu/dynasolver/index.html`

Chapter 4

Potential energy surface of the sodium trimer

The relative motion of three spin-polarized ground state sodium atoms is governed by the potential energy surface associated with the $1^4A_2'$ electronic state of Na_3. This surface determines the vibrational motion of Na_3, and, at higher energies, the reaction dynamics of collisions between sodium atoms in the $3s$ ground state and sodium molecules Na_2 in the $a^3\Sigma_u^+$ state, in the case where the individual spins of the three atoms are "aligned".

In this Chapter, we present the $1^4A_2'$ electronic state of Na_3 and the potential energy surface computed by J. Higgins *et al.* [100]. We did *not* perform any quantum-chemical computations ourselves.

The scattering calculations described in Chapter 5 are based on a pairwise-additive model potential energy surface constructed from a potential energy curve for Na_2 computed by M. Gutowski [96].

4.1   Introduction

Molecules and ions consist of positively charged nuclei and negatively charged electrons. Their most complete description is provided by their time-dependent wavefunction, whose temporal evolution is governed by the Schrödinger equation. Unfortunately, this equation cannot be solved analytically, not even for the simplest of all molecules, H_2. Approximate and numerical methods are needed in order explain the rich variety of observed phenomena.

The problem of solving the complete Schrödinger equation can be simplified due to the great difference in mass between the heavy nuclei and the light electrons: in an intuitive picture, the electrons move much faster than the nuclei, and one may expect that their motion will adapt itself almost instantaneously to any changes in the positions of the nuclei. Therefore, the usual approach is to solve the stationary Schrödinger equation for fixed positions of

the nuclei. One thus obtains electronic wavefunctions and electronic energies which parametrically depend on the nuclear coordinates. The energy of the electrons as a function of the nuclear coordinates is refered to as a *potential energy surface* (PES). The motion of the nuclei is treated in a second step, using the potential energy surfaces, and possibly couplings between different surfaces, as *input* data. The quantum-mechanical equations for the nuclear motion are derived from the Schrödinger equation (involving electronic and nuclear degrees of freedom) by expanding the total wavefunction in a basis set of electronic wavefunctions, which parametrically depend on the nuclear coordinates. In the Born-Oppenheimer approximation, all adiabiatic corrections and all non-adiabatic couplings between different electronic states are neglected.

Sophisticated methods for the calculation of potential energy surfaces have been developed over the years. A detailed description of them is beyond the scope of the present work.

Today *ab initio* potential energy surfaces are available for the lowest quartet states (total electronic spin $S = 3/2$) of all homonuclear alkali trimers: Li_3 [53, 247, 40], Na_3 [100, 247], K_3 [247], Rb_3 [247], and Cs_3 [247].

The doublet ground states $1^2E'$ (total electronic spin $S = 1/2$) of the alkali and hydrogen trimers X_3 and of their isotopes are doubly degenerate for the equilateral geometry of the nuclei. In this geometry, the two surfaces present a conical intersection, which has attracted a lot of attention over the last two decades [260, 259, 52, 269, 5, 4, 279, 149]. The conical intersection gives rise to the Jahn-Teller effect, a geometrical phase effect [189, 282]. The doublet states are not discussed in this thesis.

4.2   Sodium atom

The sodium atom ^{23}Na is composed of a nucleus which is surrounded by 11 electrons. The nucleus consists of 11 protons and 12 neutrons. The sodium atom is the second-lightest of the alkali atoms (Li, Na, K, Rb, Cs). Its electronic ground state corresponds to the configuration $1s^2\ 2s^2\ 2p^6\ 3s$. The total angular momentum (spin and orbital) of the ten inner-shell electons are zero.

The inner-shell electrons and the nucleus are called the *core.* The total angular momentum of the core is that of the nucleus, and its total electric charge is that of one proton only. In the simplest model, the core is regarded as a pointlike charge with no internal structure: in this model, the sodium atom is the same as the hydrogen atom. In a more realistic model, the core is attributed an electric polarizability, so that it becomes polarized by the Coulomb field of the valence electron. The core thus creates an electric dipole field, in addition to its Coulomb field, and both the dipole field and

Reference (first author)	method	r_e in a_0	D_e in cm^{-1}	$C_6/10^3$ in a.u.	$C_8/10^5$ in a.u.
Konowalow [140]	T	...	...	1.68	1.64
Li Li [169]	E	9.6208	174.45 ± 0.36	1.63(74)	1.570(61)
Friedman [90]	E	9.471(1)	175.76(35)	...	...
Magnier [179]	T	9.81	174	...	...
Marinescu [184]	T	...	...	1.427	1.119
Färbert [79]	E				
Derevianko [64]	T	...	...	1.556	...
Gutowski [96]	T	9.834	176.173	1.5869	1.3728
Higgins [100]	T	9.83	176.17	1.59	1.37
Ho [101]	E + T	9.617 ± 0.12	174.96 ± 1.18	...	...
Samuelis [233]	E	9.6208	...	1.5610	1.1188
Soldán [247]	T	9.853	174.025	...	...

Table 4.1: Comparison of experimental (E) and theoretical (T) potential energy curves for the $a\ ^3\Sigma_u^+$ state of Na_2.

the Coulomb field interact with the charge of the valence electron, leading to a lifting of the degeneracy between two states with the same principal quantum number n but different angular quantum numbers l and l'. In this Chapter, we do not consider the inner-shell electrons explicitly, we shall only use the "polarizible core + electron" model.

4.3   Triplet state of the sodium dimer

Compared to the singulet states of alkali dimers, fewer information is available on the triplet states, because the latter are more difficult to prepare experimentally [252]. Spectroscopic observations of rotational-vibrational levels of the triplet Na_2 potential are reported in Refs. [169, 252, 233, 62]. A comparison of characteristic values of the "a" potential found experimentally and theoretically by various groups is given in Table 4.1. The overall agreement seems to be quite good. Observations of the hyperfine structure are reported in Refs. [78] and [233].

The long-range dispersion coefficients (C_6, C_8, C_{10}, etc) are the same for the $X\ 1\Sigma_g^+$ and the $a\ ^3\Sigma_u^+$ states. At long distances, the X and the a curves only differ in the exchange term V^{exch}, which vanishes exponentially with the distance. The asymptotic forms of the two curves are given by

$$V_\pm(r) = \pm V^{\text{exch}}(r) - \frac{C_6}{r^6} - \frac{C_8}{r^8} - \frac{C_{10}}{r^{10}} - \ldots \qquad (4.1)$$

where $+$ and $-$ refer to the a and X states, respectively. Explicit expressions

for the exchange energy are derived in Refs. [244] and [198]. Sometimes the dispersion energy is represented as a damped dispersion series,

$$V(r) = \sum_n \frac{C_n}{r^n} D_n(r) \, ,$$

(4.2)

where the $D_n(r)$ are damping functions, which are unity at long distance but tend to zero for $r \to 0$ [42]. In Ref. [140] the exchange energy is approximated by a decreasing exponential, $V^{\text{exch}}(r) = Be^{-\beta r}$. W. T. Zemke and W. C. Stwalley [283] point out that the exchange energy for two ground state alkali atoms is better described by the expression

$$V^{\text{exch}}(r) = C\, r^\alpha e^{-\beta r}$$

(4.3)

of B. M. Smirnov and M. I. Chibisov [244]. Using molecular spectroscopy, C. Samuelis *et al.* [233] have determined pricise numerical values of the coefficients α and β in Smirnov's expression.

We note that the asymptotic form for the dispersion energy (4.1) needs to be corrected for very large distances due to relativistic retardation effects [48]: the interaction energy then decreases as $1/r^7$ rather than $1/r^6$.

Van der Waals interactions among atoms and molecules are discussed in several review articles (see Refs. [183, 60, 102, 223, 49, 42, 118, 264]).

See also Refs. [173], [144], [250].

Potential curve by M. Gutowski

P. Soldán *et al.* [248] used the Na_2 $a\,^3\Sigma_u^+$ potential curve calculated by M. Gutowski [96] as input data in their numerical calculations regarding low-energy collisions between Na and Na_2. As we adapted their code to compute bound state energies of Na_3 (see Chapter 5), we used the same potential curve as input data. This curve is plotted in Fig. 4.1. It is characterized by a well depth $D = 176.170$ cm^{-1} = 253.469 K and an equilibrium distance $r_{\text{e}} = 9.8265$ a$_0$ = 5.2000 Å. The long-range dispersion coefficients are

$$C_6 = 1586.9 \text{ a.u.} = 7.6477 \times 10^6 \text{ cm}^{-1}\text{Å}^6$$

(4.4)

and

$$C_8 = 1.3728 \times 10^5 \text{ a.u.} = 1.8527 \times 10^8 \text{ cm}^{-1}\text{Å}^8 \, .$$

(4.5)

Unfortunately, Ref. [96] does not give error bars for C_6 and C_8.

4.4   Lowest quartet state of the sodium trimer

The first spectroscopic data for the quartet spin state of an alkali trimer was obtained by J. Higgins *et al.* [99]. In their experiment, sodium atoms were
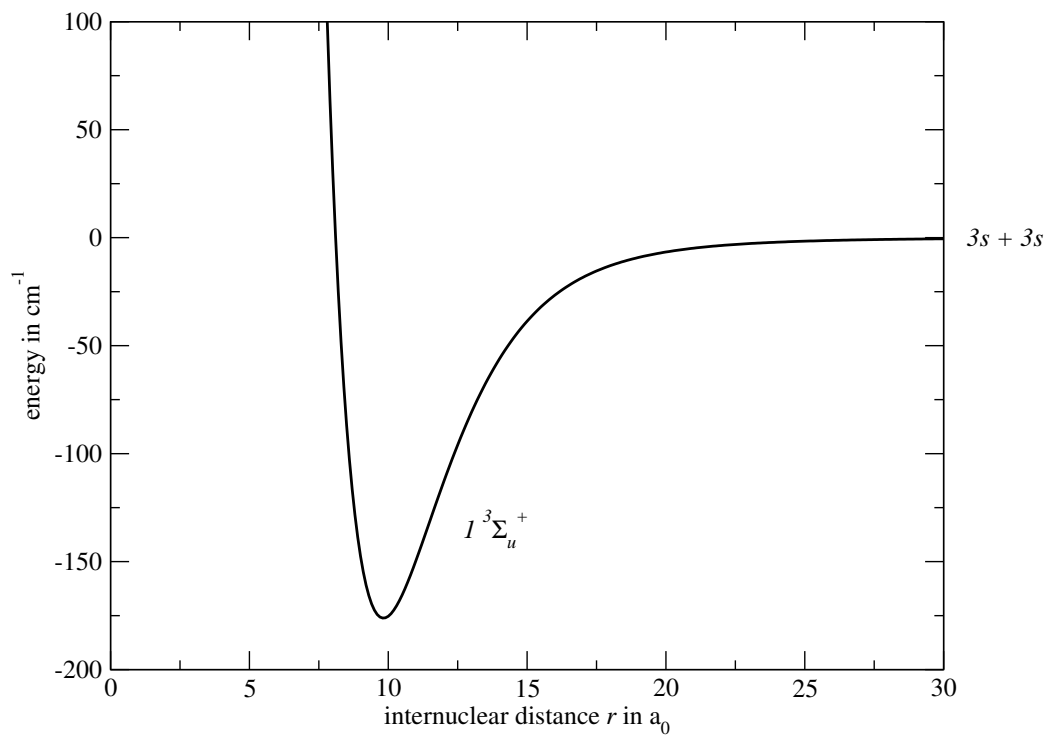
Figure 4.1: *Ab initio* potential energy curve for Na$_2$ in the a $^3\Sigma_u^+$ state, calculated by M. Gutowski *et al.*

attached to helium droplets, where they tend to form small clusters preferably in high spin states [252, 98, 226]. The sodium trimers were excited by laser to the $2\ ^4E'$ state, and the emission spectrum from relaxation to the $1\ ^4A_2'$ state was recorded.

4.4.1 Electronic model Hamiltonian

In order to explain the essential features of the potential energy surface $1\ ^4A_2'$, we define a simple model Hamiltonian for the motion of the three outer-shell electrons, interacting with each other and with the positive ionic cores. The ionic cores, which consist of the nuclei and the inner-shell electrons, are assumed fixed in space and treated as point charges with no internal structure. The model Hamiltonian can thus be written as

$$
\begin{aligned}
\hat{H} \ = \ & \hat{V}^{AB} + \hat{V}^{BC} + \hat{V}^{CA} \\
+ \ & \hat{T}_1 + \hat{V}_1^A + \hat{V}_1^B + \hat{V}_1^C \\
+ \ & \hat{T}_2 + \hat{V}_2^A + \hat{V}_2^B + \hat{V}_2^C \\
+ \ & \hat{T}_3 + \hat{V}_3^A + \hat{V}_3^B + \hat{V}_3^C \\
+ \ & \hat{V}_{12} + \hat{V}_{23} + \hat{V}_{31} \ .
\end{aligned}
\tag{4.6}
$$

Here V^{AB}, V^{BC}, V^{CA} are the potential interaction energies among the ionic cores. V_i^A, V_i^B and V_i^C are the interaction energies of the ith electron ($i = 1, 2, 3$) with the cores. V_{12}, V_{23} and V_{31} are the electron-electron energies. T_1, T_2 and T_3 are the kinetic energies of the electrons.

A more realistic Hamiltonian would include core polarization terms, which cannot be written as sums of products of two-body interactions [178, 179]. In addition, relativistic corrections would be necessary in order to explain the fine and hyperfine structure in observed spectra.

We note that the model Hamiltonian of Eq. (4.6) can be rewritten as a sum of one- and two-electron-Hamiltonians:

$$
\hat{H} = \hat{H}_{12}^{AB} + \hat{H}_{23}^{BC} + \hat{H}_{31}^{CA} - \hat{H}_1^A - \hat{H}_2^B - \hat{H}_3^C
\tag{4.7}
$$

where

$$
\begin{aligned}
\hat{H}_{12}^{AB} \ = \ & \hat{T}_1 + \hat{T}_2 + \hat{V}_1^A + \hat{V}_1^B + \hat{V}_2^A + \hat{V}_2^B + \hat{V}_{12} + \hat{V}^{AB} \\
\hat{H}_{23}^{BC} \ = \ & \hat{T}_2 + \hat{T}_3 + \hat{V}_2^B + \hat{V}_2^C + \hat{V}_3^B + \hat{V}_3^C + \hat{V}_{23} + \hat{V}^{BC} \\
\hat{H}_{31}^{CA} \ = \ & \hat{T}_3 + \hat{T}_1 + \hat{V}_3^C + \hat{V}_3^A + \hat{V}_1^C + \hat{V}_1^A + \hat{V}_{31} + \hat{V}^{CA}
\end{aligned}
\tag{4.8}
$$

and

$$
\begin{aligned}
\hat{H}_1^A \ = \ & \hat{T}_1 + \hat{V}_1^A \\
\hat{H}_2^B \ = \ & \hat{T}_2 + \hat{V}_2^B \\
\hat{H}_3^B \ = \ & \hat{T}_3 + \hat{V}_3^C .
\end{aligned}
\tag{4.9}
$$

The form of the electronic Hamiltonian (4.7) suggests that the electronic states of the diatomic fragments AB, BC and CA could be used as basis sets for calculating potential energy surfaces of the triatomic molecule ABC. In fact the expression (4.7) is the starting point for the "diatoms-in-molecules" (DIM) method [72, 73], in which the electronic structure of a polyatomic molecule is calculated using the electronic states of its monoatomic and diatomic fragments. In principle, DIM is applicable to molecules composed of an arbitrary number of atoms. It has been applied to a wide range of small molecules (see Ref. [167] and references therein).

4.4.2   Electronic wavefunction of the quartet state

The wavefunction $\psi(1,2,3)$ of the three valence electrons in the quartet spin state (total electronic spin $S = 3/2$) factorizes as

$$\psi(1,2,3) \;=\; \varphi(\mathbf{r}_1, \mathbf{r}_2, \mathbf{r}_3)\, \chi(\sigma_1, \sigma_2, \sigma_3) \qquad (4.10)$$

where $\mathbf{r}_1$, $\mathbf{r}_2$ and $\mathbf{r}_3$ are the space coordinates of the three electrons and σ_1, σ_2 and σ_3 are their spin coordinates. The quartet spin function $\chi(\sigma_1, \sigma_2, \sigma_3)$ is totally symmetric with respect to permutations of two electrons. Hence the orbital function $\varphi(\mathbf{r}_1, \mathbf{r}_2, \mathbf{r}_3)$ is totally antisymmetric.

Spin function

We denote $\hat{S}_z$ the operator defined in the spin-space of three electrons such that $1 - iS_z\alpha/\hbar$ generates an infinitesimal rotation of the spin function of three electrons about the z-axis. At present, it does not matter whether the z-axis is defined with respect to the positions of the nuclei or with respect to the laboratory. The spin function characterized by the spin projection number $M_S = 3/2$ is the product

$$\chi_{+++} \;=\; \chi_+(\sigma_1)\chi_+(\sigma_2)\chi_+(\sigma_3) \qquad (4.11)$$

where χ_+ is a one-particle spin function and eigenfunction of the one-particle spin operator $\hat{s}_z$:

$$\hat{s}_z\chi_+ \;=\; +\frac{\hbar}{2}\chi_+ \;.$$

The three other quartet spin functions (eigenfunctions of S_z with eigenvalues $\hbar/2$, $-\hbar/2$, $-3/2\hbar$) are obtained from χ_{+++} through successive application of the lowering operator $S_- = S_x - iS_y$.

Orbital function

An approximate three-electron orbital is obtained by antisymmetrizing the product wave function

$$s^A(\mathbf{r}_1)s^B(\mathbf{r}_2)s^C(\mathbf{r}_3)$$

where s^A, s^B and s^C denote spherically symmetrical orbitals centered on the nuclei A, B and C. The resulting antisymmetrical orbital is

$$
\begin{aligned}
\varphi \;=\; & \frac{1}{\sqrt{6}} \left[s^A(\mathbf{r}_1)s^B(\mathbf{r}_2)s^C(\mathbf{r}_3) - s^A(\mathbf{r}_2)s^B(\mathbf{r}_1)s^C(\mathbf{r}_3) \right. \\
& + s^A(\mathbf{r}_2)s^B(\mathbf{r}_3)s^C(\mathbf{r}_1) - s^A(\mathbf{r}_3)s^B(\mathbf{r}_2)s^C(\mathbf{r}_1) \\
& \left. + s^A(\mathbf{r}_3)s^B(\mathbf{r}_1)s^C(\mathbf{r}_2) - s^A(\mathbf{r}_1)s^B(\mathbf{r}_3)s^C(\mathbf{r}_2) \right] .
\end{aligned}
\tag{4.12}
$$

It is easy to check that this function is a basis of the A_2' representation of the D_{3h} point group (one may use the character table in Ref. [150].

The orbital (4.12) depends parametrically on the nuclear coordinates. For nuclear geometries other than equilateral, it does *not* transform according to the A_2' representation of the D_{3h} symmetry group but according to a representation of the other symmetry group. However, in order to keep the notation simple, the lowest quartet state is labelled $1\,^4A_2'$ throughout, that is, for *any* geometrical arrangement of the nuclei. The five point groups that are relevant for a system of three identical nuclei are represented in Fig. 4.4.2.

For geometries in which one atom C is situated at a large distance from diatomic molecule AB, the electronic wavefunction is conveniently expressed in terms of orbitals φ^{AB} of the diatomic molecule and orbitals s^C of the isolated atom:

$$
\varphi \;=\; \frac{1}{\sqrt{3}} \left[\varphi^{AB}(\mathbf{r}_1, \mathbf{r}_2)s^C(\mathbf{r}_3) + \varphi^{AB}(\mathbf{r}_2, \mathbf{r}_3)s^C(\mathbf{r}_1) + \varphi^{AB}(\mathbf{r}_3, \mathbf{r}_1)s^C(\mathbf{r}_2) \right]
\tag{4.13}
$$

Of course, the orbital $\varphi^{AB}(\mathbf{r}_2, \mathbf{r}_3)$ must be antisymmetric with respect to permutations of $\mathbf{r}_2$ and $\mathbf{r}_3$.

If one of the three atoms separates adiabatically from the two others, the adiabatic electronic state

$$
\mathrm{Na}_3(1^4A_2')
$$
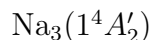
correlates to the state

$$
\mathrm{Na}(3s) + \mathrm{Na}_2(a^3\Sigma_u^+) .
$$

In fact there are no other electronic states, except excited ones, that could be physical states of Na_2 and Na after the dissociation. Therefore the wavefunction φ^{AB} in Eq. (4.13) is the lowest orbital of Σ_u^+ symmetry. In the limit of two separated atoms A and B, the molecular orbital φ^{AB} can be written

84

D_{3h}

C_{2v}

$D_{\infty h}$

$C_{\infty v}$

C_s
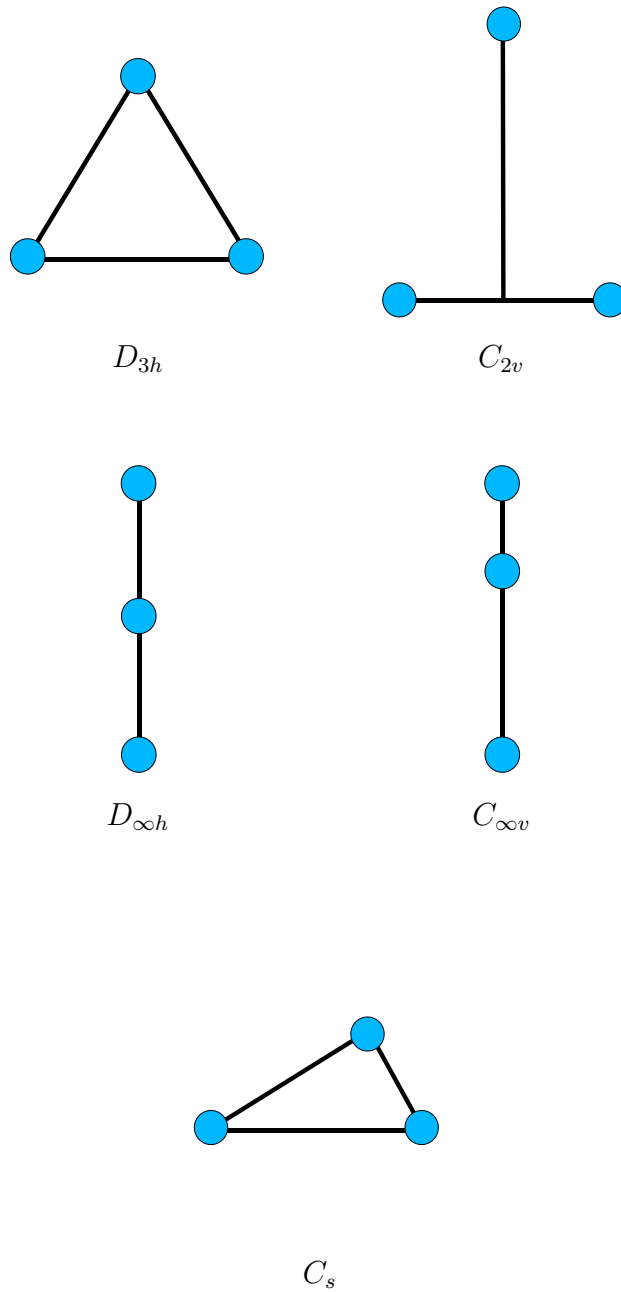
Figure 4.2: Symmetry groups of a homonuclear triatomic molecule.

as [1]

$$\varphi^{AB} = \frac{1}{\sqrt{2}} \left[s^A(\mathbf{r}_1) s^B(\mathbf{r}_2) - s^A(\mathbf{r}_2) s^B(\mathbf{r}_1) \right] \ . \tag{4.14}$$

4.4.3 Pairwise additive potential energy surface

For any triatomic system ABC, a simple model potential energy surface can be constructed using the atom-atom potentials V^{AB}, V^{BC} and V^{CA}. For large internuclear separations, the atom-atom potentials correlate respectively to the energies $(E_A + E_B)$, $(E_B + E_C)$, and $(E_C + E_A)$, where E_A, E_B and E_C are energies of the isolated atoms A, B and C.

The *pairwise additive* potential energy surface is defined as

$$V_{2b}(a, b, c) = V^{AB}(c) + V^{BC}(a) + V^{CA}(b) - E_A - E_B - E_C \ , \tag{4.15}$$

a, b, and c being the three internuclear distances. This expression is analogous to the form of Hamiltonian in Eq. (4.7). However, despite this formal resemblence, V_{2b} is not deduced immediately from (4.7), because the one- and two-electron Hamiltonians on the right-handside of Eq. (4.7) do not commute.

The use of the pairwise-additive potential energy surface as a model surface may be justified by the following arguments:

- In the asymptotic limit where one atom (say C) is infinitely far away from the two others (A and B), the pairwise additive surface describes the interaction between A and B *exactly.*

- The isotropic atom-molecule van der Waals coefficient $C_6^{\text{at}-\text{mol}}$ of the pairwise-additive potential energy surface is exactly twice the atom-atom van der Waals coefficient C_6, and one may expect that this is a reasonable first estimate for $C_6^{\text{at}-\text{mol}}$.

- In the geometry of three well-separated atoms, pairwise forces appear in a first- or second-order perturbation analysis, whereas a three-body contribution only arises in third-order [27]. The three-body correction is known as the Axilrod-Teller-Muto term (see the Appendix D).

However, the pairwise-additive surface may differ significantly from the true potential energy surface for geometries in which all three atoms are close together.

---

[1]By substituting Eq. (4.14) for φ^{AB} in Eq. (4.13), on obtains Eq. (4.12) - but this must not be seen as a mathematical proof that the $1^4 A_2'$ state correlates to the $a^3\Sigma_u^+$ molecular state and the $3s$ atomic state. It should also be noted that in the case of excited electronic states, such as those correlating to the limit $3s+3s+3p$, it is much more difficult or impossible to relate each state of the equilateral geometry univoquely to a particular state of the atom-diatom geometry.

We note that the global minimum of a pairwise additive potential surface is simply the sum of the minimum values of each pair potential. The mininum is reached at the geometry where the internuclear distances are each equal to the equilibrium distances of the pair potentials.

Pairwise-additive surfaces are usually used in calculations if better data is not available. For example, B. D. Esry *et al.* [74] have used a pairwise-additive surface for Rb_3 in order to study the recombination of three atoms at ultra-low temperatures.

We have constructed the pairwise-additive potential surface for the $1\ ^4A_2'$ state of Na_3 using the $Na_2\ a^3\Sigma_u^+$ *ab initio* potential curve by M. Gutowski [96]. At large internuclear distances, the latter is characterized by long-range atom-atom dispersion coefficients C_6 and C_8 (see Sec. 4.3), which can be related to long-range atom-molecule dispersion coefficients using Eqs. E.10 and E.12 of the Appendix E. The atom-molecule C_6 coefficient of the pairwise additive surface is exactly twice the atom-atom C_6 coefficient :

$$C_6(Na_2 - Na) \ = \ 3173.8 \text{ a.u. ;} \qquad (4.16)$$

it does not depend on the orientation of the Na_2 molecular axis with respect to the atom-molecule axis Na - Na_2.

The coefficient $C_8(Na_2-Na)$ is twice the coefficient $C_8(Na-Na)$ plus a correction which depends on the distance between the two atoms in the Na_2 molecule and on the orientation of the Na_2 molecular axis with respect to the Na atom. We have determined the atom-molecule C_8 coefficient with the internuclear distance of Na_2 fixed at the equilibrium value $r_e = 9.8265$ a.u.= 5.2000 Å. For linear Na-Na_2 configurations we obtain

$$C_8^{\parallel}(Na_2 - Na) \ = \ 2.7557 \times 10^5 \text{ a.u.,} \qquad (4.17)$$

and, for perpendicular configurations:

$$C_8^{\perp}(Na_2 - Na) \ = \ 2.7442 \times 10^5 \text{ a.u..} \qquad (4.18)$$

The value of the "pairwise additive" C_6 coefficient in Eq. (4.16) is a rough estimate for the true atom-molecule C_6 coefficient (see Sec. 4.4.5 and Ref. [228]).

4.4.4 Three-body forces for the geometry of three separated atoms

We briefly consider the situation in which all three atoms are at great distances from each other.

Van der Waals forces among three atoms were first calculated by B. M. Axilrod and E. Teller [15] and Y. Muto [195]. The induced dipole-dipole-dipole interaction energy between three *s*-state atoms has become known as

the Axilrod-Teller-Muto (ATM) term. It has the form [27]

$$E_3^{(3)}{}_{111}(a,b,c) \;=\; Z_{111}^{ABC} \times 3\frac{1 + 3\cos\alpha\cos\beta\cos\gamma}{a^3 b^3 c^3} \qquad (4.19)$$

where α, β and γ are the inner angles of the triangle formed by the atoms A, B and C. The ATM term can also be derived classically by considering the instantaneous interaction energy of three fluctuating dipole moments [92]. It has been widely used in the analysis of three-body phenomena occuring in gases [110], liquids [95], solids [174] and clusters [66, 92].

Energy corrections resulting from the interaction of three multipoles of higher orders, 2^{l_1}, 2^{l_2} and 2^{l_3}, have been derived by R. J. Bell [27] and by M. B. Doran and I. J. Zucker [66]:

$$V_3^{(3)}(a,b,c) \;=\; \sum_{l_1 l_2 l_3} Z_{l_1 l_2 l_3}^{ABC} W_{l_1 l_2 l_3}(a,b,c) \;. \qquad (4.20)$$

The geometrical factors $W_{l_1 l_2 l_3}(a,b,c)$ depend on the size and shape of the triangle formed by the three atoms. The factors $Z_{l_1 l_2 l_3}^{ABC}$ reflect intrinsic electronic properties of the interacting atoms. Upper and lower bounds of two- and three-body multipole coefficients for hydrogen, noble gas, alkali and alkaline earth atoms are given in Refs. [254] and [251].

4.4.5   Asymptotic atom - dimer interaction

We now consider the situation where atom C is located at a great distance from the diatomic molecule AB. This situation differs from the one treated in the previous Section in that the overlap of the atomic orbitals centered on A and B is no longer assumed negligible.

A perturbative analysis of the atom-molecule interaction energy now uses as unperturbed basis functions the products $\varphi_m^{AB}\varphi_k^C$ of molecular orbitals $\varphi_m^{AB}(\mathbf{r}_1, \mathbf{r}_2)$ and atomic orbitals $\varphi_k^C(\mathbf{r}_1)$. The operator of the electrostatic atom-molecule interaction energy can be expanded in a multipole series. The energy correction due to the atom-molecule interaction can be calculated by perturbation theory, using the multipole moments associated with each atomic and each molecular state. A second-order perturbation calculation yields dispersion coefficients $C_n(r,\eta)$, which depend parametrically on the internuclear distance r between A and B, and on the orientation η of the internuclear AB axis with respect to the atom C (in our notation, η is the angle between the two Jacobi vectors). See Refs. [102, 223, 49, 42, 11].

The lowest-order multipole moment of a homonuclear Σ-state diatomic molecule such as Na_2 is the quadrupole moment. The dipole moment is zero because of the geometrical symmetry of the charge density associated with the Σ-state. The multipole moments of an s-state atom all vanish due to

the spherical symmetry of the charge density. In a first-order perturbation calculation, the interaction energy between a homonuclear Σ-state molecule and an s-state atom is therefore zero. In a second-order perturbation calculation, the lowest order correction to the energy is the $1/R^6$ dipole - induced dipole interaction.

The η-dependent atom-molecule dispersion coefficients $C_n(r, \eta)$ can be expressed using spherical dispersion coefficients $C_n^{L0L}(r)$ [267]. The latter are obtained by expanding the atom-molecule interaction potential in Legendre-polynomials (see the Appendix I).[2]

Dispersion coefficients for the long-range Na($3s$) - Na$_2(a^3\Sigma_u^+)$ interaction have been calculated by M. Rérat and B. Bussery-Honvault [228] using a method of dynamic polarizabilities at imaginary frequency. For the Na$_2$ equilibrium distance fixed $r = 5.2$ Å, they have published the values

$$C_6^{000} = 3216 \text{ a.u. }, \qquad C_6^{202} = 997 \text{ a.u. .} \qquad (4.21)$$

The corresponding C_6 coefficients for perpendicular and for linear Na$-$Na$_2$ geometries are [228]:

$$C_6^{\parallel} = C_6^{000} + \frac{1}{\sqrt{5}} C_6^{202} = 3662 \text{ a.u. }, \qquad (4.22)$$

$$C_6^{\perp} = C_6^{000} - \frac{1}{2\sqrt{5}} C_6^{202} = 2993 \text{ a.u. .} \qquad (4.23)$$

We note that their computed value for C_6^{000} is quite similar to the C_6 coefficient (4.16) of the model pairwise-additive surface.

Dispersion coefficients for the Na$-$Na$_2(v, j)$ interaction

In the approach outlined above, the positions of the cores A^+, B^+ and C^+ were assumed fixed, and only the motion of the electrons was treated quantum-mechanically. The atom-molecule dispersion coefficients considered above therefore depend on the distance r between A and B and on the angle η between the two Jacobi vectors $\mathbf{r}$ and $\mathbf{R}$.

In an alternative approach, one might define atom-molecule dispersion coefficients $C_n^{Jv'j'vj}$ describing the asymptotic behaviour of the atom-molecule potential coupling matrix $V_{Jv'j'l'vjl}$ arising from the Arthurs-Dalgarno expansion [14, 204, 152]. The dispersion coefficients $C_n^{Jv'j'vj}$ can be calculated from the r- and η-dependent coefficients, or from the spherical dispersion coefficients C_n^{L0L}, using the vibrational wavefunctions $\chi_{vj}(r)$ of the AB molecule (see the Appendix I).

---

[2]Our notation C_n^{L0L} is consistent with Visser's notation in Ref. [267], where molecule-molecule dispersion coefficients are denoted $C_n^{L_a L_b L}$. In the case where "molecule" b is an S-state atom, we have $L_b = 0$ and $L_a = L$.

4.4.6 Ab initio potential surfaces

The striking feature of the existing *ab initio* potential energy surfaces for spin-aligned alkali trimers [100, 53, 247] are the *strongly attractive non-additive* forces for geometries near the equilateral (D_{3h}) equilibrium configuration. These surfaces are considerably deeper than their pairwise-additive counterparts. The three-body terms for the equilibrium geometries are reported to vary from $\approx 120\%$ for Li to 50% for Cs, compared to the value of the pairwise additive surface [247].

PES by J. Higgins et al.

Historically, the potential energy surface for Na_3 calculated by J. Higgins *et al.* [100] was the first *ab initio* surface for a spin-polarized alkali trimer. N. J. Wright and J. M. Hutson used this potential energy surface in their work on localized anharmonic modes and transition-state spectroscopy of Na_3 [278]. P. Honvault *et al.* used the surface to compute cross-sections for reactive Na + Na_2 collisions at ultralow energies [248, 219].

The *ab initio* potential surface has a global minimum value of -849.37 cm^{-1} at the equilateral triangle geometry with the bond distances at $r = 4.406$ Å, which is much smaller than the equilibrium distance $r_e = 5.2$ Å of the triplet Na_2 potential.

The three-body contribution is unrealistically large for atom - dimer geometries, leading to an atom-molecule van der Waals coefficient C_6 that is roughly four times as large as the calculated values in Eqs. (4.22) and (4.23). This error can be corrected (or at least reduced) by multiplying the three-body term with a smooth switching function [219].

The pairwise additive and the full *ab initio* PES by J. Higgins *et al.* [100] are compared in Figs. 4.3 and 4.4, for perpendicular and for linear configurations.

The full PES for linear configurations is plotted in Fig. 4.4.6 using Johnson's mapping procedure [122]. The three pathways for linear abstraction reactions,

$$
\begin{aligned}
AB + C &\leftrightarrow A + BC \\
BC + A &\leftrightarrow B + CA \\
CA + B &\leftrightarrow C + AB
\end{aligned}
$$
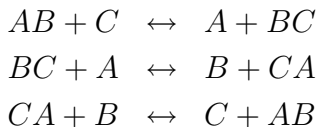
are clearly visible. In Figs. 4.6, 4.7, 4.8 and 4.9, the pairwise additive PES is plotted as a function of only the hyperradius for various nuclear geometries.

Pairwise additive PES
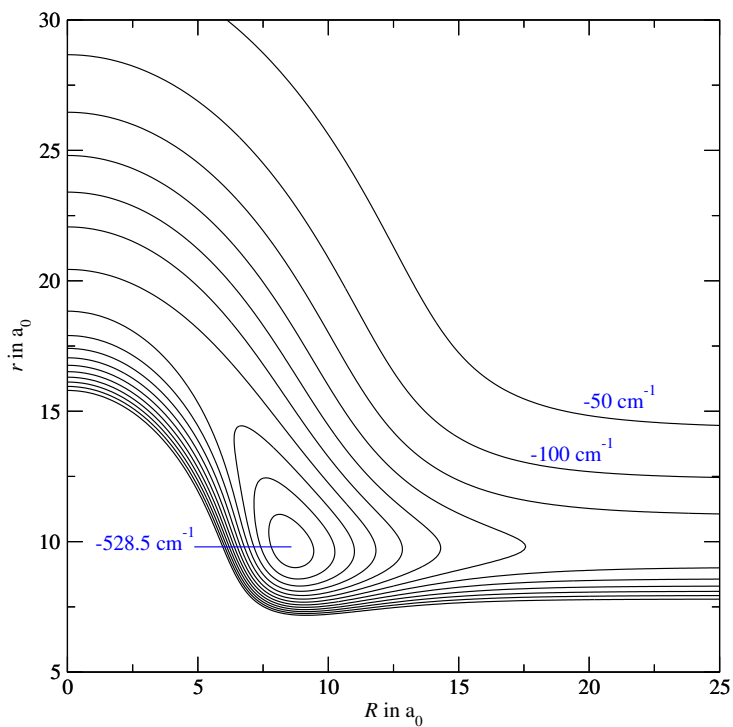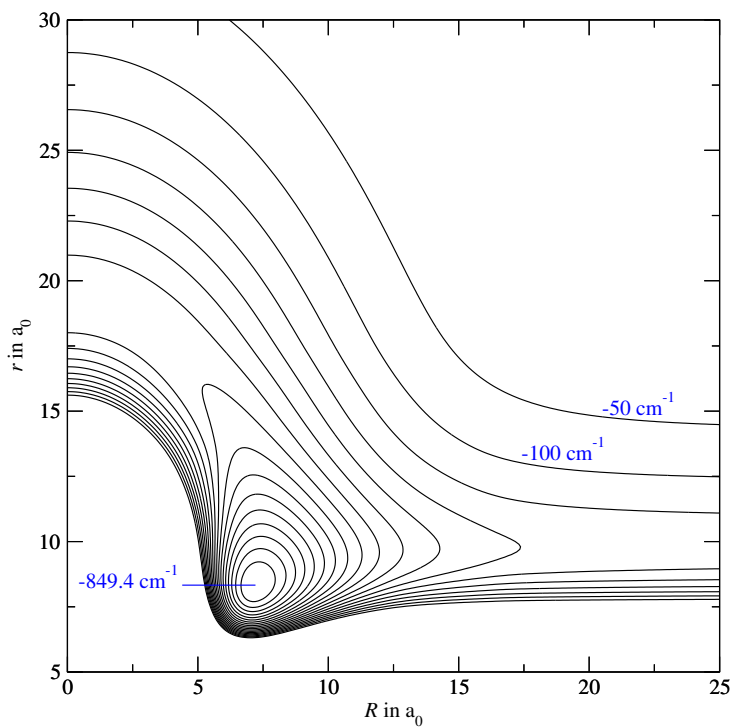
Full PES

Figure 4.3: Potential energy of Na_3 in the $1\ ^4A_2'$ state, for perpendicular geometries. The spacing between equipotential lines is 50 cm^{-1}. *Top:* Pairwise additive PES. The lowest contour (surrounding the well) corresponds to -500 cm^{-1}. *Bottom:* The full PES. The lowest contour corresponds to -800 cm^{-1}.

Pairwise additive PES
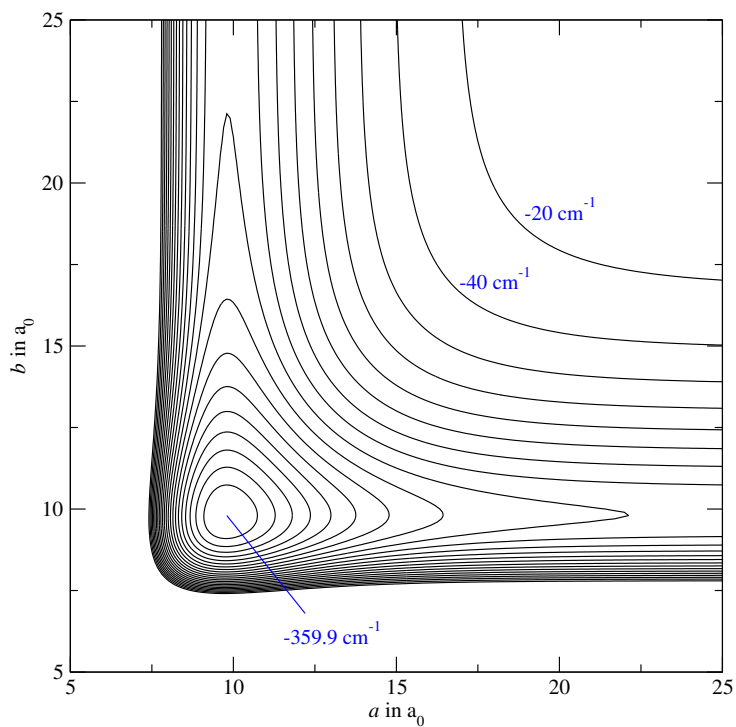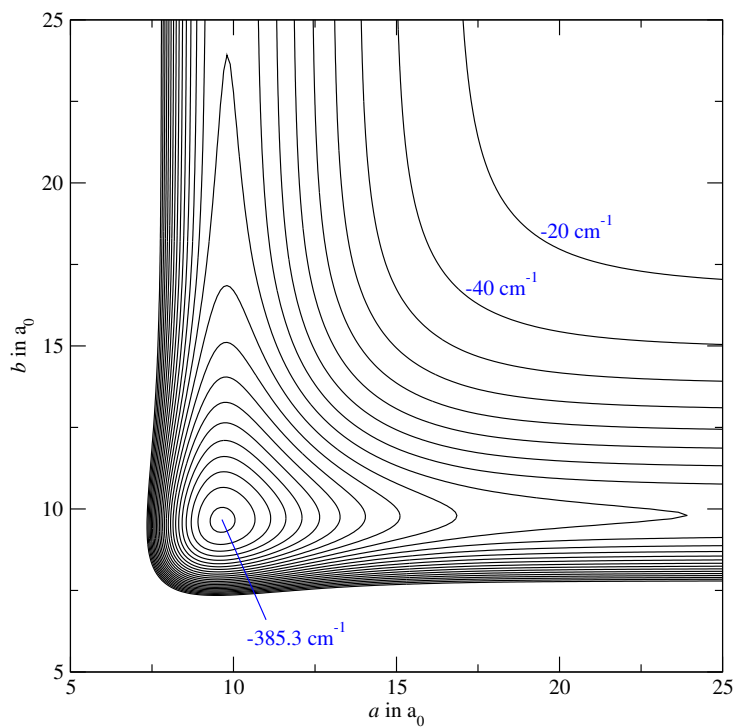
Full PES

Figure 4.4: Potential energy of Na$_3$ in the 1 $^4A'_2$ state, for linear geometries. The spacing between equipotential lines is 20 cm^{-1}. *Top:* Pairwise additive PES. The lowest contour (surrounding the well) corresponds to -340 cm^{-1}. *Bottom:* Full PES. The lowest contour corresponds to -380 cm^{-1}.
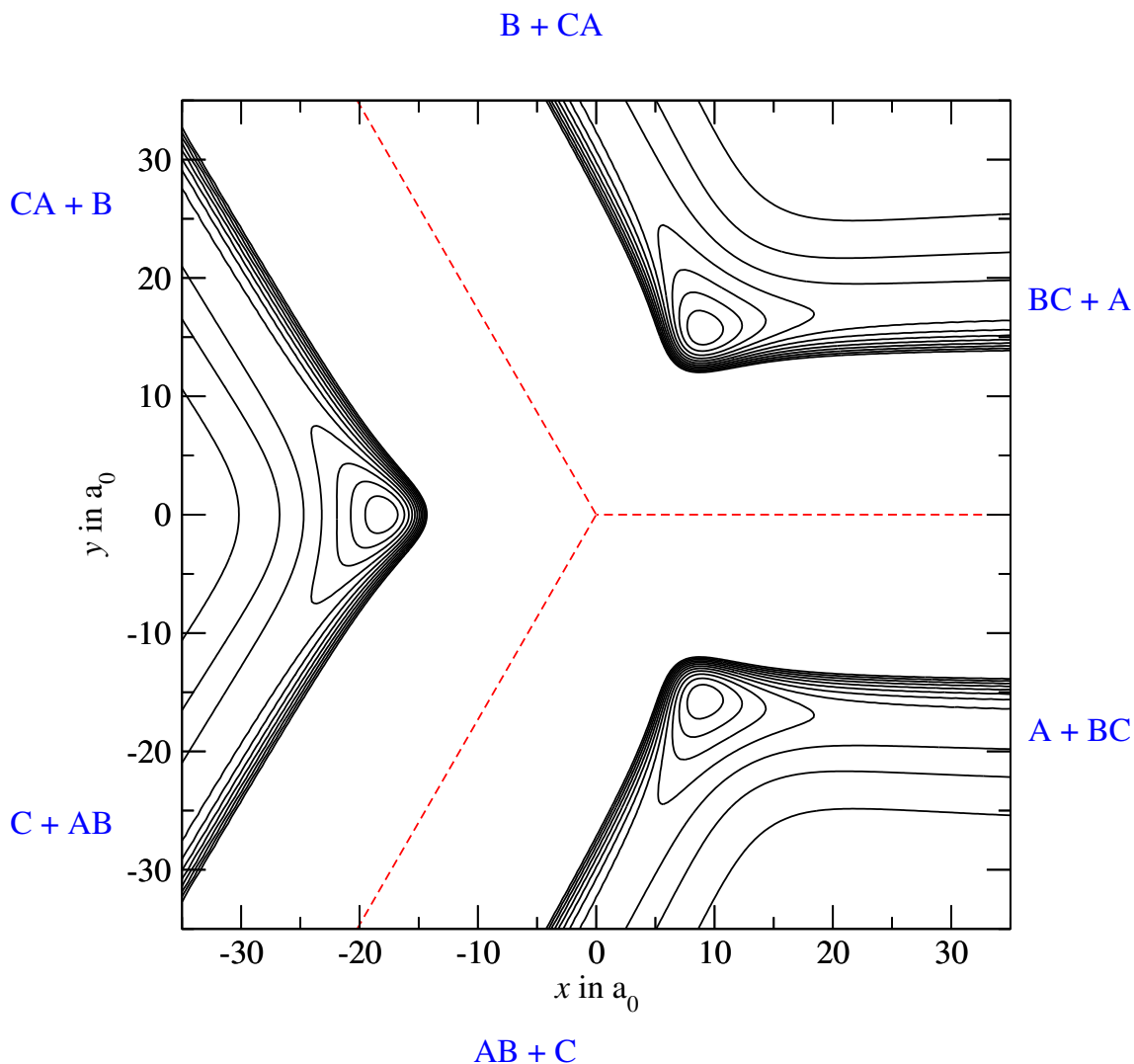
Figure 4.5: Potential energy surface $1^4A_2'$ of Na$_3$ in Johnson's (x, y, z) coordinates, for linear configurations ($z = 0$). The three-body contribution to the potential energy is included. The spacing between the contour lines is 50 cm^{-1}, and the three innermost closed contours correspond to $V = -350$ cm^{-1}. The three minima of $V = -385.3$ cm^{-1} are located at symmetrical configurations with one atom in the middle between the two others. These minima become saddlepoints if the coordinate z is allowed to vary. The three straight dashed lines starting from the origin indicate the configurations in which two atoms are at the same position, and they correspond to infinite potential ridges separating the three potential valleys. The six linear asymptotic geometries ($AB+C$, $A+BC$, $BC+A$, $B+CA$, $CA+B$, and $C+AB$), in which two atoms are at their equilibrium distance and the third atom is far away, are indicated near the corresponding asymptotic regions.
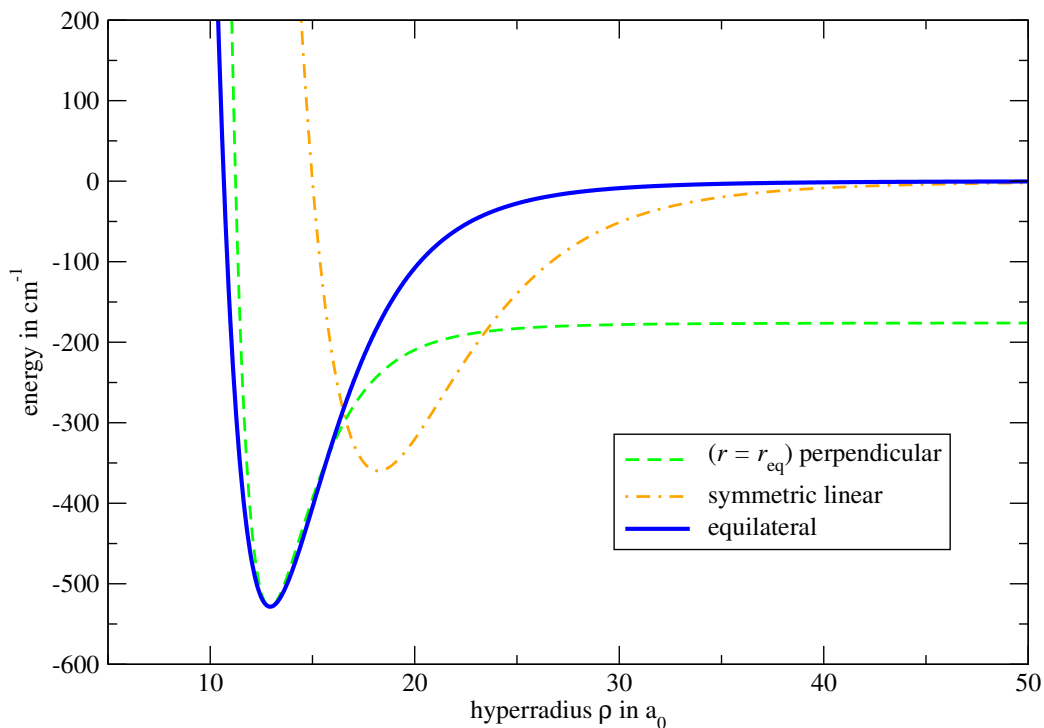
Figure 4.6: Solid line: Pairwise-additive potential energy of Na_3 for D_{3h} symmetry (equilateral triangle). The potential has a global minimum of -528.51 cm^{-1}= -760.41 K at the hyperradius $\rho = 12.932$ a$_0$ = 6.8435 Å, corresponding to the two-body equilibrium distance $r = 9.8265$ a$_0$ = 5.2000 Å. The minimum of the potential, -528.51 cm^{-1}, is three times -176.17 cm^{-1}, the minimum of the two-body triplet potential. As the hyperradius tends to infinity, the three interatomic distances become infinite, and the potential tends to the three-body continuum threshold (chosen as zero).
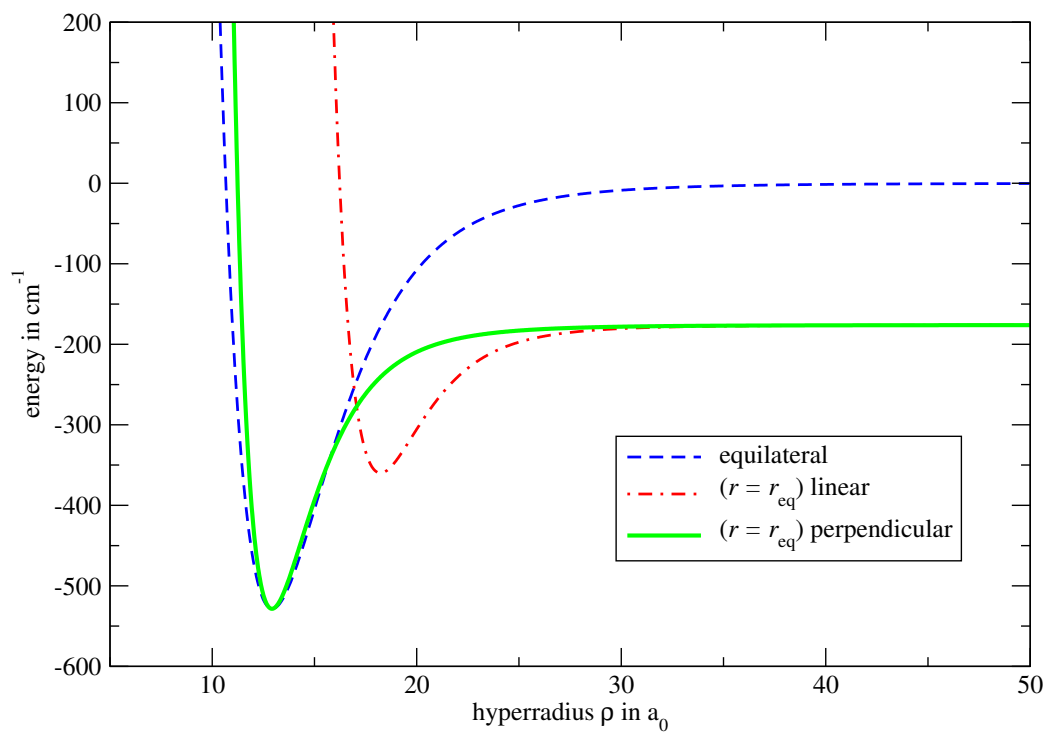
Figure 4.7: Solid line: Pairwise-additive potential energy for perpendicular symmetries C_{2v} and D_{3h}, with atoms B and C at their two-body equilibrium distance $r = 9.8$ $a_0 = 5.2$ Å, and atom A on the perpendicular bisector of the line joining B and C.
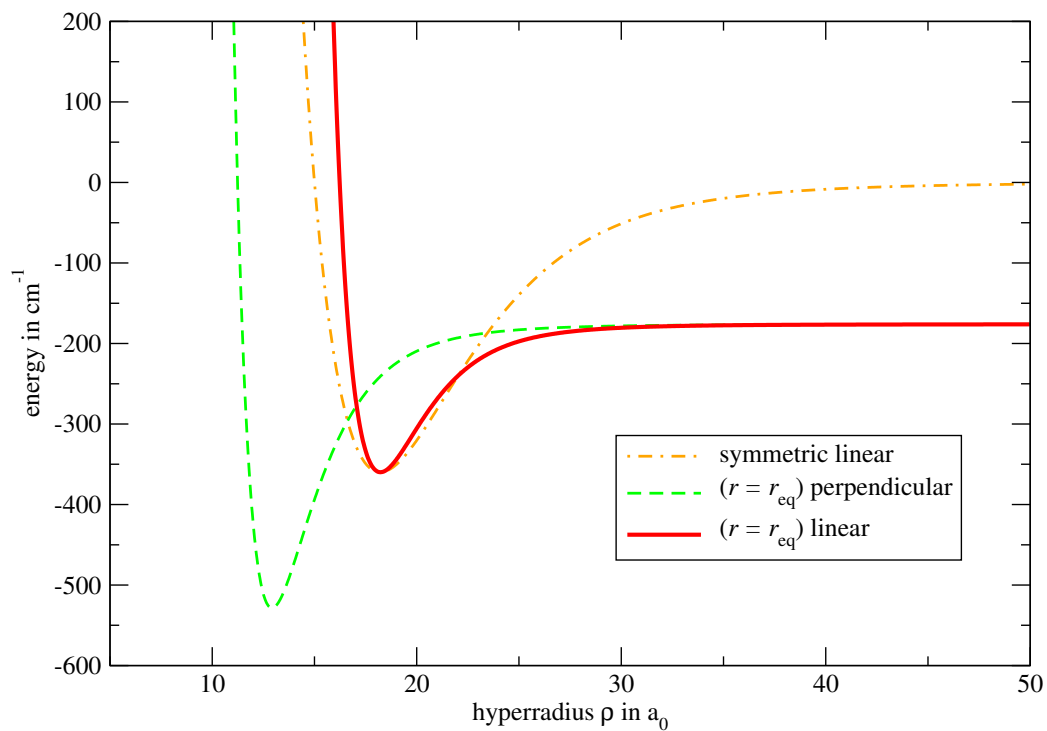
Figure 4.8: Solid line: Pairwise-additive potential energy for linear symmetries $C_{\infty v}$ and $D_{\infty h}$, with atoms B and C at their two-body equilibrium distance $r = 9.8$ a$_0$ = 5.2 Å, and atom A on the internuclear axis of B and C.
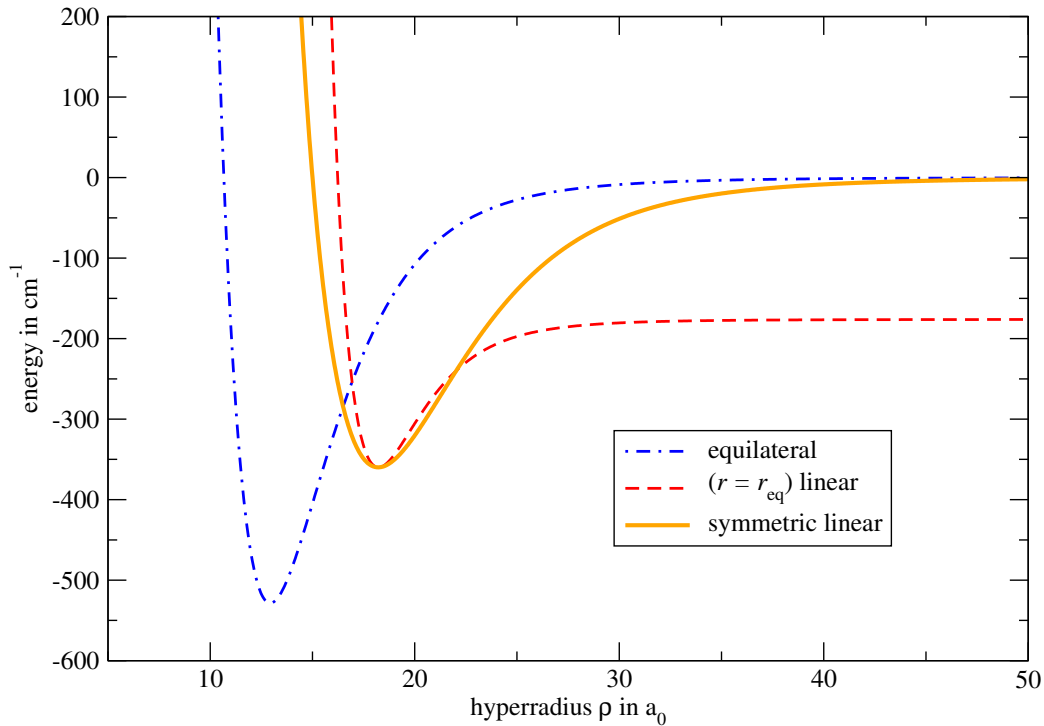
Figure 4.9: Solid line: Pairwise-additive potential energy for $D_{\infty h}$ symmetry (one atom in the middle of the two others).

4.5 Conclusion

We have described the main characteristics of the lowest quartet state of Na_3. The potential energy surface is such that abstraction and insertion reactions are energetically allowed when a sodium atom Na collides with a sodium dimer Na_2, even at very low collisional energies.

In this thesis, we have not considered the hyperfine structure of Na_3. However, hyperfine interactions play a crucial role in ultracold collisions between two alkali atoms [192]. Therefore we expect that effects arising from hyperfine interactions can also be important in Na + Na_2 collisions. It may turn out that the effects are negligible for many purposes, but this ought to be clarified.

Chapter 5

Loosely bound vibrational states of the sodium trimer

The work presented in this Chapter may be seen as an extension of the reactive scattering calculations performed by P. Honvault and J.-M. Launay *et al.* [248], who computed cross-sections for collisions between a sodium atom and a rotating and vibrating sodium dimer:

$$\mathrm{Na} + \mathrm{Na}_2(v, j) \quad \rightarrow \quad \mathrm{Na} + \mathrm{Na}_2(v', j') \ .$$
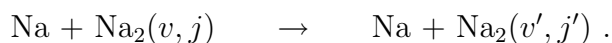
By adapting J.-M. Launay's reactive scattering code, we have computed bound state energies of Na_3 just underneath the threshold at which the Na_3 trimer may dissociate into Na and Na_2. In order to interpret these bound levels, we introduce a short-range phase shift μ which is closely related to the usual asymptotic phase shift δ but is continuous across the bound-continuum threshold. In contrast to true scattering computations, we did not compute any cross-sections.

Throughout this Chapter, the sodium trimer Na_3 is assumed to be in the lowest quartet electronic state $1\,^4A_2'$. Our computations are based on the pairwise-additive potential energy surface, constructed from M. Gutowski's [96] potential energy curve for Na_2 (see Chapter 4). The potential energy surface of this state has no barriers, so that two arbitrary points in the classically allowed region of configuration space can be connected by a path lying entirely in the classically allowed region. As a consequence, a "chemical reaction" may occur if a ground state sodium atom collides with a sodium dimer. The incident atom may replace one of the two atoms in the molecule - even at low scattering energies.

Our computations are limited to the case of zero total angular momentum

$$J \ = \ 0 \ .$$

5.1 The hyperspherical method developed by J.-M. Launay *et al.*

In order to model reactive collisions between an atom and a diatomic molecule, J.-M. Launay *et al.* developed the numerical method known as the hyperspherical diabatic-by-sector method [157, 164, 167]. For each reactive system, a potential energy surface, usually the result of *ab initio* calculations, is used as *input* data. The scattering matrix and state-to-state differential cross-sections are obtained by solving the time-independent Schrödinger equation for the nuclear motion numerically.

Up to now, the method has been used to study the following reactions:

$$
\begin{array}{rcll}
K + K_2 & \rightarrow & K_2 + K & [220] \\
Li + Li_2 & \rightarrow & Li_2 + Li & [59] \\
Na + Na_2 & \rightarrow & Na_2 & [109, 248, 219] \\
S + H_2 & \rightarrow & SH + H & [108, 23] \\
C + H_2 & \rightarrow & CH + H & [45, 17, 21] \\
O + H_2 & \rightarrow & OH + H & [107, 12, 13] \\
N + H_2 & \rightarrow & NH + H & [104, 106, 22] \\
F + D_2 & \rightarrow & DF + D & [103, 186, 105, 106] \\
Ne + H_2^+ & \rightarrow & NeH^+ + H & [111, 112] \\
He + H_2^+ & \rightarrow & HeH^+ + H & [164] \\
H + HCl & \rightarrow & H_2 + Cl & [38] \\
H_2 + Cl & \rightarrow & H + HCl & [159] \\
F + H_2 & \rightarrow & FH + H & [158, 153] \\
H + H_2 & \rightarrow & H_2 + H & [157]
\end{array}
$$
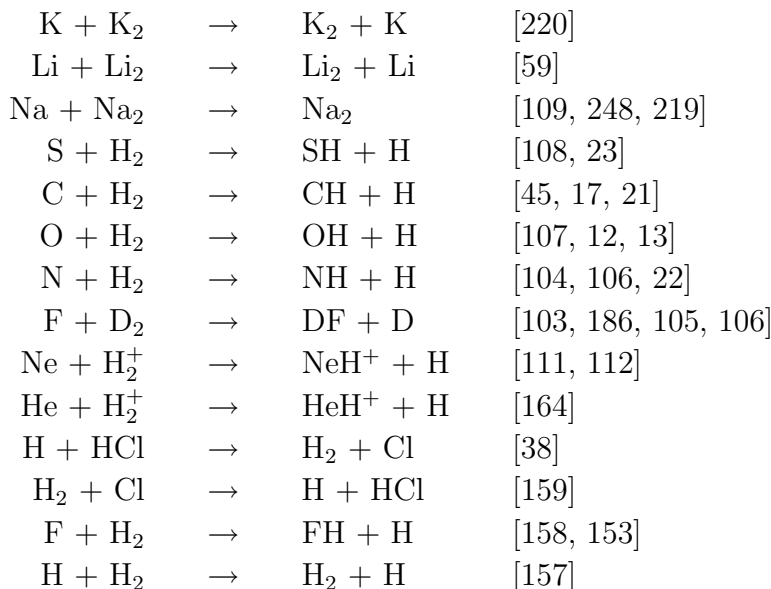
The method can be summarized as follows.

In a first step, the hyperradial kinetic energy operator associated with variations of the hyperradius ρ is *omitted*. The remaining Hamiltonian only involves partial derivative terms in the five hyperangles; we refer to it as the *angular* Hamiltonian. It is the sum of the angular kinetic energy operator and the potential energy. Its eigenfunctions are functions of the five hyperangles. We call them *potiental-adapted* angular basis functions, in order to distinguish them from hyperspherical harmonics. The angular Hamiltonian, its eigenvalues and eigenfunctions, depend parametrically on the hyperradius ρ. The hyperradial axis is divided into small sectors; within each sector, the total wavefunction is expanded in the potential-adapted angular basis functions, leading to a set of second-order coupled hyperradial differential equations.

In the second step, a fixed energy is chosen, and the hyperradial equations are used to propagate a logarithmic derivative matrix along the hyperradius,

100

starting deep in the classically forbidden region, where the three particles are close together, and ending at a large hyperradius. On the hypersphere where the propagation is stopped, the logarithmic derivative matrix is analysed in terms of asymptotic solutions using the Jacobi coordinates of all three arrangements. The matching procedure yields the reactance matrix which can be converted into the scattering matrix and state-to-state cross sections.

Finally, a remark concerning the terminology. In the case where the atoms are identical, it may be argued whether or not it makes sense to speak of a reactive collision.

In calling the scattering process

$$\text{Na} + \text{Na}_2 \quad \rightarrow \quad \text{Na} + \text{Na}_2$$
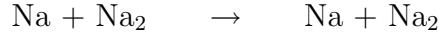
a *reaction*, we simply wish to emphasize that the corresponding scattering wavefunction may, in principle, have an important amplitude in the entire classically allowed region, in all three arrangement valleys.

5.2   Loosely bound vibrational levels of Na$_3$

In the following, our computations of vibrational levels of Na$_3$ are laid out in detail.

Atomic mass

We have used the following numerical value for the mass of the sodium atom:

$$m(^{23}\text{Na}) = m = 41877.8969 \text{ a}_0$$

The corresponding values for the reduced masses are

$$\mu(\text{Na-Na}) = \tfrac{1}{2}\, m = 20938.94845 \text{ a}_0 \ ,$$

$$\mu(\text{Na-Na}_2) = \tfrac{2}{3}\, m = 27918.59793 \text{ a}_0 \ .$$

The corresponding value for the reduced three-body mass of Na$_3$ is

$$\mu(\text{Na}_3) = \sqrt{\tfrac{1}{3}}\, m = 24178.21505 \text{ a}_0 \ .$$

5.2.1   Born-Oppenheimer approximation

The Born-Oppenheimer approximation [236] is adopted to separate the motion of the "slow" nuclei from the motion of the "fast" electrons.

The wavefunction of Na$_3$ is written as the product of a nuclear wavefunction $\psi^{(\text{nuc})}$ and an electronic wavefunction $\psi^{(\text{el})}$,

$$\psi(A, B, C, 1, 2, 3) \ = \ \psi^{(\text{nuc})}(A, B, C)\psi^{(\text{el})}(A, B, C; 1, 2, 3) \ , \qquad (5.1)$$

where (A, B, C) and $(1, 2, 3)$ are the nuclear and the electronic coordinates, respectively. The electronic wavefunction $\psi^{(el)}$ depends parametrically on the nuclear coordinates A, B, and C.

5.2.2 Symmetry of the wavefunction

The spin of a single ^{23}Na nucleus is $i = 3/2$. The spin of the electron is $s = 1/2$. Both particles are fermions.

The ^{23}Na atom consists of the nucleus and eleven electrons: it is a boson.

The complete wavefunction $\psi(A, B, C, 1, 2, 3)$ must therefore be *antisymmetric* with respect to any permutation of two nuclei ($A \leftrightarrow B$ or $B \leftrightarrow C$ or $C \leftrightarrow A$) and with respect to any permutation of two electrons ($1 \leftrightarrow 2$ or $2 \leftrightarrow 3$ or $3 \leftrightarrow 1$).

We neglect any effects linked to spin-orbit coupling, and we restrict our study to the spin-stretched states, where the nuclear and electronic spins are "parallel". The nuclear function $\psi^{(nuc)}$ and the electronic function $\psi^{(el)}$ then factorize each into a spin (χ) and an orbital (φ) function :

$$\psi^{(nuc)}(A, B, C) = \chi^{(nuc)}(A, B, C)\, \varphi^{(nuc)}(A, B, C) , \qquad (5.2)$$
$$\psi^{(el)}(A, B, C; 1, 2, 3) = \chi^{(el)}(1, 2, 3)\, \varphi^{(el)}(A, B, C; 1, 2, 3) . \qquad (5.3)$$

The nuclear spin function $\chi^{(nuc)}(A, B, C)$ is completely symmetric under permutations of the nuclear coordinates (A, B, C) and is characterized by the total nuclear spin quantum number

$$I = I_{max} = 3/2 + 3/2 + 3/2 = 9/2 . \qquad (5.4)$$

The electronic spin function $\chi^{(el)}(1, 2, 3)$ is completely symmetric under permutations of the electronic coordinates $(1, 2, 3)$ and is characterized by the total electronic spin quantum number

$$S = S_{max} = 1/2 + 1/2 + 1/2 = 3/2 . \qquad (5.5)$$

$\chi^{(el)}(1, 2, 3)$ is refered to as the quartet spin function, since its degeneracy is $2S + 1 = 4$. The complete spin function is the product of $\chi^{(nuc)}$ and $\chi^{(el)}$:

$$\chi(A, B, C, 1, 2, 3) = \chi^{(nuc)}(A, B, C)\, \chi^{(el)}(1, 2, 3) ; \qquad (5.6)$$

it is characterized by the total spin quantum number $F = 6$:

$$F = F_{max} = I_{max} + S_{max} = 9/2 + 3/2 = 6 . \qquad (5.7)$$

Hence the total wavefunction factorizes into a spin function and an orbital function:

$$\begin{aligned} \psi(A, B, C, 1, 2, 3) &= \chi^{(nuc)}(A, B, C)\, \chi^{(el)}(1, 2, 3) \ \times \\ &\times \ \varphi^{(nuc)}(A, B, C)\, \varphi^{(el)}(A, B, C; 1, 2, 3) . \end{aligned} \qquad (5.8)$$

In the following, we assume that $\varphi^{(\mathrm{el})}(A, B, C; 1, 2, 3)$ is the orbital of the $1^4A_2'$ electronic state of Na_3 (see Chapter 4). This state changes sign when two nuclei are permuted. This can easily be seen for the situation of equilateral geometry, where the electronic wavefunction is a basis of the A_2' representation of the D_{3h} point group. Therefore the wavefunction $\varphi^{(\mathrm{nuc})}(A, B, C)$ describing the relative motion of the nuclei must be *symmetric* as to ensure that the total wavefunction $\psi(A, B, C, 1, 2, 3)$ is *antisymmetric* under permutations of the nuclei.[1].

The potential energy surface $V(A, B, C)$ associated with the $1^4A_2'$ state (see Chapter 4) is used as input data for the calculations concerning the nuclear motion. The electronic wavefunction $\varphi^{(\mathrm{el})}(A, B, C; 1, 2, 3)$ itself does not appear in the scattering calculations.

5.2.3 Coordinates and the Hamiltonian

The positions of the nuclei A, B, and C in the centre-of-mass frame are indicated using the modified form of Smith-Whitten coordinates defined in Ref. [157]. These coordinates consist of the hyperradius ρ describing the size of the ABC triangle and two hyperangles θ and ϕ describing its shape (see Chapter 3).

The complete expression for the Hamiltonian can be found in Ref. [157]. The kinetic energy operator is also derived in the Appendix F. Its complete form is not needed here, because our calculations are restricted to the case of zero total orbital angular momentum, $J = 0$. In this case the wavefunction does not depend on the Euler angles, and the rotational and Coriolis coupling terms in the Hamiltonian can be omitted. Only the vibrational part must be retained.

We write the nuclear orbital wavefunction as

$$\varphi^{(\mathrm{nuc})}(A, B, C) \equiv \varphi(\rho, \theta, \phi) .$$

We shall omit the label "nuc" on φ, as there is no risk of confusion.

The Hamiltonian for $J = 0$ is given by

$$\hat{H} = -\frac{\hbar^2}{2\mu} \frac{1}{\rho^5} \frac{\partial}{\partial\rho} \rho^5 \frac{\partial}{\partial\rho} + \frac{\hbar^2}{2\mu} \hat{\Lambda}_0^2 + V(\rho, \theta, \phi) \tag{5.9}$$

---

[1]This can also be seen by considering the asymptotic limit of three separated atoms. The nuclear wavefunction then describes the motion of three bosonic atoms, and therefore it is clear that it has to be symmetric. The statement that the nuclear wavefunction is symmetric when the nuclei are fermions may seem contradictory but is readily explained by the fact that the electronic wavefunction depends parametrically on the nuclear coordinates.

where μ is the three-body reduced mass, V is the potential energy, and $\hat{\Lambda}_0^2$ is the square of the grand angular momentum operator for $J = 0$:

$$\hat{\Lambda}_0^2 \;\; = \;\; -\frac{4}{\sin 2\theta}\frac{\partial}{\partial\theta}\sin 2\theta\frac{\partial}{\partial\theta} - \frac{1}{\cos\theta}\frac{\partial^2}{\partial\phi^2} \;. \tag{5.10}$$

As discussed in Chapter 3, $\hat{H}$ takes the form

$$\hat{H} \;\; = \;\; -\frac{\hbar^2}{2\mu}\frac{1}{\rho^5}\frac{\partial}{\partial\rho}\rho^5\frac{\partial}{\partial\rho} + \hat{H}^{(\mathrm{ang})}(\rho)$$

where $\hat{H}^{(\mathrm{ang})}(\rho)$ is the ρ-dependent angular Hamiltonian

$$\hat{H}^{(\mathrm{ang})}(\rho) \;\; = \;\; \frac{\hbar^2}{2\mu}\hat{\Lambda}_0^2 + V(\rho,\theta,\phi) \;. \tag{5.11}$$

Our task is to solve the stationary Schrödinger equation for a fixed energy E:

$$\left[-\frac{\hbar^2}{2\mu}\frac{1}{\rho^5}\frac{\partial}{\partial\rho}\rho^5\frac{\partial}{\partial\rho} + \hat{H}^{(\mathrm{ang})}(\rho)\right]\varphi(\rho,\theta,\varphi) \;\; = \;\; E\,\varphi(\rho,\theta,\varphi) \;. \tag{5.12}$$

5.2.4   Adiabatic angular basis functions

We refer to the eigenfunctions $\varphi_k^{(\mathrm{ang})}(\rho;\theta,\varphi)$ $(k = 1, 2, 3, \ldots)$ of the angular Hamiltonian (5.11) as *adiabatic* angular basis functions. They depend parametrically on the hyperradius ρ, and they are solutions of the ρ-dependent angular Schrödinger equation

$$\hat{H}^{(\mathrm{ang})}(\rho)\varphi_k^{(\mathrm{ang})}(\rho;\theta,\phi) \;\; = \;\; \epsilon_k(\rho)\varphi^{(\mathrm{ang})}(\rho;\theta,\phi) \;. \tag{5.13}$$

Fig. 5.1 shows the lowest 157 computed eigenvalues

$$\epsilon_k^{(\mathrm{ang})}(\rho) \qquad (k = 1, \ldots, 157)$$

as functions of the hyperradius ρ (thin black lines). At large hyperradius $(\rho \to \infty)$ each eigenvalue $\epsilon_k^{(\mathrm{ang})}(\rho)$ tends to a distinct vibrational-rotational energy $E(v, j)$ of the diatomic molecule $Na_2(v, j)$ where v is the vibrational index, j is the rotational index. We did not compute any curves with asymptotic limits *above* the threshold for break-up into three free sodium atoms. The lowest curve $\epsilon_1^{(\mathrm{ang})}(\rho)$ tends to the energy $E(v = 0, j = 0)$ of the vibrational-rotational ground state $Na_2(v{=}0,\, j{=}0)$. The dashed line and the dot-dashed line in the figure are the pairwise-additive potential energy V, for two different geometries:
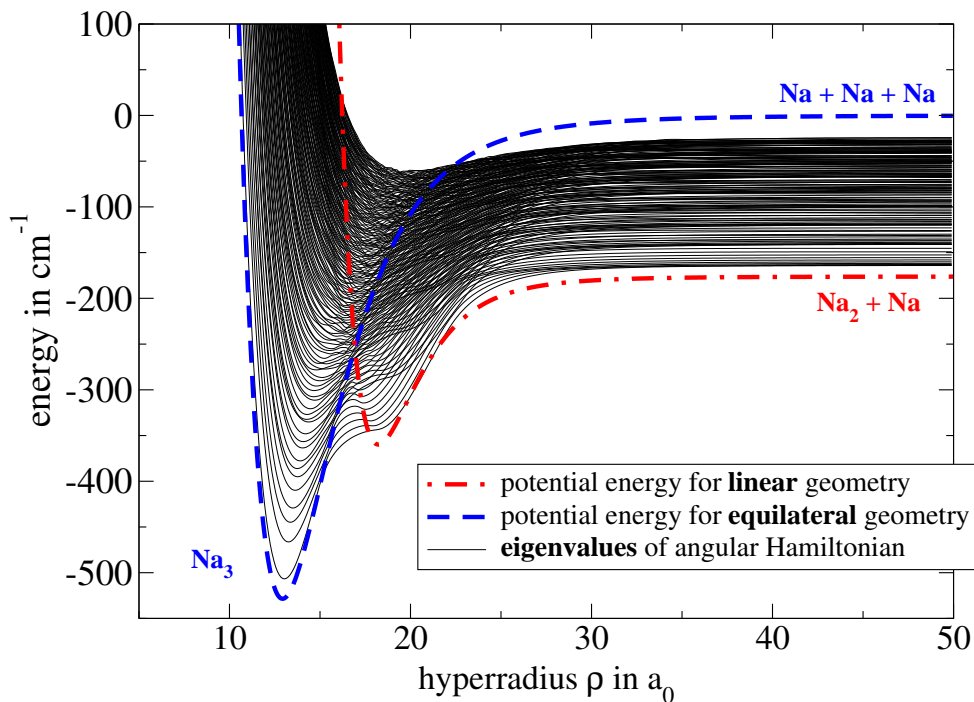
Figure 5.1: Potential energy curves and ρ-dependent eigenvalues of the angular Hamiltonian for $^{23}\text{Na}_3(1^4A_2')$ resulting from the pairwise-additive potential energy surface. Thick dashed line: Potential energy for equilateral triangle geometry D_{3h}. Thick dot-dashed line: Potential energy for linear geometry $C_{\infty v}$ with two atoms kept at their equilibrium distance $r_{\text{eq}} = 9.8$ a_0. Thin solid lines: The lowest 157 eigenvalues $\epsilon_k(\rho)$ $(k = 1, \ldots, 157)$.
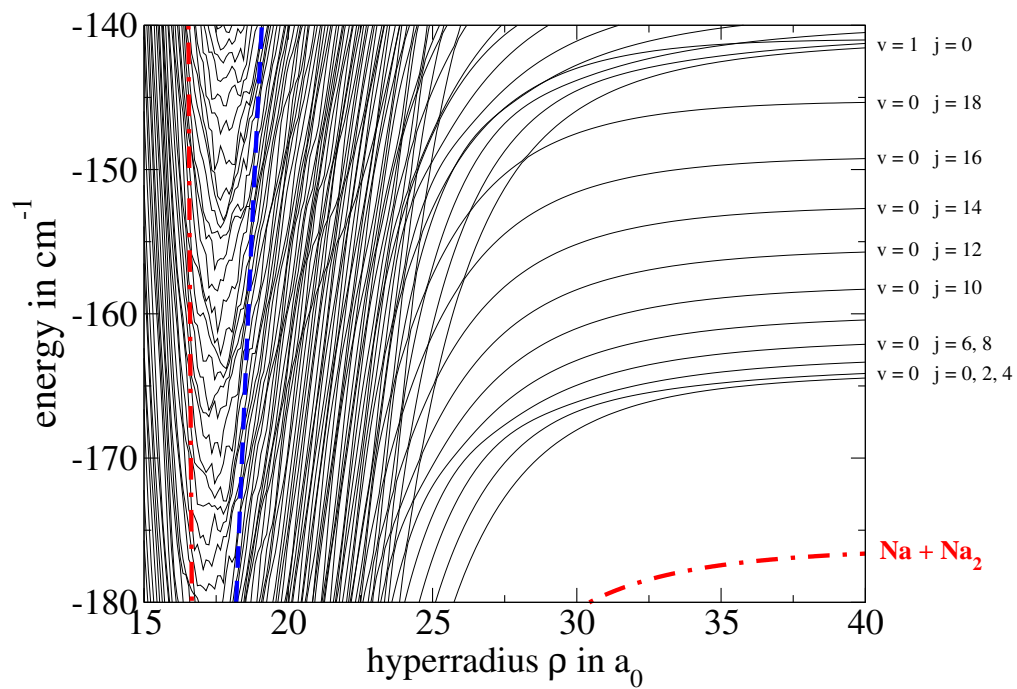
Figure 5.2: Close-up of Fig. 5.1. The lowest adiabatic curve dissociates to the Na + Na$_2$($v = 0, j = 0$) threshold.

- The dashed line indicates the potential energy for the geometry in which the three sodium atoms form an equilateral triangle. As ρ tends to infinity, this curve tends to the three-body dissociation limit, chosen as the zero in energy and equal to the energy of three separated ground state sodium atoms at rest.

- The dot-dashed line indicates the potential energy for the linear geometries in which two atoms remain together, separated by the atom-atom equilibrium distance $r_e = 9.834$ a$_0$. As $\rho \to \infty$, this curve tends to the miniumum -176.173 cm^{-1} of the atom-atom interaction potential (see Chapter 4).

Formally, the nuclear wavefunction $\varphi(\rho, \theta, \varphi)$ can be expanded at each hyperradial distance ρ in the set of adiabatic basis functions $\varphi_k^{(\text{ang})}(\rho; \theta, \varphi)$:

$$\varphi(\rho, \theta, \varphi) = \frac{1}{\rho^{5/2}} \sum_{k=1}^{\infty} \varphi_k^{(\text{ang})}(\rho; \theta, \phi) u_k(\rho) . \tag{5.14}$$

For numerical purposes, the infinite series in the above equation must be truncated at a finite value N. The Schrödinger equation (5.12) then takes the form of a system of N coupled second-order differential equations for the hyperradial functions $u_k(\rho)$:

$$-\frac{\hbar^2}{2\mu} \sum_{k=1}^{N} \langle \varphi_{k'}^{(\text{ang})}(\rho) | \left[\left(\frac{\partial^2}{\partial \rho^2} - \frac{15}{4\rho^2} \right) | \varphi_k^{(\text{ang})}(\rho) \rangle \, u_k(\rho) \right] = [E - \epsilon_{k'}(\rho)] \, u_{k'}(\rho) , \tag{5.15}$$

where the bracket notation $\langle \ldots | \ldots \rangle$ indicates the scalar product in the space of functions of the hyperangles:

$$\langle a|b \rangle \equiv \int_0^{\pi/2} d\theta \, \sin 2\theta \int_0^{2\pi} d\phi \, a^*(\theta, \phi) \, b(\theta, \phi) .$$

Using the product rule of differentiation, the coupled hyperradial equations (5.15) can be rewritten as

$$\left[\frac{\partial^2}{\partial \rho^2} - \frac{15}{4\rho^2} + \frac{2\mu}{\hbar^2} [E - \epsilon_{k'}(\rho)] \right] u_{k'}(\rho) + \sum_{k=1}^{N} \left[2P_{k'k}(\rho) \frac{\partial}{\partial \rho} + Q_{k'k}(\rho) \right] u_k(\rho) = 0 . \tag{5.16}$$

The non-adiabatic terms $P_{k'k}$ and $Q_{k'k}$ can be arranged in two matrices, $\mathbf{P}$ and $\mathbf{Q}$, the elements of which are given by

$$P_{k'k}(\rho) = \left\langle \varphi_{k'}^{(\text{ang})}(\rho) \left| \frac{\partial \varphi_k^{(\text{ang})}}{\partial \rho}(\rho) \right. \right\rangle , \tag{5.17}$$

$$Q_{k'k}(\rho) = \left\langle \varphi_{k'}^{(\text{ang})}(\rho) \left| \frac{\partial^2 \varphi_k^{(\text{ang})}}{\partial \rho^2}(\rho) \right. \right\rangle . \tag{5.18}$$

P and **Q** have certain symmetry properties, because the angular Hamiltonian $\hat{H}^{(\mathrm{ang})}$ is hermitian.[2]

Unfortunately, the non-adiabatic terms (5.17) and (5.18) are difficult to evaluate numerically. It is clear that they may vary rapidly in the vicinity of each avoided crossing between any pair of adiabatic potential curves $\epsilon_k(\rho)$ and $\epsilon_{k+1}(\rho)$. We have therefore not attempted to solve the coupled equations (5.16) numerically.

An alternative to the adiabatic angular basis could be a constant, ρ–independent basis set, consisting of hyperspherical harmonics, for example. However, a constant basis is not well-adapted either, because the shape of the classically allowed region varies with the hyperradius. A very large number of angular basis functions would be needed in order to represent the angular wavefunction accurately at *all* hyperradial distances.

The choice of angular basis set will be further discussed in Sec. 5.2.10.

5.2.5 Sector basis functions

The diabatic-by-sector method developed by J.-M. Launay *et al.* can be seen as a compromise between an adiabatic and a constant basis set. In this method, the hyperradial axis is divided into small adjoining sectors, and a potential-adapted *constant* basis set is used within each sector.

In our calculations, the range 8.2 $a_0 < \rho < 50.0$ a_0 on the hyperradial axis is divided into 297 sectors $[a_p, b_p]$ $(p = 1, \ldots, 297)$ such that $b_p = a_{p+1}$. The sector midpoints are denoted $c_p = (a_p + b_p)/2$. The angular Schrödinger equation (5.13) is solved for each distance $\rho = c_p$ through a variational expansion of $\varphi_k^{(\mathrm{ang})}(c_p; \theta, \phi)$ in a large primitive basis of symmetry-adapted hyperspherical harmonics with zero total angular momentum $J = 0$, yielding a set of $N = 135$ eigenfunctions $\varphi_k^{(\mathrm{ang})}(c_p; \theta, \phi)$ and eigenvalues $\epsilon_k(c_p)$ $(k = 1, ..., N)$. The hyperspherical harmonics retained in the primitive basis set are of even parity, and they are fully symmetric with respect to the permutation of two nuclei.

We have not performed any convergence tests, since these had already been carried out by P. Honvault and J.-M. Launay [248]. However, our

---

[2]Differentiation of the identity

$$0 = \left\langle \varphi_{k'}^{(\mathrm{ang})}(\rho) \middle| \varphi_k^{(\mathrm{ang})}(\rho) \right\rangle$$

with respect to ρ gives

$$0 = P_{kk'}^*(\rho) + P_{k'k}(\rho)$$

$$\text{and} \qquad 0 = Q_{kk'}^*(\rho) + Q_{k'k}(\rho) + 2 \left\langle \frac{\partial \varphi_{k'}^{(\mathrm{ang})}}{\partial \rho}(\rho) \middle| \frac{\partial \varphi_k^{(\mathrm{ang})}}{\partial \rho}(\rho) \right\rangle .$$

results for weakly bound levels (see Sec. 5.2.9) prove *a posteriori* that the potential-adapted angular basis set $\{\varphi_k^{(\text{ang})}, k = 1, \ldots, 135\}$ is converged and sufficiently large.

For other reactive systems, J.-M. Launay *et al.* have also performed scattering calculations for non-zero angular momentum, using angular basis functions with $J > 0$. In this case each angular basis function was a product of a symmetrical top function of definite parity and a primitive two-dimensional angular basis function [157]). We note that these ($J > 0$) angular basis functions are *not* hyperspherical harmonics, and they lead to rotational and Coriolis coupling terms.

5.2.6 Estimation of the level density

Before we proceed in our description of the diabatic-by-sector method, we shall briefly describe how we obtained a first estimate for the total number of bound states and of the level distribution in energy.

The non-adiabatic terms $\mathbf{P}$ and $\mathbf{Q}$ in the coupled hyperradial differential equations (5.16) cannot be neglected if the equations are to be solved correctly. However, by ignoring them, one can easily calculate bound levels for each adiabatic potential curve $\epsilon_k(\rho)$ and thus obtain an estimate for the total number of bound states and for their distribution in energy. Such an estimate is based on the assumption (which may be false!) that the non-adiabatic terms induce shifts of the level positions, to lower and to higher energies, but do not significantly alter the density of states.

The hyperradial Schrödinger equation associated with the k-th adiabatic curve is

$$-\frac{\hbar^2}{2\mu}\left(\frac{d^2}{d\rho^2} - \frac{15}{4\rho^2}\right) u_k(\rho) + \epsilon_k(\rho)u_k(\rho) \;=\; E\,u_k(\rho)\ . \qquad (5.19)$$

We recall that at large hyperradial distance ($\rho \to \infty$), each curve $\epsilon_k(\rho)$ tends to a distinct asymptotic energy. The asymptotic energies of the curves used in our computation ($k \leq 135$) all lie below the (Na + Na + Na) threshold to three-body break-up. Each curve therefore tends to a different vibrational-rotational level $E_{v,j}$ of an isolated $Na_2(v,j)$ diatomic molecule in the $a\,^3\Sigma_u^+$ electronic state. The lowest curve $\epsilon_1(\rho)$ tends to the Na + $Na_2(v{=}0,\ j{=}0)$ dissociation threshold.

If the non-adiabatic couplings between the adiabatic hyperangular basis functions $\varphi_k^{(\text{ang})}$ were negligible, the Na_3 complex would posess true bound states *above* the Na + $Na_2(v{=}0,\ j{=}0)$ dissociation threshold. However, due to the strong non-adiabatic coupling, there can be no such states. All true bound states lie *below* the Na + $Na_2(v{=}0,\ j{=}0)$ threshold. Above this threshold, there may only be meta-stable states, corresponding to a temporarily bound triatomic complex that will eventually decay into an Na atom and an

Na$_2$ dimer.

Neglecting all non-adiabatic couplings, we have calculated for each adiabatic potential curve $\epsilon_k(\rho)$ ($k = 1, \ldots, 135$) a discrete set of vibrational energies by solving Eq. (5.19) numerically using the Mapped Fourier Sine Grid described Chapter 2. The grid extended from $\rho_{\min} = 8.2$ a$_0$ to $\rho_{\max} = 50.0$ a$_0$. The numerical values of the k-th adiabatic potential curve $\epsilon_k(\rho)$ on the grid were obtained from the values of $\epsilon_k(\rho)$ in the sector midpoints ($\rho = c_1, \ldots, c_{297}$) by a cubic spline interpolation. We could have avoided the spline interpolation by choosing sector midpoints c_p as grid points. However, for our purpose, this would not have made any difference, since we were interested only in a first rough estimate of the level distribution and did not aim at achieving the highest possible accuracy.

Considering as *bound* only those levels with energies below the Na + Na$_2$(v=0, j=0) dissociation threshold, we found that only the lowest 69 curves support any bound levels. For the lowest curve, $\epsilon_1(\rho)$, we obtained 31 levels. For the 69th curve, which dissociates to the Na + Na$_2$($v = 2, j = 28$) threshold, we found only one bound level. We have counted a total of 640 bound vibrational levels, 13 of which have binding energies less than 1 cm^{-1}. The computed energies of *all* the 640 levels are shown in Figure 5.3.

Due to the finite size of the grid, only the states with classical turning points lying well within the borders of the grid could be calculated. The true density of states of our pairwise-additive model potential surface may therefore be greater than the computed one.

Another important numerical error arises from the choice of the grid step. In order to keep the calculations simple, we defined the grid step using the mapping procedure oulined in Ref. [276]. At short distances, up to the equilibrium distance of the lowest potential curve, the grid step was chosen constant. At larger distances, the grid step was chosen proportional to the local de Broglie wavelength

$$2\pi \left(\frac{2\mu}{\hbar^2} [E_{\max} - \epsilon_1(\rho)] - \frac{15}{4\rho^2} \right)^{-1/2} \tag{5.20}$$

associated with the lowest adiabatic curve $\epsilon_1(\rho)$ where $E_{\max}$ is a fixed energy above the atom-diatom threshold. The grid step thus defined was large compared to the many sharp variations of the adiabatic hyperradial potential curves $\epsilon_k(\rho)$ ($k = 1, 2, 3, \ldots$). We recall that the adiabatic curves are not very smooth due to the large number of narrowly avoided crossings (see Fig. 5.1). The computed level positions may therefore be quite inaccurate. However, we may hope that this error does not too much influence the resulting density of states.

Clearly the Mapped Fourier Grid method is not well suited for solving the coupled hyperradial equations (5.16) accurately, since the grid step would

(a)

(b)
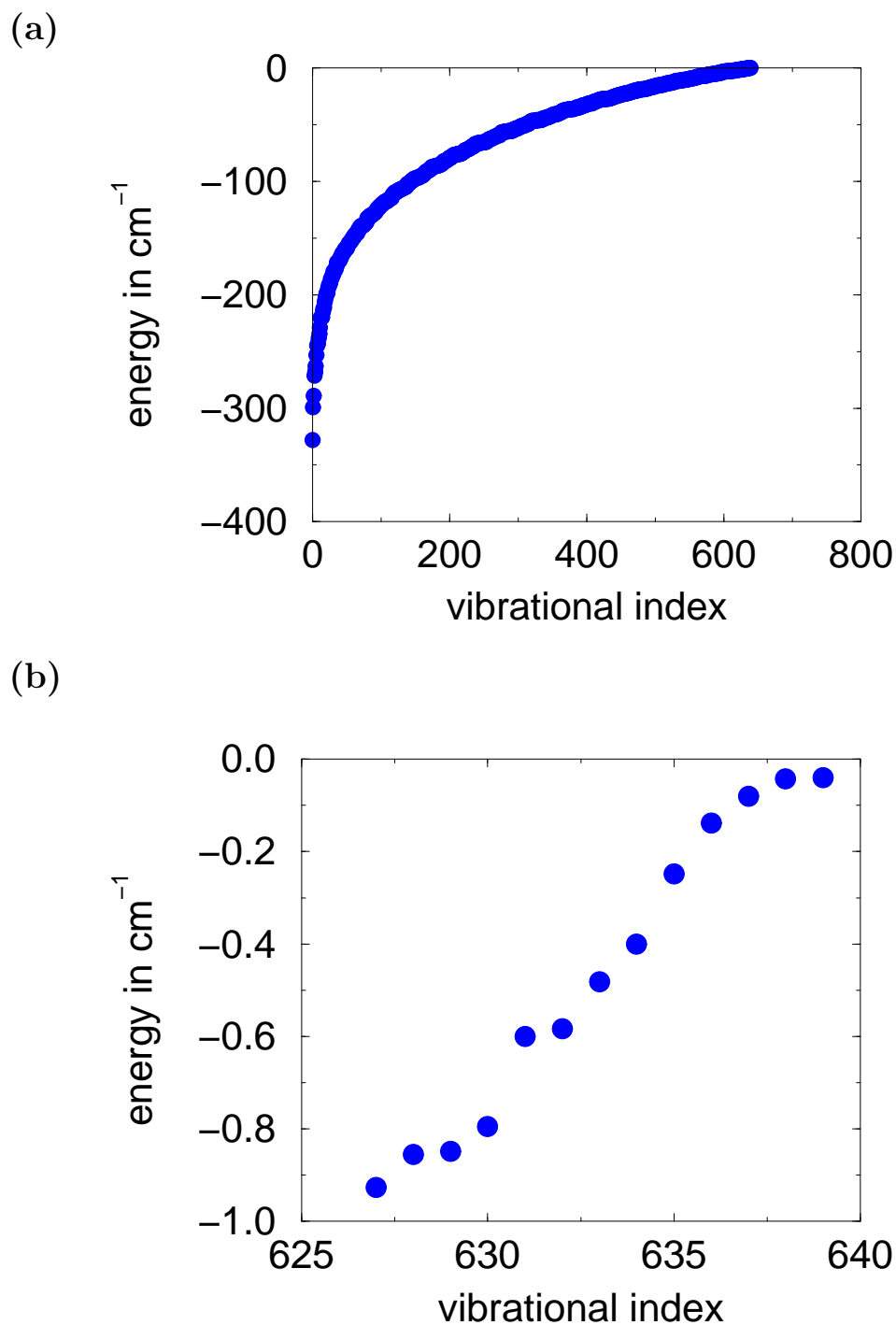
Figure 5.3: Calculated vibrational level positions of Na_3, using the hyperspherical adiabatic approximation. The zero in energy corresponds to the $Na_2(v = 0, j = 0) + Na$ dissociation threshold. The energies were computed using a Mapped Fourier Grid covering the interval 8.2 a.u. $\leq \rho \leq$ 50.0 a.u. **(a)** All computed levels. **(b)** Zoom on the levels near threshold.

have to be adapted to the sharp features of the adiabatic potential curves and the non-adiabatic terms. In the mapped grid method described in Ref. [276], the grid step is not much shorter than half the local de Broglie wavelength, but it would have to be much shorter in the present case. We believe that numerical methods involving shorter steps, such as finite difference methods, would be better adapted.

In spite of all the shortcomings of the present method, it turns out that our first estimate of the level density agrees very well with results obtained by a much more accurate approach (see Sec. 5.2.9).

Our estimate ought to be compared with numerical results by J. Wright and J. M. Hutson [278], who computed 900 bound states of Na_3 using a DVR technique. Their computations are based on the potential energy surface by J. Higgins *et al.* [100], which incorporates the three-body contribution. Unfortunately Wright's and Hutson's published results cannot be compared directly to ours, because the 900 levels they computed comprise states of all symmetries, whereas the states we computed are all of bosonic symmetry. Furthermore, the potential energy surface they used is considerably deeper than the pairwise additive surface we used.

In order to predict the true density of states of Na_3, our computations would need to be redone using a more realistic potential surface. The realistic surface must include a three-body term with the correct asymptotic behaviour. Such a surface could be modelized by introducing a damping function in order to reduce the three-body term at large hyperradii using the method by G. Quémener *et al.* [219]. Furthermore, the grid ought to be extended to a larger hyperradius.

5.2.7 Coupled hyperradial equations in the sector method

In each sector $[a_p, b_p]$ $(p = 1, \ldots, 297)$ on the ρ hyperradial axis, the wavefunction $\varphi(\rho, \theta, \varphi)$ is expanded in the angular basis functions $\varphi_k^{(\mathrm{ang})}(c_p; \theta, \phi)$ $(k = 1, \ldots, N)$:

$$\varphi(\rho, \theta, \varphi) \;=\; \frac{1}{\rho^{5/2}} \sum_{k=1}^{N} \varphi_k^{(\mathrm{ang})}(c_p; \theta, \phi) u_k(c_p; \rho) \;. \tag{5.21}$$

The Schrödinger equation (5.12) then leads to a system of N coupled second-order differential equations for the hyperradial functions $u_k(c_p; \rho)$,

$$-\frac{\hbar^2}{2\mu} \left(\frac{d^2}{d\rho^2} - \frac{15}{4\rho^2} \right) u_k(c_p; \rho) + \sum_{k'} H_{kk'}^{(\mathrm{ang})}(c_p; \rho) u_{k'}(c_p; \rho) \;=\; E \, u_k(c_p; \rho) \;. \tag{5.22}$$

The coupling matrix elements are given by

$$H_{kk'}^{(\mathrm{ang})}(c_p; \rho) \;=\; \langle \varphi_k^{(\mathrm{ang})}(c_p) | \hat{H}^{(\mathrm{ang})}(\rho) | \varphi_k^{(\mathrm{ang})}(c_p) \rangle \;. \tag{5.23}$$

The bracket notation on the right-hand side of the above equation indicates the ρ-dependent integral over the angular coordinates,

$$\int_0^{\pi/2} d\theta \, \sin 2\theta \int_0^{2\pi} d\phi \, \varphi_{k'}^{*(\mathrm{ang})}(c_p; \theta, \phi) \, \hat{H}^{(\mathrm{ang})}(\rho) \, \varphi_k^{(\mathrm{ang})}(c_p; \theta, \phi) \; ;$$

it is computed at the boundaries a_p and b_p and at the middle c_p of the pth sector and further evaluated inside the sector using a three-point Lagrange interpolation formula [157]. The $(N \times N)$-matrix $\mathbf{H}^{(\mathrm{ang})}(c_p; \rho)$ thus represents the angular Hamiltonian in the p-th sector. It is diagonal at the sector midpoint c_p and becomes non-diagonal as ρ deviates from c_p. The non-diagonal coupling elements are maximum at the sector boundaries.

It is convenient to arrange N linearly independent solutions of the coupled equations (5.22) in an $(N \times N)$-matrix $\mathbf{u}(c_p; \rho)$

$$\mathbf{u}(c_p; \rho) \;=\; \begin{pmatrix} u_{11} & \dots & u_{1N} \\ \vdots & \ddots & \vdots \\ u_{N1} & \dots & u_{NN} \end{pmatrix} , \tag{5.24}$$

so that $u_{kj}(c_p, \rho)$ is the k-th component of the j-th solution in sector p. The coupled hyperradial differential equations (5.22) can thus be written in matrix form:

$$\left[-\frac{\hbar^2}{2\mu} \left(\frac{d^2}{d\rho^2} - \frac{15}{4\rho^2} \right) + \mathbf{H}^{(\mathrm{ang})}(c_p; \rho) - E \right] \mathbf{u}(c_p; \rho) \;=\; 0 \; . \tag{5.25}$$

In principle, these equations could be solved using a finite difference propagation method such as the well-known Numerov propagator (see, for example, Refs. [54] or [32] [3]). However, in order to compute bound state energies or the reactance matrix, only the logarithmic derivative matrix is required. Wavefunctions and their derivatives are not needed explicitly. The logarithmic derivative matrix of $\mathbf{u}(c_p; \rho)$ is defined as

$$\mathbf{Z}(c_p; \rho) \;=\; \frac{\partial \mathbf{u}}{\partial \rho}(c_p; \rho) \, \mathbf{u}^{-1}(c_p; \rho) \; ; \tag{5.26}$$

it verifies a matrix Riccati equation (see the Appendix H).

5.2.8 Basis transformations at sector boundaries

In order to find the transformation law for the logarithmic derivative matrix $\mathbf{Z}(c_p; \rho)$ at the boundaries of the pth sector, we first consider the transformation of the wavefunction $\mathbf{u}(c_p; \rho)$ and its derivative $\mathbf{u}'(c_p; \rho)$. Note that we

---

[3] "The Data Analysis BriefBook" [32] can also be consulted on the World Wide Web at `http://physics.web.cern.ch/Physics/DataAnalysis/BriefBook/`

did not actually propagate $\mathbf{u}(c_p; \rho)$. In our numerical computations, only the logarithmic derivative was used.

An approximate relation between the solution matrices of sectors p and $(p+1)$ is derived from Eq. (5.21):

$$\sum_{k=1}^{N} \varphi_k^{(\text{ang})}(c_p; \theta, \phi)\, \mathbf{u}(c_p; \rho) \;\approx\; \sum_{k=1}^{N} \varphi_k^{(\text{ang})}(c_{p+1}; \theta, \phi)\, \mathbf{u}(c_{p+1}; \rho) . \qquad (5.27)$$

The above relation is approximate because the two angular basis sets

$$\{\, \varphi_k^{(\text{ang})}(c_p) \,\} \qquad \text{and} \qquad \{\, \varphi_k^{(\text{ang})}(c_{p+1}) \,\}$$

are not complete, their dimensions being finite ($N = 135$ in the present case). Eq. (5.27) would be exact if they were complete ($N \to \infty$).

In the case of *outward* propagation, the wavefunction of sector p, given by the left-hand side of Eq. (5.27), is projected on the basis functions of sector $(p+1)$. The solution matrix $\mathbf{u}(c_p; \rho)$ is thus transformed into $\mathbf{u}(c_{p+1}; \rho)$ according to

$$\mathbf{u}(c_{p+1}; \rho) \;=\; \mathbf{W}(c_{p+1}, c_p)\, \mathbf{u}(c_p; \rho) . \qquad (5.28)$$

The elements of the non-orthogonal transformation matrix $\mathbf{W}(c_{p+1}, c_p)$ are defined as the overlap integrals

$$W_{k'k}(c_{p+1}, c_p) \;=\; \langle\, \varphi_{k'}^{(\text{ang})}(c_{p+1}) \,|\, \varphi_k^{(\text{ang})}(c_p) \,\rangle . \qquad (5.29)$$

The fact that the transformations $\mathbf{W}(c_{p+1}, c_p)$ ($p = 1, 2, 3, ...$) are not orthogonal should not be seen as a short-coming of the method. If they were orthogonal, the two angular basis sets would span the same subspace, and it would not be necessary to perform a basis change in the first place!

The logarithmic derivative matrix (5.26) transforms as

$$\mathbf{Z}(c_{p+1}; \rho) \;=\; \mathbf{W}(c_{p+1}, c_p)\, \mathbf{Z}(c_p; \rho) \mathbf{W}^{-1}(c_{p+1}, c_p) . \qquad (5.30)$$

The transformations $\mathbf{W}(c_{p+1}, c_p)$ ($p = 1, 2, 3, ...$) being not orthogonal, the symmetry of the logarithmic derivative matrix is lost during the propagation. A logarithmic derivative matrix that is initially symmetric becomes increasingly non-symmetric as it is propagated from sector to sector. Clearly the angular basis sets must be chosen large enough in order to ensure that the physically important block of the reactance matrix remains sufficiently symmetric.

The procedure for *inward* propagation is analagous. The wavefunction of sector $(p+1)$, given by the right-hand side of Eq. (5.27), is projected on the basis functions of sector p. The solution matrix $\mathbf{u}(c_p; \rho)$ is computed from $\mathbf{u}(c_{p+1}; \rho)$ according to

$$\mathbf{u}(c_p; \rho) \;=\; \mathbf{W}(c_p, c_{p+1})\, \mathbf{u}(c_{p+1}; \rho) , \qquad (5.31)$$

and the logarithmic derivative matrix transforms as

$$\mathbf{Z}(c_p; \rho) \;=\; \mathbf{W}(c_p, c_{p+1})\,\mathbf{Z}(c_{p+1}; \rho)\mathbf{W}^{-1}(c_p, c_{p+1}) \;.\qquad(5.32)$$

The elements of the non-orthogonal matrix $\mathbf{W}(c_p, c_{p+1})$ are given by

$$W_{kk'}(c_p, c_{p+1}) \;=\; \langle\, \varphi_k^{(\mathrm{ang})}\,(c_p)\,|\,\varphi_{k'}^{(\mathrm{ang})}(c_{p'})\,\rangle \;.\qquad(5.33)$$

The matrices $\mathbf{W}(c_p, c_{p+1})$ and $\mathbf{W}(c_{p+1}, c_p)$, which are used respectively for inward and for outward propagation, are each other's transpose, not inverse.

Since each sector basis is incomplete, the diabatic-by-sector propagation method is not reversible. To see this, one may project a wavefunction from the basis p onto the basis $p+1$ and then back onto the basis p. Clearly one does not obtain the original wavefunction. In other words, some information about the wavefunction is lost at each sector boundary.

In order to propagate the logarithmic derivative matrix across the sectors, we have used a Fortran code written by J.-M. Launay. The code is based on D. E. Manolopoulos' version [182] of B. R. Johnson's logarithmic derivative propagator [121].

5.2.9   Logarithmic derivative shooting method

To the best of our knowledge, Frey and Howard [89] and Hutson and Jain [114] were the first to use the coupled hyperradial equations in order to compute bound state energies of triatomic systems.

We have adopted a very similar approach. It differs from the cited works only in the choice of the hyperangular basis set in which the three-body wavefunction is expanded. Frey and Howard [89] and Hutson and Jain [114] expand the wavefunction in hyperspherical harmonics, whereas we expand it in the potential-adapted diabatic basis sets which differ from sector to sector.

Our method is an example of the so-called *shooting method* for the solution of ordinary coupled differential equations [39]. For a selected trial energy E we define two logarithmic derivative matrices, $\mathbf{Z}_A$ and $\mathbf{Z}_B$, such that they correspond to hyperradial wavefunctions which decay exponentially when ρ tends to zero and when ρ tends to infinity, respectively. $\mathbf{Z}_A$ is propagated along the hyperradius ρ in the *outward* direction, starting in the energetically forbidden region at short hyperradial distance. $\mathbf{Z}_B$ is propagated in the *inward* direction, starting in the energetically forbidden region at long distance. Basis transformations are performed at the sector boundaries using Eq. (5.30) with $\mathbf{Z} \equiv \mathbf{Z}_A$ for outward and Eq. (5.32) with $\mathbf{Z} \equiv \mathbf{Z}_B$ for inward propagation. We refer to the determinant of the difference of the two matrices,

$$\det[\mathbf{Z}_A - \mathbf{Z}_B]$$

as the matching determinant. It is computed at a fixed point in the classically allowed region. If the energy equals that of a bound state, the matching determinant vanishes. Bound state energies can thus be found by repeating the propagation at different energies and searching for zeros of the matching determinant.

In order to describe a solution of the i-th adiabatic hyperradial equation (5.19) in the classically forbidden regions, it is convenient to define the function

$$\kappa_i(\rho) \;=\; \frac{1}{\hbar}\,\sqrt{2\mu[\epsilon_i(\rho) - E]} \tag{5.34}$$

where E is the energy, μ is the three-body reduced mass and $\epsilon_i(\rho)$ is the ith adiabatic potential curve.

We shall use the symbol

$$Z_{A,ij}(c_p, \rho)$$

to specify the element "ij" of the logarithmic derivative matrix $\mathbf{Z}_A(c_p, \rho)$ belonging to sector p and evaluated at the hyperradius ρ. The symbol $Z_{B,ij}(c_p, \rho)$ is defined analagously.

The outward propagation is started at the inner border ($\rho = a_1 = 8.2\ \mathrm{a_0}$) of the first sector ($p = 1$) by setting

$$Z_{A,ij}(c_1, a_1) \;=\; \delta_{ij}\kappa_i(a_1)\ . \tag{5.35}$$

The inward propagation is started at the outer border ($\rho = b_{297} = 50.0\ \mathrm{a_0}$) of the last sector ($p = 297$) by setting

$$Z_{B,ij}(c_{297}, b_{297}) \;=\; \delta_{ij}\kappa_i(b_{297})\ . \tag{5.36}$$

The matching determinant

$$\det[\mathbf{Z}_A(c_p, \rho) - \mathbf{Z}_B(c_p, \rho)]$$

is evaluated for a fixed sector number p at a fixed distance $\rho \in [a_p, b_p]$ using the Fortran routines DGECO and DGEDI of the Sun Performance Library.

Numerical results are shown in Fig. 5.4. In an energy range of 0.5 cm^{-1} below the Na - Na$_2$(v=0, j=0) atom-diatom dissociation limit, we find a total of eight bound vibrational states of Na$_3$. This result is in excellent agreement with the simple estimate described Sec. 5.2.6 which suggested that there are seven vibrational levels in this energy range (see Fig. 5.3).

We believe that the numerical accuracy of the computed bound state energies is limited mainly by two factors.

Firstly, as mentioned before, the angular basis set is incomplete in each sector. Therefore some accuracy is lost as the logarithmic derivative is propagated along the hyperradius. For this reason the numerical values for the bound state energies depend to some extent on the hyperradius at which the
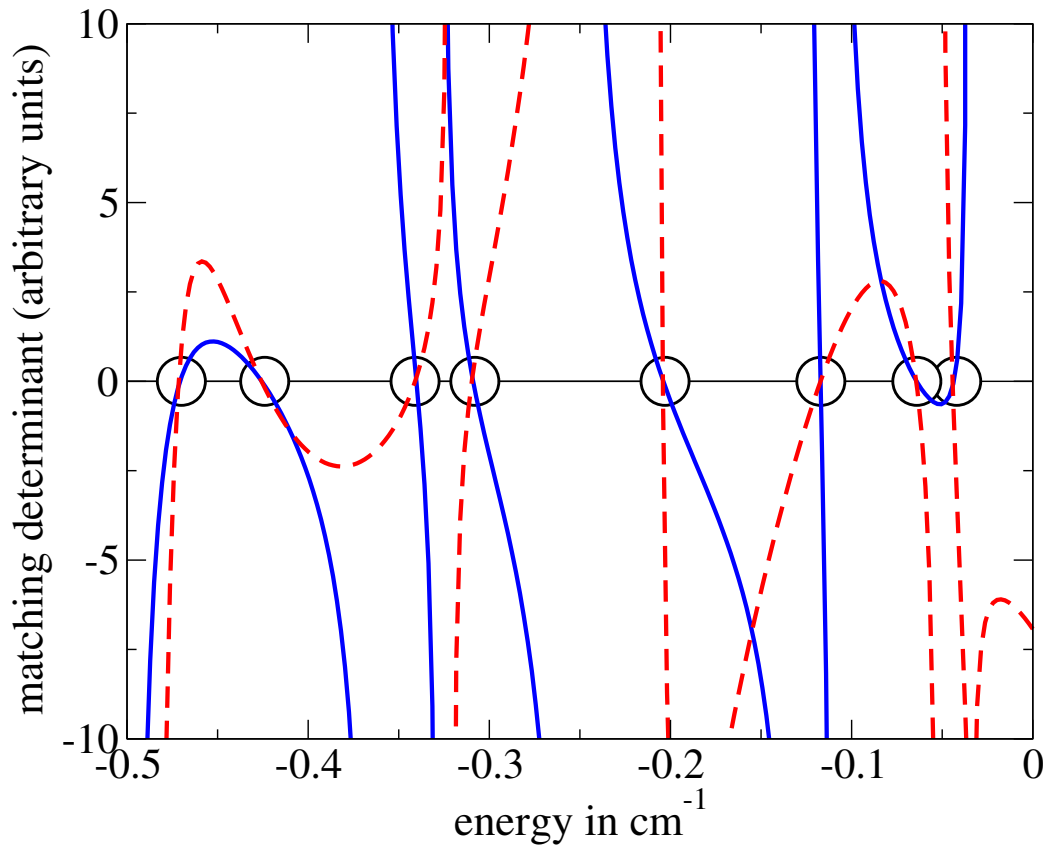
Figure 5.4: The matching determinant $\det[Z_A(E, \rho) - Z_B(E, \rho)]$ as a function of the energy E, evaluated at two hyperradial distances: $\rho = 18.1$ a_0 (full line) and $\rho = 20.1$ a_0 (dashed line). The determinant vanishes at bound state energies. The zero in energy corresponds to the Na - $Na_2(v = 0, j = 0)$ atom-diatom dissociation threshold.
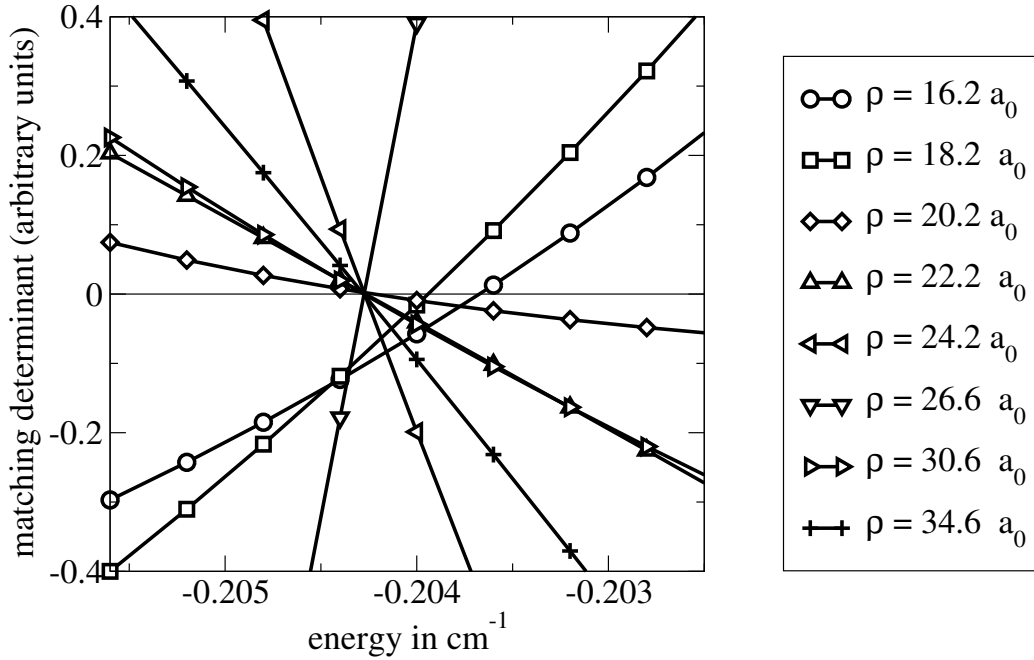
Figure 5.5: The matching determinant for energies near the bound state energy $E = -0.20(4 \pm 4)$ cm^{-1}, evaluated for eight different distances ρ.

matching determinant is evaluated. However, by computing the determinant at different hyperradial distances, we have estimated this error and found it negligible compared to the spacings between the levels (see Fig. 5.5). From this we conclude that the sector basis sets are sufficiently large.

Secondly, the propagation scheme is restricted to the interval 8.2 a$_0 < \rho < 50.0$ a$_0$, whereas the true wavefunction is defined on the interval $0 < \rho < \infty$. This could significantly affect the accuracy of the computed binding energies of levels that are so weakly bound that the amplitudes of their wavefunctions are non-negligible beyond the borders of the grid, especially at long distance. This error is more difficult to estimate because our method only yields the logarithmic derivative matrix but not the wavefunction itself. The wavefunctions are therefore difficult to visualize. Of course one could test the convergence of the computed energies by extending the grid to larger hyperradial distance. While there is no principle obstacle to extending the grid beyond $\rho = 50$ a$_0$, it cannot be done easily with the current version of the code. As mentioned in Sec. 3.3 of Chapter 3, the primitive hyperangular basis set, which is used to compute the potential-adapted basis set, becomes very inconvenient in the three asymptotic atom-diatom regions of configuration space. Moreover, the wavefunction of the least bound level may extend to arbitrarily large distances, depending on the value of the scattering length.

5.2.10 Alternative methods for solving the hyperradial equations

There are a few alternatives to the diabatic-by-sector method.

Instead of using the sector-basis sets, one may expand the wavefunction in a truely *adiabatic*, ρ-dependent angular basis set. Undoubtedly this is conceptually very appealing. The adiabatic basis can be constructed numerically by diagonalizing the angular Hamiltonian on a fine mesh of grid points on the ρ-axis. The number of mesh points would have to be larger than the number of sectors in the sector method, in order to ensure that the non-adiabatic couplings are represented accurately. However, the adiabatic basis set would be optimum at all distances, not only at the sector midpoints.

A good compromise between the sector-basis sets and the adiabatic basis could be the *split-diabatic* basis set invented by B. D. Esry and H. R. Sadeghpour [76], a ρ-dependent, potential-adapted basis set which is neither diabatic nor adiabatic and which varies less violently than the adiabatic basis.

V. Kokoouline [133] has computed bound vibrational states of the helium trimer $^4\text{He}_3$ by solving the coupled hyperradial equations in the adiabatic hyperangular basis using a hyperradial discrete variable representation (DVR), combined with a smooth variable discretization [201]. While there can be no principal obstacle to applying the same method to $^{23}\text{Na}_3$, we believe that the DVR basis set would not be very efficient in the case of Na_3, because the non-adiabatic hyperradial couplings between the adiabatic hyperangular states are much more violent for Na_3 than for He_3: in the case of He_3, the spacing between the grid points on the ρ hyperradial axis can be adapted to the local hyperradial de Broglie wavelength, but for Na_3 the grid step would have to be adapted to the sudden variations of the non-adiabatic couplings, as we already mentioned in Sec. 5.2.6.

The "Smooth Variable Discretization Enhanced Renormalized Numerov propagator" (SVDERN) developed by G. A. Parker and F. D. Colavecchia *et al.* [210, 54] is designed to propagate the R-matrix (the inverse of the logarithmic derivative matrix) along the hyperradius, using an adiabatic hyperangular basis. The SVDERN propagator could thus replace the logarithmic derivative propagator by Johnson and Manalopoulos we used in our computations.

Furthermore, the three-point Numerov recursion formula, Eq. (22) of Ref. [54], which is the basis of the SVDERN propagator, can be read as a generalized eigenvalue problem. By solving this system numerically, perhaps iteratively, it might be possible to compute bound state energies *and* wavefunctions. The proposed method is analogous to B. Lindberg's method [171] of solving the one-dimensional Schrödinger equation. We think that this algebraic method might provide a very interesting alternative to the logarithmic

derivative shooting method.

Numerov's finite difference formula relates a given grid point on the ρ hyperradial axis only with the two neighbouring grid points, whereas a DVR scheme relates each grid point with *all* the other grid points. The Numerov propagator is equivalent to a *tridiagonal* matrix representation of the Hamiltonian, whereas a DVR or pseudo-spectral scheme yields a full matrix. Therefore, if the grid step must be very small for some reason or the other (for example, if the grid step is dictated by the sharp variations of the potential coupling matrix), one may expect that the Numerov-representation of the Hamiltonian will be much more efficient than the DVR-representation.

5.3 Asymptotic analysis using Jacobi coordinates

In the previous Section, we have shown that the hyperspherical diabatic-by-sector method can be used to compute correct energies of vibrational levels of spin-polarized Na_3. The major shortcoming of the method is probably that it does not yield the wavefunctions and that it offers little insight into the structure of the bound levels. Furthermore, as explained before, it does not allow to compute the energies of states that are too weakly bound.

In order to obtain a better picture of weakly bound states, we have computed their energies by a different method. We have introduced an alternative phase shift which has some similarities with a quantum defect and which allows us to distinguish between "resonant" and "non-resonant" bound states.

Before we present our method and the results, we shall try to convey the main ideas of quantum defect theory. We shall also review the stationary scattering formalism of rearrangement collisions for the general case of three distinct atoms A, B, and C and arbitrary total angular momentum $J \geq 0$.

5.3.1 The quantum defect

In its original sense, the quantum defect δ_l is a parameter in the Rydberg formula

$$E_{nl} = -\frac{\text{const}}{(n - \delta_l)^2} \tag{5.37}$$

for the energy levels of an electron in the Coulomb field of an ionic core. The formula can be derived by writing the radial wavefunction of the excited electron at large distances as a linear combination of regular and irregular Coulomb functions and applying the bound state boundary condition. The energy levels corresponding to higly excited states are thus given by a single formula with only one parameter: the quantum defect.

The concept of a quantum defect can be extended to multichannel systems and to potentials which fall off faster than the Coulomb potential.

Although the expression "quantum defect" has its origin in the interpretation of *bound* levels, quantum defect theory is explained more easily using the language of collision theory. In the following, we try to give a short overview which is not intended to be exhaustive or mathematically rigorous.

The basic requirement for the applicability of quantum defect theory is that the configuration space can be divided into an inner region, in which all the particles may interact strongly, and one or several asymptotic regions, in which the system splits into two fragments, such as an atomic core and an electron, or a diatomic molecule and an atom. In each asymptotic region, the radial wavefunction $u(E, r)$ for the relative motion of the two fragments can be expressed as a linear combination of two energy-smooth reference functions $\bar{f}(E, r)$ and $\bar{g}(E, r)$ such that

$$u(E,r) = \bar{f}(E,r)\bar{A}(E,r) - \bar{g}(E,r)\bar{B}(E,r) \tag{5.38}$$
$$u'(E,r) = \bar{f}'(E,r)\bar{A}(E,r) - \bar{g}'(E,r)\bar{B}(E,r) \tag{5.39}$$

where r is the distance between the two fragments, E is the energy, and the prime indicates the radial derivative, $\partial/\partial r$. If $\bar{f}$ and $\bar{g}$ are exact solutions of the radial Schrödinger equation that includes the exact potential, the coefficients $\bar{A}(E, r)$ and $\bar{B}(E, r)$ do not depend on r, otherwise they verify the so-called variable phase equations [46].

Traditionally, the function $\bar{f}(E, r)$ is chosen regular in the origin ($r = 0$), and the function $\bar{g}(E, r)$ is defined such that it is locally dephased by 90° with respect to $\bar{f}(E, r)$ in the classically allowed region at short distances. While $\bar{f}(E, r)$ does not necessarily have to be regular in the origin, it is essential that $\bar{f}$ and $\bar{g}$ are linearly independent and continuous in energy. J. P. Burke *et al.* [44] defined them simply by imposing a JWKB-like initial condition at the boundary between the inner and the outer regions. Assuming that the wavefunction $u(E, r)$ is analytic in energy, the coefficients $\bar{A}(E, r)$ and $\bar{B}(E, r)$ are analytic as well and can be extrapolated across thresholds.

The usual reactance matrix $K(E)$ and the scattering matrix $S(E)$ are recovered from $\bar{A}(E, r)$ and $\bar{B}(E, r)$ using the energy-dependent linear transformation between the base pair of *short-range* solutions $\bar{f}(E, r)$ and $\bar{g}(E, r)$ and a base pair of *long-range* solutions $f(E, r)$ and $g(E, r)$. By definition, the latter are mutually dephased by 90° in the limit $r \to \infty$.

The original form of quantum defect theory was developed by M. J. Seaton in order to describe the properties of an electron in the Coulomb field of an ionic core (see his review article [240]). For these systems, the long-range reference functions $f(E, R)$ and $g(E, R)$ are Coulomb functions, which means that they never approach the sinusoidal free-particle solutions [236].

If the asymptotic interaction between the two fragments falls off faster than $1/r$, the long-range functions $f(E, R)$ and $g(E, R)$ for open channels

are chosen to behave like $j_l(kr)$ and $n_l(kr)$, respectively, when $r \to \infty$, where j_l and n_l are the Riccati-Bessel and Riccati-Neumann functions (i.e. the regular and irregular solutions of the radial Schrödinger equation for a free particle). The long-range functions for closed channels are defined such that they behave like rising and falling exponentials, $\exp(\kappa r)$ and $\exp(-\kappa r)$, respectively.

The energy-dependent linear transformation between the analytic base pair $(\bar{f}, \bar{g})$ and the pair of long-range functions (f, g) can often be described analytically using simple energy-dependent quantities, such as Milne's accumulated phase [126] or parameters measuring deviations from the JWKB approximation at energies close to thresholds [192, 222]. Using these quantities, the coefficients $\bar{A}$ and $\bar{B}$ defined in Eqs. (5.38) and (5.39) can be converted into the standard Jost functions or the K-matrix or the S-matrix.

We may cite three main applications:

- search for bound states,

- parametrization of resonances,

- analysis of threshold effects.

Quantum defect theory has been used extensively by many groups in order to interpret spectra of Rydberg atoms and molecules, as well as threshold phenomena in atomic and molecular collisions (see the reviews M. J. Seaton [240], by M. Aymar *et al.* [16] and by H. R. Sadeghpour *et al.* [230]).

There have been few attempts up to now to extend quantum defect theory to collisions between atoms and molecules. M. Raoult and G. G. Balint-Kurti [221] studied the rotational predissociation of Ar-H$_2$ within the framework of multichannel quantum defect theory (MQDT), and I. Fourré and M. Raoult [87] calculated bound states of the van der Waals complex Ar-NO using quantum defect techniques.

As far as we know, the present study is the first attempt to define a quantum defect for a reactive atom-diatom system.

Notations and formal relations

We shall denote short-range quantities by a bar. The functions $\bar{f}(E, r)$ and $\bar{g}(E, r)$ are defined by specifying their behaviour at some finite distance, whereas $f(E, r)$ and $g(E, r)$ are defined by their asymptotic behaviour for $r \to \infty$.

In analogy to Eqs. (5.38) and (5.39), the wavefunction u and its radial derivative u' can be expressed in terms of the long-range functions f and g as follows

$$u = fA - gB \tag{5.40}$$
$$u' = f'A - g'\bar{B} \tag{5.41}$$

122

The pairs (f, g) and $(\bar{f}, \bar{g})$ are related to each other by an energy-dependent matrix S (not to be confused with the S-matrix or scattering matrix) such that

$$\left(\begin{array}{cc} \bar{f} & \bar{g} \\ \bar{f}' & \bar{g}' \end{array} \right) = \left(\begin{array}{cc} f & g \\ f' & g' \end{array} \right) \left(\begin{array}{cc} S_{ff} & S_{fg} \\ S_{gf} & S_{gg} \end{array} \right) . \tag{5.42}$$

By comparing Eqs. (5.38) and (5.40), one sees that the pairs of coefficients (A, B) and $(\bar{A}, \bar{B})$ are related as follows:

$$\left(\begin{array}{c} A \\ B \end{array} \right) = \left(\begin{array}{cc} S_{ff} & -S_{fg} \\ -S_{gf} & S_{gg} \end{array} \right) \left(\begin{array}{c} \bar{A} \\ \bar{B} \end{array} \right) . \tag{5.43}$$

In the case of multi-channel systems, these quantities become matrices, and we shall denote them by bold captital letters: $\mathbf{u}$ for the solution matrix, $(\bar{\mathbf{F}}, \bar{\mathbf{G}})$ and $(\mathbf{F}, \mathbf{G})$ for the short-range and the long-range reference functions.

5.3.2 Scattering matrix for rearrangement collisions

We now consider a collision of an atom A with a diatomic molecule BC at an energy sufficiently low so that a break-up into $A + B + C$ cannot occur. In the most general case, all three arrangements of atoms are possible final states:

$$A + BC \; \rightarrow \; \left\{ \begin{array}{l} A + BC \\ B + CA \\ C + BA \end{array} \right. . \tag{5.44}$$

This means that all three sets of Jacobi coordinates are needed for a complete analysis of the scattering event.

In each arrangement valley λ, outside the reaction region, the wavefunction can be expressed conveniently using the Arthurs-Dalgarno expansion (see the Appendix I)

$$\varphi^{JM}(A, B, C) \; = \; \sum_{vjl} \mathcal{Y}_{jl}^{JM}(\hat{R}_\lambda, \hat{r}_\lambda) \, \varphi_{\lambda vj}^{(\text{vib})}(r_\lambda) \, \frac{u_{\lambda vjl}^{JM}(R_\lambda)}{R_\lambda} \tag{5.45}$$

where $\mathbf{r}_\lambda$ and $\mathbf{R}_\lambda$ are the Jacobi vectors of the λ-arrangement, $\mathcal{Y}_{jl}^{JM}$ are coupled spherical harmonics, $\varphi_{\lambda vj}^{(\text{vib})}$ is a vibrational wavefunction of the diatomic molecule of the λ-arrangement, and $u_{\lambda vjl}^{JM}(R_\lambda)$ is the radial wavefunction describing the relative motion of the atom and the diatom. The indices v and j are the vibrational and rotational quantum numbers associated with the diatomic molecule of the λ-arrangement, l is the rotational quantum number associated with the Jacobi vector $\mathbf{R}_\lambda$, J is the total angular momentum quantum number, and M is the quantum number associated with rotations of the complete system about a fixed axis in an inertial frame of reference.

Eq. (5.45) can be cast in a more general form, valid for all three arrangement valleys:

$$\varphi^{JM}(A,B,C) = \sum_{\lambda=\alpha,\beta,\gamma} \sum_{vjl} \mathcal{Y}_{jl}^{JM}(\hat{R}_\lambda,\hat{r}_\lambda)\, \varphi_{\lambda vj}^{(\text{vib})}(r_\lambda)\, \frac{u_{\lambda vjl}^{JM}(R_\lambda)}{R_\lambda}\ . \qquad (5.46)$$

This expression can be used to check whether the wavefunction $\varphi^{JM}(A,B,C)$ has the correct permutational symmetry with respect to atom exchange.

The Schrödinger equation for the wavefunction (5.46) leads to three sets ($\lambda = \alpha, \beta, \gamma$) of coupled second-order differential equations for the radial wavefunctions $u_{\lambda vjl}^{JM}(R_\lambda)$:

$$\left[-\frac{\hbar^2}{2\mu_\lambda}\left(\frac{d^2}{dR_\lambda^2} - \frac{l(l+1)}{R_\lambda^2} \right) - E \right] u_{\gamma vjl}^{JM}(R_\lambda)$$
$$+ \sum_{v'j'l'} \langle \lambda vjlJ | V | \lambda v'j'l'J \rangle\, u_{\gamma v'j'l'}^{JM}(R_\lambda)\ =\ 0\ . \qquad (5.47)$$

Here μ_λ is the reduced mass for the relative motion of the atom and the dimer in the λ-arrangement, E is the total energy, and $\langle vjlJ|V|v'j'l'J\rangle$ are the elements of the potential energy coupling matrix $\mathbf{V}(R_\lambda)$. The coupled equations (5.47) are derived in the Appendix I. Note that they are valid only in the three asymptotic regions of configuration space where the overlap of the basis functions $\mathcal{Y}_{jl}^{JM}(\hat{R}_\lambda,\hat{r}_\lambda)\varphi_{\lambda vj}^{(\text{vib})}(r_\lambda)$ and $\mathcal{Y}_{j'l'}^{JM}(\hat{R}_{\lambda'},\hat{r}_{\lambda'})\varphi_{\lambda'v'j'}^{(\text{vib})}(r_{\lambda'})$ belonging to different arrangements λ and λ' is negligible.

For each Jacobi arrangement ($\lambda = \alpha, \beta, \gamma$), it is convenient to split the potential V into the atom-atom potential and the atom-molecule interaction potential such that

$$V(A,B,C) = V_\lambda^{(\text{at}-\text{at})}(r_\lambda) + V_\lambda^{(\text{at}-\text{mol})}(r_\lambda, R_\lambda, \eta_\lambda) \qquad (5.48)$$

where η_λ is the angle between the two Jacobi vectors $\mathbf{r}_\lambda$ and $\mathbf{R}_\lambda$. The coupled equations (5.47) then take the form

$$\left[-\frac{\hbar^2}{2\mu_\lambda}\left(\frac{d^2}{dR_\lambda^2} - \frac{l(l+1)}{R_\lambda^2} \right) + E_{\lambda vj} - E \right] u_{\lambda vjl}^{JM}(R_\lambda)$$
$$+ \sum_{v'j'l'} \langle \lambda vjlJ | V_\lambda^{(\text{at}-\text{mol})} | \lambda v'j'l'J \rangle\, u_{\lambda v'j'l'}^{JM}(R_\lambda)\ =\ 0 \qquad (5.49)$$

where $E_{\lambda vj}$ is the energy of a rovibrational level of the diatomic molecule of the λ-arrangement.

The boundary conditions for the coupled equations (5.49) depend on the particular collision process one wishes to describe. Usually one specifies the initial state of the ABC system, i.e. its state before the collision. An example

124

of an initial state is the situation where atom A is at an infinite distance from molecule $BC(v,j)$ and the relative angular momentum is characterized by the fixed quantum number l.

In principal, the functions $u^{JM}_{\lambda vjl}(R_\lambda)$ can be time-dependent wavepackets. However, we assume that they are real and stationary. In the stationary picture, the scattering process can be visualized by writing each radial wavefunction $u^{JM}_{\lambda vjl}(R_\lambda)$ at large distances R_λ as a superposition of an incoming and an outgoing plane wave,

$$
u^{JM}_{\lambda vjl}(R_\lambda) = \frac{e^{-\mathrm{i}(k_{\lambda vj}R_\lambda - l\pi/2)}}{\sqrt{k_{\lambda vj}}} A_{\lambda vjl} - \frac{e^{\mathrm{i}(k_{\lambda vj}R_\lambda - l\pi/2)}}{\sqrt{k_{\lambda vj}}} B_{\lambda vjl} \qquad (5.50)
$$

with coefficients $A_{\lambda vjl}$ and $B_{\lambda vjl}$ chosen such that the set of radial wavefunctions $\{u^{JM}_{\lambda vjl}\}$ mimics a specific scattering process.

S-matrix

For each initial state $\lambda'v'j'l'$ and each energy E, we define the set of radial wavefunctions $u^{(\mathrm{S})}{}^{JM}_{\lambda vjl,\lambda'v'j'l'}(R_\lambda)$ describing the scattering from the initial state $\lambda'v'j'l'$ to all possible final states. In the asymptotic regions of configuration space, these functions are

$$
\begin{aligned}
&u^{(\mathrm{S})}{}^{JM}_{\lambda vjl,\lambda'v'j'l'}(R_\lambda) \\
&= \frac{\exp(-\mathrm{i}k_{\lambda vj}R_\lambda)}{\sqrt{k_{\lambda vj}}} \delta_{\lambda vjl,\lambda'v'j'l'} - (-1)^l \frac{\exp(\mathrm{i}k_{\lambda vj}R_\lambda)}{\sqrt{k_{\lambda vj}}} S^{JM}_{\lambda vjl,\lambda'v'j'l'}
\end{aligned}
$$

$$(5.51)$$

where $k_{\lambda vj}$ is the wavenumber for channel λvjl:

$$
k_{\lambda vj} = \frac{1}{\hbar}\sqrt{2\mu_\lambda(E - E_{\lambda vj})} . \qquad (5.52)
$$

Here μ_λ denotes the reduced mass associated with the two fragments of the λ-arrangement, and $E_{\lambda vj}$ is the combined energy of the isolated atom and the isolated diatomic molecule. The quantities $S^{JM}_{\lambda vjl,\lambda vjl}$ are the elements of the JM-block of the scattering matrix $\mathbf{S}$.

If $E > E_{\lambda vj}$, the channel λvjl is said to be *open*. For each open channel, the functions $\exp(-\mathrm{i}k_{\lambda vj})$ and $\exp(\mathrm{i}k_{\lambda vj})$ are respectively associated with a stationary flux of colliding particles and scattered particles. The S-matrix can thus be translated into differential cross sections.

If $E < E_{\lambda v j}$, the channel $\lambda v j l$ is said to be *closed*, and the wavenumber $k_{\lambda v j}$ is imaginary. Closed channels do not contribute to the flux of particles. In the asymptotic regions, the closed-channel components of the S-matrix solution $\mathbf{u}^{(\mathrm{S})}$ are

$$
u^{(\mathrm{S})}{}^{JM}_{\lambda v j l, \lambda' v' j' l'}(R_\lambda)
$$
$$
= \frac{\exp(\kappa_{\lambda v j} R_\lambda)}{\sqrt{\kappa_{\lambda v j}}} \delta_{\lambda v j l, \lambda' v' j' l'} - (-1)^l \frac{\exp(-\kappa_{\lambda v j} R_\lambda)}{\sqrt{\kappa_{\lambda v j}}} S^{JM}_{\lambda v j l, \lambda' v' j' l'}
$$
$$(5.53)$$

where

$$
\kappa_{\lambda v j} = \frac{1}{\hbar} \sqrt{2\mu_\lambda \left(E_{\lambda v j} - E \right)} . \tag{5.54}
$$

K-matrix

The S-matrix solutions (5.51) are complex-valued. Real-valued solutions, known as K-matrix solutions, are obtained by forming suitable linear combinations of the S-matrix solutions. In the asymptotic regions, the K-matrix solutions behave as follows:

$$
u^{(\mathrm{K})}{}^{JM}_{\lambda v j l, \lambda' v' j' l'}(R_\lambda)
$$
$$
= \frac{\sin(k_{\lambda v j} R_\lambda - l\pi/2)}{\sqrt{k_{\lambda v j}}} \delta_{\lambda v j l, \lambda' v' j' l'} + \frac{\cos(k_{\lambda v j} R_\lambda - l\pi/2)}{\sqrt{k_{\lambda v j}}} K^{JM}_{\lambda v j l, \lambda' v' j' l'} .
$$
$$(5.55)$$

The numbers $K^{JM}_{\lambda v j l, \lambda' v' j' l'}$ on the right-hand side are the elements of the *reactance* matrix $\mathbf{K}$, also called *reaction* matrix or simply K-matrix. Note that Eq. (5.55) only applies if the channel $\lambda v j l$ is open. Per definition, the closed-channel components of our K-matrix solution $\mathbf{u}^{(\mathrm{K})}$ are the same as those of the S-matrix solution $\mathbf{u}^{(\mathrm{S})}$.

It is convenient to express the K-matrix solutions $\mathbf{u}^{(\mathrm{K})}$ in terms of two solution matrices $\mathbf{F}$ and $\mathbf{G}$ such that

$$
u^{(\mathrm{K})}{}^{JM}_{\lambda v j l, \lambda' v' j' l'}(R_\lambda) = F^{JM}_{\lambda v j l, \lambda' v' j' l'}(R_\lambda) - G^{JM}_{\lambda v j l, \lambda' v' j' l'}(R_\lambda) K^{JM}_{\lambda v j l, \lambda' v' j' l'} . \tag{5.56}
$$

The functions $F^{JM}_{\lambda v j l, \lambda' v' j' l'}(R_\lambda)$ and $G^{JM}_{\lambda v j l, \lambda' v' j' l'}(R_\lambda)$ are defined by their asymptotic behaviour at large distances $(R_\lambda \to \infty)$ as follows:

If the channel $\lambda v j l$ is open,

$$
F^{JM}_{\lambda v j l, \lambda' v' j' l'} \to \frac{j_l(k_{\lambda v j} R_\lambda)}{\sqrt{k_{\lambda v j}}} \delta_{\lambda v j l, \lambda' v' j' l'} \to \frac{\sin(k_{\lambda v j} R_\lambda - l\pi/2)}{\sqrt{k_{\lambda v j}}} \delta_{\lambda v j l, \lambda' v' j' l'}
$$
$$(5.57)$$

$$G^{JM}_{\lambda vjl,\lambda'v'j'l'} \;\rightarrow\; \frac{n_l(k_{\lambda vj}R_\lambda)}{\sqrt{k_{\lambda vj}}}\delta_{\lambda vjl,\lambda'v'j'l'} \;\rightarrow\; -\frac{\cos(k_{\lambda vj}R_\lambda - l\pi/2)}{\sqrt{k_{\lambda vj}}}\delta_{\lambda vjl,\lambda'v'j'l'}$$

(5.58)

where j_l and n_l are the Riccati-Bessel and Riccati-Neumann functions (see the Appendix M).

If the channel λvjl is closed,

$$F^{JM}_{\lambda vjl,\lambda'v'j'l'} \;\rightarrow\; \frac{\exp(\kappa_{\lambda vj}R_\lambda)}{\sqrt{\kappa_{\lambda vj}}}\delta_{\lambda vjl,\lambda'v'j'l'}$$

(5.59)

$$G^{JM}_{\lambda vjl,\lambda'v'j'l'} \;\rightarrow\; \frac{\exp(-\kappa_{\lambda vj}R_\lambda)}{\sqrt{\kappa_{\lambda vj}}}\delta_{\lambda vjl,\lambda'v'j'l'}$$

(5.60)

when $R_\lambda \to \infty$.

The "reference functions" $F^{JM}_{\lambda vjl,\lambda'v'j'l'}$ and $G^{JM}_{\lambda vjl,\lambda'v'j'l'}$ are assumed to be *exact* solutions of the coupled differential equations (5.47) resulting from the Arthurs-Dalgarno expansion. Therefore the reactance matrix $K^{JM}_{\lambda vjl,\lambda'v'j'l'}$ does not depend on the distances R_λ. At large distances, where interchannel coupling is negligible, the matrices $\mathbf{F}$ and $\mathbf{G}$ are diagonal. If $\mathbf{F}$ and $\mathbf{G}$ were *not* chosen to be exact solutions of the coupled equations, the reactance matrix $\mathbf{K}$ would *not* be a constant but verify the K-matrix version of the variable phase equations [46].

Every solution matrix can be partitioned into blocks corresponding to open ("O") and closed channels ("C"). For example, the K-matrix solutions (5.56) can be written as

$$\mathbf{u}^{(\mathrm{K})} = \left[\begin{array}{cc} \mathbf{u}^{(\mathrm{K})}_{OO} & \mathbf{u}^{(\mathrm{K})}_{OC} \\ \mathbf{u}^{(\mathrm{K})}_{CO} & \mathbf{u}^{(\mathrm{K})}_{CC} \end{array} \right] = \left[\begin{array}{cc} \mathbf{F}_{OO} & \mathbf{F}_{OC} \\ \mathbf{F}_{CO} & \mathbf{F}_{CC} \end{array} \right] - \left[\begin{array}{cc} \mathbf{G}_{OO} & \mathbf{G}_{OC} \\ \mathbf{G}_{CO} & \mathbf{G}_{CC} \end{array} \right] \left[\begin{array}{cc} \mathbf{K}_{OO} & \mathbf{K}_{OC} \\ \mathbf{K}_{CO} & \mathbf{K}_{CC} \end{array} \right].$$

(5.61)

Each column of the matrix $\mathbf{u}^{(\mathrm{K})}$ represents a particular solution.

In the following, we choose $\kappa_{\lambda vj}$ to be *positive* if the channel λvjl is closed. The block

$$\left[\begin{array}{c} \mathbf{u}^{(K)}_{OO} \\ \mathbf{u}^{(K)}_{CO} \end{array} \right]$$

then summarizes all the solutions corresponding to physical states. They are charactized by a negligible amplitude of the wavefunction in the forbidden regions of configuration space.

The block

$$\left[\begin{array}{c} \mathbf{u}^{(K)}_{OC} \\ \mathbf{u}^{(K)}_{CC} \end{array} \right]$$

has no physical meaning because it contains the rising exponentials $\exp(\kappa_{\lambda vj}R_\lambda)$ from Eq. (5.59)

127

The open-open block of the S-matrix is obtained from the K-matrix by the Caley transformation

$$\mathbf{S}_{OO} = (1 + i\mathbf{K}_{OO})(1 - i\mathbf{K}_{OO})^{-1} . \qquad (5.62)$$

Three identical particles

If the three particles are identical, the arrangement index λ can be omitted in most of the above expressions. If the particles are bosons, Eq. (5.46) takes the form

$$\varphi^{JM}(A, B, C) = \hat{\mathcal{S}} \sum_{vjl} \mathcal{Y}_{jl}^{JM}(\hat{R}, \hat{r}) \varphi_{vj}^{(\mathrm{vib})}(r) \frac{u_{vjl}^{JM}(R)}{R} \qquad (5.63)$$

where $\hat{\mathcal{S}}$ is the symmetrisation operator and $\mathbf{R} \equiv (R, \hat{R})$ and $\mathbf{r} \equiv (r, \hat{r})$ are the Jacobi vectors of a selected arrangement, for example, the γ-arrangement.

The coupled equations (5.49) take the form

$$\left[-\frac{\hbar^2}{2\mu} \left(\frac{d^2}{dR^2} - \frac{l(l+1)}{R^2} \right) + E_{vj} - E \right] u_{vjl}^{JM}(R)$$
$$+ \sum_{v'j'l'} \langle vjlJ | V^{(\mathrm{at-mol})} | v'j'l'J \rangle \, u_{v'j'l'}^{JM}(R) = 0 \qquad (5.64)$$

where μ is the reduced mass for the relative motion of the atom and the diatomic molecule (not to be confused with the three-body reduced mass defined in Chapter 3).

5.3.3 Matching on the hypersphere

We now return to our study of the sodium trimer $\mathrm{Na}_3(^4A_2')$.

In Sec. (5.2.9), we explained how the hyperradial logarithmic derivative matrix $\mathbf{Z}$ can be propagated along the hyperradius, either in the inward or in the outward direction. In the following, we shall discuss results obtained from a logarithmic derivative matrix that was propagated in the *outward* direction, from $\rho = 8.2$ a$_0$ to $\rho = 50.0$ a$_0$.

We extracted the reactance matrix $\mathbf{K}$ [defined in Eq. (5.56)] from the hyperradial logarithmic derivative matrix given at $\rho = 50.0$ using the long-range reference functions $\mathbf{F}(R)$ and $\mathbf{G}(R)$. The numerical method for converting the hyperradial logarithmic derivative matrix into the K-matrix was developed by J.-M. Launay *et al.* and is described in Ref. [167]. It is quite complicated, because the three sets of Jacobi coordinates do not join smoothly onto the hypersperical coordinates: a segment of the surface of the hypersphere $\rho = $ const corresponds to a certain finite interval

$$R_\lambda^{\mathrm{min}} \leq R_\lambda \leq R_\lambda^{\mathrm{max}} \qquad (5.65)$$

for the Jacobi length R_λ (see Fig. 3.3 of Chapter 3).

It should be mentioned that G. A. Parker *et al.* [211] have found an elegant way to bridge the gap between hyperspherical and Jacobi regions using tangent-sphere coordinates. However, in our work the matching procedure developed by J.-M. Launay *et al.* proved to be entirely satisfactory.

5.3.4 Potential coupling matrix for Na - Na$_2$

The three sodium atoms A, B and C being identical, the Arthurs-Dalgarno expansion is the same for all three Jacobi arrangements. The radial wavefunctions can therefore be written as

$$u_{vjl}^{JM}(R)$$

where R is the distance between C and the center of mass of A and B. They are solutions of the coupled equations (5.64).

For the case of zero total angular momentum ($J = 0$), we have computed some elements of the diabatic potential energy coupling matrix $\mathbf{V}^{(\text{at}-\text{mol})}(R)$,

$$\langle vjlJ|V^{(\text{at}-\text{mol})}|v'j'l'J\rangle \ , \tag{5.66}$$

using a Fortran routine (`vr1.f`) written by J.-M. Launay[4] and using the pairwise-additive potential energy surface described in Chapter 4 as input data.

The diagonal elements of the coupling matrix (5.66) are plotted in Fig. 5.6 as functions of the distance R between the atom and the molecule. The two lowest thresholds are the ones for break-up into

$$\text{Na} + \text{Na}_2(v{=}0,\ j{=}0)$$

and

$$\text{Na} + \text{Na}_2(v = 0, j = 2) \ .$$
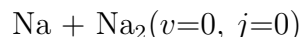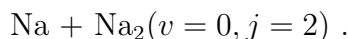
These thresholds lie at -163.7492 cm^{-1} and -163.4298 cm^{-1}, respectively, measured from the threshold to three-body (Na + Na + Na) break-up.

The influence of the non-diagonal elements on the scattering process can be assessed from Fig. 5.7. At the distance $R = 40$ a$_0$, the off-diagonal term coupling the two lowest rotational states ($v = 0, j = 0$) and ($v = 0, j = 2$) of the Na$_2$ molecule measures roughly 10% of the energy gap between the two states. This means that the diabatic coupling is probably not quite negligible at this distance. At the distance $R = 50$ a$_0$, however, the ratio between the coupling element and the energy gap is only 2%.

---

[4]Fortran routines for computing the potential coupling matrix are also available on the World Wide Web at `http://ccp7.dur.ac.uk/molcol.html`, as part of the Molcol package [85].
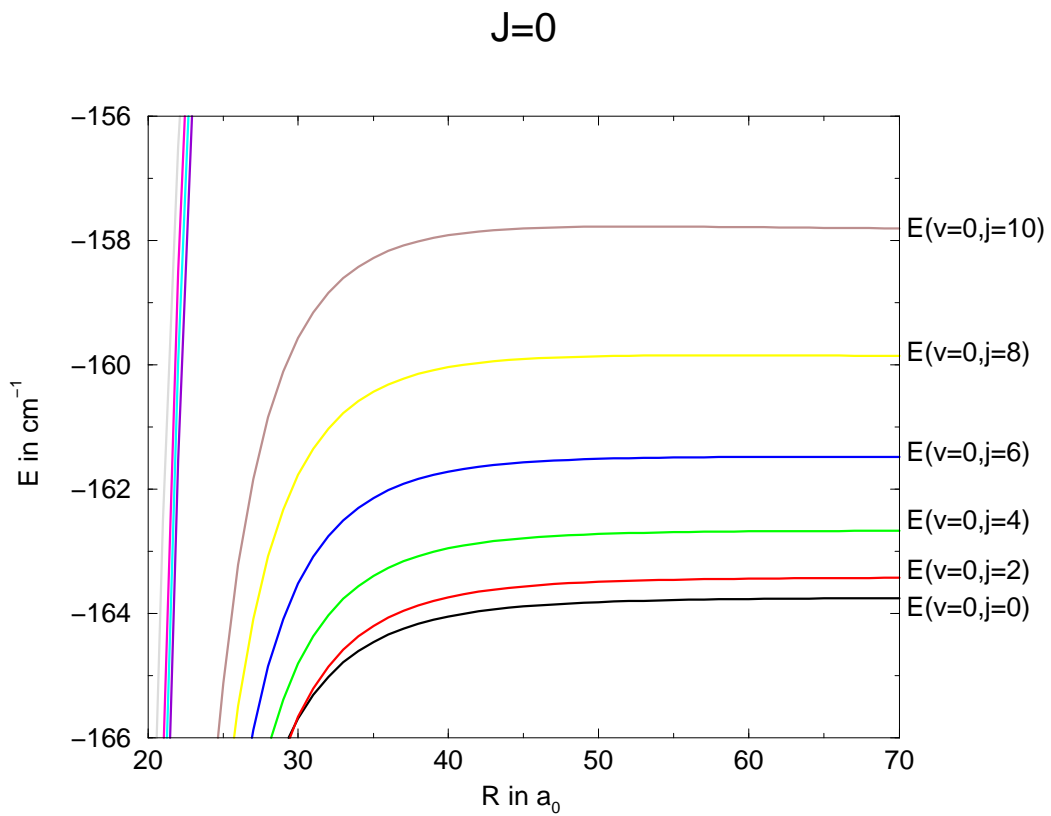
Figure 5.6: Diagonal elements V_{ii} of the potential coupling matrix for the case of zero total angular momentum ($J = 0$).
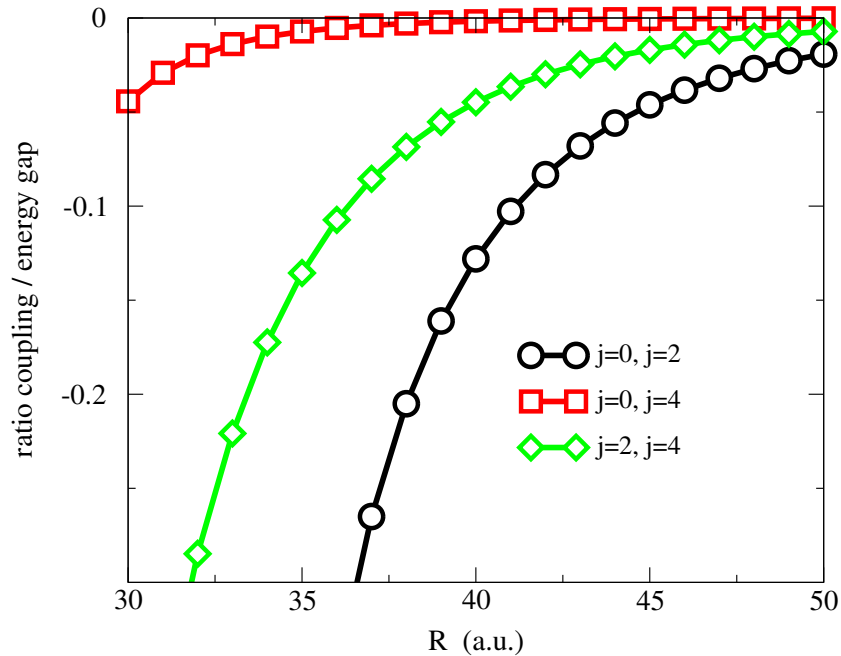
Figure 5.7: Coupling between diabatic channels. The ratio $V_{ij}/(V_{ii} - V_{jj})$ ("coupling element over energy gap") is plotted as a function of the atom-molecule distance R.

By diagonalizing the potential coupling matrix at various distances R, we obtained adiabatic potential curves which do not cross. By comparing the adiabatic curves and the diabatic curves, we concluded that the non-adiabatic coupling between the adiabatic states is probably negligible for all distances R larger than ≈ 50 a$_0$ and hence for all hyperradial distances ρ larger than ≈ 50 a$_0$[5]

In the following, we shall denote $V(R)$ the lowest of the adiabatic potential curves, which has its asymptotic limit at the Na + Na$_2$(v=0, j=0) threshold. There is no risk of confusion, $V(R)$ being the only adiabatic curve used explicitly in our scattering calculations. At distances $R \geq 35$ a$_0$, we

---

[5]We recall that the hyperradius ρ and the atom-diatom distance $\approx R$ become asymptotically equal, provided that the separation r between the two atoms forming the diatomic molecule is limited. At this point it is not necessary to distinguish between mass-scaled and unscaled Jacobi vectors, because the scaling factors are approximately 1 (see Eq. (3.27) of Chapter 3).

approximated it as[6]

$$V \;=\; E(v=0, j=0) - \frac{C_6}{R^6} - \frac{C_8}{R^8} - \frac{C_{10}}{R^{10}} \tag{5.68}$$

where

$$C_6 \;=\; 3174.60 \text{ a.u.} \tag{5.69}$$

$$C_8 \;=\; 6.6257 \times 10^5 \text{ a.u.} \tag{5.70}$$

$$C_{10} \;=\; 1.03686 \times 10^8 \text{ a.u. .} \tag{5.71}$$

We obtained these values by fitting the right-hand side of (5.68) to the computed values of the adiabatic potential curve $V(R)$. The C_6 coefficient (5.69) obtained from the fit is practically the same as the exact value (4.16) 3173.8 a.u. (= twice the dispersion coefficient of Gutowski's potential curve for the triplet state of Na_2). However, the C_8 coefficient (5.70), also derived from the fit, is too large compared to the two coefficients (4.17) and (4.18) for linear and for perpendicular geometries, 2.7557×10^5 a.u. and 2.7442×10^5 a.u. We have not tried to explain this discrepancy, but it ought to be examined more carefully.

5.3.5   Scattering at energies above threshold

In the following, the threshold for break-up into Na and $Na_2(v=0, j=0)$ is chosen as the zero in energy:

$$E(v=0, j=0) \;\equiv\; 0 \;. \tag{5.72}$$

Bound states of Na_3 are found at negative energies $(E < 0)$, scattering states of $Na + Na_2$ occur at positive energies $(E > 0)$. At energies just above

---

[6]In the actual numerical computations, we used the *mass-scaled* Jacobi length $\bar{R}$ and *mass-scaled* dispersion coefficients $\bar{C}_n$ such that

$$V \;=\; -\frac{\bar{C}_6}{\bar{R}^6} - \frac{\bar{C}_8}{\bar{R}^8} - \frac{\bar{C}_{10}}{\bar{R}^{10}} \tag{5.67}$$

where

$$\bar{C}_6 \;=\; 4887.61 \text{ a.u.}$$

$$\bar{C}_8 \;=\; 1.1779 \times 10^6 \text{ a.u.}$$

$$\bar{C}_{10} \;=\; 2.12846 \times 10^8 \text{ a.u.}$$

The unscaled and the scaled dispersion coefficients are related as follows (case of three equal masses):

$$C_n \;=\; \bar{C}_n \left(\frac{3}{4}\right)^{n/4} \;.$$

the $(E = 0)$-threshold, one of the three sodium atoms may escape to infinity, leaving behind a sodium molecule Na_2 in its vibrational-rotational ground state $(v = 0, j = 0)$.

The threshold for break-up into Na and a rotationally excited molecule $Na_2(v = 0, j = 2)$ is at

$$E(v = 0, j = 2) = 0.3194 \text{ cm}^{-1} . \tag{5.73}$$

Our scattering computations, described in this and the next few sections, are restricted to the energy range

$$-0.7 \text{ cm}^{-1} \leq E \leq 0.3 \text{ cm}^{-1} . \tag{5.74}$$

We did not extend the calculations to energies above 0.3 cm^{-1}, because this would require taking into account the first excited channel $(v = 0, j = 2, l = 2)$. In principal, this can be done very easily, but our first priority was to understand the purely elastic scattering process.

It may also be possible to extend the present calculations to somewhat lower energies. At sufficiently low energies, however, the interval (5.65) where the reactance matrix is extracted becomes strongly forbidden energetically, and the short-range reference functions $\bar{f}$ and $\bar{g}$ defined below will diverge exponentially within this interval, which could cause numerical difficulties (this remains to be tested).

In the energy range

$$0 \text{ cm}^{-1} \leq E \leq 0.3 \text{ cm}^{-1} \tag{5.75}$$

the only open channel is the elastic one,

$$\text{Na} + \text{Na}_2(v=0, j=0) \qquad \leftrightarrow \qquad \text{Na} + \text{Na}_2(v=0, j=0)$$
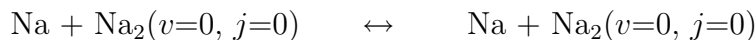
and the physically significant open-open block of the reactance matrix $\mathbf{K}(E)$ is simply a number, $K_{11}(E)$, where the index "1" stands for the channel numbers $(v = 0, j = 0, l = 0)$, v and j being the vibrational and rotational index of the Na_2 molecule and l being the partial wave number associated with the relative motion between Na and Na_2.

In order to analyse the hyperradial logarithmic derivative matrix and to obtain the K-matrix, we generated the two reference functions $\mathbf{F}(R)$ and $\mathbf{G}(R)$ defined in Eq. (5.56) numerically. In the interval (5.65) needed for the matching procedure, we approximated $\mathbf{F}(R)$ and $\mathbf{G}(R)$ by diagonal matrices, neglecting all interchannel coupling outside the hypersphere $\rho = 50.0$ a_0. The diagonal elements $F_{\nu\nu}(R)$ and $G_{\nu\nu}(R)$ associated with the *closed* channels

$$\nu \neq (v = 0, j = 0, l = 0)$$

were approximated by rising and falling exponentials, respectively.

The reference functions $f \equiv F_{11}(R)$ and $g \equiv G_{11}(R)$ associated with the *open* channel

$$\nu = (v = 0, j = 0, l = 0)$$

are defined as the solutions of the radial Schrödinger equation

$$y''(R) + \left[k^2 - \frac{2\mu V(R)}{\hbar^2} \right] y(R) = 0 \tag{5.76}$$

obeying the asymptotic boundary conditions

$$f(R) \to k^{-1/2} \sin(kR) , \qquad g(R) \to -k^{-1/2} \cos(kR) \qquad (R \to \infty) . \tag{5.77}$$

Here k is the asymptotic wavenumber, related to the energy E as

$$E = \frac{\hbar^2 k^2}{2\mu} . \tag{5.78}$$

The physical solution $u(R) \equiv u_{11}(R)$ (the "open-open" block of the solution matrix $\mathbf{u}$) is written as

$$u(R) = f(R) - g(R)K \tag{5.79}$$

where $K \equiv K_{11}$ is the open-open block of the K-matrix.

In their study of Na + Na$_2$ collisions at ultra-low energy, P. Honvault and J.-M. Launay [248] computed the functions f and g in Eq. (5.77) using the de Vogelaere integration technique [63]. In principal, we could have used the same numerical routine. However, we opted for an alternative method, based on the Milne equation [194], with the aim of extending the scattering calculations to *negative* energies and of searching for bound states. We realized later that we might as well have used the de Vogelaere algorithm, or any other suitable integration technique. This will be discussed in Sec. 5.3.9.

Since the precise manner of generating the functions f and g does not seem to matter much, we shall describe our method based on the Milne equation [194] only briefly. We write f and g in a phase-amplitude form such that

$$f(R) = a(R) \sin \phi(R) , \tag{5.80}$$
$$g(R) = -a(R) \cos \phi(R) . \tag{5.81}$$

The quantities a and ϕ are refered to, respectively, as the Milne amplitude and the accumulated phase. The Milne amplitude is a solution of Milne's equation

$$a''(R) + \frac{2\mu}{\hbar^2}[E - V(r)]a(R) - \frac{1}{a(R)^3} = 0 \tag{5.82}$$

134

a non-linear second-order differential equation. It is derived in Appendix J. We rewrite Milne's equation (5.82) as a system of two coupled first-order differential equations and solve it numerically using the fourth-order Runge-Kutta algorithm [39, 187] with a self-adjusting step size. The integration is started at a large distance, where the potential energy (5.68) is negligible compared to the energy E, using the initial values $a = k^{-1/2}$, $a = 0$. The accumulated phase $\phi(R)$ is given by the identity

$$\phi(R) \;=\; \text{const} \;+\; \int^{R} \frac{dR'}{[a(R')]^2} \;.\tag{5.83}$$

The integration constant in the above equation is chosen such that f and g verify the asymptotic boundary conditions (5.77). We computed the integral (5.83) from our numerical values for $[a(R)]^{-2}$ and $\frac{d}{dR}[a(R)]^{-2}$ on the non-equidistant grid of integration points R_i $(i = 0, 1, 2, 3, \ldots)$ by applying Hermite's trapezoidal rule [39] to each interval $[R_i, R_{i+1}]$. The integration is stopped at the inner boundary of the matching interval (5.65).

From the hyperradial logarithmic derivative matrix given at the hyperradius $\rho = 50$ a$_0$ and the values of the reference functions $\mathbf{F}$ and $\mathbf{G}$ in the matching interval (5.65), we extracted the K-matrix using the matching code developed by J.-M. Launay. We have used the matching routine as a "black box".

From the K-matrix element $K_{11}(E)$, we calculated the asymptotic s-wave phase shift $\delta(E)$ modulo π using the identity

$$\tan \delta(E) \;=\; K_{11}(E) \;.\tag{5.84}$$

The computed phase shift and its derivative with respect to the energy are plotted in Fig. 5.8, together with an alternative phase shift to be defined in Sec. 5.3.6. The derivative of $\delta(E)$ is singular at threshold $(E = 0)$, in accordance with the threshold law [150] for the s-wave phase shift:[7]

$$\tan \delta \;\propto\; E^{1/2} \;.\tag{5.85}$$

---

[7]Threshold laws and effective range expansions for scattering by long-range $1/R^n$ potentials $(n > 2)$ can be derived elegantly using the variable phase equation for the partial wave phase shift [168]. The leading terms of the Jost function at low energy can be found similarly, using the variable phase equations for the Jost function [275].

In the low-energy limit $(k \to 0)$ the tangent $\tan \delta_l$ of the lth partial wave shift δ_l is proportional to k^{2l+1} where k is the asymptotic wavenumber, provided that the potential tends to zero faster than $1/R^{2l+3}$.
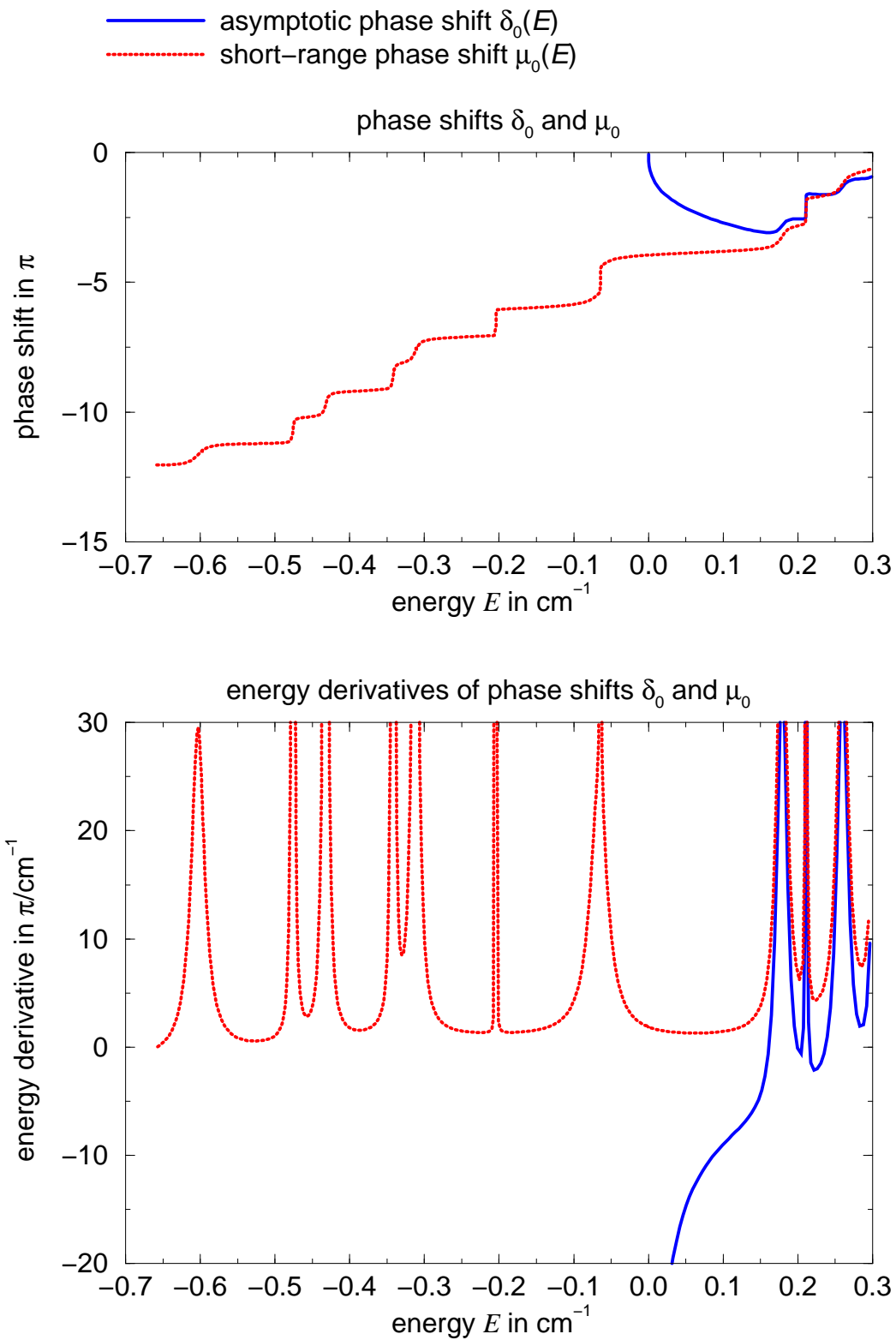
Figure 5.8: Top: The asymptotic and and the short-range phase shifts δ_0 and μ_0 as functions of the energy E. The Na$_2$ ($v = 0, j = 0$) threshold is at $E = 0$. Bottom: The derivatives of the phase shifts with respect to the energy, $d\delta_0/dE$ and $d\mu_0/dE$.

5.3.6 Scattering at energies below threshold

At energies below the atom-diatom threshold, the only physical states of the triatomic system Na + Na + Na are bound states of Na_3. However, at energies sufficiently close to the Na + $Na_2(v=0, j=0)$ threshold, the trimer may perform vibrations of very large amplitude, such that it separates temporarily into an atom and a molecule. We therefore find it appealing to regard such vibrations as collisions between Na and Na_2 at negative energy. One may expect that in those regions of configuration space in which the atom is far away from the remaining dimer, the bound state wavefunction of Na_3 resembles a continuum wavefunction, in the sense that it factorizes approximately into a vibrational-rotational function of Na_2 and a radial wavefunction describing the relative motion (the "collision") of Na and Na_2. We have therefore tried to analyse the radial wavefunction for negative energies in terms of two oscillating reference functions $\bar{f}(R)$ and $\bar{g}(R)$, in much the same manner as it is analysed for positive energies in terms of regular and irregular Riccati-Bessel functions.

Following J. P. Burke *et al.* [44], we defined the pair of short-range reference functions $\bar{f}$ and $\bar{g}$ by identifying them at a fixed distance R_0 with the two linearly independent semi-classical solutions

$$\bar{f}_{\mathrm{sc}}(R) = [k_{\mathrm{loc}}(R)]^{-1/2} \sin \int_{R_0}^{R} k_{\mathrm{loc}}(R') \, dR' \tag{5.86}$$

and

$$\bar{g}_{\mathrm{sc}}(R) = -[k_{\mathrm{loc}}(R)]^{-1/2} \cos \int_{R_0}^{R} k_{\mathrm{loc}}(R') \, dR' \tag{5.87}$$

where $k_{\mathrm{loc}}(R)$ is the local wavenumber

$$k_{\mathrm{loc}}(R) = \frac{1}{\hbar} \sqrt{2\mu[E - V(R)]} \ . \tag{5.88}$$

As before, the energy E is measured with respect to the Na + $Na_2(v=0, j=0)$ threshold, and $V(R)$ is the adiabatic potential curve (5.68). The reference functions $\bar{f}$ and $\bar{g}$ and their derivatives thus satisfy the initial conditions

$$\bar{f}(R_0) = \bar{f}_{\mathrm{sc}}(R_0) \ , \qquad \bar{g}(R_0) = \bar{g}_{\mathrm{sc}}(R_0) \ , \tag{5.89}$$

$$\bar{f}'(R_0) = \bar{f}'_{\mathrm{sc}}(R_0) \ , \qquad \bar{g}'(R_0) = \bar{g}'_{\mathrm{sc}}(R_0) \ . \tag{5.90}$$

These initial conditions imply that $\bar{f}$ and $\bar{g}$ are mutually dephased by 90° at distances $R \approx R_0$. Furthermore, they guarantee that $\bar{f}$ and $\bar{g}$ are *smooth* functions of the energy, at any fixed distance R and for all energies larger than $V(R_0)$.

In analogy with Eq. (5.79) we write[8]

$$u(R) = \bar{f}(R) - \bar{g}(R)\bar{K} \tag{5.91}$$

which defines the short-range reactance matrix $\bar{K}$. In the present single-channel formalism, $\bar{K}$ is simply a number. We define the short-range phase shift μ modulo π implicitly by the relation

$$\bar{K} = \tan\mu . \tag{5.92}$$

We might call μ a *quantum defect*. However, because of its close analogy with the ordinary long-range phase-shift δ, we prefer to call μ simply the *short-range* phase shift. $\bar{f}$ and $\bar{g}$ being continuous functions of the energy, the short-range phase shift $\mu(E)$ is continuous as well, notably at threshold $E = 0$.

We chose somewhat arbitrarily

$$R_0 = 32.57 \text{ a}_0 , \tag{5.93}$$

which is equivalent to the mass-scaled distance $\bar{R}_0 = 35.0$ a$_0$ [see Eq. (3.27)]. At this distance the potential (5.68) measures

$$V(R_0) = -0.7153 \text{ cm}^{-1} . \tag{5.94}$$

It might be possible to extend the computations to lower energies by choosing a smaller value for R_0.

We generated the functions $\bar{f}$ and $\bar{g}$ numerically for selected energies in the interval (5.74) by integrating the Milne amplitude $a(R)$ in the *outward* direction, starting at $\bar{R}_0 = 35$ a$_0$ and stopping at a distance where the potential (5.68) was negligible compared to the energy ($E < 0$ or $E > 0$).

Fig. 5.9 shows $\bar{f}$ and $\bar{g}$ for zero energy ($E = 0$) as functions of the mass-scaled distance $\bar{R}$. In the range $(\bar{R}_0, \infty)$, $\bar{f}$ and $\bar{g}$ each have only two nodes. Since the local de Broglie wavelength in the classically allowed region increases when the energy E decreases, one could expect the number of bound levels in the energy range

$$V(R_0) = -0.7153 \text{ cm}^{-1} < E < 0 \text{ cm}^{-1} \tag{5.95}$$

to be of the order of only *two*. If the energy-dependence of the logarithmic derivative of the wavefunction $u(R)$ was negligible at the distance R_0, there should be one or two, at most three, bound states in the energy range (5.95). However, our numerical results which are presented below show that the

---

[8]We use the bar on the symbols f and g to distinguish between the short-range functions $(\bar{f}, \bar{g})$ and the long-range functions (f, g). The bar on R is used to distinguish between the mass-scaled distance $\bar{R}$ and the unscaled distance R.
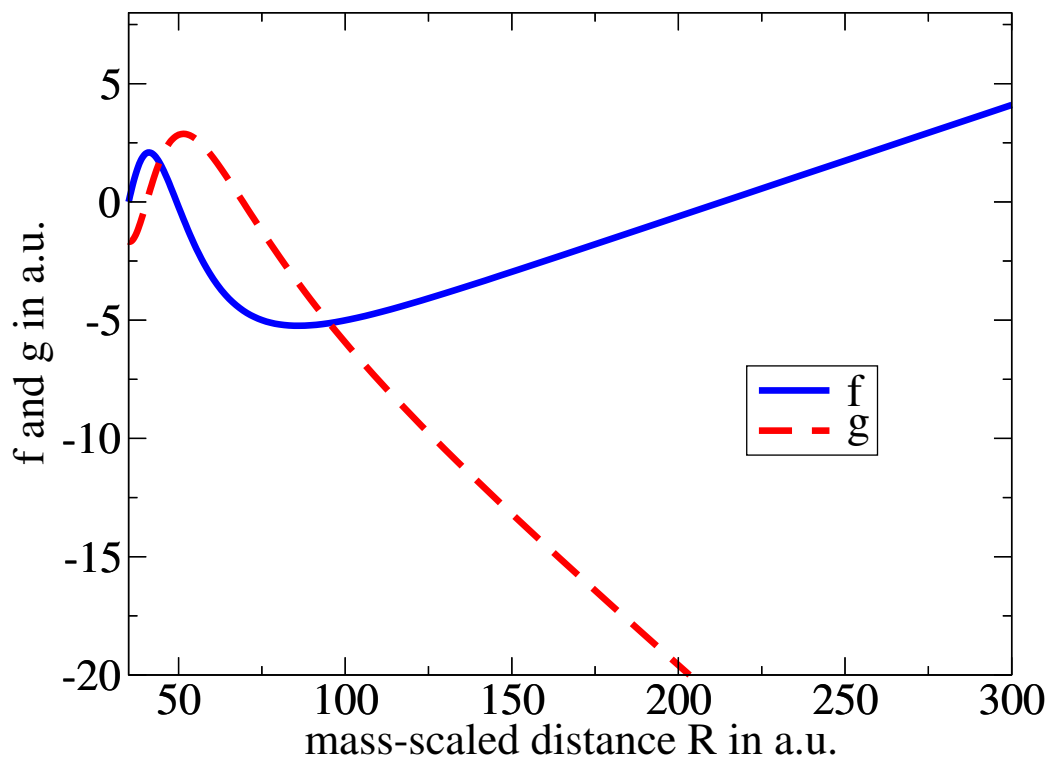
Figure 5.9: Short-range reference solutions $\bar{f}$ and $\bar{g}$ at zero energy for distances $\bar{R} \geq 35$ a$_0$.

density of states is considerably larger due to resonances in the short-range phase shift $\mu(E)$.

We computed the short-range reactance matrix $\bar{\mathbf{K}}$ by analysing the hyperradial logarithmic derivative matrix on the hypersphere $\rho = 50$ a_0 using the reference functions $\bar{f}(R)$ and $\bar{g}(R)$ in the "open" channel

$$(v = 0, \ j = 0, \ l = 0) \ \equiv \ \text{"1"}$$

and the usual rising and decaying exponential functions in the other channels.

From the element $\bar{K}(E) \equiv \bar{K}_{11}(E)$ of the short-range reactance matrix $\bar{\mathbf{K}}$ we obtained the short-range phase shift $\mu(E)$, *à l'addition d'un multiple de π près*[9]. It is plotted in Fig. 5.8, along with the conventional phase shift $\delta(E)$.

5.3.7   Resonances

In the energy range (5.74), the calculated short-range phase shift $\mu(E)$ passes through ten resonances, seven of which lie below the bound-continuum threshold (see Fig. 5.8). Fig. 5.10 shows the behaviour of the phase shift $\mu(E)$ near the resonance $E_0 = 0.064357$ cm^{-1}. The three resonances found above threshold manifest themselves also in the long-range phase shift $\delta(E)$.

In the vicinity of each resonance, the short-range phase shift $\mu(E)$ increases rapidly by roughly π over an energy range Γ, the width of the resonance. At energies sufficiently close to the centre E_0 of the resonance, the phase shift can be approximated by the formula

$$\mu(E) \ = \ \mu(E_0) - \arctan \frac{\Gamma}{2(E - E_0)} \tag{5.96}$$

which is analogous to Eq. (134,10) of Ref. [150] (Landau and Lifchitz, *Mécanique Quantique*) describing a resonance in the long-range phase-shift $\delta(E)$. The fitted values E_0 and Γ are given in Table 5.1.

According to Landau and Lifchitz [150], the width of a resonance in the conventional phase-shift $\delta(E)$ can be interpreted as the probability per unit time for the system to decay. Naively, one could try to interpret resonances in $\mu(E)$ in the same manner, be the energy positive or negative. The width of each resonance in $\mu(E)$ could thus be seen as the probability per unit time for a quasi-bound Na$_3$ complex to decay into an Na atom and an Na$_2(v=0$, $j=0)$ molecule. Of course, if the energy is negative, the distance between the two fragments must remain finite. At negative energies, the Na atom and the Na$_2$ molecule remain weakly bound by the van der Waals force, and they will collide after one vibrational period to form once again a quasi-stable trimer such that the three atoms remain close together for a while.

---

[9]modulo π
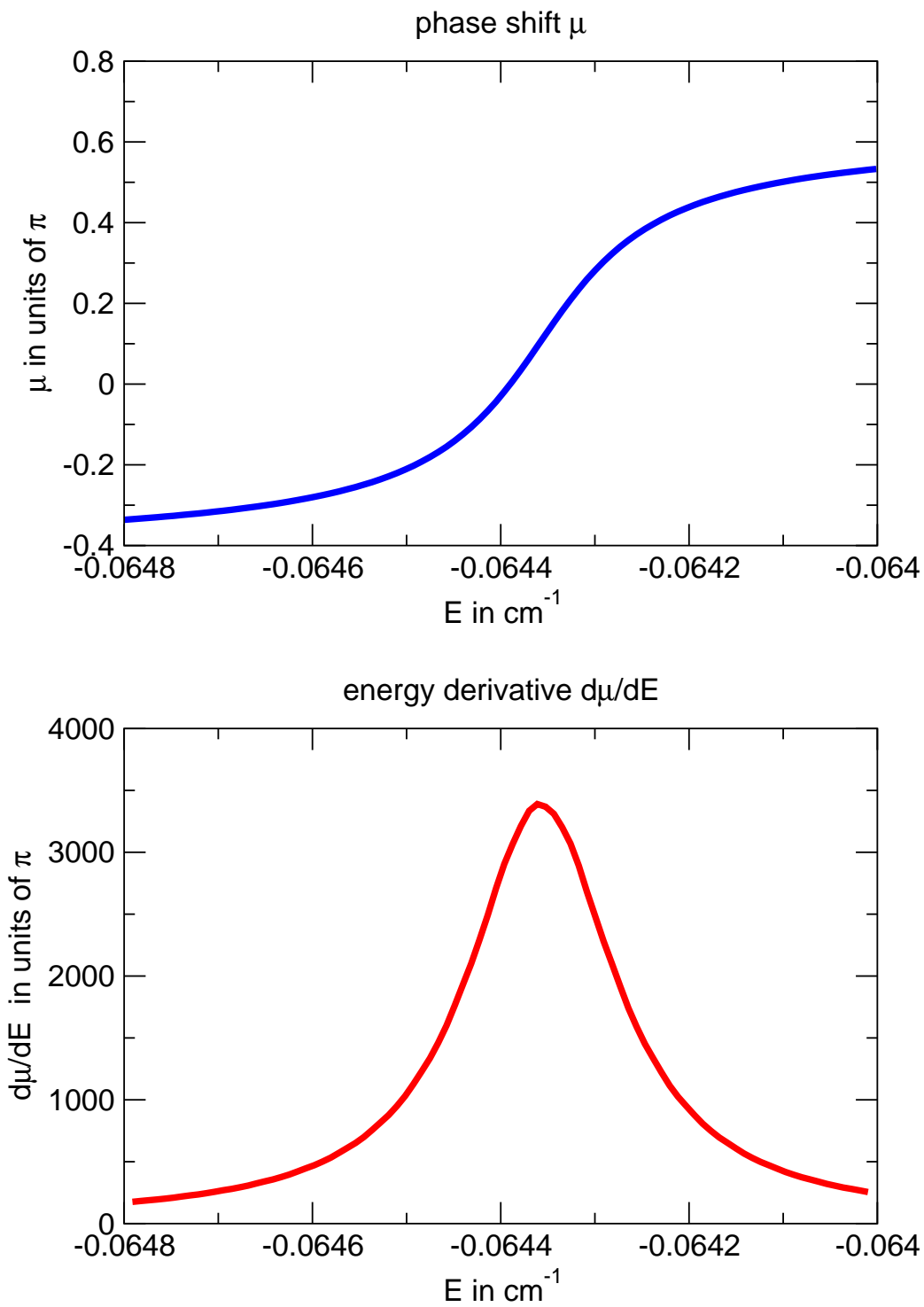
Figure 5.10: The short-range phase shift μ and its derivative $\frac{d\mu}{dE}$ as functions of the energy E near the resonance $E_0 = -0.064357$ cm^{-1}.

Position E_0 in cm^{-1}	Width Γ in cm^{-1}	Level index w
0.210879	0.00023	-
0.259748	0.016	-
0.178728	0.015	-
-0.064357	0.00019	3
-0.204273	7.2×10^{-5}	5
-0.31222	0.0095	6
-0.341782	0.0026	7
-0.432213	0.0057	8
-0.475856	0.0022	9
-0.603184	0.021	10

Table 5.1: Resonances in the short-range phase shift $\mu(E)$. The index w indicates the vibrational level of Na$_3$ associated with the resonance (see the main text and Table 5.2)

Perhaps this simple picture is correct only if the relative motion of the Na atom and the Na$_2$(v=0, j=0) molecule is semi-classical. In this case the reference functions $\bar{f}(R)$ and $\bar{g}(R)$ display many regular oscillations and resemble continuum wavefunctions, except in the outer classically forbidden region. In order to interpret the motion in the classically allowed region at intermediate distances, the short-range phase shift μ could then be used in much the same manner as one uses the asymptotic phase shift δ to analyse the oscillating continuum functions.

It is well known [245, 93, 82] that every isolated resonance in the asymptotic phase shift $\delta(E)$ can be related to a time-delay of the scattered wavepacket. We think that it should be possible to extend the theory of time-delay to resonances below threshold, provided that the relative motion of the colliding partners is locally that of a free particle, so that the stationary radial wavefunction is approximated sufficiently well by a plane wave on a sufficiently large interval.

Quasi-bound states of triatomic systems are discussed, for example, in Ref. [146].

5.3.8 Bound states

If the energy E is negative, the short-range reference functions $\bar{f}$ and $\bar{g}$ behave asymptotically as

$$\bar{f}(R) \quad \rightarrow \quad \exp(\kappa R)\, A(E) \qquad (5.97)$$

$$\bar{g}(R) \quad \rightarrow \quad \exp(\kappa R)\, B(E) \tag{5.98}$$

when $R \rightarrow \infty$. Here κ is given by

$$\kappa \;=\; \frac{\sqrt{2\mu(-E)}}{\hbar} \;. \tag{5.99}$$

The coefficients A and B in Eqs. (5.97) and (5.97) are energy-dependent amplitude functions. The wavefunction $u(R)$ accordingly behaves as

$$u(R) \quad \rightarrow \quad \exp(\kappa R)[A(E) - B(E)K(E)] \qquad (R \rightarrow \infty) \;. \tag{5.100}$$

At energies E such that

$$A(E) - B(E)\bar{K}(E) \;=\; 0 \tag{5.101}$$

the wavefunction $u(R)$ decays exponentially when $R \rightarrow \infty$. Such energies correspond to bound states.[10] By comparing Eqs. (5.97), (5.98) and (5.80), (5.81), one sees that the Milne amplitude $a(R)$ diverges as $\exp(\kappa R)$ and that Milne's accumulated phase $\phi(R)$ converges to an energy-dependent value $\beta(E)$:

$$\lim_{R\rightarrow\infty} \phi(R) \;=\; \beta(E) \;. \tag{5.102}$$

The bound state condition (5.101) can thus be written as

$$\sin\beta(E) + \cos\beta(E)\, \bar{K}(E) \;=\; 0 \;. \tag{5.103}$$

By searching for zeros of the function

$$D(E) \;\equiv\; \sin\beta(E) + \cos\beta(E)\, \bar{K}(E) \tag{5.104}$$

(see Fig. 5.11), we obtained numerical values for the energies of ten weakly bound states in the energy range

$$-0.6 \text{ cm}^{-1} \;\leq\; E \;< 0 \text{ cm}^{-1} \;. \tag{5.105}$$

These energies are listed in Table 5.2, along with values obtained by the hyperradial method described in Sec. 5.2.

The values $E^{(1)}$ and $E^{(2)}$ agree very well, in the sense that the differences $|E^{(2)} - E^{(1)}|$ are small compared to the spacings between two different vibrational levels. The logarithmic derivative matching method does not yield the

---

[10]The condition (5.101) can be generalized to the case where more than one channel are treated like locally open channels. If there are N locally open channels, the bound state condition takes the form

$$\det[\mathbf{A}(E) - \mathbf{B}(E)\bar{\mathbf{K}}(E)] \;=\; 0$$

where $\mathbf{A}$, $\mathbf{B}$ and $\bar{\mathbf{K}}$ are square matrices of dimension $N \times N$.
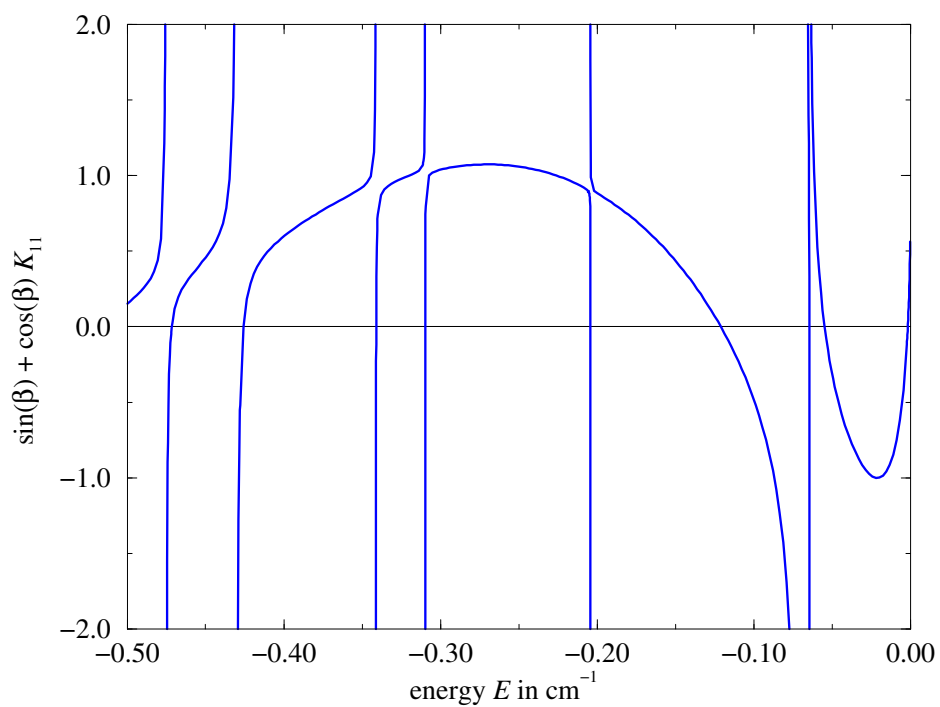
Figure 5.11: The quantity $D = \sin(\beta) + \cos(\beta)K$ as a function of the energy E. Bound state energies are zeros of D.

| Level | Computed energy | | Comment |
| | using HS coord. | using HS + Jacobi coord. | |
w	$E^{(1)}$ in cm^{-1}	$E^{(2)}$ in cm^{-1}	
1	not found	-0.001615	-
2	-0.0440	-0.05472	-
3	-0.0642	-0.06446	R
4	-0.11715	-0.12102	-
5	-0.2041	-0.204291	R
6	-0.3093	-0.309728	R
7	-0.3407	-0.341034	R
8	-0.4257	-0.42578	R
9	-0.4710	-0.471537	R
10	-0.5205	-0.5205	R

Table 5.2: Computed energies of highly excited vibrational levels of $Na_3(^4A_2')$. The zero in energy lies at the threshold for break-up into Na and Na_2. The energies $E^{(1)}$ were obtained by the hyperradial method described in Sec. 5.2.9. The energies $E^{(2)}$ were deduced from the reactance matrix $\bar{K}$ and the short-range phase-shift μ. Energies near resonances of μ are marked by the letter "R".

energy of the very last, least bound level ("1"), which is readily explained by the fact that the wavefunction of the last level is not negligible outside the hypersphere ($\rho = 50$ a$_0$).

In order to make appearant the link between the resonances and the bound state energies , we have plotted the latter in Fig. 5.3.8 together with the energy derivative of the short-range phase shift $\mu(E)$. The figure shows that each resonance of $\mu(E)$ is directly linked to a bound state, and only the weakly bound states "1", "2", and "4" (see Table 5.2) are not caused by resonances.

In the previous paragraph, we suggested interpreting the width of the resonances in μ as the probability for a metastable Na$_3$ trimer to decay into a weakly bound Na + Na$_2(v{=}0, j{=}0)$ van der Waals complex. If this interpretation is justified, we may expect that at large distances ($\bar{R} \geq 35$ a$_0$) the amplitudes of the stationary normalized wavefunctions for the non-resonant bound states "1", "2" and "4" will be *larger* than those of the resonant states "3" and "5", "6", "7", "8", "9", "10". In order to verify whether this hypothesis is true, it would be necessary to compute not only the phase shift, but also to generate the complete normalized wavefunctions of these weakly bound levels. Unfortunately, this cannot be done easily with the scattering code we used. A DVR method should be more appropriate. However, we are not aware of any DVR code designed to compute the *very weakly* bound states that are the subject of the present study.

It should be noted that *all* computed values $E^{(2)}$ are slightly smaller than the corresponding values $E^{(1)}$. In the case of the very weakly bound levels "2", "3", perhaps also "4", this systematic error might be explained by the neglect of the wavefunctions' exponentially decreasing tails outside the hypersphere ($\rho = 50$ a$_0$) in the hyperradial method.

In our calculations using the Jacobi coordinates there are probably many other sources of error:

- Some accuracy may be lost due to the matching between hyperspherical and Jacobi coordinates.

- At energies sufficiently far below the $E(v = 0, j = 0)$ threshold, the exponential growth of our reference functions $\bar{f}(R)$ and $\bar{g}(R)$ starts at a short distance, such that $\bar{f}(R)$ and $\bar{g}(R)$ tend to become linearly dependent within the matching interval (5.65). If the linear dependence is too strong, the K-matrix cannot be computed correctly.

- All interchannel coupling was assumed negligible outside the hypersphere $\rho = 50$ a$_0$.

- Our adiabatic potential curve $V(R)$ may not have been realistic enough.
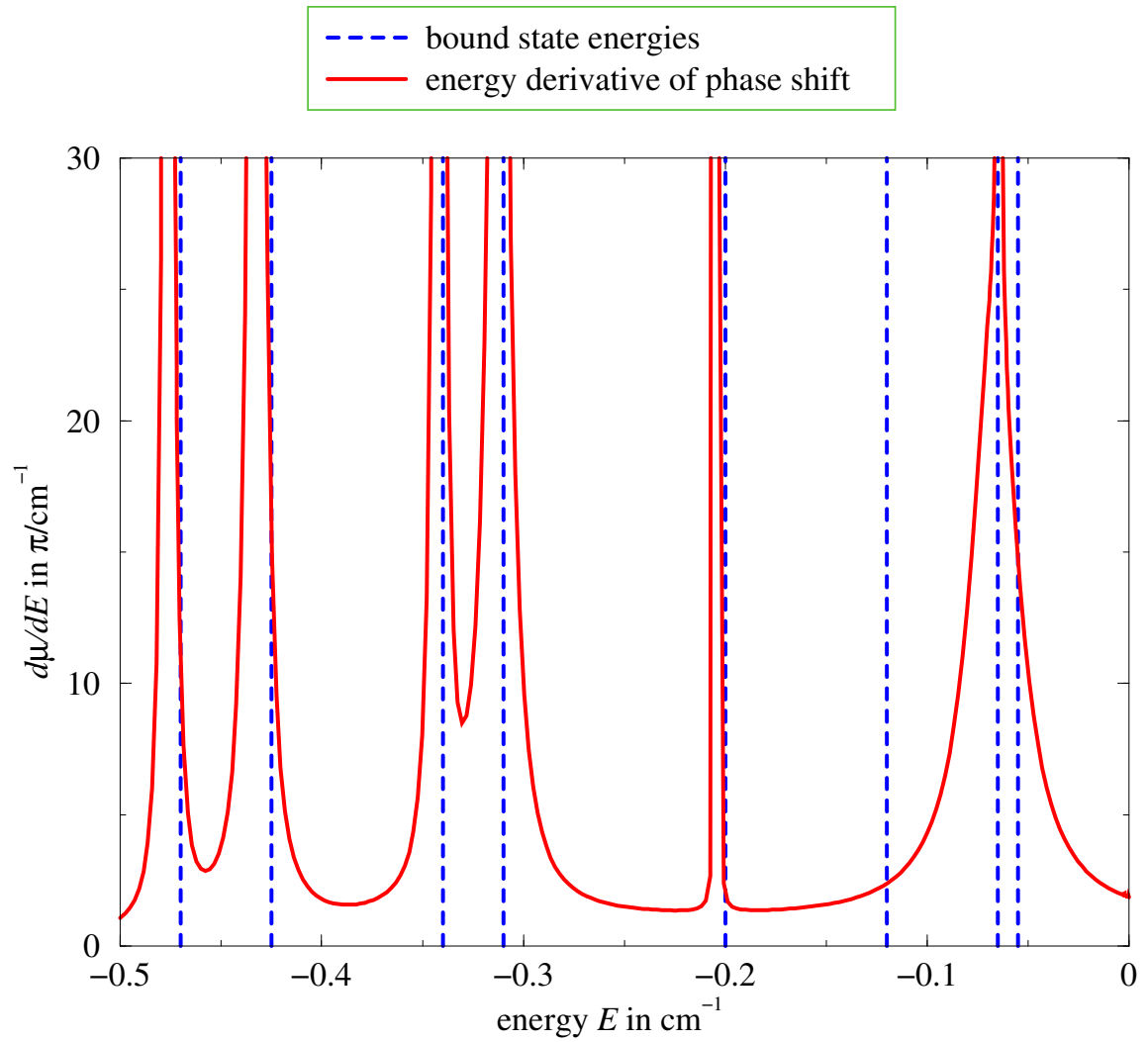
Figure 5.12: Resonances and bound state energies. Full red line: the energy-derivative $\frac{d\mu}{dE}$. Dashed blue lines: bound state energies.

It is striking that the numerical error is larger in the case of the non-resonant states "1", "2", and "4", compared to the resonant states. This could be explained by our earlier hypothesis, namely that the wavefunctions of the non-resonant states have a relatively large amplitude at large distance, i. e. outside the hypersphere $\rho = 50$ a$_0$. For these levels, the numerical values $E^{(2)}$, deduced from the short-range reactance matrix $\bar{\mathbf{K}}$, should therefore be considered as more reliable than the values $E^{(1)}$ which were obtained using only hyperspherical coordinates.

We expect that the computed value for the binding energy of the very last bound level ("1") is extremely sensitive to any changes in the long-range part of the adiabatic potential $V(R)$, in particular to the value of the C_6 coefficient. It would be important to check to what extent the results for the other bound levels depend on the numerical values of the C_6, C_8 and C_{10} coefficients used to approximate the potential at large distances. If it is true that the wavefunctions of the non-resonant states "1", "2", "4" extend far into the Jacobi regions, their energies should be more sensitive to the form of the potential curve $V(R)$.

5.3.9   Comment on the Milne equation

Many authors [44, 192, 126] have used the Milne equation (5.82) in order to generate a base pair of linearly independent solutions $f(R)$ and $g(R)$ of the radial Schrödinger equation numerically and to obtain the accumulated phase parameter $\beta(E)$ defined in Eq. (5.102).

We believe that the method has two major drawbacks.

Firstly, it is difficult to test the numerical accuracy of the solutions $f(R)$ and $g(R)$ if these are constructed from the Milne amplitude $a(R)$ and Milne's accumulated phase $\phi(R)$ using Eqs. (5.80), (5.81) and (5.83). In fact $f(R)$ and $g(R)$ given by these equations are such that their Wronskian

$$ W[f, g] \; = \; f(R)g'(R) - f'(R)g(R) \tag{5.106} $$

equals exactly one, $W[f, g] = 1$, whether the Milne amplitude $a(R)$ solves Milne's equation (5.82) or not. Therefore, if $f(R)$ and $g(R)$ are generated from Milne's amplitude and the corresponding accumulated phase, the Wronskian (5.106) cannot be used to check whether $f(R)$ and $g(R)$ solve the radial Schrödinger equation (5.76).

Secondly, the Milne amplitude may vary violently if the JWKB approximation fails. In this case a very small step size may be needed to solve the Milne equation numerically, leading to a loss in numerical accuracy. This is especially worrying, because there is no simple means to check the accuracy of the computed functions $f(R)$ and $g(R)$, their Wronskian being constant by definition.

In order to investigate the Wigner threshold law, we integrated Milne's amplitude in the inward direction, starting in the asymptotic region at large distance using JWKB-like initial conditions $a = k^{-1/2}$, $a' = 0$ at an energy-dependent distance where the potential C_6/R^6 potential was negligible. We found it impossible to compute the amplitude correctly at extremely low energies because it assumed a step-like behaviour. We did not experience the same kind of problem when integrating the Milne amplitude in the outward direction, again starting with JWKB-like initial conditions: in this case the Milne amplitude became oscillatory (not step-like) at large distances,

$$a(R) \rightarrow A + B\sin(kR + \gamma) \qquad (R \rightarrow \infty) \qquad (5.107)$$

A, B and γ being constants such that $a(R)$ is positive at all distances, i.e. $0 < B < A$. In the limiting case where the JWKB approximation is valid on the entire range $R_0 \leq R \leq \infty$, the constants A and B were found to be $A \approx k^{1/2}$, $B \approx 0$, as expected.

To summarize, we believe that it is generally more convenient to generate the reference functions $f(R)$ and $g(R)$ independently from each other by solving the radial Schrödinger equation directly using a standard integration technique, such as the Numerov algorithm (see the Appendix K) or de Vogelaere's method [63].

The Milne amplitude and Milne's accumulated phase could, however, be useful in order to study deviations from the JWKB approximation. If needed, Milne's accumulated phase parameter $\beta(E)$, defined for negative energies, can be obtained from the ratio between $f(R)$ and $g(R)$ at distances sufficiently far in the forbidden region:

$$\tan\beta(E) = -\lim_{R\to\infty} \frac{f(R)}{g(R)} . \qquad (5.108)$$

5.3.10 Determine the scattering length from spectroscopic data?

The accurate determination of atom-atom scattering lengths is a challenging problem [115]. In our group, A. Crubellier *et al.* [57] determined the Na-Na scattering length using the long-range part of the atom-atom interaction potential and experimental data for loosely bound levels close underneath the atom-atom dissociation threshold.

The present numerical study of bound states of Na_3 was partly motivated by the wish to find out whether the scattering length [150] for collisions between Na atoms and $Na_2(v{=}0, j{=}0)$ molecules might be deduced from spectroscopic data of weakly bound vibrational levels of Na_3, assuming that such data could be obtained experimentally.

Fig. 5.8 shows that the computed short-range phase shift $\mu(E)$ modulo π is approximately constant, except near the resonances. Each resonance is associated with a rapid increase of μ by approximately π as the energy E is scanned across the resonance. Thus the phase shift μ (modulo π) at threshold might be approximated reasonably well by the phase shift at the bound state energies "1", "2" or "4".

If the energy of one of the non-resonant states could be *measured* experimentally, the corresponding short-range phase shift μ or the element $\bar{K}$ of the short-range reactance matrix could be obtained by requiring the radial wavefunction (5.91) to vanish exponentially at large distance $(R \rightarrow \infty)$ at the *experimental* value of the energy. The experiment could replace the numerical method that we used to describe the reaction region, where the potential is not known sufficiently well as to allow to predict the correct value of the scattering length.

In order to generate the radial wavefunction (5.91), only the long-range part of the atom-molecule interaction potential $V(R)$ would need to be known accurately.

The short-range phase shift μ thus determined could be related to the scattering length α using the long-range behaviour of the short-range reference functions $\bar{f}$ and $\bar{g}$. The quality of the result will depend on the precise manner in which $\bar{f}$ and $\bar{g}$ are defined. Clearly, they should be chosen as to minimize the energy-dependence of the short-range phase shift $\mu(E)$. For this purpose one could try to define them by a JWKB-like initial condition at a distance *shorter* than the distance $R_0 = 32.57$ a_0 we used in our computations (see Eq. 5.93).

The method proposed is roughly equivalent to the following intuitive way of proceeding:

1. Measure the energy E_{bound} of one of the very weakly bound non-resonant states of Na-Na$_2$.

2. Generate the corresponding radial wavefunction $u_{\text{bound}}(R)$ by solving the radial Schrödinger equation numerically through *inward* integration at the energy E_{bound}. Start the integration in the outer classically forbidden region where the wavefunction behaves as $\sim \exp(-\kappa R)$. Stop at a distance R_0 where the information regarding the adiabatic potential curve $V(R)$ becomes insufficient.

3. At the distance R_0, match the zero-energy wavefunction u_{zero} to the bound-state wavefunction u_{bound}:

$$
\begin{aligned}
u_{\text{zero}}(R) &= u_{\text{bound}}(R) \\
u'_{\text{zero}}(R) &= u'_{\text{bound}}(R) \qquad\qquad (R = R_0)
\end{aligned}
$$

4. Integrate $u_{\mathrm{zero}}(R)$ in the *outward* direction using the radial Schrödinger equation for zero energy. Stop at a distance where $u_{\mathrm{zero}}(R)$ has reached its asymptotic form

$$u_{\mathrm{zero}}(R) = (r - \alpha) \ \times \mathrm{const.}$$

The parameter α thus obtained could be an estimate for the scattering length.

At the present stage, we do not know how such weakly bound states could be measured experimentally. Besides, it must be tested whether the available information regarding the long-range part of the Na-Na$_2$ potential is accurate enough to obtain an estimate for the scattering length, or at least to predict its sign, if experimental data for these weakly bound states was available. Finally, it would be very important to clarify the possible influence of the interactions that give rise to the atomic hyperfine structure.

5.4 Solving the coupled equations in the three Jacobi regions

Jacobi coordinates provide a much more natural description of the triatomic system than hyperspherical coordinates if one atom is relatively far away from the two others. Their geometrical meaning is clear, and they are better suited than hyperspherical coordinates for analysing the relatively weak interactions between the atom and the molecule at intermediate and large distances.

The existing version of the reactive scattering code developed by J.-M. Launay *et al.* does not allow to take into account any residual couplings between the asymptotic channels vjl outside the hypersphere $\rho = \rho_{\mathrm{max}}$ (as before, v and j label the rotational-vibrational states of the diatomic molecule, and l is the partial wave number for the relative motion between the atom and the dimer). Therefore the hyperradial logarithmic derivative matrix must be propagated up to a relatively large hyperradius ρ_{max}, before it can be analysed in terms of asymptotic solutions expressed in Jacobi coordinates.

It would be a great step forward if the hyperradial logarithmic derivative matrix could be analysed on a *smaller* hypersphere. The numerical efficiency of the scattering code could probably be greatly improved, and it would become possible to study the role of the weak couplings between the atom and the molecule at large and intermediate distances.

The project of analysing the wavefunction on a smaller hypersphere is not finished yet. We shall summarize what has been accomplished so far, and describe a numerical method that could be used to convert a "short-range" reactance matrix, obtained at a relatively short hyperradius, into the asymptotic reactance matrix.

5.4.1 The problem of linear dependence

In order to improve the description of collisions between Na and Na_2, it would be desirable to stop the propagation of the hyperradial logarithmic derivative matrix $\mathbf{Z}(\rho)$ at a hyperradius ρ_0 considerably smaller than 50 a_0. In principal, the asymptotic K-matrix could be obtained by analysing $\mathbf{Z}$ at the distance $\rho_0 << 50$ a_0 using the reference functions $\mathbf{F}(R)$ and $\mathbf{G}(R)$ obeying the K-matrix boundary conditions described in Sec. (5.3.2). Our initial aim was therefore to generate the matrices $\mathbf{F}(R)$ and $\mathbf{G}(R)$ by *inward* integration, in direct analogy to the method described in Sec. 5.3.5. The integration was to be started at a very large distance R, where the atom-molecule interaction potential is negligible, and stopped at the inner border R^{min} of the matching interval (5.65). The only difference between the proposed scheme and the existing one is that the matching interval (5.65) would lie closer to the origin, so that $\mathbf{F}(R)$ and $\mathbf{G}(R)$ would no longer be diagonal due to the interchannel couplings at distances shorter than ≈ 50 a_0.

It is a well-known phenomenon that linearly independent solutions of differential equations can become numerically indistinguishable due to the limited number of digits on a computer. The problem can sometimes be overcome by propagating not the solution matrix itself but its logarithmic derivative matrix, using for example, the Johnson-Manolopoulos propagator [121, 182].

However, in the present case, knowing the logarithmic derivatives of $\mathbf{F}$ and $\mathbf{G}$ is not sufficient for converting the hyperradial logarithmic derivative matrix into the K-matrix: the functions $\mathbf{F}$ and $\mathbf{G}$ themselves and their radial derivatives $\mathbf{F}'$ and $\mathbf{G}'$ are needed for the matching procedure linking hyperspherical and Jacobi coordinates.

J.-M. Launay [155] tested the following stabilization technique in order to propagate $\mathbf{F}$ and $\mathbf{G}$ from large to small distances.

At a certain distance R_1, where the N numerical solutions summarized in the $(N \times N)$-matrix $\mathbf{F}(R) \equiv \mathbf{F}^{(0)}(R)$ start to become linearly dependent, the matrix $\mathbf{F}^{(0)}$ is replaced by

$$\mathbf{F}^{(1)}(R) \;=\; \mathbf{F}^{(0)}(R)\,\mathbf{S}_F^{(1)} \tag{5.109}$$

where $\mathbf{S}_F^{(1)}$ is the stabilizing matrix

$$\mathbf{S}_F^{(1)} \;\equiv\; \left[\mathbf{F}^{(0)}(R_1)\right]^{-1} . \tag{5.110}$$

The procedure is repeated at several distances, $R_2, R_3, \ldots, R_M$ such that

$$R_M \;<\; \ldots \;<\; R_2 \;<\; R_1 . \tag{5.111}$$

The stabilizing matrices

$$\mathbf{S}_F^{(m)} \;=\; \left[\mathbf{F}^{(m-1)}(R_m)\right]^{-1} \qquad (m = 1, 2, \ldots, M) \tag{5.112}$$

152

are stored in memory. The solution $\mathbf{F}^{(M)}$ obtained after M stabilizations is related to $\mathbf{F}^{(0)}$ using

$$\mathbf{F}^{(M)}(R) \;=\; \mathbf{F}^{(0)}(R)\,\mathbf{S}_F^{(1)}\,\mathbf{S}_F^{(2)}\cdots\mathbf{S}_F^{(M)} \tag{5.113}$$

The matrix $\mathbf{F}^{(M)}(R)$ is well-conditioned at short distances $(R \approx R_M)$, in particular in the matching interval (5.65), whereas $\mathbf{F}^{(0)}(R)$ is well-conditioned at long distances $(R \to \infty)$. This means that the product of all stabilizations tends to be singular, symbolically:

$$\mathbf{S}_F^{(1)}\,\mathbf{S}_F^{(2)}\cdots\mathbf{S}_F^{(M)} \;\approx\; \infty \tag{5.114}$$

The stabilization procedure for $\mathbf{G}$ is analagous:

$$\mathbf{G}^{(M)}(R) \;=\; \mathbf{G}^{(0)}(R)\,\mathbf{S}_G^{(1)}\,\mathbf{S}_G^{(2)}\cdots\mathbf{S}_G^{(M)} \tag{5.115}$$

By analysing the hyperradial logarithmic derivative matrix using the stabilized functions $\mathbf{F}^{(M)}$ and $\mathbf{G}^{(M)}$ one obtains a "local" K-matrix $\mathbf{K}^{(M)}$ that is related to the asymptotic K-matrix $\mathbf{K} \equiv \mathbf{K}^{(0)}$ as follows:

$$\mathbf{K}^{(0)} \;=\; \mathbf{S}_G^{(1)}\,\mathbf{S}_G^{(2)}\cdots\mathbf{S}_G^{(M)}\,\mathbf{K}^{(M)}\left[\mathbf{S}_F^{(M)}\right]^{-1}\cdots\left[\mathbf{S}_F^{(2)}\right]^{-1}\left[\mathbf{S}_F^{(1)}\right]^{-1}. \tag{5.116}$$

The above equation suggests that the local K-matrix $\mathbf{K}^{(M)}$ might be converted into the asymptotic K-matrix $\mathbf{K}^{(0)}$ numerically by performing the following series of operations:

$$\begin{aligned}
\mathbf{K}^{(M-1)} &\;=\; \mathbf{S}_G^{(M)}\,\mathbf{K}^{(M)}\left[\mathbf{S}_F^{(M)}\right]^{-1} \\[2mm]
\mathbf{K}^{(M-2)} &\;=\; \mathbf{S}_G^{(M-1)}\,\mathbf{K}^{(M-1)}\left[\mathbf{S}_F^{(M-1)}\right]^{-1} \\[2mm]
&\;\;\vdots\;\;\vdots\;\;\vdots \\[2mm]
\mathbf{K}^{(1)} &\;=\; \mathbf{S}_G^{(2)}\,\mathbf{K}^{(2)}\left[\mathbf{S}_F^{(2)}\right]^{-1} \\[2mm]
\mathbf{K}^{(0)} &\;=\; \mathbf{S}_G^{(1)}\,\mathbf{K}^{(1)}\left[\mathbf{S}_F^{(1)}\right]^{-1}
\end{aligned} \tag{5.117}$$

Although these equations are formally correct, J.-M. Launay found that the algorithm was *unstable* [155].

In order to examine this problem, we implemented two different numerical methods for solving the coupled equations (5.47) arising from the Arthurs-Dalgarno expansion.

In the first method, we generated the reference functions $\mathbf{F}(R)$ and $\mathbf{G}(R)$ numerically by solving the coupled equations (5.47) directly, either by a fourth-order Runge-Kutta scheme which is easy to implement but not very precise, or by the Numerov propagator described in the Appendix K.

In the second method, we expressed the wavefunction and its radial derivative in terms of two amplitude functions and rewrote the coupled second-order differential equations (5.47) as a system of coupled variable phase equations. The variable phase equations are derived by comparing the wavefunction at each distance R to two linearly independent reference functions $\mathbf{F}^{\text{ref}}(R)$ and $\mathbf{G}^{\text{ref}}(R)$. We defined the reference functions as solutions of the second-order equations without the non-diagonal coupling terms. Thus $\mathbf{F}^{\text{ref}}$ and $\mathbf{G}^{\text{ref}}$ are diagonal matrices at every distance R. We solved the resulting variable phase equations using the fourth-order Runge-Kutta method, by propagating the amplitude matrices along the radial coordinate R, either in the inward or in the outward directions, using various initial conditions. The reference functions $\mathbf{F}^{\text{ref}}$ and $\mathbf{G}^{\text{ref}}$ were generated "on the fly", in the course of the propagation along R. The amplitude functions are very convenient, as they allow to monitor the effect of channel couplings very easily. They become constant if the non-diagonal coupling terms are negligible.

In the numerical tests, we retained only the three lowest channels of the Arthurs-Dalgarno expansion. The corresponding diabatic potential curves (see Fig. 5.6) tend to the thresholds

$$E(v = 0, j = 0) \ ,$$

$$E(v = 0, j = 2) \ ,$$

$$E(v = 0, j = 4) \ .$$

The potential coupling elements, used as input data, were computed using the code `vr1.f` mentioned in Sec. 5.3.4.

The numerical details of the various methods are not important at this point. Our aim was only to find out whether the linear dependence of numerical solutions is linked to the integration method used. We found that this is *not* the case: every method we used gave the same results. The phenomenon of "linear dependence" is "mathematical", not "numerical": each numerical solution, seen individually, is correct, but the various solutions become indistinguishable in the course of the integration, unless all channels retained in the computations are open.

Fig. 5.13 shows the open-channel components $F_{11}(R)$ and $G_{11}(R)$ of the solution matrices $\mathbf{F}(R)$ and $\mathbf{G}(R)$ for the two-channel model

$$"1" \qquad \equiv \qquad (v = 0, j = 0, l = 0) \qquad (\text{open})$$

and

$$"2" \qquad \equiv \qquad (v = 0, j = 2, l = 2) \qquad (\text{closed}) \ .$$
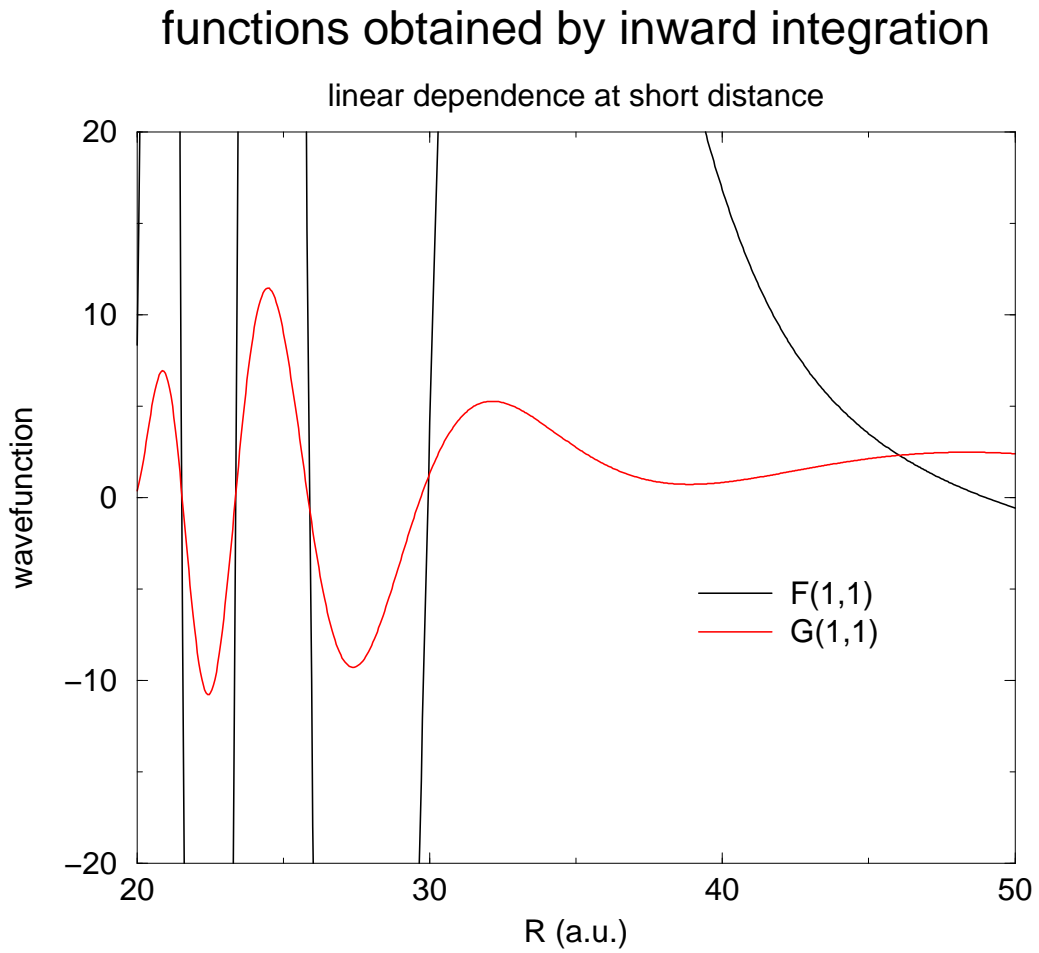
Figure 5.13: The reference functions $F_{11}(R)$ and $G_{11}(R)$ obtained by inward integration.

For a fixed energy between the thresholds $E(v = 0, j = 0)$ and $E(v = 0, j = 2)$, we integrated $\mathbf{F}$ and $\mathbf{G}$ from large to small distances using K-matrix boundary conditions such that

$$\begin{pmatrix} F_{11} & F_{12} \\ F_{21} & F_{22} \end{pmatrix} \rightarrow \begin{pmatrix} \sin(kR)/\sqrt{k} & 0 \\ 0 & \exp(\kappa R) \end{pmatrix} \qquad (R \rightarrow \infty) \quad (5.118)$$

and

$$\begin{pmatrix} G_{11} & G_{12} \\ G_{21} & G_{22} \end{pmatrix} \rightarrow \begin{pmatrix} -\cos(kR)/\sqrt{k} & 0 \\ 0 & \exp(-\kappa R) \end{pmatrix} \qquad (R \rightarrow \infty)$$

$$(5.119)$$

At distances larger than approximately 50 a_0, F_{11} and G_{11} are mutually dephased by 90°, although this is not clearly visible in the figure. The figure shows that F_{11} and G_{11} are not JWKB-like. In fact their amplitudes grow toward the inner region, which can only be due to the interaction with the closed channel "2". This growth in amplitude is much more pronounced for F_{11} than for G_{11}, which may be explained by their different nodal structures at distances $R \approx 40$ a_0, where channel "2" is still "locally closed" but starts to influence the behaviour of both F_{11} and G_{11}. For numerical purposes, F_{11} and G_{11} must be considered linearly dependent at distances smaller than approximately 30 a_0: their nodes are same.

We suspect that the scheme (5.117) for the computation of the K-matrix fails because $\mathbf{F}$ and $\mathbf{G}$ are stabilized *separately*. The stabilizations ensure that each of the matrices $\mathbf{F}$, $\mathbf{G}$, $\mathbf{F}'$, $\mathbf{G}'$ remains well-conditioned, but they do *not* guarantee that the matrix

$$\begin{pmatrix} \mathbf{F} & \mathbf{G} \\ \mathbf{F}' & \mathbf{G}' \end{pmatrix} \qquad (5.120)$$

of dimension $(2N \times 2N)$ is well-conditioned, too!

5.4.2 Linear dependence: a simple model

In order to understand the numerical problems arising from exponentially diverging solutions, we consider the simple equation

$$y''(x) - y(x) = 0 . \qquad (5.121)$$

Two linearly independent solutions are given by

$$f(x) = \cosh x , \qquad g(x) = \sinh x . \qquad (5.122)$$

Clearly they become indistinguishable numerically when x is sufficiently large. This can be seen by computing the Wronskian

$$W(x) = f(x)g'(x) - g(x)f'(x) \qquad (5.123)$$

156

x	error in single precision mode	error in double precision mode
0.0	0.000D+00.0	0.000D+00
1.0	0.238D−06.0	0.666D−15
2.0	−0.954D−06.0	−0.178D−14
3.0	0.153D−04.0	−0.284D−13
4.0	0.610D−04.0	0.114D−12
5.0	0.000D+00.0	0.182D−11
6.0	0.391D−02.0	0.728D−11
7.0	0.312D−01.0	−0.582D−10
8.0	−0.250D+00.0	0.000D+00
9.0	−0.100D+01.0	0.373D−08
10.0	0.230D+02.0	0.298D−07
11.0	−0.100D+01.0	−0.119D−06
12.0	−0.100D+01.0	0.191D−05
13.0	−0.100D+01.0	−0.763D−05
14.0	−0.100D+01.0	−0.610D−04
15.0	−0.100D+01.0	0.000D+00
16.0	−0.100D+01.0	−0.781D−02
17.0	−0.100D+01.0	0.000D+00
18.0	−0.100D+01.0	0.000D+00
19.0	−0.100D+01.0	−0.400D+01
20.0	−0.100D+01.0	−0.100D+01

Table 5.3: Numerical error for the Wronskian $fg' - g'f$ using Fortran's single and double precision modes.

using the numerical values for f, g', g and f'. Although the Wronskian equals exactly 1, the numerical result is zero if x is sufficiently large (see Table 5.3).

In order to illustrate a simple stabilization method we show how the Wronskian of $\cosh x$ and $\sinh x$ can be computed *numerically* for very large values of x.

In a *Gedankenexperiment* we integrate $f \equiv f^{(0)}$ and $g \equiv g^{(0)}$ from $x = 0$ to $x = 1$. At $x = 1$ we perform the first stabilization:

$$\left(\begin{array}{cc} f^{(1)}(x) & g^{(1)}(x) \\ f'^{(1)}(x) & g'^{(1)}(x) \end{array} \right) = \left(\begin{array}{cc} f^{(0)}(x) & g^{(0)}(x) \\ f'^{(0)}(x) & g'^{(0)}(x) \end{array} \right) \left(\begin{array}{cc} S_{ff}^{(1)} & S_{fg}^{(1)} \\ S_{gf}^{(1)} & S_{gg}^{(1)} \end{array} \right) \qquad (5.124)$$

where

$$\left(\begin{array}{cc} S_{ff}^{(1)} & S_{fg}^{(1)} \\ S_{gf}^{(1)} & S_{gg}^{(1)} \end{array} \right) = \left(\begin{array}{cc} g'^{(0)}(1) & -g^{(0)}(1) \\ -f'^{(0)}(1) & f^{(0)}(1) \end{array} \right) \qquad (5.125)$$

so that

$$\left(\begin{array}{cc} f^{(1)}(1) & g^{(1)}(1) \\ f'^{(1)}(1) & g'^{(1)}(1) \end{array} \right) = \left(\begin{array}{cc} 1 & 0 \\ 0 & 1 \end{array} \right). \qquad (5.126)$$

157

In the interval
$$1 < x \le 2,$$
the Wronskian (5.123) is computed from the Wronskian
$$W^{(1)}(x) \;=\; f^{(1)}(x)g'^{(1)}(x) - f'^{(1)}(x)g^{(1)}(x) \tag{5.127}$$
of the stabilized solutions using the identity
$$W(x) \;=\; \left(S_{gf}^{(1)}S_{fg}^{(1)} - S_{ff}^{(1)}S_{gg}^{(1)}\right)^{-1} W^{(1)}(x). \tag{5.128}$$

The stabilized solutions $f^{(m)}(x)$ and $g^{(m)}(x)$ for the interval
$$m \;\le\; x \;\le\; m+1 \tag{5.129}$$
can be defined iteratively. The Wronskian $W(x)$ in this interval can be computed as follows:

$$
\begin{aligned}
W(x) \;=\;& \left(S_{ff}^{(m)}S_{gg}^{(m)} - S_{gf}^{(m)}S_{fg}^{(m)}\right)^{-1} \times \\
&\cdots \\
&\times \left(S_{ff}^{(2)}S_{gg}^{(2)} - S_{gf}^{(2)}S_{fg}^{(2)}\right)^{-1} \times \\
&\times \left(S_{ff}^{(1)}S_{gg}^{(1)} - S_{gf}^{(1)}S_{fg}^{(1)}\right)^{-1} W^{(m)}(x)
\end{aligned}
\tag{5.130}
$$

In our example, the stabilizing matrices are all explicitly given by

$$
\begin{pmatrix} S_{ff}^{(m)} & S_{fg}^{(m)} \\ S_{gf}^{(m)} & S_{gg}^{(m)} \end{pmatrix}
= \begin{pmatrix} \cosh 1 & -\sinh 1 \\ -\sinh 1 & \cosh 1 \end{pmatrix}.
\tag{5.131}
$$

Thus the numerical values
$$S_{ff}^{(m)}S_{gg}^{(m)} - S_{gf}^{(m)}S_{fg}^{(m)} \qquad (m = 1, 2, 3, \ldots)$$
are all very nearly 1, which explains why the iterative procdure (5.130) will give a very accurate result for the Wronskian at distances where it cannot be computed directly.

The example may not be very convincing, since Eq. (5.130) only states the trivial fact that the Wronskian is constant. However, the scheme (5.130) fails if the stabilizations are not performed at sufficiently small intervals. For instance, if the first stabilization is performed at $x = 100$, the numerical value for
$$S_{ff}^{(1)}S_{gg}^{(1)} - S_{gf}^{(1)}S_{fg}^{(1)}$$
will be exactly zero, and the numerical value for $W(x)$ at distances $x \gg 1$ will be wrong.

One can construct other simple examples using the functions $\sinh x$ and $\cosh x$ to show that the stabilizations *are* useful. For example, using the stabilization technique, it is possible to invert the matrix

$$\left(\begin{array}{cc} \cosh x & \sinh x \\ \sinh x & \cosh x \end{array} \right)$$

numerically at any distance x, *without* using the analytical value of its determinant.

5.4.3 A modified stabilization scheme

We now return to our study of the coupled equations (5.47) and the problem of computing the K-matrix, assuming that the hyperradial logarithmic derivative matrix is given at a relatively *small* hyperradius.

In analogy to Eq. (5.124), we define the following scheme in order to stabilize the solution matrix (5.120) at M distances

$$R_M \; < \; R_{M-1} \; < \; \ldots \; < \; R_2 \; < \; R_1 \; :$$

$$\left(\begin{array}{cc} \mathbf{F}^{(m)}(R) & \mathbf{G}^{(m)}(R) \\ \mathbf{F}'^{(m)}(R) & \mathbf{G}'^{(m)}(R) \end{array} \right) = \left(\begin{array}{cc} \mathbf{F}^{(m-1)}(R) & \mathbf{G}^{(m-1)}(R) \\ \mathbf{F}'^{(m-1)}(R) & \mathbf{G}'^{(m-1)}(R) \end{array} \right) \left(\begin{array}{cc} \mathbf{S}_{FF}^{(m)} & \mathbf{S}_{FG}^{(m)} \\ \mathbf{S}_{GF}^{(m)} & \mathbf{S}_{GG}^{(m)} \end{array} \right) \tag{5.132}$$

with a stabilizing matrix given by

$$\left(\begin{array}{cc} \mathbf{S}_{FF}^{(m)} & \mathbf{S}_{FG}^{(m)} \\ \mathbf{S}_{GF}^{(m)} & \mathbf{S}_{GG}^{(m)} \end{array} \right) = \left(\begin{array}{cc} \mathbf{G}'^{(m-1)}(R_m) & -\mathbf{F}'^{(m-1)}(R_m) \\ -\mathbf{G}^{(m-1)}(R_m) & \mathbf{F}^{(m-1)}(R_m) \end{array} \right)^T . \tag{5.133}$$

According to this scheme,

$$\left(\begin{array}{cc} \mathbf{F}^{(m)}(R_m) & \mathbf{G}^{(m)}(R_m) \\ \mathbf{F}'^{(m)}(R_m) & \mathbf{G}'^{(m)}(R_m) \end{array} \right) = \left(\begin{array}{cc} 1 & 0 \\ 0 & 1 \end{array} \right) \tag{5.134}$$

where "1" stands for the unit matrix of dimension $(N \times N)$.

In the two adjoining intervals $[R_{m+1}, R_m]$ and $[R_m, R_{m-1}]$, we write the wavefunction $\mathbf{u}(R)$ (we may assume that it has been deduced from the hyperspherical region) as

$$\mathbf{u}(R) \; = \; \mathbf{F}^{(m)}(R)\mathbf{A}^{(m)} - \mathbf{G}^{(m)}(R)\mathbf{B}^{(m)} . \tag{5.135}$$

and as

$$\mathbf{u}(R) \; = \; \mathbf{F}^{(m-1)}(R)\mathbf{A}^{(m-1)} - \mathbf{G}^{(m-1)}(R)\mathbf{B}^{(m-1)} . \tag{5.136}$$

By comparing these two equations one sees that the amplitudes $\left(\mathbf{A}^{(m)}, \mathbf{B}^{(m)}\right)$ and $\left(\mathbf{A}^{(m-1)}, \mathbf{B}^{(m-1)}\right)$ are related as

$$\begin{pmatrix} \mathbf{S}_{FF}^{(m)} & -\mathbf{S}_{FF}^{(m)} \\ -\mathbf{S}_{GF}^{(m)} & \mathbf{S}_{GG}^{(m)} \end{pmatrix} \begin{pmatrix} \mathbf{A}^{(m)} \\ \mathbf{B}^{(m)} \end{pmatrix} = \begin{pmatrix} \mathbf{A}^{(m-1)} \\ \mathbf{B}^{(m-1)} \end{pmatrix} . \tag{5.137}$$

The corresponding K-matrices

$$\mathbf{K}^{(m)} = \mathbf{B}^{(m)} \left[\mathbf{A}^{(m)}\right]^{-1} \tag{5.138}$$

and

$$\mathbf{K}^{(m-1)} = \mathbf{B}^{(m-1)} \left[\mathbf{A}^{(m-1)}\right]^{-1} \tag{5.139}$$

are related as

$$\mathbf{K}^{(m-1)} = \left[-\mathbf{S}_{GF}^{(m)} + \mathbf{S}_{GG}^{(m)}\mathbf{K}^{(m)}\right] \left[\mathbf{S}_{FF}^{(m)} - \mathbf{S}_{FG}^{(m)}\mathbf{K}^{(m)}\right]^{-1} . \tag{5.140}$$

The above equation suggests that the "local" K-matrix $\mathbf{K}^{(M)}$, obtained from an analysis of the wavefunction on the hypersphere, might be converted into the asymptotic K-matrix $\mathbf{K}^{(0)}$ in a series of steps using the stabilizing matrices (5.133). The original recurrence relation (5.117), which J.-M. Launay had found unstable, is recovered from (5.140) by setting $\mathbf{S}_{GF} = 0$ and $\mathbf{S}_{FG} = 0$.

We have presented the steps leading to the recurrence relation (5.140) in the way in which we had discovered it naively, starting from the initial idea of integrating two linearly independent K-matrix reference functions $\mathbf{F}$ and $\mathbf{G}$ in the *inward* direction and using a stabilization technique.

In reality, their is no reason whatsoever for starting the propagation at a large distance! In fact the reference functions $\mathbf{F}^{(m)}$ and $\mathbf{G}^{(m)}$ used in each interval $[R_{m+1}, R_m]$ do not depend on the values of the functions used in the other intervals. In each interval $[R_{m+1}, R_m]$, the $2N$ functions summarized in the matrices $\mathbf{F}^{(m)}$ and $\mathbf{G}^{(m)}$ form a *complete* and well-conditioned basis set in the space of solutions of the coupled equations (5.47). Since the basis functions $\mathbf{F}^{(m+1)}$ and $\mathbf{G}^{(m+1)}$ do not depend on the basis functions $\mathbf{F}^{(m)}$ and $\mathbf{G}^{(m)}$, the basis functions in each sector can be generated independently from those of the other sectors. In particular, there is no need for storing them; they can be generated at the time when they are needed.

The propagation scheme could thus be the following:

1. Generate a base pair of reference functions $\mathbf{F}^{(M)}(R)$ and $\mathbf{G}^{(M)}(R)$ in the matching interval (5.65), which in our present notation is the interval

$$[R_M, R_{M-1}] .$$

In order to minimize the problems of linear dependence within this interval, define $\mathbf{F}^{(M)}$ and $\mathbf{G}^{(M)}$ by the initial condition

$$\begin{pmatrix} \mathbf{F}^{(M)}(R_{\text{mid}}) & \mathbf{G}^{(M)}(R_{\text{mid}}) \\ \mathbf{F}'^{(M)}(R_{\text{mid}}) & \mathbf{G}'^{(M)}(R_{\text{mid}}) \end{pmatrix} = \begin{pmatrix} \mathbf{diag} \end{pmatrix} \tag{5.141}$$

160

where R_{mid} is the *midpoint*

$$\frac{R_{M-1} - R_M}{2}$$

of the matching interval. (**diag**) is a diagonal matrix of dimension $(2N \times 2N)$, which could be defind such that $\mathbf{F}^{(M)}$ and $\mathbf{G}^{(M)}$ and their derivatives match semiclassical solutions at the distance R_{mid}.

2. Use the existing matching code to determine two coefficient matrices $\mathbf{A}^{(M)}$ and $\mathbf{B}^{(M)}$ such that

$$\mathbf{u}(R) \;=\; \mathbf{F}^{(M)}(R)\mathbf{A}^{(M)} - \mathbf{G}^{(M)}(R)\mathbf{B}^{(M)} \tag{5.142}$$

where $\mathbf{u}(R)$ is the solution matrix that matches the N wavefunctions given on the hypersphere.

3. Compute the "local" K-matrix

$$\mathbf{K}^{(M)} \;=\; \mathbf{B}^{(M)} \left[\mathbf{A}^{(M)} \right]^{-1} . \tag{5.143}$$

$\mathbf{K}^{(M)}$ could then be transformed into the asymptotic K-matrix $\mathbf{K}^{(0)}$ in a series of M steps,

$$\mathbf{K}^{(M)} \;\to\; \mathbf{K}^{(M-1)} \;\to\; \ldots \;\to\; \mathbf{K}^{(2)} \;\to\; \mathbf{K}^{(1)} \;\to\; \mathbf{K}^{(0)} \tag{5.144}$$

using the recurrence relation (5.140). For that purpose, a well-conditioned matrix

$$\begin{pmatrix} \mathbf{F}^{(m)}(R) & \mathbf{G}^{(m)}(R) \\ \mathbf{F}'^{(m)}(R) & \mathbf{G}'^{(m)}(R) \end{pmatrix} \tag{5.145}$$

would have to be generated for each sector $[R_m, R_{m-1}]$ by solving the coupled equations (5.47) within the sector. For each sector boundary a transformation matrix relating the basis sets of sectors $[R_{m+1}, R_m]$ and $[R_m, R_{m-1}]$ would have to be computed, so that $\mathbf{K}^{(m)}$ can be transformed into $\mathbf{K}^{(m-1)}$:

$$\begin{pmatrix} \mathbf{S}_{FF}^{(m)} & \mathbf{S}_{FG}^{(m)} \\ \mathbf{S}_{GF}^{(m)} & \mathbf{S}_{GG}^{(m)} \end{pmatrix} \tag{5.146}$$
$$= \begin{pmatrix} \mathbf{G}^{(m-1)}(R) & -\mathbf{F}'^{(m-1)}(R) \\ -\mathbf{G}'^{(m-1)}(R) & \mathbf{F}'^{(m-1)}(R) \end{pmatrix}^T \begin{pmatrix} \mathbf{F}^{(m)}(R) & \mathbf{G}^{(m)}(R) \\ \mathbf{F}'^{(m)}(R) & \mathbf{G}'^{(m)}(R) \end{pmatrix} .$$

The right-hand side of (5.146) cannot be evaluated at an arbitrary distance R, due to the problems of linear dependence: it must be evaluated at the boundary $R = R_m$, where both

$$\begin{pmatrix} \mathbf{F}^{(m)}(R) & \mathbf{G}^{(m)}(R) \\ \mathbf{F}'^{(m)}(R) & \mathbf{G}'^{(m)}(R) \end{pmatrix} \quad \text{and} \quad \begin{pmatrix} \mathbf{F}^{(m-1)}(R) & \mathbf{G}^{(m-1)}(R) \\ \mathbf{F}'^{(m-1)}(R) & \mathbf{G}'^{(m-1)}(R) \end{pmatrix}$$

are assumed to be sufficiently "well-conditioned".

We believe that the method (5.144) could be numerically stable, provided that the sectors are chosen small enough. However we did not test it.

In fact, the suggested method means that $2N$ linearly independent solutions of the coupled equations (5.47) would have to be generated only to convert the short-range K-matrix, which represents only N solutions, into the asymptotic K-matrix.

5.4.4   K-matrix propagator

A far more efficient procedure could be obtained by defining, for each interval $[R_m, R_{m-1}]$, the basis functions $\mathbf{F}^{(m)}(R)$ and $\mathbf{G}^{(m)}(R)$ such that they are *diagonal*. This could be achieved, for example, by setting all non-diagonal elements of the potential coupling matrix $\mathbf{V}(R)$ in Eq. (5.47) artificially to zero and solving the resulting uncoupled equations in each interval $[R_m, R_{m-1}]$ using JWKB-like initial conditions. The diagonal functions $\mathbf{F}^{(m)}$ and $\mathbf{G}^{(m)}$ could thus be generated numerically very rapidly, for example using the single-channel version of the Numerov propagator (Numerov's integration method is described in Appendix K). The matrices (5.146) for the transformations at sector boundaries then become diagonal as well. Of course, the diagonal functions $\mathbf{F}^{(m)}$ and $\mathbf{G}^{(m)}$ do not solve the coupled equations (5.47), except at distances where the non-diagonal elements of the potential coupling matrix are negligible. This means that the K-matrix $\mathbf{K}^{(m)}(R)$ is no longer a constant but verifies the K-matrix version of the *variable phase equations*, a system of N coupled non-linear first-order differential equations.

Thus, instead of computing $2N$ solutions of N coupled *second-order* linear differential equations, one now needs to solve only a system of N coupled *first-order* non-linear differential equations, and one may expect that the numerical effort will be considerably less. It should be noted that every K-matrix $\mathbf{K}^{(m)}(R)$ may become singular for certain values of R. This should not a problem: if $\mathbf{K}^{(m)}$ shows signs of becoming singular, the propagation could be continued using the inverse matrix, $\left[\mathbf{K}^{(m)}\right]^{-1}$, until the inverse matrix in its turn shows signs of becoming singular.

Only the functions $\mathbf{F}^{(M)}(R)$ and $\mathbf{G}^{(M)}(R)$ used in the matching interval (5.65) must be *exact* solutions of the coupled equations (5.47), since they serve to analyse the hyperradial logarithmic derivative matrix. The short-range K-matrix $\mathbf{K}^{(M)}$ obtained by the matching procedure could be transformed into $\mathbf{K}^{(M-1)}(R_{M-1})$ using the transformation matrix (5.146) (with $m \equiv M$, $R \equiv R_{M-1}$).

Given the diagonal sector basis functions $\mathbf{F}^{(M-1)}(R)$ and $\mathbf{G}^{(M-1)}(R)$, one could use the variable phase equations to propagate the K-matrix

$$\mathbf{K}^{(M-1)}(R)$$

from R_{M-1} to R_{M-2}, where one transforms it into

$$\mathbf{K}^{(M-2)}(R)$$

and so on. The final result will be the asymptotic K-matrix $\mathbf{K}^{(0)}(R)$.

It should be possible to reduce the number of closed channels in the course of the propagation. In order to eliminate channel i at the sector boundary R_m, one could define $F_{ij}^{(m)}(R)$ and $G_{ij}^{(m)}(R)$ as rising and falling exponentials:

$$F_{ij}^{(m)}(R) = \delta_{ij} \exp(\kappa_i R) , \qquad\qquad\qquad (5.147)$$

$$G_{ij}^{(m)}(R) = \delta_{ij} \exp(-\kappa_i R) , \qquad j = 1, \ldots, N . \qquad (5.148)$$

Then the K-matrix $\mathbf{K}^{(m)}$ deduced from $\mathbf{K}^{(m+1)}$ at the boundary R_m is such that that all elements $K_{ij}^{(m)}(R)$ $(j = 1, \ldots, N)$ can be omitted at distances $R > R_m$. Of course more than one channel might be omitted at the same distance.

The suggested K-matrix propagation method is very similar to the variable-phase algorithm developed by R. Martinazzo *et al.* [185]. Martinazzo's algorithm could perhaps be used without any further modification, but the matching interval would have to be treated separately.

5.5 Note regarding Efimov and halo states

It should be mentioned that a system of three particles may posess bound or quasi-bound states at energies closely underneath the threshold for break-up into *three* free particles: Efimov states and halo (or Borromean) states [71, 75, 69, 117].

As far as we know, the Efimov effect has not yet been observed experimentally, but it has been the subject of many theoretical investigations. Most of the models rely on hyperspherical coordinates.

If at least one of the two-body subsystems posesses a bound state, there cannot be any true three-body bound states at energies above the threshold for break-up into one particle and a bound two-body complex. There can only be long-lived metastable states, since the formation of a two-body bound subsystem will release enough kinetic energy for the third body to be ejected from the three-body complex.

However, a recent study on Rb_3 suggests that Efimov states could have a very long lifetime due to the fact that the overlap integral (the Franck-Condon factor) for a transition between the Efimov state and an atom-diatom scattering state is extremely small [132].

It might be interesting to examine theoretically and numerically whether Efimov states exist for Na_3. Since these states are diffuse (by definition), it would probably not be necessary to analyse them using Jacobi coordinates. A hyperspherical description might be sufficient.

5.6 Conclusion

We have computed energies of very weakly bound vibrational states of the sodium trimer Na_3 in its quartet spin state, using a pairwise-additive model potential energy surface as input data. Our calculations show that J.-M. Launay's hyperspherical reactive scattering code, which had previously been used only for energies above the atom-diatom breakup threshold, can easily be extended to energies below this threshold.

We have analysed the hyperradial logarithmic derivative matrix on the hypersphere $\rho = 50$ a_0 using two energy-smooth reference functions, thereby treating the weakly bound states and the low-energy scattering states on the same footing. We have computed a "short-range phase shift" and found that it shows a number of sharp resonances, both in the bound and in the continuum part of the spectrum. Each resonance below threshold might be associated with a quasi-stable vibrating Na_3 trimer that can *temporarily* dissociate into a weakly bound $Na + Na_2(v=0, j=0)$ van der Waals complex. In contrast, each resonance above threshold is undoubtedly associated with a quasi-bound Na_3 complex that may *permanently* dissociate into Na and $Na_2(v=0, j=0)$. We did not translate the asymptotic scattering phase shift into elastic cross sections, since this had already been done by P. Honvault *et al.* [248].

The influence of quasi-bound states on cross-sections in non-reactive atom-molecule collisions has been investigated numerically by N. Balakrishnan *et al.* [18, 263]. In their quantum mechanical investigation of rovibrational relaxation of H_2 and D_2 by collisions with Ar atoms, they demonstrated a dramatic change in the behaviour of the rate coefficients at low temperatures when the van der Waals potential supports a quasibound level very close to the dissociation threshold. We expect that similar effects might be observed in the collisions of Na and Na_2, although these collisions are of the reactive type.

We pointed out that the computation of the potential-adapted hyperangular basis functions is very time-consuming. In order to improve the numerical efficiency, we suggest analysing the hyperradial logarithmic derivative on a smaller hypersphere and converting the short-range K-matrix into the asymptotic K-matrix in a series of steps, perhaps using an existing K-matrix propagation scheme. It should thus become possible to study collisions involving molecules in much higher excited vibrational states than is presently possible, and to study the effects of the relatively weak interchannel couplings at intermediate and large distances between the Na atom and the Na_2 molecule.

The proposed K-matrix propagation scheme is not the only way in which the numerical efficiency could be enhanced. In particular it might be possible to compute the potential-adapted hyperangular basis functions in a more

efficient manner, for example using Faddeev equations or B-spline techniques [75, 138]. The B-spline technique could be more flexible compared to the expansion in hyperspherical harmonics, since the B-splines can be tailored to cover the energetically allowed region. Thus it could become possible to compute the potential-adapted hyperangular basis set at arbitrary distances (far beyond $\rho > 50$ a$_0$). However, we think that computing the hyperangular basis set by a new method does not promise the same conceptual advantages as using Jacobi coordinates at intermediate and large distances. Besides, it would require very important modifications of the existing code.

Chapter 6

Prospects for the photoassociation of Na$_3$

This last Chapter is based on notes I made during a visit to Prof. E. Tiemann's group at the Institute of Quntum Optics (University of Hannover).

6.1 Motivation

Photoassociation reactions between two colliding atoms and a photon have been observed for well over ten years. Photoassociation spectroscopy has became a routine technique.

Interestingly it seems that the formation of a *triatomic* system by photoassociation has never been observed, in contrast to photodissociative processes (the decay of a metastable triatomic molecule into a dimer and an atom under emission of a photon). At the present stage we are not aware of any established theoretical model describing the "inverse" process: the *formation* of a triatomic molcule by absorption of a photon.

A triatomic molecule, for example the sodium trimer Na$_3$, can split into three sodium atoms Na, or into a sodium atom Na and a sodium molecule Na$_2$. This means that there may be two very different approaches to forming a trimer. A photoassociation reaction could start when three atoms collide,

$$\mathrm{Na}(3s) + \mathrm{Na}(3s) + \mathrm{Na}(3s) + h\nu \rightarrow \mathrm{Na}_3(3s + 3s + 3p)$$
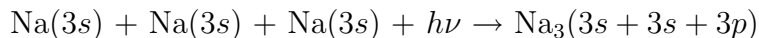
or when an atom collides with a diatomic molecule,

$$\mathrm{Na}(3s) + \mathrm{Na}_2(3s + 3s) + h\nu \rightarrow \mathrm{Na}_3(3s + 3s + 3p) \ .$$
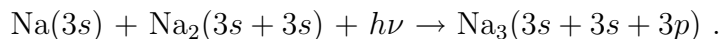
The energy of the photon is needed to lift the system from a three-body or two-body continuum state in the electronic ground state to a bound vibrational state of an electronically excited molecule. If the triatomic molecule

is formed from an atom and a dimer, the photon is also required for the conservation of the total momentum.

There may be many variants and limiting case of these schemes, because the diatomic molecule has many internal degrees of freedom: electronic, vibrational, rotational. In particular it should make an important difference whether the dimer is initially in a low-lying or in a very loosely bound vibrational level. If the dimer is very weakly bound, the two schemes obviously resemble each other.

The atom-atom photoassociation cross-sections are known to depend critically on the overlap integrals (the Franck-Condon factors) between the radial wavefunction in the entrance (continuum) channel and the radial wavefunction in the exit (bound) channel. The overlap must be sufficiently large for the photoassociation process to be efficient. The concept of overlap integrals can be generalized to electronic transitions in a triatomic system, and one might use it to estimate which of the two proposed processes, photoassocation of Na and Na_2 or of three Na atoms, is more likely.

6.1.1 Photoassociation of three atoms

Let us consider three ground state sodium atoms in a cold gas.

By absorbing a photon they may reach a potential energy surface correlated to the threshold for dissociation into

$$Na(3s) + Na(3s) + Na(3p) \ .$$
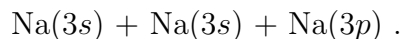
Here we shall only use a simple *classical* picture.

We may assume that the three atoms spend comparitively more time in the regions of configuration space where they are *slow*, which means that they are more likely to absorb a photon in these regions. If the three atoms are excited from the electronic ground state to the excited state when their mutual distances are large, they will have a large potential energy on the excited surface - we may assume that their energy lies *above* the atom-diatom dissociation threshold. After the absorption of the photon, the three atoms may collide, and two of them may form a deeply bound diatomic molecule, thereby releasing enough energy for the third atom to escape to infinity. The described process is a *quenching* process on the excited potential energy surface. It is *not* the desired formation of a bound triatomic molecule.

Can the three atoms absorb the photon at the moment where they are close together, near the minimum of the excited potential energy surface? In this case they might reach a deeply bound vibrational level of the excited state. Unfortunately, the probability of such an event will generally be small, because the three atoms will be *fast* when they are near together, and the *time* they spend near the minimum of the ground potential energy surface

will be short - unless they are in resonance with a quasibound vibrational state of Na_3 in the ground electronic state.

This simple argumentation suggests that the prospects for a photoassociation of three free sodium atoms may not be particularly good, except if resonances with quasibound states of Na_3 could be exploited.

Also it cannot be ruled out that there are long-lived *quasi-bound* states closely underneath the threshold for break-up into $Na(3s) + Na(3s) + Na(3p)$. In such states, the three atoms could be relatively far away from each other, so that they do not immediatly decay into a strongly bound Na_2 molecule and an Na atom. Of course, the question is then whether such weakly bound states could be called *molecules.*

6.1.2   Photoassociation of an atom and a dimer

A more promising route to forming stable triatomic molecules might be to prepare a mixture of ground state Na atoms and Na_2 molecules.

Let us consider an Na atom and an $Na_2(v,j)$ molecule in a low-lying rotational-vibrational state (v,j). As they approach each other slowly on the ground potential energy surface $Na(3s) + Na(3s) + Na(3s)$, they will eventually reach a point at which they may absorb a photon that transfers them to a weekly bound vibrational state on the *excited* potential energy surface $Na(3s) + Na(3s) + Na(3p)$, in close analogy to the atom - atom photoassociation reaction.

In Chapter 5 we reported numerous resonances in the Na - $Na_2(v=0,j=0)$ elastic scattering phase shift. We mentioned that each resonance corresponds to a quasi-bound Na_3 trimer. One may expect that similar resonances exist for the potential energy surfaces correlated to the $Na(3s) + Na(3s) + Na(3p)$ dissociation threshold. Every resonance, on the ground as well as on the excited potential energy surface could perhaps be exploited for a photoassociation reaction.

We would like to point out the important difference between this proposed mechanism, *forming a trimer from an atom and a dimer*, and the idea we mentioned before, *forming a trimer from three free atoms.* We suggested that there is a region in configuration space where the slowly colliding Na atom and the Na_2 molecule may absorb a photon. At an energy *above* the $Na(3s) + Na(3s) + Na(3s)$ dissociation threshold, the three Na atoms may of course reach the same region in configuration space. However, their relative motion will be much faster, and the probability for absorbing the photon will therefore be greatly reduced (unless the total energy is concentrated on a fast vibrating and rotating Na_2 dimer, which is very unlikely: how should this dimer have been formed?)

6.2 Electronic states of an equilateral homonuclear alkali trimer

A large number of different electronic states might intervene in a photoassociation of three identical alkali atoms. In this Section we construct the states adapted to D_{3h} equilateral geometry, for the two different thresholds $s+s+s$ (all three atoms in the s ground state) and $s + s + p$ (two atoms in the s ground state, one atom in the p excited state).

The D_{3h} point group has the following 12 elements (we use the notation of Ref. [150]):

- E: the identity.[1]

- σ_h: reflexion by the horizontal plane.

- C_3, C_3^2: rotations of 120° and 240° about the vertical axis,

- $\sigma_h C_3$, $\sigma_h C_3^2$: rotation-reflexions. The element $\sigma_h C_3$ is also denoted S_3. Note that the element $\sigma_h C_3^2$ is *not* equal to S_3^2:

$$S_3^2 \;=\; (\sigma_h C_3)(\sigma_h C_3) \;=\; \sigma_h^2 C_3^2 = C_3^2 \;.$$

- U_2^A, U_2^B, U_2^C: rotations of 180° around the horizontal axis passing trough core A, B, and C, respectively.

- σ_v^A, σ_v^B, σ_v^C: rotations of 180° around the horizontal axis passing trough core A, B, and C, respectively, followed by the reflexion σ_h.

Tables 6.1 is the D_{3h} multiplication table. For each pair (A, B) of group elements A and B, it indicates the product AB. Its entries are arranged according to the following scheme:

$$
\begin{array}{|cccc|}
\hline
E & \dots & B & \dots \\
\vdots & & \vdots & \\
A & \dots & A \cdot B & \dots \\
\vdots & & \vdots & \\
\hline
\end{array}
$$

Table 6.2 is the D_{3h} character table taken from Ref. [150]. For each irreducible representation (left column), the table gives the character of each of the six classes. The letters "x" and "y" are meant to indicate that the x- and y-components of a vector (x, y, z) are the basis of an E' representation, whereas the z-component is the basis of the A_2' representation, assuming that the z-axis is chosen as the principal axis of symmetry.

---

[1]Note that the symbol E also indicates two-dimensional representations of a point group

E	C_3	C_3^2	σ_h	$\sigma_h C_3$	$\sigma_h C_3^2$	U_2^A	U_2^B	U_2^C	σ_v^A	σ_v^B	σ_v^C
C_3	C_3^2	E	$\sigma_h C_3$	$\sigma_h C_3^2$	σ_h	U_2^C	U_2^A	U_2^B	σ_v^C	σ_v^A	σ_v^B
C_3^2	E	C_3	$\sigma_h C_3^2$	σ_h	$\sigma_h C_3$	U_2^B	U_2^C	U_2^A	σ_v^B	σ_v^C	σ_v^A
σ_h	$\sigma_h C_3$	$\sigma_h C_3^2$	E	C_3	C_3^2	σ_v^A	σ_v^B	σ_v^C	U_2^A	U_2^B	U_2^C
$\sigma_h C_3$	$\sigma_h C_3^2$	σ_h	C_3	C_3^2	E	σ_v^C	σ_v^A	σ_v^B	U_2^C	U_2^A	U_2^B
$\sigma_h C_3^2$	σ_h	$\sigma_h C_3$	C_3^2	E	C^3	σ_v^B	σ_v^C	σ_v^A	U_2^B	U_2^C	U_2^A
U_2^A	U_2^B	U_2^C	σ_v^A	σ_v^B	σ_v^C	E	C_3	C_3^2	σ_h	$\sigma_h C_3$	$\sigma_h C_3^2$
U_2^B	U_2^C	U_2^A	σ_v^B	σ_v^C	σ_v^A	C_3^2	E	C_3	$\sigma_h C_3^2$	σ_h	$\sigma_h C_3$
U_2^C	U_2^A	U_2^B	σ_v^C	σ_v^A	σ_v^B	C_3	C_3^2	E	$\sigma_h C_3$	$\sigma_h C_3^2$	σ_h
σ_v^A	σ_v^B	σ_v^C	U_2^A	U_2^B	U_2^C	σ_h	$\sigma_h C_3$	$\sigma_h C_3^2$	E	C_3	C_3^2
σ_v^B	σ_v^C	σ_v^A	U_2^B	U_2^C	U_2^A	$\sigma_h C_3^2$	σ_h	$\sigma_h C_3$	C_3^2	E	C_3
σ_v^C	σ_v^A	σ_v^B	U_2^C	U_2^A	U_2^B	$\sigma_h C_3$	$\sigma_h C_3^2$	σ_h	C_3	C_3^2	E

Table 6.1: Multiplication table of the D_{3h} symmetry group.

D_{3h}	E	σ_h	$2C_3$	$2S_3$	$3U_2$	$3\sigma_v$
A_1'	1	1	1	1	1	1
A_2'	1	1	1	1	-1	-1
A_1''	1	-1	1	-1	1	-1
A_2''; z	1	-1	1	-1	-1	1
E'; x, y	2	2	-1	-1	0	0
E''	2	-2	-1	1	0	0

Table 6.2: Character table for the D_{3h} point group.

6.2.1 Orbitals for a single electron

The orbital wavefunction of an electron in a spherically symmetrical potential can be written $\varphi_{nlm}(\mathbf{r})$, where n, l, and m are the principal, angular momentum, and magnetic quantum numbers, respectively, and $\mathbf{r}$ is the cartesian position vector pointing from the centre of symmetry to the electron. Any such wavefunction, centered on one of the cores, A, B, or C, is a stationary state of the electron, provided that the internuclear distances $\overline{AB}$, $\overline{BC}$, and $\overline{CA}$ are large compared to the typical size of the orbital.[2]

Since we shall only consider orbitals with the same principal quantum number ($n = 3$ in the case of Na_3 in its ground electronic state), we drop this quantum number in our notations. An s-orbital $\varphi_{n00}(\mathbf{r})$ is denoted $s(\mathbf{r})$. The p-orbitals $\varphi_{n1m}(\mathbf{r})$ ($m = -1, 0, 1$) are denoted $p_{-1}(\mathbf{r})$, $p_0(\mathbf{r})$, and $p_1(\mathbf{r})$, but we shall never use them; we shall use linear combinations instead, p_x, p_y and p_z, which are real-valued and easier to visualize. p_z is the same as p_0 (up to a factor of module 1) and is symmetrical under rotations about the z-axis. The p_x- and p_y-orbitals are obtained from p_z by rotations of $90°$ about the y- and the x-axis, and they are symmetrical under rotations about the x- and the y-axis, respectively.

We now consider the situation in which the three cores form an equilateral triangle (D_{3h} geometry). The results obtained here could also be useful for the geometries of lower symmetry C_{2v} and C_s, since the latter are subgroups of D_{3h}. Linear geometries ($C_{\infty h}$ and $D_{\infty h}$) need to be examined separately, as they are continuous groups and not subgroups of D_{3h}.

The molecular plane spanned by the atoms A, B and C is refered to as the *horizontal* plane. In the D_{3h} geometry, the principal axis of symmetry is perpendicular to this plane, and we may think of it as pointing *upwards*. As we look downwards onto the molecular plane, the three cores A, B, and C appear anti-clockwise.

In order to facilitate the symmetry operations involving atomic orbitals centered on the cores, we define three cartesian coordinate systems $(xyz)^A$, $(xyz)^B$ and $(xyz)^C$, centered on A, B, and C, respectively. They are related to each other by rotations of $\pm 120°$ around the principal axis (see Fig. 6.1). The z^A-, z^B- and z^C-axis are all taken parallel to the principal axis, and they point upwards. The x^A-, x^B- and x^C-axis are chosen so that they point outwards, away from the centre of the ABC triangle. The y^A-, y^B- and y^C-axis are finally chosen such that each coordinate system is right-handed.

By centering the orbitals s, p_x, p_y and p_z on core A and by orienting them with respect to the cartesian coordinate system $(xyz)^A$, we obtain orbitals s^A, p_x^A, p_y^A, and p_z^A. s- and p-orbitals centered on B and C are defined

---

[2]The size of the orbital may be defined as the diameter of the classically allowed region of the electron in the core's Coulomb field.
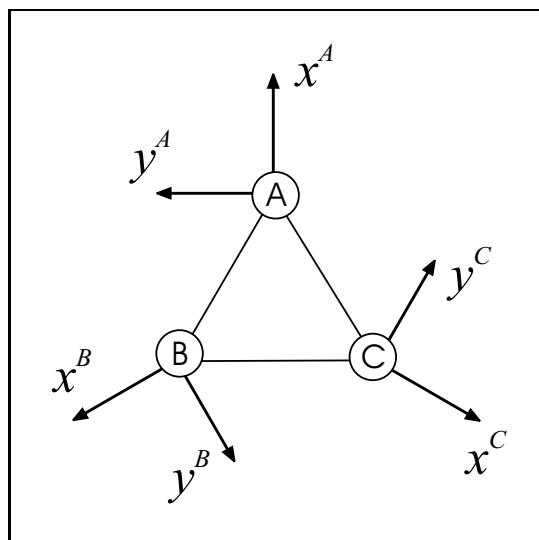
Figure 6.1: Cartesian coordinate systems centered on A, B and C. The z-direction is perpendicular to the molecular plane.

analogously. The p-orbitals are sketched in Fig. 6.2.

We note that the p_x and p_y orbitals are unchanged by reflections by the molecular plane, whereas the p_z orbitals change sign. The behaviour of the various s- and p-orbitals under D_{3h} symmetry operations is summarized in Table 6.3.

The twelve orbitals considered here can be divided into four basis sets, each consisting of three orbitals:

$$(s^A,\ s^B,\ s^C)\ ;\qquad (p_x^A,\ p_x^B,\ p_x^C)\ ;\qquad (p_y^A,\ p_y^B,\ p_y^C)\ ;\qquad (p_z^A,\ p_z^B,\ p_z^C)\ .$$

The D_{3h} symmetry operations only relate orbitals belonging to the same set (see Table 6.3), which means that each of the four sets is a basis of a three-dimensional (and hence reducible) representation of D_{3h}. We have not constructed the irreducible representations, because we use the single-electron orbitals only as "building blocks" for the three-electron states (see the next paragraph).

6.2.2   Orbitals for three electrons

Using the single-electron orbitals defined in Sec. 6.2.1, we may easily construct three-electron orbitals adapted to D_{3h} symmetry, considering the following four cases separately :

- $s + s + s$: only s-orbitals are occupied.

- $s+s+p_x$: two electrons are in s-orbitals, one electron is in a p_x-orbital.
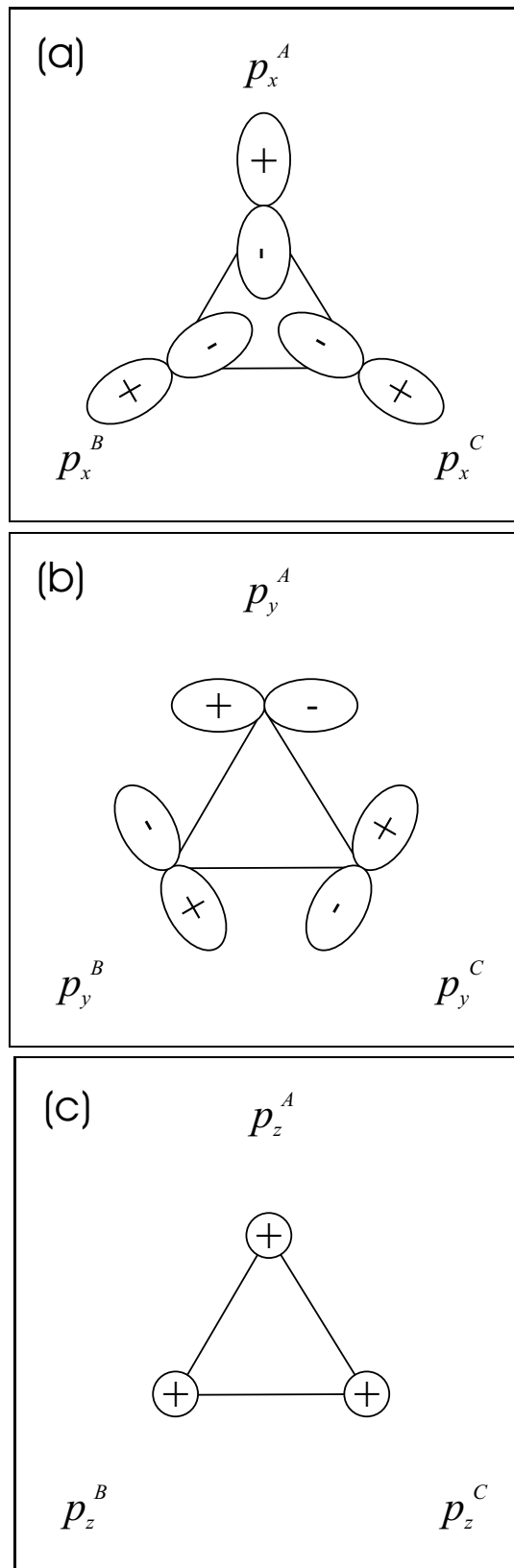
Figure 6.2: Schematic representation of atomic p-orbitals centered on A, B and C: (**a**) the p_x-orbitals, (**b**) the p_y-orbitals, and (**c**) the p_z-orbitals. The p_z-orbitals are positive for $z > 0$ and negative for $z < 0$.

E	C_3	C_3^2	σ_h	$\sigma_h C_3$	$\sigma_h C_3^2$	U_2^A	U_2^B	U_2^C	σ_v^A	σ_v^B	σ_v^C
s^A	s^B	s^C	s^A	s^B	s^C	s^A	s^C	s^B	s^A	s^C	s^B
s^B	s^C	s^A	s^B	s^C	s^A	s^C	s^B	s^A	s^C	s^B	s^A
s^C	s^A	s^B	s^C	s^A	s^B	s^B	s^A	s^C	s^B	s^A	s^C
p_x^A	p_x^B	p_x^C	p_x^A	p_x^B	p_x^C	p_x^A	p_x^C	p_x^B	p_x^A	p_x^C	p_x^B
p_x^B	p_x^C	p_x^A	p_x^B	p_x^C	p_x^A	p_x^C	p_x^B	p_x^A	p_x^C	p_x^B	p_x^A
p_x^C	p_x^A	p_x^B	p_x^C	p_x^A	p_x^B	p_x^B	p_x^A	p_x^C	p_x^B	p_x^A	p_x^C
p_y^A	p_y^B	p_y^C	p_y^A	p_y^B	p_y^C	$-p_y^A$	$-p_y^C$	$-p_y^B$	$-p_y^A$	$-p_x^C$	$-p_x^B$
p_y^B	p_y^C	p_y^A	p_y^B	p_y^C	p_y^A	$-p_y^C$	$-p_y^B$	$-p_y^A$	$-p_y^C$	$-p_x^B$	$-p_x^A$
p_y^C	p_y^A	p_y^B	p_y^C	p_y^A	p_y^B	$-p_y^B$	$-p_y^A$	$-p_y^C$	$-p_y^B$	$-p_x^A$	$-p_x^C$
p_z^A	p_z^B	p_z^C	$-p_z^A$	$-p_z^B$	$-p_z^C$	$-p_z^A$	$-p_z^C$	$-p_z^B$	p_z^A	p_z^C	p_z^B
p_z^B	p_z^C	p_z^A	$-p_z^B$	$-p_z^C$	$-p_z^A$	$-p_z^C$	$-p_z^B$	$-p_z^A$	p_z^C	p_z^B	p_z^A
p_z^C	p_z^A	p_z^B	$-p_z^C$	$-p_z^A$	$-p_z^B$	$-p_z^B$	$-p_z^A$	$-p_z^C$	p_z^B	p_z^A	p_z^C

Table 6.3: Symmetry properties of single-electron orbitals s, p_x, p_y, and p_z, centered on the cores A, B and C for the D_{3h} equilateral triangle geometry.

- $s+s+p_y$: two electrons are in s-orbitals, one electron is in a p_y-orbital.

- $s+s+p_z$: two electrons are in s-orbitals, one electron is in a p_z-orbital.

We only consider the situation where there is exactly one valence electron near each core. Ionic states are not considered in this thesis.

The three-electron orbitals for D_{3h}-symmetry are listed on the next pages. They are generally neither symmetrical nor antisymmetrical with respect to electron exchange. Therefore they must not be seen as physical states but only as building blocks for constructing the physical spin-orbit states with the correct permutational symmetry.

Orbitals which can be simply obtained from the listed ones by permuting the coordinates $(1, 2, 3)$ are not indicated.

Orbitals $(s + s + s)$

The orbital

$$
\begin{aligned}
\varphi\{A_1' \, s^3\}(1,2,3) \;=\; & [\, s^A(1)\, s^B(2)\, s^C(3) + s^B(1)\, s^A(2)\, s^C(3) \\
+ \;& s^B(1)\, s^C(2)\, s^A(3) + s^C(1)\, s^B(2)\, s^A(3) \\
+ \;& s^C(1)\, s^A(2)\, s^B(3) + s^A(1)\, s^C(2)\, s^B(3)\,]\,/\,\sqrt{6}
\end{aligned}
\tag{6.1}
$$

is the basis of the A_1' representation.

The orbital

$$
\begin{aligned}
\varphi\{A_2' \, s^3\}(1,2,3) \;=\; & [\, s^A(1)\, s^B(2)\, s^C(3) - s^B(1)\, s^A(2)\, s^C(3) \\
+ \;& s^B(1)\, s^C(2)\, s^A(3) - s^C(1)\, s^B(2)\, s^A(3) \\
+ \;& s^C(1)\, s^A(2)\, s^B(3) - s^A(1)\, s^C(2)\, s^B(3)\,]\,/\,\sqrt{6}
\end{aligned}
\tag{6.2}
$$

is the basis of the A_2' representation.

The orbitals

$$
\left\{
\begin{aligned}
\varphi_1\{E' \, s^3\}(1,2,3) \;=\; & [\, 2\, s^A(1)\, s^B(2)\, s^C(3) \\
& - s^B(1)\, s^C(2)\, s^A(3) \\
& - s^C(1)\, s^A(2)\, s^B(3)\,]\,/\,\sqrt{6} \\
\varphi_2\{E' \, s^3\}(1,2,3) \;=\; & [\, s^B(1)\, s^C(2)\, s^A(3) - s^C(1)\, s^A(2)\, s^B(3)\,]\,/\,\sqrt{2}
\end{aligned}
\right.
\tag{6.3}
$$

form the basis of an E' representation. An equivalent (complex-valued) basis is given by

$$
\left\{
\begin{aligned}
\varphi\{E' \, s^3\}(1,2,3) \;=\; & [\, s^A(1)\, s^B(2)\, s^C(3) \\
& + s^B(1)\, s^C(2)\, s^A(3)\, e^{-i\frac{2\pi}{3}} \\
& + s^C(1)\, s^A(2)\, s^B(3)\, e^{i\frac{2\pi}{3}}\,]\,/\,\sqrt{3} \\
\varphi^*\{E' \, s^3\}(1,2,3) \;=\; & [\, s^A(1)\, s^B(2)\, s^C(3) \\
& + s^B(1)\, s^C(2)\, s^A(3)\, e^{i\frac{2\pi}{3}} \\
& + s^C(1)\, s^A(2)\, s^B(3)\, e^{-i\frac{2\pi}{3}}\,]\,/\,\sqrt{3}
\end{aligned}
\right.
\tag{6.4}
$$

The basis functions (6.3) and (6.4) are related as

$$
\left\{
\begin{aligned}
\varphi \;&=\; (\varphi_1 + i\varphi_2)\,/\,\sqrt{2} \\
\varphi^* \;&=\; (\varphi_1 - i\varphi_2)\,/\,\sqrt{2}
\end{aligned}
\right.
\,.
\tag{6.5}
$$

Orbitals $(s + s + p_x)$

The orbital

$$\begin{aligned}
\varphi\{A_1'\, s^2 p_x\}(1,2,3) &= [\, s^A(1)\, s^B(2)\, p_x^C(3) + s^B(1)\, s^A(2)\, p_x^C(3) \\
&+ \; s^B(1)\, s^C(2)\, p_x^A(3) + s^C(1)\, s^B(2)\, p_x^A(3) \\
&+ \; s^C(1)\, s^A(2)\, p_x^B(3) + s^A(1)\, s^C(2)\, p_x^B(3)\,]\,/\,\sqrt{6}
\end{aligned}$$

(6.6)

is the basis of the A_1' representation.

The orbital

$$\begin{aligned}
\varphi\{A_2'\, s^2 p_x\}(1,2,3) &= [\, s^A(1)\, s^B(2)\, p_x^C(3) - s^B(1)\, s^A(2)\, p_x^C(3) \\
&+ \; s^B(1)\, s^C(2)\, p_x^A(3) - s^C(1)\, s^B(2)\, p_x^A(3) \\
&+ \; s^C(1)\, s^A(2)\, p_x^B(3) - s^A(1)\, s^C(2)\, p_x^B(3)\,]\,/\,\sqrt{6}
\end{aligned}$$

(6.7)

is the basis of the A_2' representation.

The orbitals

$$\left\{ \begin{aligned}
\varphi_1\{E'\, s^2 p_x\}(1,2,3) &= [\, 2\, s^A(1)\, s^B(2)\, p_x^C(3) \\
&- \; s^B(1)\, s^C(2)\, p_x^A(3) \\
&- \; s^C(1)\, s^A(2)\, p_x^B(3)\,]\,/\,\sqrt{6} \\
\varphi_2\{E'\, s^2 p_x\}(1,2,3) &= [\, s^B(1)\, s^C(2)\, p_x^A(3) - \; s^C(1)\, s^A(2)\, p_x^B(3)\,]\,/\,\sqrt{2}
\end{aligned} \right.$$

(6.8)

form the basis of an E' representation. An equivalent (complex-valued) basis is given by

$$\left\{ \begin{aligned}
\varphi\{E'\, s^2 p_x\}(1,2,3) &= [\, s^A(1)\, s^B(2)\, p_x^C(3) \\
&+ s^B(1)\, s^C(2)\, p_x^A(3)\, e^{-i\frac{2\pi}{3}} \\
&+ s^C(1)\, s^A(2)\, p_x^B(3)\, e^{i\frac{2\pi}{3}}\,]\,/\,\sqrt{3} \\
\varphi^*\{E'\, s^2 p_x\}(1,2,3) &= [\, s^A(1)\, s^B(2)\, p_x^C(3) \\
&+ s^B(1)\, s^C(2)\, p_x^A(3)\, e^{i\frac{2\pi}{3}} \\
&+ s^C(1)\, s^A(2)\, p_x^B(3)\, e^{-i\frac{2\pi}{3}}\,]\,/\,\sqrt{3}
\end{aligned} \right.$$

(6.9)

The basis functions (6.8) and (6.9) are related as

$$\left\{ \begin{aligned}
\varphi &= (\varphi_1 + i\varphi_2)\,/\,\sqrt{2} \\
\varphi^* &= (\varphi_1 - i\varphi_2)\,/\,\sqrt{2}
\end{aligned} \right. .$$

(6.10)

Orbitals $(s + s + p_y)$

The orbital

$$
\begin{aligned}
\varphi\{A_2'\ s^2 p_y\}(1,2,3) \ =\ & [\, s^A(1)\, s^B(2)\, p_y^C(3) + s^B(1)\, s^A(2)\, p_y^C(3) \\
+\ & s^B(1)\, s^C(2)\, p_y^A(3) + s^C(1)\, s^B(2)\, p_y^A(3) \\
+\ & s^C(1)\, s^A(2)\, p_y^B(3) + s^A(1)\, s^C(2)\, p_y^B(3)\,]\,/\,\sqrt{6}
\end{aligned}
$$

$$(6.11)$$

is the basis of the A_2' representation.

The orbital

$$
\begin{aligned}
\varphi\{A_1'\ s^2 p_y\}(1,2,3) \ =\ & [\, s^A(1)\, s^B(2)\, p_y^C(3) - s^B(1)\, s^A(2)\, p_y^C(3) \\
+\ & s^B(1)\, s^C(2)\, p_y^A(3) - s^C(1)\, s^B(2)\, p_y^A(3) \\
+\ & s^C(1)\, s^A(2)\, p_y^B(3) - s^A(1)\, s^C(2)\, p_y^B(3)\,]\,/\,\sqrt{6}
\end{aligned}
$$

$$(6.12)$$

is the basis of the A_1' representation.

The orbitals

$$
\left\{
\begin{aligned}
\varphi_1\{E'\ s^2 p_y\}(1,2,3) \ =\ & [\, 2\, s^A(1)\, s^B(2)\, p_y^C(3) \\
& -\ s^B(1)\, s^C(2)\, p_y^A(3) \\
& -\ s^C(1)\, s^A(2)\, p_y^B(3)\,]\,/\,\sqrt{6} \\
\varphi_2\{E'\ s^2 p_y\}(1,2,3) \ =\ & [\, s^B(1)\, s^C(2)\, p_y^A(3) -\ s^C(1)\, s^A(2)\, p_y^B(3)\,]\,/\,\sqrt{2}
\end{aligned}
\right.
$$

$$(6.13)$$

form the basis of an E' representation. An equivalent (complex-valued) basis is given by

$$
\left\{
\begin{aligned}
\varphi\{E'\ s^2 p_y\}(1,2,3) \ =\ & [\, s^A(1)\, s^B(2)\, p_y^C(3) \\
& +\ s^B(1)\, s^C(2)\, p_y^A(3)\, e^{-\mathrm{i}\frac{2\pi}{3}} \\
& +\ s^C(1)\, s^A(2)\, p_y^B(3)\, e^{\mathrm{i}\frac{2\pi}{3}}\,]\,/\,\sqrt{3} \\
\varphi^*\{E'\ s^2 p_y\}(1,2,3) \ =\ & [\, s^A(1)\, s^B(2)\, p_y^C(3) \\
& +\ s^B(1)\, s^C(2)\, p_y^A(3)\, e^{\mathrm{i}\frac{2\pi}{3}} \\
& +\ s^C(1)\, s^A(2)\, p_y^B(3)\, e^{-\mathrm{i}\frac{2\pi}{3}}\,]\,/\,\sqrt{3}
\end{aligned}
\right.
$$

$$(6.14)$$

The basis functions (6.13) and (6.14) are related as

$$
\left\{
\begin{aligned}
\varphi \ &=\ (\varphi_1 + \mathrm{i}\varphi_2)\,/\,\sqrt{2} \\
\varphi^* \ &=\ (\varphi_1 - \mathrm{i}\varphi_2)\,/\,\sqrt{2}
\end{aligned}
\right. .
$$

$$(6.15)$$

179

Orbitals $(s + s + p_z)$

The orbital

$$
\begin{aligned}
\varphi\{A_1'' \, s^2 p_z\}(1,2,3) \;=\; & [\, s^A(1) \, s^B(2) \, p_z^C(3) + s^B(1) \, s^A(2) \, p_z^C(3) \\
& + \; s^B(1) \, s^C(2) \, p_z^A(3) + s^C(1) \, s^B(2) \, p_z^A(3) \\
& + \; s^C(1) \, s^A(2) \, p_z^B(3) + s^A(1) \, s^C(2) \, p_z^B(3) \,] \, / \, \sqrt{6}
\end{aligned}
$$

(6.16)

is the basis of the A_1'' representation.

The orbital

$$
\begin{aligned}
\varphi\{A_2'' \, s^2 p_z\}(1,2,3) \;=\; & [\, s^A(1) \, s^B(2) \, p_z^C(3) - s^B(1) \, s^A(2) \, p_z^C(3) \\
& + \; s^B(1) \, s^C(2) \, p_z^A(3) - s^C(1) \, s^B(2) \, p_z^A(3) \\
& + \; s^C(1) \, s^A(2) \, p_z^B(3) - s^A(1) \, s^C(2) \, p_z^B(3) \,] \, / \, \sqrt{6}
\end{aligned}
$$

(6.17)

is the basis of the A_2'' representation.

The orbitals

$$
\left\{
\begin{aligned}
\varphi_1\{E'' \, s^2 p_z\}(1,2,3) \;=\; & [\, 2 \, s^A(1) \, s^B(2) \, p_z^C(3) \\
& - \; s^B(1) \, s^C(2) \, p_z^A(3) \\
& - \; s^C(1) \, s^A(2) \, p_z^B(3) \,] \, / \, \sqrt{6} \\
\varphi_2\{E'' \, s^2 p_z\}(1,2,3) \;=\; & [\, s^B(1) \, s^C(2) \, p_z^A(3) - \; s^C(1) \, s^A(2) \, p_z^B(3) \,] \, / \, \sqrt{2}
\end{aligned}
\right.
$$

(6.18)

form the basis of an E'' representation. An equivalent (complex-valued) basis is given by

$$
\left\{
\begin{aligned}
\varphi\{E'' \, s^2 p_z\}(1,2,3) \;=\; & [\, s^A(1) \, s^B(2) \, p_z^C(3) \\
& + \; s^B(1) \, s^C(2) \, p_z^A(3) \, e^{-i\frac{2\pi}{3}} \\
& + \; s^C(1) \, s^A(2) \, p_z^B(3) \, e^{i\frac{2\pi}{3}} \,] \, / \, \sqrt{3} \\
\varphi^*\{E'' \, s^2 p_z\}(1,2,3) \;=\; & [\, s^A(1) \, s^B(2) \, p_z^C(3) \\
& + \; s^B(1) \, s^C(2) \, p_z^A(3) \, e^{i\frac{2\pi}{3}} \\
& + \; s^C(1) \, s^A(2) \, p_z^B(3) \, e^{-i\frac{2\pi}{3}} \,] \, / \, \sqrt{3}
\end{aligned}
\right.
$$

(6.19)

The basis functions (6.18) and (6.19) are related as

$$
\left\{
\begin{aligned}
\varphi \;&=\; (\varphi_1 + i\varphi_2) \, / \, \sqrt{2} \\
\varphi^* \;&=\; (\varphi_1 - i\varphi_2) \, / \, \sqrt{2}
\end{aligned}
\right. .
$$

(6.20)

6.2.3 Spin functions

We denote $\chi_+(\sigma)$ and $\chi_-(\sigma)$ the eigenfunctions of the single-electron spin operator $\hat{s}_z$, with respective eigenvalues $\hbar/2$ and $-\hbar/2$:

$$\hat{s}_z \chi_+(\sigma) = \frac{\hbar}{2}\chi_+(\sigma) , \qquad \hat{s}_z \chi_-(\sigma) = -\frac{\hbar}{2}\chi_-(\sigma) . \qquad (6.21)$$

σ is the single-electron "spin coordinate", with possible values $+1/2$ and $-1/2$. Explicitly,

$$\begin{aligned}
\chi_+(1/2) &= 1 , & \chi_+(-1/2) &= 0 , \\
\chi_-(1/2) &= 0 , & \chi_-(-1/2) &= 1 .
\end{aligned} \qquad (6.22)$$

Symmetry properties for D_{3h} geometry

The behaviour of the single-electron spin functions $\chi_+(\sigma)$ and $\chi_-(\sigma)$ under D_{3h} symmetry operations is summarized in Table 6.2.3. We have not used these relations, but they might be useful in order to establish selection rules for transitions between spin-coupled states.

In a rotation of angle ϕ around the axis $\mathbf{n}$, the spin function $\chi(\sigma)$ of a spin-1/2 particle transforms as:

$$\chi \to e^{-i\phi\mathbf{n}\cdot\mathbf{s}}\chi = \left[\cos\left(\frac{\phi}{2}\right) - 2\,i\,\mathbf{n}\cdot\hat{\mathbf{s}}\left(\sin\frac{\phi}{2}\right) \right] \chi . \qquad (6.23)$$

In the (χ_+, χ_-) basis, the rotation operator $e^{-i\phi\mathbf{n}\cdot\mathbf{s}}$ is represented by the matrix

$$e^{-i\phi\mathbf{n}\cdot\hat{\mathbf{s}}} = \cos\left(\frac{\phi}{2}\right)\begin{pmatrix} 1 & 0 \\ 0 & 1 \end{pmatrix} - i\sin\left(\frac{\phi}{2}\right)\begin{pmatrix} n_z & n_x - in_y \\ n_x + in_y & -n_z \end{pmatrix} . \qquad (6.24)$$

Like the orbital angular momentum states, the spin states are pseudo-vectors: in rotations they behave like vectors, but they are unaffected by the inversion:[3]

$$I\chi_+(\sigma) = \chi_+(\sigma) , \qquad I\chi_-(\sigma) = \chi_-(\sigma) . \qquad (6.25)$$

Thus I is represented by the unity matrix:

$$I = \begin{pmatrix} 1 & 0 \\ 0 & 1 \end{pmatrix} \qquad (6.26)$$

Eqs. (6.24) and (6.26) can be used to obtain matrix representations of rotations and reflexions in the (χ_+, χ_-) basis (a reflexion can be expressed

---

[3]In principal one could also assume that the inversion gives a minus sign: $I\chi = -\chi$, so that $I^2 = E$, as required. We have not investigated this alternative.

as rotation of $180°$ followed by the inversion). In the (χ_+, χ_-) basis, the D_{3h} elements are represented by the following matrices:

$$
E = \begin{pmatrix} 1 & 0 \\ 0 & 1 \end{pmatrix} \qquad\qquad Q = \begin{pmatrix} -1 & 0 \\ 0 & -1 \end{pmatrix}
$$

$$
C_3 = \begin{pmatrix} e^{-i\frac{\pi}{3}} & 0 \\ 0 & e^{i\frac{\pi}{3}} \end{pmatrix} \qquad\qquad C_3 Q = \begin{pmatrix} e^{i\frac{2\pi}{3}} & 0 \\ 0 & e^{-i\frac{2\pi}{3}} \end{pmatrix}
$$

$$
C_3^2 = \begin{pmatrix} e^{-i\frac{2\pi}{3}} & 0 \\ 0 & e^{i\frac{2\pi}{3}} \end{pmatrix} \qquad\qquad C_3^2 Q = \begin{pmatrix} e^{i\frac{\pi}{3}} & 0 \\ 0 & e^{-i\frac{\pi}{3}} \end{pmatrix}
$$

$$
\sigma_h = \begin{pmatrix} -i & 0 \\ 0 & i \end{pmatrix} \qquad\qquad \sigma_h Q = \begin{pmatrix} i & 0 \\ 0 & -i \end{pmatrix}
$$

$$
\sigma_h C_3 = \begin{pmatrix} e^{-i\frac{5\pi}{6}} & 0 \\ 0 & e^{i\frac{5\pi}{6}} \end{pmatrix} \qquad\qquad \sigma_h C_3 Q = \begin{pmatrix} e^{i\frac{\pi}{6}} & 0 \\ 0 & e^{-i\frac{\pi}{6}} \end{pmatrix}
$$

$$
\sigma_h C_3^2 = \begin{pmatrix} e^{i\frac{5\pi}{6}} & 0 \\ 0 & e^{-i\frac{5\pi}{6}} \end{pmatrix} \qquad\qquad \sigma_h C_3^2 Q = \begin{pmatrix} e^{-i\frac{\pi}{6}} & 0 \\ 0 & e^{i\frac{\pi}{6}} \end{pmatrix}
$$

$$
U_2^A = \begin{pmatrix} 0 & -i \\ -i & 0 \end{pmatrix} \qquad\qquad U_2^A Q = \begin{pmatrix} 0 & i \\ i & 0 \end{pmatrix}
$$

$$
U_2^B = \begin{pmatrix} 0 & e^{-i\frac{\pi}{6}} \\ e^{-i\frac{5\pi}{6}} & 0 \end{pmatrix} \qquad\qquad U_2^B Q = \begin{pmatrix} 0 & e^{i\frac{5\pi}{6}} \\ e^{i\frac{\pi}{6}} & 0 \end{pmatrix}
$$

$$
U_2^C = \begin{pmatrix} 0 & e^{i\frac{\pi}{6}} \\ e^{i\frac{5\pi}{6}} & 0 \end{pmatrix} \qquad\qquad U_2^C Q = \begin{pmatrix} 0 & e^{-i\frac{5\pi}{6}} \\ e^{-i\frac{\pi}{6}} & 0 \end{pmatrix}
$$

$$
\sigma_v^A = \begin{pmatrix} 0 & -1 \\ 1 & 0 \end{pmatrix} \qquad\qquad \sigma_v^A Q = \begin{pmatrix} 0 & 1 \\ -1 & 0 \end{pmatrix}
$$

$$
\sigma_v^B = \begin{pmatrix} 0 & e^{-i\frac{2\pi}{3}} \\ e^{-i\frac{\pi}{3}} & 0 \end{pmatrix} \qquad\qquad \sigma_v^B Q = \begin{pmatrix} 0 & e^{i\frac{\pi}{3}} \\ e^{i\frac{2\pi}{3}} & 0 \end{pmatrix}
$$

$$
\sigma_v^C = \begin{pmatrix} 0 & e^{-i\frac{\pi}{3}} \\ e^{-i\frac{2\pi}{3}} & 0 \end{pmatrix} \qquad\qquad \sigma_v^C Q = \begin{pmatrix} 0 & e^{i\frac{2\pi}{3}} \\ e^{i\frac{\pi}{3}} & 0 \end{pmatrix}
$$

$$(6.27)$$

The above set of matrices is a *binary* representation of D_{3h}: each group element is represented by two different matrices. The rotation of 2π around an arbitrary axis is denoted Q following Ref. [150]. It commutes with all group elements. Strictly speaking, the binary representation is not a representation of the symmetry group, since it does not reflect the group structure exactly. In particular, two matrices representing two commuting group elements do not necessarily commute. This can be demonstrated by the following exam-

ple:

$$\sigma_h U_2^A = \begin{pmatrix} -i & 0 \\ 0 & i \end{pmatrix} \begin{pmatrix} 0 & -i \\ -i & 0 \end{pmatrix} = \begin{pmatrix} 0 & -1 \\ 1 & 0 \end{pmatrix} = \sigma_v^A$$

$$U_2^A \sigma_h = \begin{pmatrix} 0 & -i \\ -i & 0 \end{pmatrix} \begin{pmatrix} -i & 0 \\ 0 & i \end{pmatrix} = \begin{pmatrix} 0 & 1 \\ -1 & 0 \end{pmatrix} = \sigma_v^A Q$$

This clearly shows the need for introducing Q in order to obtain a complete group.

However, the binary representation is a true representation of the *double* group D'_{3h}, defined as the direct product of D_{3h} and the group formed by the two elements E and Q. Since Q commutes with all elements of D_{3h}, the order of D'_{3h} is $2 \times 12 = 24$ (twice the order of D_{3h}). Table 6.2.3 is the first quadrant of the D'_{3h} multiplication table. It indicates the products AB, for all elements A and B belonging to D_{3h}. The products $(QA)B$, $A(QB)$ and $(QA)(QB)$ are not listed due to lack of space, but they can be found very easily from the table using the identities

$$(QA)B = Q(AB), \qquad A(QB) = Q(AB), \qquad (QA)(QB) = AB . \quad (6.28)$$

E	C_3	C_3^2	σ_h	$\sigma_h C_3$	$\sigma_h C_3^2$	U_2^A	U_2^B	U_2^C	σ_v^A	σ_v^B	σ_v^C
C_3	C_3^2	Q	$\sigma_h C_3$	$\sigma_h C_3^2$	$\sigma_h Q$	$U_2^C Q$	U_2^A	U_2^B	$\sigma_v^C Q$	σ_v^A	σ_v^B
C_3^2	Q	$C_3 Q$	$\sigma_h C_3^2$	$\sigma_h Q$	$\sigma_h C_3 Q$	$U_2^B Q$	$U_2^C Q$	U_2^A	$\sigma_v^B Q$	$\sigma_v^C Q$	σ_v^A
σ_h	$\sigma_h C_3$	$\sigma_h C_3^2$	Q	$C_3 Q$	$C_3^2 Q$	σ_v^A	σ_v^B	σ_v^C	$U_2^A Q$	$U_2^B Q$	$U_2^C Q$
$\sigma_h C_3$	$\sigma_h C_3^2$	$\sigma_h Q$	$C_3 Q$	$C_3^2 Q$	E	$\sigma_v^C Q$	σ_v^A	σ_v^B	U_2^C	$U_2^A Q$	$U_2^B Q$
$\sigma_h C_3^2$	$\sigma_h Q$	$\sigma_h C_3 Q$	$C_3^2 Q$	E	C^3	$\sigma_v^B Q$	$\sigma_v^C Q$	σ_v^A	U_2^B	U_2^C	$U_2^A Q$
U_2^A	U_2^B	U_2^C	$\sigma_v^A Q$	$\sigma_v^B Q$	$\sigma_v^C Q$	Q	$C_3 Q$	$C_3^2 Q$	σ_h	$\sigma_h C_3$	$\sigma_h C_3^2$
U_2^B	U_2^C	$U_2^A Q$	$\sigma_v^B Q$	$\sigma_v^C Q$	σ_v^A	C_3^2	Q	$C_3 Q$	$\sigma_h C_3^2 Q$	σ_h	$\sigma_h C_3$
U_2^C	$U_2^A Q$	$U_2^B Q$	$\sigma_v^C Q$	σ_v^A	σ_v^B	C_3	C_3^2	Q	$\sigma_h C_3 Q$	$\sigma_h C_3^2 Q$	σ_h
σ_v^A	σ_v^B	σ_v^C	U_2^A	U_2^B	U_2^C	$\sigma_h Q$	$\sigma_h C_3 Q$	$\sigma_h C_3^2 Q$	Q	$C_3 Q$	$C_3^2 Q$
σ_v^B	σ_v^C	$\sigma_v^A Q$	U_2^B	U_2^C	$U_2^A Q$	$\sigma_h C_3^2$	$\sigma_h Q$	$\sigma_h C_3 Q$	C_3^2	Q	$C_3 Q$
σ_v^C	$\sigma_v^A Q$	$\sigma_v^B Q$	U_2^C	$U_2^A Q$	$U_2^B Q$	$\sigma_h C_3$	$\sigma_h C_3^2$	$\sigma_h Q$	C_3	C_3^2	Q

Table 6.4: Multiplication table of the binary point group D'_{3h}. Only the first quadrant of the table is shown (see text for details).

D'_{3h}	E	Q	σ_h	C_3	C_3^2	$\sigma_h C_3$	$\sigma_h C_3 Q$	$3U_2$	$3\sigma_v$
			$\sigma_h Q$	$C_3^2 Q$	$C_3 Q$	$\sigma_h C_3^2$	$\sigma_h C_3^2 Q$	$3U_2 Q$	$3\sigma_v Q$
E'_1	2	-2	0	1	-1	$\sqrt{3}$	$-\sqrt{3}$	0	0
E'_2	2	-2	0	1	-1	$-\sqrt{3}$	$\sqrt{3}$	0	0
E'_3	2	-2	0	-2	2	0	0	0	0

Table 6.5: Character table for the binary representations of the D_{3h} point group.

6.2.4 Spin functions for three electrons

The spin space of three electrons has the dimension $2^3 = 8$. A basis of this space is given by the product states

$$\chi_{m_1}(1)\,\chi_{m_2}(2)\,\chi_{m_3}(3)\;,$$

where each of the quantum numbers (m_1, m_2, m_3) can assume the values $+1/2$ and $-1/2$. The spin operator associated with the ith electron is denoted $\hat{\mathbf{s}}(i)$ $(i = 1, 2, 3)$.

The total electronic spin operator is the sum

$$\hat{\mathbf{S}} = \hat{\mathbf{s}}(1) + \hat{\mathbf{s}}(2) + \hat{\mathbf{s}}(3)\;. \tag{6.29}$$

The operator

$$\hat{\mathbf{S}}^2 = \sum_{i=1}^{3}[\,\hat{s}_x^2(i) + \hat{s}_y^2(i) + \hat{s}_z^2(i)\,]$$

has the eigenvalues $\hbar^2 S(S+1)$, where the spin quantum number S is either $S = 1/2$ (doublet states) or $S = 3/2$ (quartet states). The eight-dimensional spin space is the sum of a four-dimensional space of doublet states and a four-dimensional space of quartet states:

$$1/2 \otimes 1/2 \otimes 1/2 \;=\; 1/2 \otimes (0 \oplus 1) \;=\; 1/2 \oplus 1/2 \oplus 3/2\;. \tag{6.30}$$

The quartet spin functions with positive spin projections $M_S = +3/2$ and $M_S = +1/2$ are given by

$$
\begin{aligned}
\chi_{\frac{3}{2}\frac{3}{2}}(1,2,3) &= \chi_+(1)\chi_+(2)\chi_+(3)\;, &(6.31)\\
\chi_{\frac{3}{2}\frac{1}{2}}(1,2,3) &= [\,\chi_-(1)\chi_+(2)\chi_+(3) \\
&\quad + \chi_+(1)\chi_-(2)\chi_+(3) \\
&\quad + \chi_+(1)\chi_+(2)\chi_-(3)\,] \,/\, \sqrt{3}\;. &(6.32)
\end{aligned}
$$

185

E	C_3	σ_h	U_2^A	σ_v^A
χ_+	$e^{-i\frac{\pi}{3}}\chi_+$	$-i\chi_+$	$-i\chi_-$	$-\chi_-$
χ_-	$e^{i\frac{\pi}{3}}\chi_-$	$i\chi_-$	$-i\chi_+$	χ_+

Table 6.6: Symmetry properties of the single-electron spin functions χ_+ and χ_- for the D_{3h} equilateral triangle geometry.

The corresponding states with negative spin projections $M_S = -1/2$ and $M_S = -3/2$ are obtained from the above expressions by replacing χ_+ by χ_- and χ_- by χ_+. The quartet spin states are totally symmetrical with respect to permutations of the electrons (each quartet spin states is a basis of the totally symmetrical representation of the permutation group S_3).

Two mutually orthogonal doublet states with positive spin projection $M_S = +1/2$ may be defined as:

$$
\begin{aligned}
\chi_{\frac{1}{2}\frac{1}{2}}^{(1)}(1,2,3) &= [\, 2\chi_+(1)\chi_+(2)\chi_-(3) \\
&\quad - \chi_-(1)\chi_+(2)\chi_+(3) \\
&\quad - \chi_+(1)\chi_-(2)\chi_+(3)\,] \,/\, \sqrt{6}\,, \quad (6.33) \\
\chi_{\frac{1}{2}\frac{1}{2}}^{(2)}(1,2,3) &= [\, \chi_+(1)\chi_-(2)\chi_+(3) \\
&\quad - \chi_-(1)\chi_+(2)\chi_+(3)\,] \,/\, \sqrt{2}\,. \quad (6.34)
\end{aligned}
$$

$\chi_{\frac{1}{2}\frac{1}{2}}^{(1)}$ and $\chi_{\frac{1}{2}\frac{1}{2}}^{(2)}$ form the basis of a two-dimensional irreducible representation of the permutation group S_3. We note that they are real.

Sometimes it is convenient to use the following two linear combinations of $\chi_{\frac{1}{2}\frac{1}{2}}^{(1)}$ and $\chi_{\frac{1}{2}\frac{1}{2}}^{(2)}$:

$$
\chi_{\frac{1}{2}\frac{1}{2}} = \left[\chi_{\frac{1}{2}+\frac{1}{2}}^{(1)} + i\chi_{\frac{1}{2}+\frac{1}{2}}^{(2)} \right] \,/\, \sqrt{2} \quad (6.35)
$$

$$
\chi_{\frac{1}{2}\frac{1}{2}}^{*} = \left[\chi_{\frac{1}{2}+\frac{1}{2}}^{(1)} - i\chi_{\frac{1}{2}+\frac{1}{2}}^{(2)} \right] \,/\, \sqrt{2} \quad (6.36)
$$

$\chi_{\frac{1}{2}\frac{1}{2}}$ is complex-valued, and $\chi_{\frac{1}{2}\frac{1}{2}}^{*}$ is its complex conjugate. Explicitly,

$$
\begin{aligned}
\chi_{\frac{1}{2}\frac{1}{2}}(1,2,3) &= [\, \chi_-(1)\chi_+(2)\chi_+(3) \\
&\quad + \chi_+(1)\chi_-(2)\chi_+(3)\, e^{-i\frac{2\pi}{3}} \\
&\quad + \chi_+(1)\chi_+(2)\chi_-(3)\, e^{i\frac{2\pi}{3}} \,] \,/\, \sqrt{3}\,, \quad (6.37)
\end{aligned}
$$

$$
\chi_{\frac{1}{2}\frac{1}{2}}^{*}(1,2,3) = [\, \chi_-(1)\chi_+(2)\chi_+(3)
$$

$$+\chi_+(1)\chi_-(2)\chi_+(3)\,e^{\mathrm{i}\frac{2\pi}{3}}$$
$$+\chi_+(1)\chi_+(2)\chi_-(3)\,e^{-\mathrm{i}\frac{2\pi}{3}}\,]\,/\,\sqrt{3}\;. \qquad (6.38)$$

Permuting spins 2 and 3 amounts to replacing $\chi_{\frac{1}{2}\frac{1}{2}}$ by its complex conjugate:

$$\hat{\mathcal{P}}_{132}\,\chi_{\frac{1}{2}\frac{1}{2}}(1,2,3) = \chi_{\frac{1}{2}\frac{1}{2}}(1,3,2) = \chi^*_{\frac{1}{2}\frac{1}{2}}(1,2,3)$$

Cyclic permutations of the spins 1, 2, and 3 only affect the phase of $\chi_{\frac{1}{2}\frac{1}{2}}$:

$$\hat{\mathcal{P}}_{312}\,\chi_{\frac{1}{2}\frac{1}{2}}(1,2,3) = \chi_{\frac{1}{2}\frac{1}{2}}(3,1,2) = e^{-\mathrm{i}\frac{2\pi}{3}}\,\chi_{\frac{1}{2}\frac{1}{2}}(1,2,3)\;,$$

$$\hat{\mathcal{P}}_{231}\,\chi_{\frac{1}{2}\frac{1}{2}}(1,2,3) = \chi_{\frac{1}{2}\frac{1}{2}}(2,3,1) = e^{\mathrm{i}\frac{2\pi}{3}}\,\chi_{\frac{1}{2}\frac{1}{2}}(1,2,3)\;.$$

Analogous expressions hold for the doublet function with negative spin projections, $\chi_{\frac{1}{2},-\frac{1}{2}}(1,2,3)$ and $\chi^*_{\frac{1}{2},-\frac{1}{2}}(1,2,3)$.

6.2.5 Spin-orbit states

The complete stationary wavefunction $\psi(1,2,3)$ describing the three open-shell electrons "1", "2" and "3" can be written as an antisymmetrized product, such as

$$\hat{\mathcal{A}}\,\chi(1,2,3)\,\varphi(1,2,3) \qquad (6.39)$$

or

$$\hat{\mathcal{A}}\,\chi(2,1,3)\,\varphi(1,2,3) \qquad (6.40)$$

where χ and φ are spin and orbital functions, respectively, and $\hat{\mathcal{A}}$ is the antisymmetrization operator for three electrons.

Substituting for $\varphi(1,2,3)$ the D_{3h} basis functions defined in Sec. 6.2.2 yields electronic wavefunctions $\psi(1,2,3)$ with the correct permutational and spatial symmetries (the procedure may yield the same function $\psi(1,2,3)$ more than once). As a consequence of the antisymmetrization procedure $\hat{\mathcal{A}}$, many terms may cancel. In some cases *all* terms cancel, in agreement with the Pauli exclusion principle, and the resulting function $\psi(1,2,3)$ will be zero.

Every spin-orbital $\psi(1,2,3)$ that is an element of a basis of an irreducible representation of D_{3h} can also be obtained by substituting for $\varphi(1,2,3)$ in Eq. (6.39) a certain function that is *not* an element of a basis of an irreducible representation of D_{3h}. As a trivial example, we may consider the wavefunction $\psi\{^4A_2'\}$ of the lowest quartet state

$$\psi\{^4A_2'\}(1,2,3) = \hat{\mathcal{A}}\,\chi(1,2,3)\,s^A(1)s^B(2)s^C(3)\,/\,\sqrt{6} \qquad (6.41)$$

where $\chi(1,2,3)$ is a quartet spin function. In fact, the product

$$s^A(1)s^B(2)s^C(3)$$

Asymptotic limit	Doublet states $S = 1/2$				Quartet states $S = 3/2$	
$s+s+s$	$^2E'$				$^4A'_2$	
$s+s+p_x$	$^2A'_1$	$^2A'_2$	$^2E'(\alpha)$	$^2E'(\beta)$	$^4A'_2$	$^4E'$
$s+s+p_y$	$^2A'_1$	$^2A'_2$	$^2E'(\alpha)$	$^2E'(\beta)$	$^4A'_1$	$^4E'$
$s+s+p_z$	$^2A''_1$	$^2A''_2$	$^2E''(\alpha)$	$^2E''(\beta)$	$^4A''_1$	$^4E''$

Table 6.7: Electronic states of an alkali trimer X_3.

on the right-hand side is *not* the basis of an irreducible representation of D_{3h}.

Every quartet state $\psi\{S = 3/2\}(1, 2, 3)$ can be written as the product of a completely symmetrical spin function and a totally antisymmetrical orbital function. The doublet states $\psi\{S = 1/2\}(1, 2, 3)$, in contrast, do *not* factorize into a spin function and an orbital function.

The dimensions of the four spin-orbit subspaces

$$s + s + s$$

$$s + s + p_x$$

$$s + s + p_y$$

$$s + s + p_z$$

can be found by choosing as their basis states antisymmetrical three-electron states of the form

$$
\begin{aligned}
\psi(1, 2, 3) &= \hat{\mathcal{A}} \; \chi_{m_1}(1) \, \chi_{m_2}(2) \, \chi_{m_3}(3) \times \\
&\times \; \varphi^A(1) \, \varphi^B(2) \, \varphi^C(3)
\end{aligned}
\tag{6.42}
$$

where χ_m is a single-electron spin function and φ^A, φ^B, φ^C are single-electron orbitals (not necessarily identical ones) centered respectively on A, B, and C. The "$s + s + s$"-space has dimension 8 (four doublet and four quaret states). The "$s + s + p_x$", "$s + s + p_y$" and "$s + s + p_z$" spaces each have dimension 24 (twelve doublet and twelve quartet states).

Finally, we point out that according to the Jahn-Teller theorem [150], the D_{3h} geometry cannot be stable in the case of the degenerate electronic states (E' or E''), .

6.2.6   Selection rules for electric dipole transitions

Considering the three nuclei as *fixed* in space (in the xy plane), one may establish selection rules for electric dipole transitions between two electronic

	E'; x, y	A_2''; z
A_1'	E'	A_2''
A_2'	E'	A_1''
A_1''	E''	A_2'
A_2''	E''	A_1'
E'	$A_1' + A_2' + E'$	E''
E''	$A_1'' + A_2'' + E''$	E'

Table 6.8: Selection rules for electric dipole transitions for D_{3h} nuclear geometry. The left column indicates the initial states, the two columns on the right indicate possible final states for the two possible polarizations of the electric field (parallel to the xy plane, parallel to the z axis)

states of the X_3 complex. We only consider the case of equilateral geometry (D_{3h}).

We established the selection rules summarized in Table 6.8 following the procedure described in Ref. [150], using the fact that the electric field components parallel and perpendicular to the molecular plane transform as the E' and A_2'' representations of D_{3h}, respectively (see the D_{3h} character table 6.2). The results are given in Table 6.8.

For example, spin-polarized Na_3 trimers in the electronic ground state

$$^4A_2' \ (3s + 3s + 3s)$$

might be transfered by an electromagnetic wave to electronically excited states

$$^4E' \ (3s + 3s + 3p) \qquad \text{or} \qquad ^4A_1'' \ (3s + 3s + 3p)$$

(see Table 6.8). The wave can be linearly or circularly polarized. By orienting the molecules parallel or perpendicular to the electric component of the electromagnetic wave, it might be possible to excite them selectively either to $^4E'$ or to $^4A_1''$ states.

Note that we have derived these selection rules using the molecular point group D_{3h}. A clearer approach might be to use the nuclear permutation - inversion group [43]).

6.2.7   Nuclear spin

The nuclear spin degrees of freedom need to be considered in order to establish the *statistical weights* for transitions between various rotational-vibrational

levels of the ground and the excited electronic states [150, 43]. We do not derive the statistical weights here, we only present the essential facts concerning the spin of the ^{23}Na nucleus.

The nuclear spin of a single ^{23}Na atom is $i = 3/2$ [1]. Its projections on a fixed axis can therefore be $I_M = -3/2,\ -1/2,\ 1/2,\ 3/2$.

The spin space $i_1 \otimes i_2 \otimes i_3$ of three sodium nuclei therefore has dimension $4^3 = 64$. It splits into several subspaces each characterized by a quantum number I, which lies between $1/2$ and $9/2$:

$$3/2 \otimes 3/2 \otimes 3/2 = 2 \times 1/2 \oplus 4 \times 3/2 \oplus 3 \times 5/2 \oplus 2 \times 7/2 \oplus 9/2 . \quad (6.43)$$

The three nuclei being identical fermions, the complete wavefunction of the triatomic system must be *antisymmetric* with respect to a permutation of two nuclei. The wavefunction may be written as

$$\psi = \hat{\mathcal{A}}_{ABC}\, \chi^{\mathrm{nuc}}(A, B, C)\, \phi^{\mathrm{nuc}}(A, B, C)\, \psi^{\mathrm{el}}(A, B, C, 1, 2, 3) \,/\, \sqrt{6}$$

$$(6.44)$$

where

$$\psi^{\mathrm{el}} = \hat{\mathcal{A}}_{123}\, \chi^{\mathrm{el}}(1, 2, 3)\, \varphi^{\mathrm{el}}(A, B, C, 1, 2, 3) \qquad (6.45)$$

is the electronic wavefunction. Here $\hat{\mathcal{A}}_{ABC}$ and $\hat{\mathcal{A}}_{123}$ are the antisymmetrization operators with respect to the nuclei ABC and the electrons 123.

6.2.8 Nuclear permutations

When two nuclei are permuted, the coordinate system with respect to which the electronic wavefunction is defined changes. Therefore the electronic wavefunction changes as well. For example,

$$\hat{\mathcal{P}}_{BAC}\, \psi^{\mathrm{el}}(A, B, C, 1, 2, 3)$$

is *not* the same as

$$\psi^{\mathrm{el}}(B, A, C, 1, 2, 3) .$$

In order to understand this, we may examine the effect of the permutation $\hat{\mathcal{P}}_{BAC}$ on the orbital function $p_z^A(1)s^B(2)s^C(3)$. One might think that it could be sufficient to permute the indices A and B, resulting in $p_z^B(1)s^A(2)s^C(3)$. However, the coordinate systems $(xyz)^A$, $(xyz)^B$, and $(xyz)^C$ (see Fig. 6.1) which were used to define the orbitals p_z^A, s^B, and s^C, do not only change their origins by also their orientations. These coordinate systems transform as follows:

$$\hat{\mathcal{P}}_{BAC}: \quad \begin{cases} (xyz)^A & \rightarrow & (x, -y, -z)^B \\ (xyz)^B & \rightarrow & (x, -y, -z)^A \\ (xyz)^C & \rightarrow & (x, -y, -z)^C \end{cases}$$

After the permutation

$$\mathcal{P}_{BAC}$$

, the electronic wavefunction is given by $-p_z^B(1)s^A(2)s^C(3)$, the atomic orbitals being defined with respect to the new coordinate system.

The nuclear permutation $\mathcal{P}_{BAC}$ has the effect of rotating the electronic wavefunction by $180°$ about the axis $M_{AB}C$ where M_{AB} is the point at half distance between A and B:

$$\hat{\mathcal{P}}_{BAC}\varphi(1,2,3) = U_2^C\varphi(1,2,3) \ . \tag{6.46}$$

Cyclic permutations of the nuclei have the effect of rotating the electronic wavefunction by $120°$ about the principal axis (perpendicular to the molecular plane):

$$\hat{\mathcal{P}}_{CAB} \ = \ \hat{\mathcal{P}}_{BAC} \circ \hat{\mathcal{P}}_{ACB} = U_2^C \circ U_2^A = C_3 \ . \tag{6.47}$$

6.3   Conclusion

We have constructed symmetry-adapted electronic states of an equilateral alkali trimer correlated to the $(s + s + s)$ and the $(s + s + p)$ dissociation thresholds, respectively, using basis sets of atomic orbitals and neglecting all physical interactions, notably the electrostatic forces.

If placed in an external electromagnetic wave, for example a laser beam, the triatomic system might be transfered from its electronic ground state to one of the excited electronic states correlated to the $(s + s + p)$ dissociation limit. The electromagnetic wave could thus induce a photoassociation reaction.

We have indicated the selection rules for electric dipole transitions between the electronic ground states $(s+s+s)$ and the exited electronic states $(s + s + p)$ for *fixed* positions of the nuclei, assuming that the nuclei form an equilateral triangle. If the molecular symmetry differs markedly from the equilateral one, other selection rules must be used.

In the next step the role of vibrational and rotational degrees of freedom should be considered. In particular the statistical weights for transitions between different rotational-vibrational levels should be establishd. Perhaps it could be convenient to use a free software package for group theory such as GAP [237].

Chapter 7

Conclusions and Perspectives

In this thesis we discussed various aspects related to the physics of two and three interacting atoms.

We showed that the Mapped Fourier Sine Grid is a simple and very efficient method for solving the radial Schrödinger equation numerically. The spurious solutions resulting from the standard mapped Fourier grid method remain somewhat mysterious, but it has become evident that they are sensitive to the behaviour of the grid basis functions near the borders of the grid. We did not fully exploit the grid method in our study devoted to the sodium trimer, but it should be clear that the discrete Fourier transform is a very versatile algorithm, and it may be useful for many different applications. In particular it could be interesting to combine it with the cartesian-like coordinates described by R. T. Pack [206]: one could thus obtain a three-dimensional representation of the vibrational wavefunction of a triatomic system.

We have presented the first numerical study of extremely weakly bound vibrational states of the sodium trimer. By adopting a scattering formalism, we obtained converged values for the energies of bound levels lying very closely underneath the atom-diatom dissociation threshold, including the very last bound level. By defining a short-range phase-shift we have been able to distinguish between resonant and non-resonant bound states. Although the method in its present form does not allow to compute three-dimensional vibrational wavefunctions, it offers a lot of insight, and it shows the close similarity between the weakly bound vibrational levels and low-energy scattering states. The project of using Jacobi coordinates in the three atom-dimer regions of configuration space where couplings are not negligible is still underway. Its success would be a great step forward, as it could allow to study slow collisions of atoms and molecules in high-lying vibrational states, which are of great interest in photoassociation experiments.

Finally we raised some simple questions concerning the possibility of forming trimers by photoassociation: either from three atoms or from an atom

and a dimer. The study shows that there are many electronically excited states which may intervene in a photassociation of Na_3. Therefore there could be many paths leading to the formation of Na_3 by photoassociation. It would be important to obtain a clearer picture of the electronic states and the corresponding potential energy surfaces correlated to the $Na(3s) + Na(3s) + Na(3p)$ dissociation limit.

Appendix A

Fundamental constants

speed of light in vacuum	c =	$299\,792\,458$ ms^{-1}
Planck constant	h =	$6.626\,069\,3(11) \times 10^{-34}$ J s
Boltzmann constant	k_B =	$1.380\,650\,5(24) \times 10^{-23}$ J K^{-1}
elementary charge	q_e =	$1.602\,176\,53(14) \times 10^{-19}$ C
electron mass	m_e =	$9.109\,382\,6(16) \times 10^{-31}$ kg
proton mass	m_p =	$1.672\,621\,71(29) \times 10^{-27}$ kg
electron rest energy	$m_e c^2$ =	$8.187\,104\,7(14) \times 10^{-14}$ J
	=	$0.510\,998\,918(44)$ MeV
proton rest energy	$m_p c^2$ =	$1.503\,277\,43(26) \times 10^{-10}$ J
	=	$938.272\,029(80)$ MeV

These are the 2002 CODATA recommended values [258].

Appendix B

Matrix elements for the mapped Fourier sine grid

The elements D_{ij} ($i = 0, \ldots, N$, $j = 1, \ldots, N-1$) of the rectangular matrix D defined in Eq. (2.60) can be evaluated using the trigonometric sum rule

$$1 + 2 \sum_{k=1}^{\nu} \cos(k\,z) \;=\; \frac{\sin\left[\left(\nu + \frac{1}{2}\right)z\right]}{\sin\left(\frac{z}{2}\right)} \qquad (z \in \mathbb{C}) . \qquad \text{(B.1)}$$

$$
\begin{aligned}
D_{ij} \;&=\; \sum_{k=1}^{N-1} C_{ik}\, k\, S^{\dagger}{}_{kj} \\
&=\; \alpha_i \frac{2}{N} \sum_{k=1}^{N-1} k\, \cos\left(k\frac{\pi}{N}i\right)\, \sin\left(k\frac{\pi}{N}j\right) \\
&=\; \alpha_i \frac{1}{N} \sum_{k=1}^{N-1} k\, \left[\sin\left(k\frac{\pi}{N}(i+j)\right) - \sin\left(k\frac{\pi}{N}(i-j)\right)\right] \\
&=\; \alpha_i \frac{1}{N} \left[\left.\sum_{k=1}^{N-1} k\, \sin\left(k\frac{m\pi}{N}\right)\right|_{m=i+j} - \left.\sum_{k=1}^{N-1} k\, \sin\left(k\frac{m\pi}{N}\right)\right|_{m=i-j}\right]
\end{aligned}
$$

$$\text{(B.2)}$$

For $m \neq 0$:

$$
\begin{aligned}
\sum_{k=1}^{N-1} k\, \sin\left(k\frac{m\pi}{N}\right) \;&=\; \left.-\frac{\partial}{\partial\beta} \sum_{k=1}^{N-1} \sin(k\beta)\right|_{\beta=\frac{m\pi}{N}} \\
&=\; \left.-\frac{\partial}{\partial\beta} \frac{\sin[(N-\frac{1}{2})\beta]}{2\sin\frac{\beta}{2}}\right|_{\beta=\frac{m\pi}{N}}
\end{aligned}
$$

$$= -\frac{(N - \frac{1}{2})\cos[(N - \frac{1}{2})\beta]\sin\frac{\beta}{2} - \frac{1}{2}\sin[(N - \frac{1}{2})\beta]\cos\frac{\beta}{2}}{2\sin^2\frac{\beta}{2}}\Bigg|_{\beta=\frac{m\pi}{N}}$$

$$= -\frac{(N - \frac{1}{2})(-1)^m \cos(\frac{m\pi}{2N})\sin(\frac{m\pi}{2N}) + \frac{1}{2}(-1)^m \sin(\frac{m\pi}{2N})\cos(\frac{m\pi}{2N})}{2\sin^2(\frac{m\pi}{2N})}$$

$$= -\frac{N}{2}(-1)^m \cot\left(\frac{m\pi}{2N}\right) \tag{B.3}$$

For $m = 0$, the sum is 0.

The final result is Eq. (2.60).

Appendix C

Rayleigh-Ritz variational method

C.1 Ritz variational principle

The Ritz variational principle [187] states that the functional

$$E\{\psi\} \;=\; \frac{\langle\psi|\hat{H}|\psi\rangle}{\langle\psi|\psi\rangle} \;, \tag{C.1}$$

defined on the space of square-integrable functions $\psi(q)$, is stationary if $\psi(q)$ is a solution of the Schrödinger equation: :

$$\delta E\{\psi\} \;=\; 0 \tag{C.2}$$

$$\Leftrightarrow \quad \hat{H}\,\psi(q) \;=\; E\,\psi(q) \;. \tag{C.3}$$

C.2 Expansion of the wavefunction in basis functions

In order to find an approximate solution of (C.3), the trial solution $\psi(q)$ is expanded in a finite set of basis functions $u_k(q)$:

$$\psi(q) \;=\; \sum_{k=1}^{N} u_k(q)c_k \;. \tag{C.4}$$

The task is then to determine the set of coefficients $\{c_k\}$ that render the functional (C.1) stationary. For this purpose it is convenient to rewrite Eq. (C.1) as

$$E\{\psi\}\,\langle\psi|\psi\rangle \;=\; \langle\psi|\hat{H}|\psi\rangle \;. \tag{C.5}$$

The coefficients c_k and their complex conjugates c_k^* can be treated as independent variables. Deriving (C.5) with respect to c_m and using the condition

$$\frac{\partial E\{\psi(c_1, \ldots, c_N)\}}{\partial c_k} = 0 \qquad (k = 1, \ldots, N) \qquad \text{(C.6)}$$

gives the identity

$$\sum_{l=1}^{N} \langle u_k | \hat{H} - E\{\psi\} | u_l \rangle c_l = 0 \qquad \text{(C.7)}$$

which can be rewritten as

$$\sum_{l=1}^{N} H_{kl}\, c_l = E\{\psi\} \sum_{l=1}^{N} S_{kl}\, c_l \qquad \text{(C.8)}$$

where H_{kl} and S_{kl} denote the Hamiltonian and overlap matrix elements:

$$H_{kl} = \langle u_k | \hat{H} | u_l \rangle , \qquad S_{kl} = \langle u_k | u_l \rangle . \qquad \text{(C.9)}$$

Solving the eigenvalue problem (C.8) yields a set of wavefunctions $\psi_k(q)$ and expectation values $E_k = E\{\psi_k\}$ $(k = 1, \ldots, N)$ such that

$$E_1 < E_2 < \ldots < E_N . \qquad \text{(C.10)}$$

C.3 Upper bound for the ground state energy

According to the Ritz-Rayleigh theory, the lowest expectation value E_1 is an *upper* bound for the ground state energy $E_1^{(\text{exact})}$:

$$E_1^{(\text{exact})} \leq E_1 . \qquad \text{(C.11)}$$

The upper bound E_1 can be lowered by increasing the size N of the basis set $\{u_k\}$ $(k = 1, \ldots, N)$.

C.4 Upper bounds for energies of excited states

By choosing a basis set *orthogonal* to the *exact* ground state, the Rayleigh-Ritz method can be used to find an upper bound for the energy of the first excited state [187, 236].

Upper bounds for the energies of higher excited states can also be derived. For example, an upper bound for the energy of the second excited state is obtained by choosing the expansion functions orthogonal to the *exact* wavefunctions of both the ground and the first excited state.

We note that the functions ψ_k ($k = 1, \ldots, N$) obtained by solving (C.8) are mutually orthogonal. If ψ_1 is a good approximation to the ground state, one may expect that ψ_2 will be an appproximation to the first excited state and that its associated energy E_2 will be an *upper bound* for the exact energy - although the functions ψ_k ($k = 2, \ldots, N$) are only approximately orthogonal to the exact ground state. The argument can be extended to higher states. By solving (C.8), one generally obtains a set of N_{max} ($N_{\text{max}} < N$) energy levels E_k ($k = 1, \ldots, N_{\text{max}}$), which may be considered as converged and which constitute upper bounds for the true energies.

We wish to point out again that an approximate solution ψ_k ($1 < k \leq N_{\text{max}}$) is not exactly orthogonal to the exact wavefunctions of the lower levels. Therefore, it cannot be ruled out that some of the solutions $\psi_{k'}$ ($k < k' \leq N_{\text{max}}$) are spurious in the sense that their energy does not converge to a lower value when the dimension N of the basis set is increased.

Appendix D

Long-range interactions between three atoms

In this Appendix we derive the asymptotic expressions for the interaction energies of three well-separated atoms using perturbation theory. The internuclear distances are assumed sufficiently large so that the mutual overlap of the electronic orbitals centered on different atoms is negligible. The wavefunctions then need not be antisymmetrized with respect to electrons attached to different nuclei.

D.0.1 Zero-order wavefunction and interaction potential

The electronic coordinates of atoms A, B, and C are denoted 1, 2, and 3, respectively. The correspondig s - orbitals are $\varphi_0^A(1)$, $\varphi_0^B(2)$ and $\varphi_0^C(3)$, with energies are E_0^A, E_0^B, and E_0^C.

The electronic wavefunction of the three separated atoms is the product

$$\varphi^{(0)}(1, 2, 3) \;=\; \varphi_0^A(1)\varphi_0^B(2)\varphi_0^C(3) \;, \tag{D.1}$$

and the total energy of the non-interacting atoms is

$$E^{(0)} \;=\; E_0^A + E_0^B + E_0^C \;. \tag{D.2}$$

Note that we have not anti-symmetrized $\varphi^{(0)}$ with respect to permutations of the electrons, since we only consider the case where the internuclear distances are large compared to the typical size of the atomic orbitals. In fact the multipole expansion of the potential energy operator is not possible for antisymmetrized wavefunctions.

If necessary, the wavefunction can be antisymmetrized in a final step, *after* the perturbative corrections have been performed.

The potential $V^{ABC}(123)$ describing the interaction of the three atoms is the sum of the pair potentials $V^{AB}(12)$, $V^{BC}(23)$ and $V^{CA}(31)$(which each tend to zero with increasing internuclear distance):

$$V(ABC)(123) = V(AB)(12) + V(BC)(23) + V(CA)(31) \qquad \text{(D.3)}$$

The effect of the interaction potential on the energy of the system will be analyzed using perturbation theory. The total energy of the interacting atoms is therefore written as

$$E = E^{(0)} + E^{(1)} + E^{(2)} + E^{(3)} + \dots , \qquad \text{(D.4)}$$

where $E^{(n)}$ is the correction of order n.

Throughout this section, the indices k_1, k_2, k_3 label the electronic states of the atoms A, B, and C, respectively. The two-atom states $|{}^{A}_{k_1}{}^{B}_{k_2}\rangle$, $|{}^{B}_{k_2}{}^{C}_{k_3}\rangle$ and $|{}^{C}_{k_3}{}^{A}_{k_1}\rangle$ correspond to the wavefunctions $|\varphi^A_{k_1}(1)\varphi^B_{k_2}(2)\rangle$, $\varphi^B_{k_2}(2)\varphi^C_{k_3}(3)$ and $\varphi^C_{k_3}(3)\varphi^A_{k_1}(1)$. The three-atom state $|{}^{A}_{k_1}{}^{B}_{k_2}{}^{C}_{k_3}\rangle$ correspond to the wavefunction $\varphi^A_{k_1}(1)\varphi^B_{k_2}(2)\varphi^C_{k_3}(3)$.

D.0.2   First order correction

The first order correction to the energy of the non-degenerate ground state is given by

$$E^{(1)} = \langle {}^{ABC}_{0\,0\,0}|\hat{V}^{AB}_{12} + \hat{V}^{BC}_{23} + \hat{V}^{CA}_{31}|{}^{ABC}_{0\,0\,0}\rangle, \qquad \text{(D.5)}$$

which simplifies as

$$E^{(1)} = \langle {}^{AB}_{0\,0}|\hat{V}^{AB}_{12}|{}^{AB}_{0\,0}\rangle + \langle {}^{BC}_{0\,0}|\hat{V}^{BC}_{23}|{}^{BC}_{0\,0}\rangle + \langle {}^{CA}_{0\,0}|\hat{V}^{CA}_{31}|{}^{CA}_{0\,0}\rangle. \qquad \text{(D.6)}$$

Due to the spherical symmetry of the s-orbitals, the three terms in the sum vanish, so that the first-order correction is zero: $E^{(1)} = 0$, just as in the case of two interacting s-state atoms.

D.0.3   Second order correction

The second order correction is given by

$$E^{(2)} = -\sum_{k_1 k_2 k_3}{}' \left[(E^A_{k_1} + E^B_{k_2} + E^C_{k_3}) - (E^A_0 + E^B_0 + E^C_0)\right]^{-1} \times$$
$$\times \ \langle {}^{ABC}_{0\,0\,0}|\hat{V}^{AB}_{12} + \hat{V}^{BC}_{23} + \hat{V}^{CA}_{31}|{}^{A\ B\ C}_{k_1 k_2 k_3}\rangle \times$$
$$\times \ \langle {}^{A\ B\ C}_{k_1 k_2 k_3}|\hat{V}^{AB}_{12} + \hat{V}^{BC}_{23} + \hat{V}^{CA}_{31}|{}^{ABC}_{0\,0\,0}\rangle. \qquad \text{(D.7)}$$

The symbol $\sum'$ means that the sum includes only the terms with $(k_1, k_2, k_3) \neq (0, 0, 0)$. The sums in the above formula simplify, yielding a pairwise additive

term:

$$
\begin{aligned}
E^{(2)} \;=\; & -\sum_{k_1 k_2}{}' \frac{|\langle {}^{AB}_{0\,0}|\hat{V}^{AB}_{12}|{}^{A\ B}_{k_1 k_2}\rangle|^2}{(E^A_{k_1} + E^B_{k_2}) - (E^A_0 + E^B_0)} \\
& -\sum_{k_2 k_3}{}' \frac{|\langle {}^{BC}_{0\,0}|\hat{V}^{BC}_{23}|{}^{B\ C}_{k_2 k_3}\rangle|^2}{(E^B_{k_1} + E^C_{k_2}) - (E^B_0 + E^C_0)} \\
& -\sum_{k_3 k_1}{}' \frac{|\langle {}^{CA}_{0\,0}|\hat{V}^{CA}_{31}|{}^{A\ B}_{k_3 k_1}\rangle|^2}{(E^C_{k_1} + E^A_{k_2}) - (E^C_0 + E^A_0)}
\end{aligned}
\tag{D.8}
$$

Thus the second order correction is the sum of the asymptotic two-body potentials.

D.0.4 Third order correction

The third order correction in energy[1] is :

$$
\begin{aligned}
E^{(3)} \;=\; & \sum_{\substack{k_1 k_2 k_3 \\ k'_1 k'_2 k'_3}}{}' \left[(E^A_{k_1} + E^B_{k_2} + E^C_{k_3}) - (E^A_0 + E^B_0 + E^C_0) \right]^{-1} \times \\
& \times \left[(E^A_{k'_1} + E^B_{k'_2} + E^C_{k'_3}) - (E^A_0 + E^B_0 + E^C_0) \right]^{-1} \times \\
& \times \langle {}^{ABC}_{0\,0\,0}|\hat{V}^{AB}_{12} + \hat{V}^{BC}_{23} + \hat{V}^{CA}_{31}|{}^{A\ B\ C}_{k_1 k_2 k_3}\rangle \times \\
& \times \langle {}^{A\ B\ C}_{k_1 k_2 k_3}|\hat{V}^{AB}_{12} + \hat{V}^{BC}_{23} + \hat{V}^{CA}_{31}|{}^{A\ B\ C}_{k'_1 k'_2 k'_3}\rangle \times \\
& \times \langle {}^{A\ B\ C}_{k'_1 k'_2 k'_3}|\hat{V}^{AB}_{12} + \hat{V}^{BC}_{23} + \hat{V}^{CA}_{31}|{}^{ABC}_{0\,0\,0}\rangle.
\end{aligned}
\tag{D.9}
$$

The above sum can be decomposed into two- and three-body terms [27]:

$$
E^{(3)} \;=\; E^{(3)}_2 + E^{(3)}_3.
\tag{D.10}
$$

The two-body term is

$$
E^{(3)}_2 \;=\; \sum_{\substack{k_1 k_2 \\ k'_1 k'_2}}{}' \frac{\langle {}^{AB}_{0\,0}|\hat{V}^{AB}_{12}|{}^{A\ B}_{k_1 k_2}\rangle \langle {}^{A\ B}_{k_1 k_2}|\hat{V}^{AB}_{12}|{}^{A\ B}_{k'_1 k'_2}\rangle \langle {}^{A\ B}_{k'_1 k'_2}|\hat{V}^{AB}_{12}|{}^{AB}_{0\,0}\rangle}{(E^A_{k_1} + E^B_{k_2} - E^A_0 - E^B_0)(E^A_{k'_1} + E^B_{k'_2} - E^A_0 - E^B_0)}
$$

---

[1]We are using the formula of Ref. [150] for the third-order correction due to a perturbation $\hat{V}$:

$$
E^{(3)}_n \;=\; \sum_{\substack{km \\ m\neq n, k\neq n, k\neq m}} \frac{V_{nm} V_{mk} V_{kn}}{\hbar^2 \omega_{mn} \omega_{kn}},
$$

with the frequencies $\omega_{mn} = \frac{E^{(0)}_m - E^{(0)}_n}{\hbar}$ and the matrix elements $V_{nm} = \langle {}^{(0)}_n|\hat{V}|{}^{(0)}_m\rangle$ of the perturbation $\hat{V}$.

$$+\sum_{\substack{k_2 k_3 \\ k_2' k_3'}}' \frac{\langle^{BC}_{0\,0}|\hat{V}^{BC}_{23}|^{B\,C}_{k_2 k_3}\rangle\langle^{B\,C}_{k_2 k_3}|\hat{V}^{BC}_{23}|^{B\,C}_{k_2' k_3'}\rangle\langle^{B\,C}_{k_2' k_3'}|\hat{V}^{BC}_{23}|^{BC}_{0\,0}\rangle}{(E^B_{k_2}+E^C_{k_3}-E^B_0-E^C_0)(E^B_{k_2'}+E^C_{k_3'}-E^B_0+E^C_0)}$$

$$+\sum_{\substack{k_3 k_1 \\ k_3' k_1'}}' \frac{\langle^{CA}_{0\,0}|\hat{V}^{CA}_{31}|^{C\,A}_{k_3 k_1}\rangle\langle^{C\,A}_{k_3 k_1}|\hat{V}^{CA}_{31}|^{C\,A}_{k_3' k_1'}\rangle\langle^{C\,A}_{k_3' k_1'}|\hat{V}^{CA}_{31}|^{CA}_{0\,0}\rangle}{(E^C_{k_3}+E^A_{k_1}-E^C_0-E^A_0)(E^C_{k_3'}-E^C_0+E^A_{k_1'}-E^A_0)}.$$

<div align="right">(D.11)</div>

The three-body contribution contains products of matrix elements belonging to different atoms:

$$
\begin{aligned}
E_3^{(3)} \;=\;+\; & \sum_{k_1 k_2 k_3}' \frac{\langle^{AB}_{0\,0}|\hat{V}^{AB}_{12}|^{A\,B}_{k_1 k_2}\rangle\langle^{B\,C}_{k_2 0}|\hat{V}^{BC}_{23}|^{BC}_{0\,k_3}\rangle\langle^{C\,A}_{k_3 k_1}|\hat{V}^{CA}_{31}|^{CA}_{0\,0}\rangle}{(E^A_{k_1}+E^B_{k_2}-E^A_0-E^B_0)(E^C_{k_3}+E^A_{k_1}-E^C_0-E^A_0)} \\[2ex]
& +\sum_{k_1 k_2 k_3}' \frac{\langle^{AB}_{0\,0}|\hat{V}^{AB}_{12}|^{A\,B}_{k_1 k_2}\rangle\langle^{C\,A}_{0\,k_1}|\hat{V}^{CA}_{31}|^{C\,A}_{k_3 0}\rangle\langle^{B\,C}_{k_2 k_3}|\hat{V}^{BC}_{23}|^{BC}_{0\,0}\rangle}{(E^A_{k_1}+E^B_{k_2}-E^A_0-E^B_0)(E^B_{k_2}+E^C_{k_3}-E^B_0-E^C_0)} \\[2ex]
=\;+\; & \sum_{k_2 k_3 k_1}' \frac{\langle^{BC}_{0\,0}|\hat{V}^{BC}_{23}|^{B\,C}_{k_2 k_3}\rangle\langle^{C\,A}_{k_3 0}|\hat{V}^{CA}_{31}|^{CA}_{0\,k_1}\rangle\langle^{A\,B}_{k_1 k_2}|\hat{V}^{AB}_{12}|^{AB}_{0\,0}\rangle}{(E^B_{k_2}+E^C_{k_3}-E^B_0-E^C_0)(E^A_{k_1}+E^B_{k_2}-E^A_0-E^B_0)} \\[2ex]
& +\sum_{k_2 k_3 k_1}' \frac{\langle^{BC}_{0\,0}|\hat{V}^{BC}_{23}|^{B\,C}_{k_2 k_3}\rangle\langle^{AB}_{0\,k_2}|\hat{V}^{AB}_{12}|^{A\,B}_{k_1 0}\rangle\langle^{C\,A}_{k_3 k_1}|\hat{V}^{CA}_{31}|^{CA}_{0\,0}\rangle}{(E^B_{k_2}+E^C_{k_3}-E^B_0-E^C_0)(E^C_{k_3}+E^A_{k_1}-E^C_0-E^A_0)} \\[2ex]
=\;+\; & \sum_{k_2 k_3 k_1}' \frac{\langle^{BC}_{0\,0}|\hat{V}^{BC}_{23}|^{B\,C}_{k_2 k_3}\rangle\langle^{C\,A}_{k_3 0}|\hat{V}^{CA}_{31}|^{CA}_{0\,k_1}\rangle\langle^{A\,B}_{k_1 k_2}|\hat{V}^{AB}_{12}|^{AB}_{0\,0}\rangle}{(E^B_{k_2}+E^C_{k_3}-E^B_0-E^C_0)(E^A_{k_1}+E^B_{k_2}-E^A_0-E^B_0)} \\[2ex]
& +\sum_{k_2 k_3 k_1}' \frac{\langle^{BC}_{0\,0}|\hat{V}^{BC}_{23}|^{B\,C}_{k_2 k_3}\rangle\langle^{AB}_{0\,k_2}|\hat{V}^{AB}_{12}|^{A\,B}_{k_1 0}\rangle\langle^{C\,A}_{k_3 k_1}|\hat{V}^{CA}_{31}|^{CA}_{0\,0}\rangle}{(E^B_{k_2}+E^C_{k_3}-E^B_0-E^C_0)(E^C_{k_3}+E^A_{k_1}-E^C_0-E^A_0)}
\end{aligned}
$$

<div align="right">(D.12)</div>

D.0.5 Multipole expansions of the potentials

The two-body interaction potentials V^{AB}_{12}, V^{BC}_{23} and V^{CA}_{31} in the above formulae can be expanded in multipole series [116, 151]. The second-order and the third-order corrections $E^{(2)}$ and $E^{(3)}$ to the energy are then calculated using the atomic multipole moments associated with the atomic states $\varphi^A_{k_1}(1)$, $\varphi^B_{k_2}(2)$ and $\varphi^A_{k_3}(3)$. The third-order three-body term $E_3^{(3)}$ can thus be written as [27, 66]:

$$E_3^{(3)}(a,b,c) \;=\; \sum_{l_1 l_2 l_3} Z^{ABC}_{l_1 l_2 l_3} W_{l_1 l_2 l_3}(a,b,c) \tag{D.13}$$

where (a,b,c) are the internuclear distances, and l_1, l_2 and l_3 indicate the orders of atomic multipole moments, corresponding to monopoles $(l=0)$,

dipoles ($l = 1$), quadrupole ($l = 2$), octupoles ($l = 3$) and so on. The W functions are geometrical factors depending only on the relative positions of the three nuclei, while the Z constants only depend on the species of atoms A, B and C. Explicit expressions for the Z and W factors can be found in Ref. [27].

Dipole - dipole - dipole interaction

The lowest order contribution to the three-body energy $E_3^{(3)}$ is the dipole-dipole-dipole term [27], first calculated by B. M. Axilrod and E. Teller [15] and Y. Muto [195]:

$$E_3^{(3)}{}_{111}(a, b, c) \;=\; Z_{111}^{ABC} \times 3\frac{1 + 3\cos\alpha\cos\beta\cos\gamma}{a^3 b^3 c^3}, \qquad \text{(D.14)}$$

where α, β and γ are the inner angles of the triangle formed by the atoms A, B and C (note the identity $\alpha + \beta + \gamma = 180°$).

Appendix E

Dispersion coefficients of the pairwise additive potential energy surface

In this Apendix, we define dispersion coefficients for a pairwise additive potential energy surface of a general triatomic system ABC. We consider the situation where the distance R between atom C and the centre of mass of AB is great compared to the distance r between A and B. The potential energy may then be exanded in powers of $1/R$.

The atom - atom potentials are denoted $V^{AB}(c)$, $V^{BC}(a)$ and $V^{CA}(b)$, where a, b, c are the bond lengths. The potentials V^{BC} and V^{CA} are assumed to behave asymptotically as

$$V^{BC}(a) = -\frac{C_6^{B-C}}{a^6} - \frac{C_8^{B-C}}{a^6} \tag{E.1}$$

$$V^{CA}(b) = -\frac{C_6^{C-A}}{b^6} - \frac{C_8^{C-A}}{b^8}. \tag{E.2}$$

In the case where a and b are large, the pairwise additive potential energy

$$V^{AB}(c) + V^{BC}(a) + V^{CA}(b) \tag{E.3}$$

may therefore be written as

$$V = -\frac{C_6^{B-C}}{a^6} - \frac{C_8^{B-C}}{a^6} - \frac{C_6^{C-A}}{b^6} - \frac{C_8^{C-A}}{b^8} + V^{AB}(c), \tag{E.4}$$

with all powers of a and b of order higher than 8 neglected. By expressing the bond lengths a and b in terms of the internal Jacobi coordinates r, R

and η, the potential energy takes the form [1]

$$V(r, R, \eta) = V^{AB}(r) - \frac{C_6^{B-C}}{\left[R^2 + \left(\frac{m_A r}{m_A + m_B}\right)^2 - 2R\frac{m_A r}{m_A + m_B}\cos\eta\right]^3}$$

$$- \frac{C_8^{B-C}}{\left[R^2 + \left(\frac{m_A r}{m_A + m_B}\right)^2 - 2R\frac{m_A r}{m_A + m_B}\cos\eta\right]^4}$$

$$- \frac{C_6^{C-A}}{\left[R^2 + \left(\frac{m_B r}{m_A + m_B}\right)^2 + 2R\frac{m_B r}{m_A + m_B}\cos\eta\right]^3}$$

$$- \frac{C_8^{C-A}}{\left[R^2 + \left(\frac{m_B r}{m_A + m_B}\right)^2 + 2R\frac{m_B r}{m_A + m_B}\cos\eta\right]^4}$$

$$(E.5)$$

In the situation where atoms A and B are close together and atom C is far from the complex AB, the distance c is small compared to both a and b. The potential energy may then be expanded in powers of $\frac{r}{R}$, with r and η fixed. The eigth-order result is

$$V(r, R, \eta) = V^{AB}(r) - \frac{C_6^{AB-C}}{R^6} - \frac{C_7^{AB-C}(r, \eta)}{R^7} - \frac{C_8^{AB-C}(r, \eta)}{R^8} \quad (R >> r),$$

$$(E.6)$$

where the atom-molecule multipole coefficients C_6^{AB-C} and C_8^{AB-C} for fixed distance r and fixed angle η and without three-body contribution are given by

$$C_6^{AB-C} = C_6^{B-C} + C_6^{C-A} \tag{E.7}$$

$$C_7^{AB-C} = -6\cos\eta\, C_6^{B-C}\frac{m_A r}{m_A + m_B}$$
$$+ 6\cos\eta\, C_6^{C-A}\frac{m_B r}{m_A + m_B} \tag{E.8}$$

$$C_8^{AB-C} = C_8^{B-C} + 3(8\cos^2\eta - 1)C_6^{B-C}\left(\frac{m_A r}{m_A + m_B}\right)^2$$
$$+ C_8^{C-A} + 3(8\cos^2\eta - 1)C_6^{C-A}\left(\frac{m_B r}{m_A + m_B}\right)^2. \tag{E.9}$$

Thus the atom - molecule van der Waals coefficient C_6^{AB-C} deduced from the pairwise additive PES is simply the sum of the atom - atom coefficients C_6^{B-C}

---

[1] The Jacobi length r and the bond length c are identical. However, when we use Jacobi coordinates, we rather write r instead of c.

and C_6^{C-A}. The coefficients C_7^{AB-C} and C_8^{AB-C} depend on the orientation of the internuclear axis joining A and B with respect to the position of atom C.

If the atoms A and B are identical, the atom - molecule dispersion coefficients of the pairwise additive PES are given by

$$C_6^{A_2-C} = 2C_6 \tag{E.10}$$

$$C_7^{A_2-C} = 0 \tag{E.11}$$

$$C_8^{A_2-C} = 2C_8 + \frac{3r^2C_6}{2}(8\cos^2\eta - 1) \tag{E.12}$$

where $C_6 \equiv C_6^{B-C} = C_6^{C-A}$ and $C_8 \equiv C_8^{B-C} = C_8^{C-A}$ denote the atom - atom dispersion coefficients.

Appendix F

Kinetic energy operator in curvilinear coordinates

The general expression of the Schrödinger equation in non-cartesian coordinates was derived by Boris Podolsky [216]. The form of the Laplacian in curvilinear coordinates was further discussed by H. Essen [77] and L. J. Schaad [234].

Podolsky's formula is the starting point for various partitioned-matrix methods, which were developed to separate rotational from vibrational contributions to the kinetic energy. In this Appendix, we re-derive Podolsky's expression for the kinetic energy operator. Next we present a partitioned-matrix method in its general form and finally apply it to Smith-Whitten coordinates.

F.1 Laplacian in curvilinear coordinates

Using mass-scaled Jacobi coordinates, the kinetic energy operator of an N-body system has the form of the Laplacian operator in $f = 3N$ dimensions, which is multiplied by $-\hbar^2/(2\mu)$, μ being the N-body reduced mass. Its form in arbitrary coordinates can be obtained using the chain rule of differentiation. However, the calculations usually become very tedious. It is more convenient to transform the Laplacian using tensor analysis. The resulting expression for the kinetic energy operator is known as Podolsky's formula [216]. It can be derived as follows.

We consider a tranformation between the coordinates q^i and an alternative set of coordinates $\bar{q}^i$ $(i = 1, ..., f)$. By definition, the quantities A_{kl}^{ij} form the components of a relative tensor of weight w if they transform as

$$\bar{A}_{kl}^{ij} = \frac{\partial \bar{q}^i}{\partial q^\alpha} \frac{\partial \bar{q}^j}{\partial q^\beta} \frac{\partial q^\gamma}{\partial \bar{q}^k} \frac{\partial q^\delta}{\partial \bar{q}^l} A_{\gamma\delta}^{\alpha\beta} \left| \frac{\partial q}{\partial \bar{q}} \right|^w . \tag{F.1}$$

The determinant $\left|\frac{\partial q}{\partial \bar{q}}\right|$ in the above equation is called the Jacobian of the coordinate transformation [187]. The metric tensor associated with the coordinates q^i is denoted g_{ij}. Its inverse is g^{ij}:

$$g^{ij}g_{jk} = \delta_{ik} . \tag{F.2}$$

It can be shown that the square root of the determinant of the metric tensor is a relative scalar of weight 1,

$$\sqrt{|\bar{g}|} = \left|\frac{\partial q}{\partial \bar{q}}\right| \sqrt{|g|} . \tag{F.3}$$

The weight of a relative tensor by increased by $+1$ by multiplying it with $\sqrt{|\bar{g}|}$. One can show that the divergence of a relative vector R^i of weight 1,

$$\text{div}R = \frac{\partial R^i}{\partial q^i}, \tag{F.4}$$

is a relative scalar of weight 1.

The wavefunction ψ is a scalar because its value at an arbitrary point in space does not depend on the choice of coordinates. The quantities

$$R_i = |g|^{1/2}\frac{\partial \psi}{\partial q^i} \tag{F.5}$$

form a relative covariant vector of weight 1. It can be shown that its divergence,

$$\text{div}R = \frac{\partial R^i}{\partial q^i} = \frac{\partial}{\partial q^i}|g|^{1/2}g^{ij}\frac{\partial \psi}{\partial q^j} , \tag{F.6}$$

is a relative scalar of weight 1. Therefore

$$|g|^{-1/2}\text{div}R = |g|^{-1/2}\frac{\partial}{\partial q^i}|g|^{1/2}g^{ij}\frac{\partial \psi}{\partial q^j} \tag{F.7}$$

is a scalar. We have thus obtained the following transformation law:

$$|\bar{g}|^{-1/2}\frac{\partial}{\partial \bar{q}^i}|\bar{g}|^{1/2}\bar{g}^{ij}\frac{\partial \psi}{\partial \bar{q}^j} = |g|^{-1/2}\frac{\partial}{\partial q^i}|g|^{1/2}g^{ij}\frac{\partial \psi}{\partial q^j} . \tag{F.8}$$

Let now the $\bar{q}^i$ be Cartesian coordinates ($\bar{q}^i = x^i$) with metric tensor $\bar{g}_{ij} = \delta_{ij}$ (the identity matrix). Then the above equation becomes:

$$\Delta\psi = \frac{\partial}{\partial x^i}\delta^{ij}\frac{\partial \psi}{\partial x^j} = |g|^{-1/2}\frac{\partial}{\partial q^i}|g|^{1/2}g^{ij}\frac{\partial \psi}{\partial q^j} . \tag{F.9}$$

The kinetic energy operator thus takes the form:

$$\hat{T}\psi = -\frac{\hbar^2}{2\mu}\sum_{i,j=1}^{f}|g|^{-1/2}\frac{\partial}{\partial q^i}|g|^{1/2}g^{ij}\frac{\partial \psi}{\partial q^j} . \tag{F.10}$$

This is the result derived by B. Podolsky's [216].

214

F.2 Partitioned matrix method

In the centre-of-mass frame, the system of N particles is described by $3N-3$ coordinates. In an attempt to separate rotational from vibrational motion, one may split these coordinates into $3N-6$ vibrational coordinates describing the relative positions of the particles and 3 Euler angles indicating the orientation of a body-fixed system of axis with respect to space-fixed axis.

A widely used procedure for deriving vibrational Hamiltonians is Wilson's G-matrix method [277]. In an extended version [177] it accounts also for the rotational motion associated with the Euler angles. Rotational-vibrational Hamiltonians are also discussed in Refs. [214, 41, 264, 88].

The method outlined below follows Johnson's method [124], which in turn is similar to the partitioned matrix procedure by X. Chapuisat *et al.* [50]. In contrast to Johnson, we first outline the general approach, and apply it to Smith-Whitten coordinates later (see Sec. F.3). While formula (26) of Ref. [124] seems to be specific to Smith-Whitten coordinates, our resulting expression, Eq. (F.23), is quite general.

The coordinates are collectively denoted q^i $(i = 1, .., 3N-3)$. Their conjugated momentum operators are

$$\hat{p}_i = -i\hbar \frac{\partial}{\partial q^i} . \tag{F.11}$$

Later we will need the matrix of operators $\hat{\mathbf{p}}^T = (\hat{p}_1, ..., \hat{p}_{3N-3})$. The elements g_{ij} of the metric tensor are arranged in the matrix $\mathbf{g}$. Following Ref. [124], we partition it into four blocks,

$$\mathbf{g} = \begin{pmatrix} \mathbf{G} & \mathbf{C} \\ \mathbf{C}^T & \mathbf{K} \end{pmatrix} , \tag{F.12}$$

in such a way that $\mathbf{G}$ and $\mathbf{K}$ are associated with vibrational and rotational coordinates, respectively. $\mathbf{G}$ and $\mathbf{K}$ are of dimensions $(3N-6) \times (3N-6)$ and 3×3, respectively. The off-diagonal blocks $\mathbf{C}$ and $\mathbf{C}^T$ are linked to Coriolis coupling between the vibrational and rotational degrees of freedom. In the following we will need the matrix

$$\mathbf{U} = (\mathbf{K} - \mathbf{C}^T \mathbf{G}^{-1} \mathbf{C})^{-1} . \tag{F.13}$$

We note that the metric tensor can be written as the product

$$\mathbf{g} = \begin{pmatrix} \mathbf{1} & \mathbf{0} \\ \mathbf{C}^T \mathbf{G}^{-1} & \mathbf{U}^{-1} \end{pmatrix} \begin{pmatrix} \mathbf{G} & \mathbf{C} \\ \mathbf{0} & \mathbf{1} \end{pmatrix} , \tag{F.14}$$

and its determinant is therefore

$$|g| = \begin{vmatrix} \mathbf{1} & \mathbf{0} \\ \mathbf{C}^T \mathbf{G}^{-1} & \mathbf{U}^{-1} \end{vmatrix} \begin{vmatrix} \mathbf{G} & \mathbf{C} \\ \mathbf{0} & \mathbf{1} \end{vmatrix} = \frac{|G|}{|U|} . \tag{F.15}$$

The inverse of the metric tensor is

$$\mathbf{g}^{-1} = \begin{pmatrix} \mathbf{G}^{-1} + \mathbf{G}^{-1}\mathbf{C}\mathbf{U}\mathbf{C}^T\mathbf{G}^{-1} & -\mathbf{G}^{-1}\mathbf{C}\mathbf{U} \\ -\mathbf{U}\mathbf{C}^T\mathbf{G}^{-1} & \mathbf{U} \end{pmatrix} , \tag{F.16}$$

which can be verified by direct multiplication. Using matrix notation, the kinetic energy operator (F.10) takes the form

$$2\mu\hat{T} = |g|^{-1/2}\hat{\mathbf{p}}^T|g|^{1/2}\mathbf{g}^{-1}\hat{\mathbf{p}} . \tag{F.17}$$

Using the product rule for differentiation,

$$\hat{\mathbf{p}}|g|^{1/2} = \frac{1}{2}|g|^{-1/2}(\hat{\mathbf{p}}|g|) + |g|^{1/2}\hat{\mathbf{p}} , \tag{F.18}$$

the kinetic energy operator can be written as

$$2\mu\hat{T} = (\mathbf{p}' + \hat{\mathbf{p}})^T\mathbf{g}^{-1}\hat{\mathbf{p}} , \tag{F.19}$$

where the column vector $\mathbf{p}'$ is defined as

$$\mathbf{p}' = \frac{1}{2|g|}(\hat{\mathbf{p}}|g|) . \tag{F.20}$$

The entries of $\mathbf{p}'$ are not operators but numbers: the operator $\hat{\mathbf{p}}$ in the above expression is understood to act only on $|g|$ but not on any symbols that could be written to the right of the closing bracket). The column vectors $\hat{\mathbf{p}}$ and $\mathbf{p}'$ are split into vibrational and rotational parts:

$$\hat{\mathbf{p}} = \begin{pmatrix} \hat{\mathbf{P}} \\ \hat{\mathbf{J}} \end{pmatrix} , \qquad \mathbf{p}' = \begin{pmatrix} \mathbf{P}' \\ \mathbf{J}' \end{pmatrix} . \tag{F.21}$$

In the general treatment of this section, $\hat{\mathbf{J}}$ is not necessarily the angular momentum vector. However it is closely related, since the components of the matrix $\hat{\mathbf{J}}$ generate infinitesimal changes in the orientation coordinates (for example, in the Euler angles). Using the above definitions, Eq. (F.19) becomes

$$2\mu\hat{T} = \begin{pmatrix} \hat{\mathbf{P}} + \mathbf{P}' \\ \hat{\mathbf{J}} + \mathbf{J}' \end{pmatrix}^T \begin{pmatrix} \mathbf{G}^{-1} + \mathbf{G}^{-1}\mathbf{C}\mathbf{U}\mathbf{C}^T\mathbf{G}^{-1} & -\mathbf{G}^{-1}\mathbf{C}\mathbf{U} \\ -\mathbf{U}\mathbf{C}^T\mathbf{G}^{-1} & \mathbf{U} \end{pmatrix} \begin{pmatrix} \hat{\mathbf{P}} \\ \hat{\mathbf{J}} \end{pmatrix} , \tag{F.22}$$

which can be rewritten as

$$\boxed{\begin{aligned} 2\mu\hat{T} = {} & (\hat{\mathbf{P}} + \mathbf{P}')^T\mathbf{G}^{-1}\hat{\mathbf{P}} \\ & + \left[(\hat{\mathbf{P}} + \mathbf{P}')^T + (\hat{\mathbf{J}} + \mathbf{J}')^T\mathbf{G}^{-1}\mathbf{C}\right]\mathbf{U}\left(\hat{\mathbf{J}} - \mathbf{C}^T\mathbf{G}^{-1}\hat{\mathbf{P}}\right) . \end{aligned}}$$
$$\tag{F.23}$$

Remark: Eq. (F.23) has been derived by separating the coordinates into vibrational and rotational ones. However, Eq. (F.23) is valid for *any* coordinates that are divided into two sets.

F.3 Kinetic energy operator in Smith-Whitten coordinates

In order to derive the kinetic energy operator in Smith-Whitten coordinates, we first calculate the metric tensor g_{ij}. Since g_{ij} can depend only on the relative positions of the three particles but not on the Euler angles (α, β, γ), it may be derived by choosing as coordinates $(\rho, \Theta, \Phi, \Omega_x, \Omega_y, \Omega_z)$ where $(\Omega_x, \Omega_y, \Omega_z)$ are the Cartesian components of an infinitesimal rotation vector $\mathbf{\Omega}$. The space-fixed mass-weighted Jacobi vectors $\bar{\mathbf{r}}'$ and $\bar{\mathbf{R}}'$ are then obtained from $(\rho, \Theta, \Phi, \Omega_x, \Omega_y, \Omega_z)$ using

$$\bar{\mathbf{r}}' = \bar{\mathbf{r}} + \mathbf{\Omega} \times \bar{\mathbf{r}} \tag{F.24}$$
$$\bar{\mathbf{R}}' = \bar{\mathbf{R}} + \mathbf{\Omega} \times \bar{\mathbf{R}} . \tag{F.25}$$

where $\bar{\mathbf{r}}$ and $\bar{\mathbf{R}}$ are the mass-weighted Jacobi vectors.

Using an abbreviated notation, $\mathrm{ss} \equiv \sin \Theta \sin \Phi$, $\mathrm{sc} \equiv \sin \Theta \cos \Phi$, $\mathrm{cs} \equiv \cos \Theta \sin \Phi$, and $\mathrm{cc} \equiv \cos \Theta \cos \Phi$, we have:

$$
\begin{pmatrix} \bar{r}'_x \\ \bar{r}'_y \\ \bar{r}'_z \\ \bar{R}'_x \\ \bar{R}'_y \\ \bar{R}'_z \end{pmatrix}
= \rho \begin{pmatrix} \mathrm{cc} \\ -\mathrm{ss} \\ 0 \\ \mathrm{cs} \\ \mathrm{sc} \\ 0 \end{pmatrix}
+ \rho \begin{pmatrix} \Omega_z \mathrm{ss} \\ \Omega_z \mathrm{cc} \\ -\Omega_x \mathrm{ss} - \Omega_y \mathrm{cc} \\ -\Omega_z \mathrm{sc} \\ \Omega_z \mathrm{cs} \\ \Omega_x \mathrm{sc} - \Omega_y cs \end{pmatrix} ,
\tag{F.26}
$$

The Jacobian

$$
\begin{pmatrix}
\partial \bar{r}'_x/\partial \rho & \partial \bar{r}'_x/\partial \Theta & \partial \bar{r}'_x/\partial \Phi & \partial \bar{r}'_x/\partial \Omega_x & \partial \bar{r}'_x/\partial \Omega_y & \partial \bar{r}'_x/\partial \Omega_z \\
\partial \bar{r}'_y/\partial \rho & \partial \bar{r}'_y/\partial \Theta & \partial \bar{r}'_y/\partial \Phi & \partial \bar{r}'_y/\partial \Omega_x & \partial \bar{r}'_y/\partial \Omega_y & \partial \bar{r}'_y/\partial \Omega_z \\
\partial \bar{r}'_z/\partial \rho & \partial \bar{r}'_z/\partial \Theta & \partial \bar{r}'_z/\partial \Phi & \partial \bar{r}'_z/\partial \Omega_x & \partial \bar{r}'_z/\partial \Omega_y & \partial \bar{r}'_z/\partial \Omega_z \\
\partial \bar{R}'_x/\partial \rho & \partial \bar{R}'_x/\partial \Theta & \partial \bar{R}'_x/\partial \Phi & \partial \bar{R}'_x/\partial \Omega_x & \partial \bar{R}'_x/\partial \Omega_y & \partial \bar{R}'_x/\partial \Omega_z \\
\partial \bar{R}'_y/\partial \rho & \partial \bar{R}'_y/\partial \Theta & \partial \bar{R}'_y/\partial \Phi & \partial \bar{R}'_y/\partial \Omega_x & \partial \bar{R}'_y/\partial \Omega_y & \partial \bar{R}'_y/\partial \Omega_z \\
\partial \bar{R}'_z/\partial \rho & \partial \bar{R}'_z/\partial \Theta & \partial \bar{R}'_z/\partial \Phi & \partial \bar{R}'_z/\partial \Omega_x & \partial \bar{R}'_z/\partial \Omega_y & \partial \bar{R}'_z/\partial \Omega_z
\end{pmatrix}
$$

is easily evaluated. The result for $(\Omega_x, \Omega_y, \Omega_z) = (0, 0, 0)$ is [1]

$$
\begin{pmatrix}
\mathrm{cc} & -\mathrm{sc} & -\mathrm{cs} & 0 & 0 & \mathrm{ss} \\
-\mathrm{ss} & -\mathrm{cs} & -\mathrm{sc} & 0 & 0 & \mathrm{cc} \\
0 & 0 & 0 & -\mathrm{ss} & -\mathrm{cc} & 0 \\
\mathrm{cs} & -\mathrm{ss} & \mathrm{cc} & 0 & 0 & -\mathrm{sc} \\
\mathrm{sc} & \mathrm{cc} & -\mathrm{ss} & 0 & 0 & \mathrm{cs} \\
0 & 0 & 0 & \mathrm{sc} & -\mathrm{cs} & 0
\end{pmatrix}
\begin{pmatrix} 1 \\ \rho \\ \rho \\ \rho \\ \rho \\ \rho \end{pmatrix} .
\tag{F.27}
$$

---

[1] It seems that Eq. (19) of Ref. [123] contains three errors.

From Eq. (F.27), we can evaluate the metric tensor $\mathbf{g}$. Following Johnson [123], we transform the result from the Smith-Whitten angular coordinates Θ and Φ to the modified angular coordinates

$$
\begin{aligned}
\theta &= \frac{\pi}{2} - 2\Theta \ , \\
\phi &= \frac{\pi}{2} - 2\Phi \ .
\end{aligned}
\tag{F.28}
$$

The conjugated momentum operators are

$$
\hat{\mathbf{P}} = \begin{pmatrix} \hat{p}_\rho \\ \hat{p}_\theta \\ \hat{p}_\phi \end{pmatrix} = -i\hbar \begin{pmatrix} \partial/\partial\rho \\ \partial/\partial\theta \\ \partial/\partial\phi \end{pmatrix}
\tag{F.29}
$$

and

$$
\hat{\mathbf{J}} = \begin{pmatrix} \hat{J}_x \\ \hat{J}_y \\ \hat{J}_z \end{pmatrix} = -i\hbar \begin{pmatrix} \partial/\partial\Omega_x \\ \partial/\partial\Omega_y \\ \partial/\partial\Omega_z \end{pmatrix} \ .
\tag{F.30}
$$

The operators $(\hat{J}_x, \hat{J}_y, \hat{J}_z)$ in the above expression are the body-frame components of the angular momentum operator $\hat{\mathbf{J}}$, because they generate infinitesimal rotations of the wavefunction around the body-fixed x-, y- and z-axis, respectively. They can easily be expressed in terms of the Euler angles (α, β, γ) and the operators $\partial/\partial\alpha$, $\partial/\partial\beta$ and $\partial/\partial\gamma$. The details can be found in Ref. [123, 124]

The final expression for the metric tensor is

$$
\mathbf{g} = \left(\begin{array}{ccc|ccc}
1 & 0 & 0 & 0 & 0 & 0 \\
0 & \frac{\rho^2}{4} & 0 & 0 & 0 & 0 \\
0 & 0 & \frac{\rho^2}{4} & 0 & 0 & \frac{\rho^2}{2}\cos(\theta) \\
\hline
0 & 0 & 0 & \frac{I_x}{\mu} & 0 & 0 \\
0 & 0 & 0 & 0 & \frac{I_y}{\mu} & 0 \\
0 & 0 & \frac{\rho^2}{2}\cos(\theta) & 0 & 0 & \frac{I_z}{\mu}
\end{array} \right) \ ,
\tag{F.31}
$$

where I_x, I_y and I_z are the principal moments of inertia. The $\mathbf{g}$ matrix (F.31) has been split into four blocks, as in Eq. (F.12). They are:

$$
\mathbf{G} = \begin{pmatrix} 1 & 0 & 0 \\ 0 & \rho^2/4 & 0 \\ 0 & 0 & \rho^2/4 \end{pmatrix} \ , \qquad \mathbf{K} = \frac{1}{\mu} \begin{pmatrix} I_x & 0 & 0 \\ 0 & I_y & 0 \\ 0 & 0 & I_z \end{pmatrix} \ ,
\tag{F.32}
$$

and

$$
\mathbf{C} = \frac{\rho^2}{2}\cos(\theta) \begin{pmatrix} 0 & 0 & 0 \\ 0 & 0 & 0 \\ 0 & 0 & 1 \end{pmatrix} \ .
\tag{F.33}
$$

The matrix $\mathbf{U}$ defined in Eq. (F.13) is:

$$
\mathbf{U} = \mu \begin{pmatrix} I_x & 0 & 0 \\ 0 & I_y & 0 \\ 0 & 0 & I_z \sin^2\theta \end{pmatrix}^{-1} = \frac{1}{\rho^2} \begin{pmatrix} \frac{2}{1-\sin\theta} & 0 & 0 \\ 0 & \frac{2}{1+\sin\theta} & 0 \\ 0 & 0 & \frac{1}{\sin^2\theta} \end{pmatrix} . \tag{F.34}
$$

The determinants of $\mathbf{G}$ and $\mathbf{U}$ are:

$$
|G| = \frac{\rho^4}{16}, \qquad |U| = \frac{4}{\rho^6 \sin^2\theta \cos^2\theta} . \tag{F.35}
$$

The determinant of the metric tensor is

$$
|g| = \frac{|G|}{|U|} = \frac{\rho^{10} \sin^2\theta \cos^2\theta}{64} . \tag{F.36}
$$

The quantities $\mathbf{P}'$ and $\mathbf{J}'$ of Eq. (F.21) are easily evaluated:

$$
\mathbf{P}' = -i\hbar \begin{pmatrix} 5/\rho \\ 2\cot(2\theta) \\ 0 \end{pmatrix} , \qquad \mathbf{J}' = \begin{pmatrix} 0 \\ 0 \\ 0 \end{pmatrix} \tag{F.37}
$$

The operators $\mathbf{C}^T \mathbf{G}^{-1} \hat{\mathbf{P}}$ and $(\hat{\mathbf{P}} + \mathbf{P}')^T \mathbf{G}^{-1} \mathbf{C}$ are also found easily:

$$
\mathbf{C}^T \mathbf{G}^{-1} \hat{\mathbf{P}} = -2i\hbar \cos\theta \begin{pmatrix} 0 \\ 0 \\ \partial/\partial\phi \end{pmatrix} ,
$$

$$
(\hat{\mathbf{P}} + \mathbf{P}')^T \mathbf{G}^{-1} \mathbf{C} = -2i\hbar \cos\theta \, (0, 0, \partial/\partial\phi) . \tag{F.38}
$$

By substituting Eqs. (F.29), (F.30), (F.37) and (F.38) into the general expression (F.23), we obtain the final result: [2]

$$
\begin{aligned}
\hat{T} = & -\frac{\hbar^2}{2\mu} \left[\frac{1}{\rho^5} \frac{\partial}{\partial\rho} \rho^5 \frac{\partial}{\partial\rho} + \frac{4}{\rho^2} \frac{1}{\sin(2\theta)} \frac{\partial}{\partial\theta} \sin(2\theta) \frac{\partial}{\partial\theta} + \frac{4}{\rho^2} \frac{1}{\cos^2(\theta)} \frac{\partial^2}{\partial\phi^2} \right] \\
& + \frac{\hbar^2}{\mu\rho^2} \left[\frac{1}{1-\sin(\theta)} \left(\frac{\hat{J}_x}{i\hbar} \right)^2 + \frac{1}{1+\sin(\theta)} \left(\frac{\hat{J}_y}{i\hbar} \right)^2 + \frac{1}{2\sin^2(\theta)} \left(\frac{\hat{J}_z}{i\hbar} \right)^2 \right] \\
& + 2 \frac{i\hbar}{\mu\rho^2} \frac{\cos(\theta)}{\sin^2(\theta)} \hat{J}_z \frac{\partial}{\partial\phi} .
\end{aligned} \tag{F.39}
$$

The kinetic energy operator (F.39) is a sum of vibrational, rotational and Coriolis terms:

$$
\hat{T} = \hat{T}_{\text{vib}} + \hat{T}_{\text{rot}} + \hat{T}_{\text{cor}} . \tag{F.40}
$$

---

[2]The following formulas are used:

$$
\frac{\partial^2}{\partial\rho^2} + \frac{5}{\rho} \frac{\partial}{\partial\rho} = \frac{1}{\rho^5} \frac{\partial}{\partial\rho} \rho^5 \frac{\partial}{\partial\rho}
$$

$$
\frac{\partial^2}{\partial\theta^2} + 2\cot(2\theta) \frac{\partial}{\partial\theta} = \frac{1}{\sin(2\theta)} \frac{\partial}{\partial\theta} \sin(2\theta) \frac{\partial}{\partial\theta}
$$

The rotational energy term in Eq. (F.39),

$$\hat{T}_{\text{rot}} \;=\; \frac{1}{2}\left(\frac{\hat{J}_x^2}{I_x} + \frac{\hat{J}_y^2}{I_y} + \frac{\hat{J}_z^2}{I_z \sin\theta}\right) \tag{F.41}$$

is the Hamiltonian not of a rigid but of a *fluid* rotator [41] (it differs from the rigid rotator Hamiltonian in the factor $1/\sin\theta$ associated with $\hat{J}_z^2$).

Appendix G

Rotations of a rigid body

This Appendix summarizes the quantum theory of a rotating rigid body. We define the three Euler angles, the angular momentum operator and the Hamiltonian. We show that the Wigner D-functions, defined as matrix elements of the operator of finite rotations, are eigenfunctions of a symmetric top.

The following discussion excludes cylindrically symmetric bodies, such as linear molecules, since these bodies have only two rotational degrees of freedom. Linear molecules are briefly discussed in Sec. G.5.

G.1 Euler angles

In order to indicate the orientation of a rigid body with respect to a *space-fixed* Cartesian coordinate system xyz, we introduce a *body-fixed* system $\xi\eta\zeta$, which is attached to the body and performs the same rotations as the body. We shall regard the xyz-axes as non-rotated and the $\xi\eta\zeta$-axes as rotated, and we shall always reason in terms of *active* rotations (of a rigid body, of a wavefunction, of a coordinate axis).

An arbitrary orientation of the $\xi\eta\zeta$-system can be achieved by three successive rotations about different coordinate axis. Conventionally, these are made by [187]

1. Rotating xyz by angle α ($0 \leq \alpha < 2\pi$) about the z-axis to give $x'y'z'$.

2. Rotating $x'y'z'$ by angle β ($0 \leq \alpha < \pi$) about the y'-axis to give $x''y''z''$.

3. Rotating $x''y''z''$ by angle γ ($0 \leq \gamma < 2\pi$) about the z''-axis to give $\xi\eta\zeta$.

Note that some of the axis coincide: $z = z'$, $z'' = \zeta$, and $y' = y''$. The y'-axis is called the *nodal line*. The three angles (α, β, γ) are called *Euler angles*.

We call an arbitrary axis **n** *space-fixed* if it remains fixed to the xyz coordinates as the Euler angles are varied. For each space-fixed axis **n**,

a *body-fixed axis* $\mathbf{n}^{\mathrm{BF}}$ is obtained by rotating $\mathbf{n}$ through the Euler angles (α, β, γ). The orientation of $\mathbf{n}^{\mathrm{BF}}$ relative to the $\xi\eta\zeta$-axes is thus the same as the direction of $\mathbf{n}$ relative to the xyz-axes.

G.2 Rigid body

In quantum mechanics, the rotational motion of a rigid body is described by a wavefunction $\varphi(\alpha, \beta, \gamma)$, the arguments of which are the three Euler angles. The wavefunction is normalized as follows [150]:

$$\int_0^{2\pi} d\alpha \int_0^{\pi} d\beta \int_0^{2\pi} d\gamma \, \sin\beta \, |\varphi(\alpha, \beta, \gamma)|^2 \;=\; 1 \; . \tag{G.1}$$

The quantity $d\alpha \, d\beta \, d\gamma \, \sin\beta \, |\varphi(\alpha, \beta, \gamma)|^2$ is interpreted as the probability that the Euler angles relating the xyz- and the $\xi\eta\zeta$-axes are (α, β, γ), with uncertainty $d\alpha \, d\beta \, d\gamma$.

In the following we shall assume that the $\xi\eta\zeta$-axes are the principal axis of inertia of the body.

G.2.1 Angular momentum operator $\hat{\mathbf{J}}$

The angular momentum operator of the rigid body is denoted $\hat{\mathbf{J}}$. Its Cartesian components $\hat{J}_x$, $\hat{J}_y$ and $\hat{J}_z$ generate infinitesimal rotations of any function of the Euler angles about the x-, y-, and z-axis, respectively. They may be written as differential operators in the Euler angles [150], but these expressions are not needed here. An infinitesimal rotation of a function $\varphi(\alpha, \beta, \gamma)$ about an axis $\mathbf{u}$ can be written as follows:

$$(1 - \mathrm{i}\Omega\mathbf{u}.\hat{\mathbf{J}}/\hbar) \, \varphi(\alpha, \beta, \gamma) \;=\; \varphi(\tilde{\alpha}, \tilde{\beta}, \tilde{\gamma}) \; . \tag{G.2}$$

In the above equation, (α, β, γ) and $(\tilde{\alpha}, \tilde{\beta}, \tilde{\gamma})$ are the Euler angles describing the orientation of the $\xi\eta\zeta$-axes with respect to the xyz-axes before and after the infinitesimal rotation about $\mathbf{u}$, respectively.

The space-fixed and the body-fixed projections of $\hat{\mathbf{J}}$ commute [150]:

$$[\mathbf{n}.\hat{\mathbf{J}}, \mathbf{n}^{\mathrm{BF}}.\hat{\mathbf{J}}] \;=\; 0 \; . \tag{G.3}$$

This translates the fact that a rotation of the body about a body-fixed axis $\mathbf{n}^{\mathrm{BF}}$ commutes with a rotation about the corresponding space-fixed axis. Note that the body fixed-projections $\hat{J}_\xi$, $\hat{J}_\eta$, and $\hat{J}_\zeta$ verify anormal commutation relations [150].

G.2.2 Hamiltonian

The rotational Hamiltonian of a rigid body with principal moments of inertia I_A, I_B, and I_C and principal axis $\xi\eta\zeta$ has the form [150]:

$$\hat{H}_{\text{rot}} = \frac{1}{2}\left(\frac{\hat{J}_\xi^2}{I_A} + \frac{\hat{J}_\eta^2}{I_B} + \frac{\hat{J}_\zeta^2}{I_C}\right) . \tag{G.4}$$

Spherical top

The principal moments of inertia of a spherical top are all equal: $I_A = I_B = I_C \equiv I$. The Hamiltonian and its energy levels are thus given by

$$\hat{H}_{\text{rot}} = \frac{\hat{\mathbf{J}}^2}{2I} , \tag{G.5}$$

$$\hat{E}_j^{(\text{rot})} = \frac{\hbar^2 j(j+1)}{2I} . \tag{G.6}$$

Its eigenfunctions are the symmetric top wavefunctions (G.30).

Symmetric top

In the case where two principal moments are equal ($I_A = I_B \neq I_C$), the Hamiltonian (G.4) is rewritten as

$$\hat{H}_{\text{rot}} = \frac{\hat{\mathbf{J}}^2}{2I_A} + \frac{1}{2}\left(\frac{1}{I_C} - \frac{1}{I_A}\right)\hat{J}_\zeta^2 , \tag{G.7}$$

which means that its energy levels are given by

$$E_{jk}^{(\text{rot})} = \frac{\hbar^2 j(j+1)}{2I_A} + \frac{\hbar^2}{2}\left(\frac{1}{I_C} - \frac{1}{I_A}\right)k^2 . \tag{G.8}$$

Its eigenfunctions, the symmetric top wavefunctions, are given in Eq. (G.30).

Asymmetric top

If the three principal moments all differ ($I_A \neq I_B \neq I_C \neq I_A$), the eigenvalues and eigenfunctions of the Hamiltonian (G.4) are not known analytically. However, the eigenfunctions can be expanded in symmetric top functions [212, 150]:

$$\varphi_{jm}(\alpha, \beta, \gamma) = \sum_{k=-j}^{j} \varphi_{jmk}^{(\text{symtop})}(\alpha, \beta, \gamma)\, C_{jmk} . \tag{G.9}$$

The Hamiltonian (G.4) is thus represented by a Hermitian matrix, and its eigenvalues and eigenfunctions $\varphi_{jm}(\alpha, \beta, \gamma)$ can be calculated numerically.

G.3 Wigner D-function

In order to define the Wigner D-function, we consider a physical system not connected to the rigid body. The coordinates of the system are collectively denoted q. Its wavefunction with respect to the fixed xyz-axes is written $\varphi(q)$.

The system can be purely fictitious, but in order visualize the system's wavefunction $\varphi(q)$, it may be helpful to choose as system an isolated particle with Cartesian coordinates $q = (x, y, z)$.

G.3.1 Rotation operator

The wavefunction $\varphi(q)$ can be rotated by means of the rotation operator

$$\hat{D}(\alpha, \beta, \gamma) \;=\; \hat{D}_{z''}(\gamma)\hat{D}_{y'}(\beta)\hat{D}_{z}(\alpha) \;. \tag{G.10}$$

The rotated wavefunction,

$$\varphi^{\mathrm{BF}}(q) \;=\; \hat{D}(\alpha, \beta, \gamma)\,\varphi(q) \;, \tag{G.11}$$

remains fixed with respect to the $\xi\eta\zeta$-axes as the Euler angles are varied, and we therefore call $\varphi^{\mathrm{BF}}(q)$ body-fixed. The non-rotated function $\varphi(q)$ is called space-fixed.

In Eq. (G.10), the rotation operator $\hat{D}(\alpha, \beta, \gamma)$ has been written as a product of three rotations involving the original axes xyz as well as the primed axes $x'y'z'$ and $x''y''z''$. It is usually more convenient to express $\hat{D}(\alpha, \beta, \gamma)$ in terms of rotations about the original (unprimed) axes: [1]

$$\hat{D}(\alpha, \beta, \gamma) \;=\; \hat{D}_{z}(\alpha)\hat{D}_{y}(\beta)\hat{D}_{z}(\gamma) \tag{G.12}$$

G.3.2 Angular momentum operator $\hat{\mathbf{L}}$

The angular momentum operator of the system is denoted $\hat{\mathbf{L}}$. Its projections $\hat{L}_x$, $\hat{L}_y$, and $\hat{L}_z$ generate infinitesimal rotations of the wavefunction $\varphi(q)$ about the space-fixed x-, y-, and z-axis, respectively. They can be written

---

[1]We may express (G.10) also in terms of rotations about the rotated axes $\xi\eta\zeta$:

$$\hat{D}(\alpha, \beta, \gamma) \;=\; \hat{D}_{\zeta}(\alpha)\hat{D}_{\eta}(\beta)\hat{D}_{\zeta}(\gamma) \;.$$

The equivalence of (G.10) and (G.12) can be seen as follows:

$$\begin{aligned}
\hat{D}_{z''}(\gamma) &= \hat{D}_{y'}(\beta)\hat{D}_{z'}(\gamma)\hat{D}_{y'}^{\dagger}(\beta) \\
&= \hat{D}_{z}(\alpha)\hat{D}_{y}(\beta)\hat{D}_{z}(\gamma)\hat{D}_{z}^{\dagger}(\alpha)\hat{D}_{y'}^{\dagger}(\beta) \\
\Rightarrow \quad \hat{D}_{z''}(\gamma)\hat{D}_{y'}(\beta)\hat{D}_{z}(\alpha) &= \hat{D}_{z}(\alpha)\hat{D}_{y}(\beta)\hat{D}_{z}(\gamma) \;.
\end{aligned}$$

as differential operators in the coordinates q, but the explicit expressions are not needed here. The operator of finite rotations (G.12) can be expressed in terms of $\hat{L}_y$ and $\hat{L}_z$ as follows:

$$\hat{D}(\alpha, \beta, \gamma) \;=\; e^{-\mathrm{i}\alpha\hat{L}_z/\hbar}\, e^{-\mathrm{i}\beta\hat{L}_y/\hbar}\, e^{-\mathrm{i}\gamma\hat{L}_z/\hbar} \,. \tag{G.13}$$

Eq. (G.13) is given here only for the sake of clarity; we do not need it in this Appendix.

G.3.3   Wigner rotation matrix

Instead of the arbitrary function $\varphi(q)$, we now consider a set of functions $\varphi_{jm}(q)$ $(m = -j, \ldots, 0, \ldots, j)$ forming a basis of the jth irreducible representation of the rotation group $O(3)$. The $\varphi_{jm}(q)$ are chosen to be normalized eigenfunctions of the operators $\hat{\mathbf{L}}^2$ and $\hat{L}_z$ such that

$$\hat{\mathbf{L}}^2 \varphi_{jm}(q) \;=\; \hbar^2 j(j+1)\, \varphi_{jm}(q) \,, \tag{G.14}$$

$$\hat{L}_z \varphi_{jm}(q) \;=\; \hbar m\, \varphi_{jm}(q) \,. \tag{G.15}$$

The Wigner D-functions $D_{mk}^{(j)}(\alpha, \beta, \gamma)$ are defined as the matrix elements of the rotation operator (G.10) in the φ_{jm}-basis: [2]

$$D_{mk}^{(j)}(\alpha, \beta, \gamma) \;=\; \int \varphi_{jm}^*(q)\hat{D}(\alpha, \beta, \gamma)\varphi_{jk}(q)\, dq \,, \tag{G.16}$$

or, more compactly:

$$\boxed{D_{mk}^{(j)}(\alpha, \beta, \gamma) \;=\; \langle jm|\hat{D}(\alpha, \beta, \gamma)|jk\rangle} \,. \tag{G.17}$$

Explicit formulas for the Wigner D-functions can be found in Refs. [150] and [70]. Note that the cited books use different conventions for the Euler angles, and our definition (G.17) differs from the definitions in both [150] and [70] due to the fact that Landau and Edmonds consider passive rotations (rotations of coordinate axes), whereas we perform active rotations (rotations of the wavefunction). [3].

---

[2] We assume that the φ_{jm} $(m = -j, \ldots, j)$ verify the usual phase convention:

$$(\hat{L}_x - \mathrm{i}\hat{L}_y)\, \varphi_{jm}(q) \;=\; \varphi_{jm}(q)\, \times\ \ (\text{real constant})$$

[3] A. R. Edmonds' definitions are the following [70]:

$$\begin{aligned}\hat{D}(\alpha\beta\gamma) &= e^{\mathrm{i}\alpha\hat{L}_z}\, e^{\mathrm{i}\beta\hat{L}_y}\, e^{\mathrm{i}\gamma\hat{L}_z} & [\ \text{Edmonds (\ 4.1.9)}\ ] \\ D_{m'm}^{(j)}(\alpha\beta\gamma) &= \langle jm'|\hat{D}(\alpha\beta\gamma)|jm\rangle & [\ \text{Edmonds (\ 4.1.10)}\ ]\end{aligned}$$

They are analagous to Eqs. (G.13) and (G.17). If the angles α and γ are permuted, our operator (G.13) becomes the inverse of [Edmonds (\ 4.1.9)].

G.4 Symmetric top wavefunctions

The Schrödinger equation for a symmetric top is a second-order differential equation in the three Euler angles that can be solved analytically [145]. Its solutions, the symmetric-top wavefunctions, are proportional to Wigner D-functions [150].

In this paragraph, we show that the Wigner-D functions (G.17), defined as matrix elements of the operator of finite rotations, are eigenfunction of $\hat{\mathbf{J}}^2$, $\hat{J}_z$, and $\hat{J}_\zeta$, where $\hat{J}_z$ is the projection of the angular momentum operator $\hat{\mathbf{J}}$ on the space-fixed z-axis and $\hat{J}_\zeta$ is its projection on the body-fixed ζ-axis. We thereby show that the Wigner-D functions are indeed eigenfunctions of a symmetric top. Our derivation is based purely on geometrical considerations and has some similarities with the proof given in Ref. [61].

G.4.1 Rotation of the rotation operator

The operator of finite rotations $\hat{D}(\alpha, \beta, \gamma)$, considered as a function of the Euler angles (α, β, γ), can be rotated using the operator $\hat{\mathbf{J}}$ defined in Eq. (G.2). The rotated function is:

$$(1 - i\Omega \mathbf{u}.\hat{\mathbf{J}}/\hbar)\,\hat{D}(\alpha, \beta, \gamma) \;=\; \hat{D}(\tilde{\alpha}, \tilde{\beta}, \tilde{\gamma})\;, \qquad (G.18)$$

where $(\tilde{\alpha}, \tilde{\beta}, \tilde{\gamma})$ are the Euler angles of the $\xi\eta\zeta$-system after the infinitesimal rotation. The above equation is a special case of Eq. (G.2).

At this point we remark that the operator symbol on the D-function indicates that $\hat{D}(\alpha, \beta, \gamma)$ is an operator defined in the space of functions of q, whereas the operator symbol on the angular momentum operator $\mathbf{J}$ indicates that $\hat{\mathbf{J}}$ is defined in the space of functions of (α, β, γ).

G.4.2 Equivalence of $\hat{\mathbf{J}}$ and $\hat{\mathbf{L}}$

Clearly, there are two formally different methods to rotate the body-fixed wavefunction $\hat{D}(\alpha, \beta, \gamma)\,\varphi(q)$ by an infinitesimal angle Ω about an axis $\mathbf{u}$:

- One can vary the Euler angles (α, β, γ), in other words, apply the operator $\hat{\mathbf{J}}$ on $\hat{D}(\alpha, \beta, \gamma)\,\varphi(q)$ and use (G.18). The rotated wavefunction is

$$(1 - i\Omega \mathbf{u}.\hat{\mathbf{J}}/\hbar)\,\hat{D}(\alpha, \beta, \gamma)\,\varphi(q) \;=\; \hat{D}(\tilde{\alpha}, \tilde{\beta}, \tilde{\gamma})\,\varphi(q)\;. \quad (G.19)$$

- One can vary q, that is, apply the operator $\hat{\mathbf{L}}$ on $(G.11)$:

$$(1 - i\Omega \mathbf{u}.\hat{\mathbf{L}}/\hbar)\,\hat{D}(\alpha, \beta, \gamma)\,\varphi(q) \;=\; \hat{D}(\tilde{\alpha}, \tilde{\beta}, \tilde{\gamma})\,\varphi(q)\;. \quad (G.20)$$

Combining equations (G.19) and (G.20) yields the identity: [4]

$$\boxed{\hat{\mathbf{J}}\,\hat{D}(\alpha,\beta,\gamma)\,\varphi(q) \;=\; \hat{\mathbf{L}}\,\hat{D}(\alpha,\beta,\gamma)\,\varphi(q)} \;. \qquad \text{(G.22)}$$

G.4.3   Space-fixed and body-fixed angular momentum operators

The operator $(1-i\Omega\mathbf{n}.\hat{\mathbf{L}}/\hbar)$ rotates the wavefunction $\varphi(q)$ by an infinitesimal angle Ω about the space-fixed axis $\mathbf{n}$, whereas the operator $(1 - i\Omega\mathbf{n}^{\mathrm{BF}}.\hat{\mathbf{L}}/\hbar)$ rotates it about the associated body-fixed axis $\mathbf{n}^{\mathrm{BF}}$. The space-fixed and the body-fixed angular momentum operators are related by the unitary transformation

$$\boxed{\mathbf{n}^{\mathrm{BF}}.\hat{\mathbf{L}} \;=\; \hat{D}(\alpha,\beta,\gamma)\,\mathbf{n}.\hat{\mathbf{L}}\,\hat{D}^{\dagger}(\alpha,\beta,\gamma)} \;. \qquad \text{(G.23)}$$

Projection of (G.22) on the space-fixed axis $\mathbf{n}$ gives:

$$\mathbf{n}.\hat{\mathbf{J}}\,\hat{D}(\alpha,\beta,\gamma)\,\varphi(q) \;=\; \mathbf{n}.\hat{\mathbf{L}}\,\hat{D}(\alpha,\beta,\gamma)\,\varphi(q) \;. \qquad \text{(G.24)}$$

Projection of (G.22) on the body-fixed axis $\mathbf{n}^{\mathrm{BF}}$ and use of (G.23) leads to

$$\mathbf{n}^{\mathrm{BF}}.\hat{\mathbf{J}}\,\hat{D}(\alpha,\beta,\gamma)\,\varphi(q) \;=\; \hat{D}(\alpha,\beta,\gamma)\,\mathbf{n}.\hat{\mathbf{L}}\,\varphi(q) \;. \qquad \text{(G.25)}$$

We shall also need the following relation, which follows immediately from (G.22):

$$\hat{\mathbf{J}}^2\,\hat{D}(\alpha,\beta,\gamma)\,\varphi(q) \;=\; \hat{\mathbf{L}}^2\,\hat{D}(\alpha,\beta,\gamma)\,\varphi(q) \;. \qquad \text{(G.26)}$$

G.4.4   The Wigner D-functions as eigenfunctions of a symmetric top

The effect of the operators $\hat{\mathbf{J}}^2$, $\hat{J}_z$ and $\hat{J}_\zeta$ on the Wigner D-functions (G.17) can now be calculated very easily. Eq. (G.26) yields:

$$\begin{aligned}
\hat{\mathbf{J}}^2 D^{(j)}_{mk}(\alpha,\beta,\gamma) &= \langle jm|\hat{\mathbf{J}}^2\hat{D}(\alpha,\beta,\gamma)|jk\rangle \\
&= \langle jm|\hat{\mathbf{L}}^2\hat{D}(\alpha,\beta,\gamma)|jk\rangle \\
&= \hbar^2 j(j+1)\,D^{(j)}_{mk}(\alpha,\beta,\gamma) \;.
\end{aligned} \qquad \text{(G.27)}$$

---

[4]We recall that $\mathbf{u}.\hat{\mathbf{J}}$ and $\mathbf{u}.\hat{\mathbf{L}}$ are differential operators in the Euler angles and in the q-variables, respectively. Equation (G.22) could be written more concicely using brackets indicating the order of operations:

$$[\hat{\mathbf{J}}\,\hat{D}](\alpha,\beta,\gamma)\,\varphi(q) \;=\; \hat{\mathbf{L}}\,[\hat{D}(\alpha,\beta,\gamma)\,\varphi](q) \;. \qquad \text{(G.21)}$$

On the left-hand side of Eq. (G.21), the operator $\hat{\mathbf{J}}$ transforms the operator $\hat{D}(\alpha,\beta,\gamma)$, and the transformed operator $[\hat{\mathbf{J}}\,\hat{D}](\alpha,\beta,\gamma)$ is then applied on $\varphi(q)$. On the right-hand side, the operator $\hat{\mathbf{L}}$ transforms the function $\varphi^{\mathrm{BF}}(q) = \hat{D}(\alpha,\beta,\gamma)\,\varphi(q)$.

In order to evaluate the effect of $\hat{J}_z$ and $\hat{J}_\zeta$, we make the unit vector $\mathbf{n}$ point into the z-direction, so that $\mathbf{n}$ and $\mathbf{n}^{\mathrm{BF}}$ become $\mathbf{e}_z$ and $\mathbf{e}_\zeta$, respectively. Using Eqs. (G.24) and (G.25), we obtain

$$
\begin{aligned}
\hat{J}_z D_{mk}^{(j)}(\alpha, \beta, \gamma) &= \langle jm|\hat{J}_z \hat{D}(\alpha, \beta, \gamma)|jk\rangle \\
&= \langle jm|\hat{L}_z \hat{D}(\alpha, \beta, \gamma)|jk\rangle \\
&= \hbar m \, D_{mk}^{(j)}(\alpha, \beta, \gamma) \ ,
\end{aligned}
\tag{G.28}
$$

$$
\begin{aligned}
\hat{J}_\zeta D_{mk}^{(j)}(\alpha, \beta, \gamma) &= \langle jm|\hat{J}_\zeta \hat{D}(\alpha, \beta, \gamma)|jk\rangle \\
&= \langle jm|\hat{D}(\alpha, \beta, \gamma)\hat{L}_z|jk\rangle \\
&= \hbar k \, D_{mk}^{(j)}(\alpha, \beta, \gamma) \ .
\end{aligned}
\tag{G.29}
$$

We have thus shown that the Wigner D-function $D_{mk}^{(j)}(\alpha, \beta, \gamma)$ is an eigenfunction of $\hat{\mathbf{J}}^2$, $\hat{J}_z$, and $\hat{J}_\zeta$, with respective eigenvalues $\hbar^2 j(j+1)$, $\hbar m$, and $\hbar k$. The Wigner D-functions are thus the eigenfunctions of a symmetric top.

G.4.5 Normalization

Normalized symmetric top wavefunctions are defined as follows [150]:

$$
\boxed{\varphi_{jmk}^{(\mathrm{symtop})}(\alpha, \beta, \gamma) \; = \; \mathrm{i}^j \sqrt{\tfrac{2j+1}{8\pi^2}} \, D_{mk}^{(j)}(\alpha, \beta, \gamma)} \ .
\tag{G.30}
$$

It can be shown that they are normalized in agreement with (G.1).

G.5 Rotation of a linear molecule

The orientation of the internuclear axis of a *linear* molecule is described using only two Euler angles: the polar and azimuthal angles of spherical coordinates, θ $(0 \leq \theta \leq \pi)$ and ϕ $(0 \leq \phi < 2\pi)$. One may still define a rotated coordinate system $\xi\eta\zeta$, but this system is not strictly "body-fixed": the $\xi\eta\zeta$-axes does in general not perform the same rotation as the molecular axis when the Euler angles are varied. This may be visualized as follows.

The direction of the molecular axis is indicated by the unit vector $\mathbf{n}$ with space-fixed components

$$
\begin{aligned}
n_x &= \sin\theta\cos\phi \ , \tag{G.31} \\
n_x &= \sin\theta\sin\phi \ , \tag{G.32} \\
n_x &= \cos\theta \ . \tag{G.33}
\end{aligned}
$$

The $\xi\eta\zeta$-axes may then be identified with the unit vectors $(\mathbf{n}, \mathbf{e}_\theta, \mathbf{e}_\phi)$, where $\mathbf{e}_\theta$ and $\mathbf{e}_\phi$ are given by:

$$\mathbf{e}_\theta = \frac{\partial \mathbf{n}}{\partial \theta}, \qquad \mathbf{e}_\phi = \frac{\partial \mathbf{n}}{\partial \phi} .$$

$(\mathbf{n}, \mathbf{e}_\theta, \mathbf{e}_\phi)$ are the familiar unit vectors of spherical coordinates.

We first consider a rotation of the molecular axis $\mathbf{n}$ about the z-axis, $\mathbf{n}$ pointing initially in the x-direction. As the azimuthal angle ϕ is varied, $\mathbf{n}$ describes a circle with radius 1 in the xy-plane. The vector $\mathbf{e}_\theta$ remains constant (pointing into the negative z-direction), and the vector $\mathbf{e}_\phi$ changes uniformly with ϕ.

We next assume that $\mathbf{n}$ again points into the the x-direction, and we consider a rotation about the y-axis, so that $\mathbf{n}$ now describes a circle with radius 1 in the xz-plane. As $\mathbf{n}$ passes across the pole ($\theta = 0$), the unit vectors $\mathbf{e}_\theta$ and $\mathbf{e}_\phi$ become $-\mathbf{e}_\theta$ and $-\mathbf{e}_\phi$, respectively. This shows in a spectactular manner that the "body-fixed" system $\xi\eta\zeta$ does not perform the same rotation as the molecular axis! Whenever the internuclear axis passes exactly across the pole, the "body-fixed" axis changes abruptly. If the axis gets near the pole without touching it, $\mathbf{e}_\theta$ and $\mathbf{e}_\phi$ vary smoothly. However, they vary more rapidly near the pole than on the equator.

The discussion shows that the $\xi\eta\zeta$ axes are only "partly body-fixed". As a consequence, the angular momentum operator $\mathbf{u}.\hat{\mathbf{J}}$, which generates an infinitesimal rotation of the internuclear axis $\mathbf{n}$ about an axis $\mathbf{u}$, generates a *different* infinitesimal rotation of the $\xi\eta\zeta$-axes (except when $\mathbf{u}$ is parallel to the space-fixed z-axis). Rotations of the *entire* molecule, including electrons attached to the $\xi\eta\zeta$-system [5], can therefore *not* be performed using only the nuclear angular momentum operator $\hat{\mathbf{J}}$: one also needs the electronic angular momentum operator $\hat{\mathbf{L}}$ (which generates rotations of the electrons only, leaving the internuclear axis unchanged).

---

[5]In the Born-Oppenheimer approach, the positions of the electrons are described with respect to the rotated axes, $\xi\eta\zeta$.

Appendix H

Logarithmic derivative matrix

A system of N coupled linear second-order differential equations without first-derivative terms can be written as

$$\Psi''(x) = W(x)\Psi(x) \tag{H.1}$$

where the $\Psi(x)$ is an $N{\times}N$-matrix of N linearly independent solution vectors:

$$\Psi = \begin{pmatrix} \Psi_1 & \dots & \Psi_{1N} \\ \vdots & \ddots & \vdots \\ \Psi_N & \dots & \Psi_{1N} \end{pmatrix} \tag{H.2}$$

The logarithmic derivative matrix $Z(x)$ is defined as

$$Z = \Psi'\Psi^{-1} \; ; \tag{H.3}$$

it is invariant under transformations in the solution space. This is seen by replacing in Eq. (H.3) Z by $\tilde{Z}A$, where A is a constant coefficient matrix of dimension $N \times N$. In other words, the relation $\tilde{\Psi}' = Z\tilde{\Psi}$ holds for any linear combination of solutions. In a basis transformation (frame transformation), the solution matrix Ψ and the log derivative matrix become $\tilde{\Psi} = U\Psi$ and $\tilde{Z} = UZU^{-1}$, respectively.

Differentiation of the identity $Z\Psi = \Psi'$ and elimination of the second derivative using Eq. (H.1) yields the matrix Riccati equation

$$Z'(x) = W(x) - Z(x)^2. \tag{H.4}$$

The R-matrix is defined as the inverse $R = Z^{-1}$ of the log derivative matrix. It verifies a similar equation:

$$R'(x) = 1 - R(x)W(x)R(x) \; . \tag{H.5}$$

Bound state energies can be found by the "shooting method" explained as follows.

One log derivative matrix, $Z_A(x)$, is obtained by *outward* integration, starting in the inner forbidden region. Another log derivative matrix, $Z_B(x)$, is obtained by *inward* integration, staring in the outer forbidden region. The respective initial conditions are

$$Z_A(x) \; = \; \begin{pmatrix} \kappa_1(x) & & 0 \\ & \ddots & \\ 0 & & \kappa_N(x) \end{pmatrix} \qquad Z_B(x) = \begin{pmatrix} -\kappa_1(x) & & 0 \\ & \ddots & \\ 0 & & -\kappa_N(x) \end{pmatrix} ,$$

(H.6)

where the quantities κ_i $(i = 1, \ldots, N)$ are defined via the diagonal elements of the coupling matrix W:

$$\kappa_i(x) = \sqrt{-W_{ii}(x)} \qquad (i = 1, \ldots, N) .$$

(H.7)

Let $\phi(x) = \begin{pmatrix} \phi_1(x) \\ \vdots \\ \phi_N(x) \end{pmatrix}$ be a particular solution satisfying the boundary conditions for both $x \to 0$ and $x \to \infty$. Its derivative ϕ' may then be obtained from ϕ using either Z_A or Z_B:

$$\phi'(x) \; = \; Z_A(x)\phi(x) \; = \; Z_B(x)\phi(x) .$$

(H.8)

This means that

$$[Z_A(x) - Z_B(x)]\phi(x) \; = \; 0 .$$

(H.9)

Bound states are thus characterized by the condition

$$\boxed{\det[Z_A(x) - Z_B(x)] \; = \; 0} .$$

(H.10)

In practice, the matching distance needs to be chosen in the classically allowed region.

Appendix I

Scattering equations in Jacobi coordinates

In this Appendix we present the space-fixed coupled equations for the relative motion of an atom C and a diatomic molecule AB in a Σ electronic state. These equations are obtained by the Arthurs-Dalgarno expansion [14] of the wavefunction using a space-fixed frame. Scattering equations using a body-fixed reference frame can be found in Refs. [204] and [152].

I.0.1 Hamiltonian and angular momentum

We use the space-fixed Jacobi coordinates $\mathbf{r} = \overrightarrow{AB}$ and $\mathbf{R} = \overrightarrow{(AB)C}$. The potential is written as the sum of the diatomic potential V_{AB} and the atom-molecule interaction potential V_{AB-C}:

$$V(r, R, \eta) = V_{AB}(r) + V_{AB-C}(r, R, \eta) , \tag{I.1}$$

where η is the angle between the Jacobi vectors $\mathbf{r}$ and $\mathbf{R}$. The Hamiltonian can be split as

$$\hat{H} = \hat{H}_{AB} + \hat{H}_{AB-C} \tag{I.2}$$

where $\hat{H}_{AB}$ and $\hat{H}_{AB-C}$ are defined as

$$\hat{H}_{AB} = -\frac{\hbar^2}{2\mu_{AB}} \left[\frac{1}{r} \frac{\partial^2}{\partial r^2} r + \frac{1}{r^2} \left(\frac{\hat{\mathbf{j}}}{i\hbar} \right)^2 \right] + V_{AB}(r) , \tag{I.3}$$

$$H_{AB-C} = -\frac{\hbar^2}{2\mu_{AB-C}} \left[\frac{1}{R} \frac{\partial^2}{\partial R^2} R + \frac{1}{R^2} \left(\frac{\hat{\mathbf{l}}}{i\hbar} \right)^2 \right] + V_{AB-C}(r, R, \eta) . \tag{I.4}$$

Here $\hat{\mathbf{j}}$ and $\hat{\mathbf{l}}$ are the angular momentum operators associated with the Jacobi vectors $\mathbf{r}$ and $\mathbf{R}$, respectively. The total angular momentum operator is

$$\hat{\mathbf{J}} = \hat{\mathbf{l}} + \hat{\mathbf{j}} . \tag{I.5}$$

I.0.2 Channel basis functions and coupled equations

The eigenfunctions of $\hat{H}_{AB}$ are rotational-vibrational functions $\varphi_{vj}^{(\text{vib})}(r)Y_{jm_j}(\Omega_r)$ such that

$$(\hat{H}_{AB} - E_{vj})\,\varphi_{vj}^{(\text{vib})}(r)\,Y_{jm_j}(\Omega_r) \;=\; 0\;, \qquad (I.6)$$

where E_{vj} are rotational-vibrational energy levels of the moleceule AB. Eigenfunctions of $\mathbf{J}^2$, J_z, $\mathbf{l}^2$ and $\mathbf{j}^2$ are constructed using Clebsch-Gordon coefficients:

$$\mathcal{Y}_{jl}^{JM}(\Omega_R,\Omega_r) \;=\; \sum_{m_l=-l}^{l}\sum_{m_j=-j}^{j}\langle JMlj|m_lm_j\rangle\,Y_{lm_l}(\Omega_R)Y_{jm_j}(\Omega_r) \qquad (I.7)$$

The channel functions $\varphi_{vj}^{(\text{vib})}(r)\mathcal{Y}_{jl}^{JM}(\Omega_R,\Omega_r)$ are eigenfunctions of $\mathbf{J}^2$, J_z, $\mathbf{l}^2$, $\mathbf{j}^2$ and $\hat{H}_{AB}$:

$$\left[\hat{\mathbf{J}}^2 - \hbar^2 J(J+1)\right]\varphi_{vj}^{(\text{vib})}\,\mathcal{Y}_{jl}^{JM} \;=\; 0 \qquad (I.8)$$

$$(J_z - \hbar M)\,\varphi_{vj}^{(\text{vib})}\,\mathcal{Y}_{jl}^{JM} \;=\; 0 \qquad (I.9)$$

$$\left[\hat{\mathbf{l}}^2 - \hbar^2 l(l+1)\right]\varphi_{vj}^{(\text{vib})}\,\mathcal{Y}_{jl}^{JM} \;=\; 0 \qquad (I.10)$$

$$\left(\hat{j}_z - \hbar m_j\right)\varphi_{vj}^{(\text{vib})}\,\mathcal{Y}_{jl}^{JM} \;=\; 0 \qquad (I.11)$$

$$\left(\hat{H}_{AB} - E_{vj}\right)\varphi_{vj}^{(\text{vib})}\,\mathcal{Y}_{jl}^{JM} \;=\; 0 \qquad (I.12)$$

At fixed distance R, the wavefunction $\varphi^{JM}(R,\Omega_R,r,\Omega_r)$ (eigenfunction of $\mathbf{J}^2$ and J_z) is expanded in the basis functions $\varphi_{vj}^{(\text{vib})}\mathcal{Y}_{jl}^{JM}$:

$$\varphi^{JM}(R,r,\Omega_R,\Omega_r) \;=\; \sum_{vjl}\varphi_{vj}^{(\text{vib})}(r)\mathcal{Y}_{jl}^{JM}(\Omega_R,\Omega_r)\frac{u_{vjl}^{JM}(R)}{R} \qquad (I.13)$$

The stationary Schrödinger equation $(\hat{H} - E)\varphi^{JM} = 0$ then leads to a system of coupled second-order differential equations for the channel functions $u_{vjl}^{JM}(R)$:

$$\left[-\frac{\hbar^2}{2\mu_{AB-C}}\left(\frac{d^2}{dR^2} - \frac{l(l+1)}{R^2}\right) + E_{vj} - E\right]u_{vjl}^{JM}(R)$$
$$+ \sum_{v'j'l'}\langle vjlJ|V_{AB-C}|v'j'l'J\rangle\,u_{v'j'l'}^{JM}(R) \;=\; 0\;. \qquad (I.14)$$

For each distance R, the elements of the potential coupling matrix are given by

$$\langle v'j'l'J|V_{AB-C}|vjlJ\rangle$$

$$
= \int_0^\infty dr\, r^2 \int d\Omega_r \int d\Omega_R\, \varphi_{v'j'}^{\text{(vib)}*}(r)\, \mathcal{Y}_{j'l'}^{*\,JM}(\Omega_r, \Omega_R)\, \times
$$

$$
\times\, V_{AB-C}(r, R, \eta)\, \varphi_{vj}^{\text{(vib)}}(r)\, \mathcal{Y}_{jl}^{JM}(\Omega_r, \Omega_R)\,; \tag{I.15}
$$

they are functions of R. Note that they do not dependent on the quantum number M associated with $\hat{J}_z$.

In the case of two identical atoms ($A = B$), the potential V_{AB-C} is unchanged under the transformations $\mathbf{r} \to -\mathbf{r}$ and $\mathbf{R} \to -\mathbf{R}$. The matrix elements (I.15) therefore vanish unless $j + j'$ and $l + l'$ are pair.

I.0.3 Expansion of the interaction potential in Legendre polynomials

If the interaction potential is expanded in Legendre-polynomials,

$$
V_{AB-C}(r, R, \eta) \;=\; \sum_{L=1}^{\infty} (2L+1)^{-1/2} P_L(\cos\eta) V_{AB-C}^L(r, R)\,, \tag{I.16}
$$

the R-dependent potential matrix elements take the form

$$
\langle v'j'l'J | V_{AB-C} | vjlJ \rangle \;=\; \sum_{L=0}^{\infty} (2L+1)^{-1/2} \langle \varphi_{v'j'}^{\text{(vib)}} | V_{AB-C}^L | \varphi_{vj}^{\text{(vib)}} \rangle\, f_{j'l'Ljl}^J \tag{I.17}
$$

where

$$
\langle \varphi_{v'j'}^{\text{(vib)}} | V_{AB-C}^L | \varphi_{vj}^{\text{(vib)}} \rangle \;=\; \int_0^\infty dr\, r^2\, \varphi_{v'j'}^{\text{(vib)}*}(r)\, V_{AB-C}^L(r, R)\, \varphi_{vj}^{\text{(vib)}}(r)\,, \tag{I.18}
$$

$$
f_{j'l'Ljl}^J \;=\; \int d\Omega_R \int d\Omega_r\, \mathcal{Y}_{j'l'}^{JM*}(\Omega_r, \Omega_R)\, P_L(\cos\eta)\, \mathcal{Y}_{jl}^{JM}(\Omega_r, \Omega_R) \tag{I.19}
$$

The $f_{j'l'Ljl}^J$ are Percival-Seaton coefficients, known analytically in terms of $3j$ and $6j$ coefficients [204].

I.0.4 Spherical dispersion coefficients

At large distances R, the components $V_{AB-C}^L(r, R)$ of the atom-molecule interaction potential $V_{AB-C}(r, R, \eta)$ can be developed in a series of inverse powers of R:

$$
V_{AB-C}^L(r, R) \;=\; -\sum_n R^{-n} C_n^{L0L}(r)\,. \tag{I.20}
$$

The dispersion coefficients C_n^{L0L} are a special case of the coefficients $C_n^{L_a L_b L}$ used in Refs. [267] and [228] for potentials describing molecule-molecule

interactions. The asymptotic behaviour of the potential coupling matrix elements (I.17) is obtained by inserting (I.20) into Eq. (I.17):

$$\langle v'j'l'J|V_{AB-C}|vjlJ\rangle = -\sum_n \frac{C_n^{Jv'j'vj}}{R^n} \tag{I.21}$$

with dispersion coefficients $C_n^{Jv'j'vj}$ given by

$$C_n^{Jv'j'vj} = \sum_{L=0}^{\infty} (2L+1)^{-1/2} \langle \varphi_{v'j'}^{(\text{vib})}|C_n^{L0L}|\varphi_{vj}^{(\text{vib})}\rangle \, f_{j'lL'jl}^J \,. \tag{I.22}$$

Appendix J

Milne equation

The radial Schrödinger equation for the lth partial wave can be written as

$$u''(r) + [k(r)]^2 u(r) = 0 \tag{J.1}$$

where

$$k(r) = \sqrt{\frac{2\mu}{\hbar^2}[E - V(r)] - \frac{l(l+1)}{r^2}} \ . \tag{J.2}$$

Our aim is to construct two linearly independent solutions $f(r)$ and $g(r)$, which we write in a phase-amplitude form [194]:

$$\begin{pmatrix} f & g \\ f' & g' \end{pmatrix} = \begin{pmatrix} a \sin \phi & -a \cos \phi \\ a' \sin \phi + \frac{w}{a} \cos \phi & -a' \cos \phi + \frac{w}{a} \sin \phi \end{pmatrix} \ . \tag{J.3}$$

The Wronskian of f and g is constant:

$$w = fg' - f'g = a^2 \phi' = \text{const} \ . \tag{J.4}$$

Milne's accumulated phase is defined as

$$\phi(r) = w \int_{r_0}^r \frac{dr'}{a^2(r')} \tag{J.5}$$

where r_0 is the starting point of the integration. Equation (J.5) is known as Milne's first equation. The amplitude $a(r)$ satisfies Milne's second equation [194]:

$$a''(r) + k^2(r)a(r) - \frac{w^2}{a(r)^3} = 0 \ . \tag{J.6}$$

In the case of a constant potential ($k = \text{const}$), the stationary solution ($a^{\text{stat}} = k^{-1/2}$) is *stable*, see Fig. J.1.

The first-order JWKB approximation for the Milne phase and amplitude is

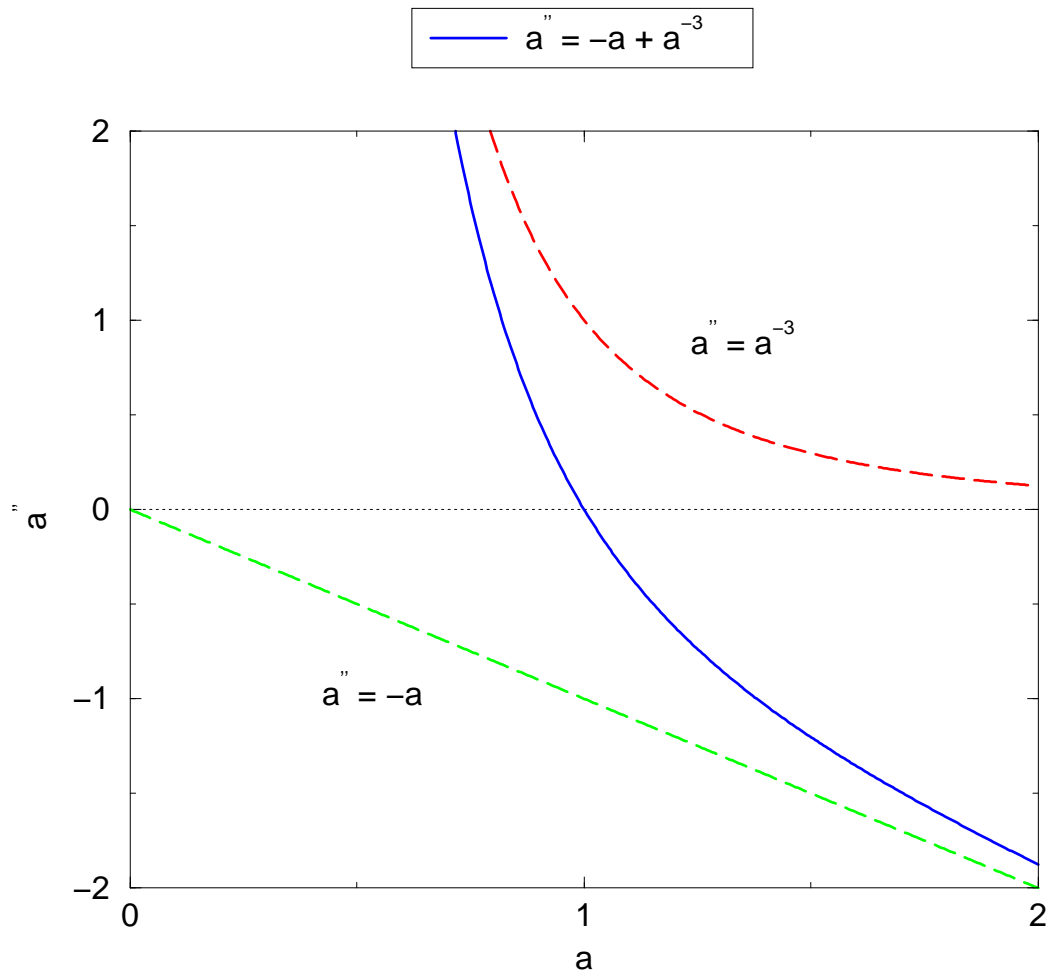$$a(r) = k^{-1/2}(r), \qquad \phi(r) = \int_{r_0}^r k(r')dr' \tag{J.7}$$

Figure J.1: The second derivative a'' as a function of the Milne amplitude a, for $k = 1$. The stationary solution $a(R) = 1$ is *stable* because a'' decreases as a increases.

in accordance with Milne's first (but not second) equation.

For numerical purposes, a rule is needed that determines the distance at which the propagation of the Milne amplitude can be stopped and at which the numerical solutions can be connected to asymptotic solutions. There are several possibilities. One needs to distinguish between bound and continuum energies.

- Below threshold ($\epsilon < 0$, $\kappa = \sqrt{-2\mu E}$): We found it useful to consider the square of the Milne amplitude multiplied. We multiply it by κ in order to obtain a dimensionless quantity. We stop the integration when $1/[a(r)^2\kappa]$ becomes less than some small constant, typically 10^{-4}. Numerically we found that the accumlated phase $\phi(r)$ has then practically reached its limit β.

- If the energy lies above threshold ($\epsilon > 0$, $k = \sqrt{2\mu E}$), we stop the integration when the energy ϵ becomes negligible compared to the potential energy.

Milne equation for strongly closed channels

In classically forbidden regions the solutions of the Schr ödinger equations $f(r)$ and $g(r)$ do no oscillate but show an exponentially increasing or decreasing behaviour. For such regions, it seems natural to replace the sine and cosine in expression (J.3) by cosinus hyperbolicus and sinus hyperbolicus [87, 126] [1]:

$$\begin{pmatrix} f & g \\ f' & g' \end{pmatrix} = \begin{pmatrix} a\sinh\phi & a\cosh\phi \\ a'\sinh\phi - \frac{w}{a}\cosh\phi & a'\cosh\phi - \frac{w}{a}\sinh\phi \end{pmatrix} \quad (J.8)$$

where w is the Wronskian of solutions f and g:

$$w = fg' - f'g = -a^2\phi' = \text{const}. \quad (J.9)$$

Solving Eq. (J.8) for a, a', ϕ, w gives:

$$w = fg' - f'g \quad (J.10)$$

$$a = \sqrt{g^2 - f^2} \quad (J.11)$$

$$a' = \frac{gg' - ff'}{a} \quad (J.12)$$

$$\phi = \frac{1}{2}\ln\frac{g+f}{g-f}. \quad (J.13)$$

---

[1]We again use a short-hand notation, omitting the dependence of tn the radial coordinate r. Note that f, g, a and ϕ are all functions of r: $f(r)$, $g(r)$, $a(r)$, $\phi(r)$. Only the Wronskian w is a constant.

One sees that Milne's accumulated phase $\phi(r)$ is given by the integral

$$\phi(r) \;=\; -w \int_{r_0}^{r} \frac{dr'}{a^2(r)} \;.$$ (J.14)

Note the minus sign.

Milne's second equation for a and a' reads

$$a''(r) - \kappa^2(r)a(r) + \frac{w^2}{a^3(r)} \;=\; 0 \;.$$ (J.15)

Equations (J.6) and (J.15) only differ in the sign of the cubic term a^{-3} (note that $k^2 = -\kappa^2$). Fig. J.2 shows the second derivative a'' as a function of the amplitude a for the special case of a constant potential ($\kappa^2 = $ const). One sees that the equilibrium solution, $a(r) = \kappa^{-1/2}$, is *unstable*.

The JWKB approximation for solutions in the classically forbidden region is

$$w \;=\; 1 \,, \qquad a^{\mathrm{JWKB}}(r) \;=\; \kappa(r)^{-1/2}, \qquad \phi^{\mathrm{JWKB}}(r) \;=\; -\int_{r_0}^{r} \kappa(r')dr' \quad \text{(J.16)}$$

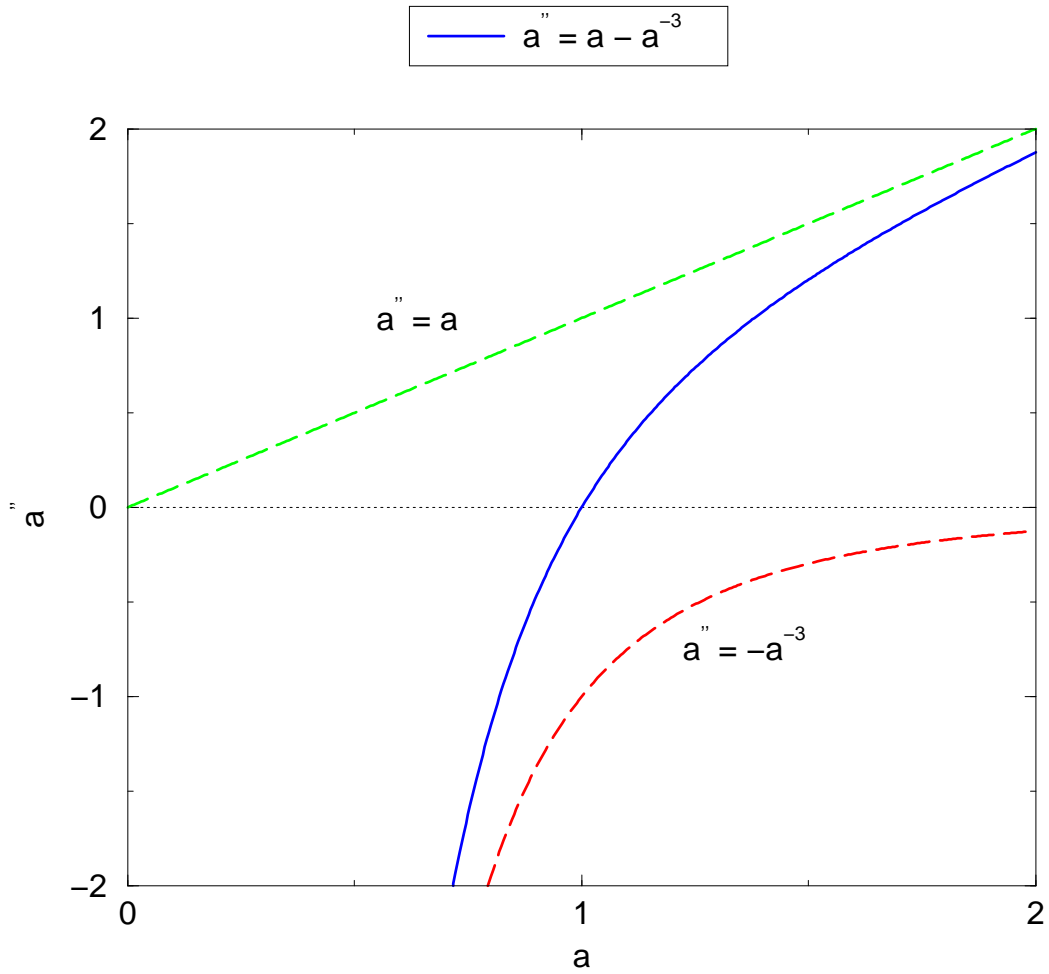in accordance with Milne's first equation, Eq. (J.9).

Figure J.2: The second derivative a'' as a function of the Milne amplitude a, for $\kappa = 1$. The stationary solution $(a = 1, a' = 0)$ is *unstable* because a'' increases as a increases.

Appendix K

Numerov's finite difference formula

The coupled second-order differential equations are written as

$$\Psi''(x) + W(x)\Psi(x) = 0 . \tag{K.1}$$

We define the differences

$$a_i = x_i - x_{i-1} \tag{K.2}$$
$$b_i = x_{i+1} - x_i \tag{K.3}$$

and consider the Taylor expansions of Ψ and its second derivative:

$$\Psi_{i+1} = \Psi_i + b_i\Psi_i' + \frac{b_i^2}{2}\Psi_i'' + \frac{b_i^3}{3!}\Psi_i^{(3)} + \frac{b_i^4}{4!}\Psi_i^{(4)} + \frac{b_i^5}{5!}\Psi_i^{(5)} + \frac{b_i^6}{6!}\Psi_i^{(6)} + \cdots \tag{K.4}$$

$$\Psi_{i+1}'' = \Psi_i'' + b_i\Psi_i^{(3)} + \frac{b_i^2}{2}\Psi_i^{(4)} + \frac{b_i^3}{3!}\Psi_i^{(5)} + \frac{b_i^4}{4!}\Psi_i^{(6)} + \cdots \tag{K.5}$$

$$\Psi_{i-1} = \Psi_i - a_i\Psi_i' + \frac{a_i^2}{2}\Psi_i'' - \frac{a_i^3}{3!}\Psi_i^{(3)} + \frac{a_i^4}{4!}\Psi_i^{(4)} - \frac{a_i^5}{5!}\Psi_i^{(5)} + \frac{a_i^6}{6!}\Psi_i^{(6)} - \cdots \tag{K.6}$$

$$\Psi_{i-1}'' = \Psi_i'' - a_i\Psi_i^{(3)} + \frac{a_i^2}{2}\Psi_i^{(4)} - \frac{a_i^3}{3!}\Psi_i^{(5)} + \frac{a_i^4}{4!}\Psi_i^{(6)} - \cdots \tag{K.7}$$

where $\Psi_i = \Psi(x_i)$.

Add Ψ_{i+1}/b_i and Ψ_{i-1}/a_i and use Eqs. (K.4) and (K.6). The first derivative term cancels strictly. The higher odd derivative terms cancel approximately:

$$\frac{\Psi_{i+1}}{b_i} + \frac{\Psi_{i-1}}{a_i} = \left(\frac{1}{b_i} + \frac{1}{a_i}\right)\Psi_i + \frac{1}{2}(b_i + a_i)\Psi_i'' + \frac{1}{3!}(b_i^2 - a_i^2)\Psi_i^{(3)} +$$
$$+ \frac{1}{4!}(b_i^3 + a_i^3)\Psi_i^{(4)} + \frac{1}{5!}(b_i^4 - a_i^4)\Psi_i^{(5)} + \frac{1}{6!}(b_i^5 + a_i^5)\Psi_i^{(6)} + \cdots \tag{K.8}$$

$$\frac{\Psi''_{i+1}}{b_i} + \frac{\Psi''_{i-1}}{a_i} = \left(\frac{1}{b_i} + \frac{1}{a_i}\right)\Psi''_i + \frac{1}{2}(b_i + a_i)\Psi_i^{(4)} + \frac{1}{3!}(b_i^2 - a_i^2)\Psi_i^{(5)} +$$

$$+\frac{1}{4!}(b_i^3 + a_i^3)\Psi_i^{(6)} + \cdots \tag{K.9}$$

Multiply Eq. (K.9) by $(a_i^2 - a_i b_i + b_i^2)/12$ and subtract the result from Eq. (K.8) to cancel the fourth derivative term. This gives

$$\frac{1}{b_i}\left[1 + \frac{1}{12}(a_i^2 - a_i b_i + b_i^2)W_{i+1}\right]\Psi_{i+1} + \frac{1}{a_i}\left[1 + \frac{1}{12}(a_i^2 - a_i b_i + b_i^2)W_{i-1}\right]\Psi_{i-1}$$

$$= \left(\frac{1}{b_i} + \frac{1}{a_i}\right)\left[1 + \frac{1}{12}(a_i^2 - 7a_i b_i + b_i^2)W_i\right]\Psi_i$$

$$+\frac{1}{6}(b_i^2 - a_i^2)\Psi_i^{(3)} - \frac{1}{360}(b_i^2 - a_i^2)(2b_i^2 - 5a_i b_i + 2a_i^2)\Psi_i^{(5)}$$

$$+\mathcal{O}(b_i^5 + a_i^5)\Psi_i^{(6)} \tag{K.10}$$

The grid step should be chosen constant so that the terms proportional to $(b_i^2 - a_i^2)$ cancel. Omitting derivatives of order 6 and higher gives the finite difference formula

$$\frac{1}{b_i}\left[1 + \frac{1}{12}a_i b_i W_{i+1}\right]\Psi_{i+1} + \frac{1}{a_i}\left[1 + \frac{1}{12}a_i b_i W_{i-1}\right]\Psi_{i-1}$$

$$= \left(\frac{1}{b_i} + \frac{1}{a_i}\right)\left[1 - \frac{5}{12}a_i b_i W_i\right]\Psi_i . \tag{K.11}$$

In this equation, the original operator $d^2/dx^2 + W$ from Eq. (K.1) is represented by a tridiagonal matrix.

Eq. (K.11) is known as Numerov's formula. It is mainly used as a recursion formula to solve initial value problems.

Appendix L

Density of states of a system of free particles

In this Appendix, we derive the expression for the density of states of n free particles.

L.1 Volume of a sphere in n dimensions

The volume of sphere in a cartesian space of n-dimensions can be calculated recursively:

$$V_{n+1}(r) \;=\; \int_{-r}^{r} dz \, V_n \left(\sqrt{r^2 - z^2} \right) \tag{L.1}$$

Comparing this expression with

$$V_n(r) \;=\; a_n r^n \tag{L.2}$$

leads to a recursion formula for the coefficients a_n:

$$a_n \;=\; 2a_{n-1} \int_0^{\pi/2} d\theta \, \cos^n \theta \;. \tag{L.3}$$

The integral in the above equation can be calculated recursively using partial integration. The result for $n \geq 2$ is

$$\int_0^{\pi/2} d\theta \, \cos^n \theta \;=\; \begin{cases} \frac{(n-1)!!}{n!!} & (n \text{ odd}) \\ \frac{\pi}{2} \frac{(n-1)!!}{n!!} & (n \text{ pair}) \end{cases} \tag{L.4}$$

so that

$$a_n \;=\; \begin{cases} 2 \frac{(n-1)!!}{n!!} \, a_{n-1} & (n \text{ odd}) \\ \pi \frac{(n-1)!!}{n!!} \, a_{n-1} & (n \text{ pair}) \end{cases} . \tag{L.5}$$

The volume V_n of a sphere with radius r in a space of dimension n ($n = 1, 2, 3, \ldots$) can thus be calculated according to the following scheme:

$$
\begin{aligned}
V_1(r) &= \tfrac{1}{1!!} & &= 1 \\
V_1(r) &= \tfrac{2}{1!!}\, r & &= 2r \\
V_2(r) &= \tfrac{1}{2!!}\,(2\pi)\, r^2 & &= \pi r^2 \\
V_3(r) &= \tfrac{2}{3!!}\,(2\pi)\, r^3 & &= \tfrac{4}{3}\,\pi\, r^3 \\
V_4(r) &= \tfrac{1}{4!!}\,(2\pi)^2\, r^4 & &= \tfrac{1}{2}\,\pi^2\, r^4 \\
V_5(r) &= \tfrac{2}{5!!}\,(2\pi)^2\, r^5 & &= \tfrac{8}{15}\,\pi^2\, r^5 \\
V_6(r) &= \tfrac{1}{6!!}\,(2\pi)^3\, r^6 & &= \tfrac{1}{6}\,\pi^3\, r^6 \\
V_7(r) &= \tfrac{2}{7!!}\,(2\pi)^3\, r^7 & &= \tfrac{16}{105}\,\pi^3\, r^7 \\
V_8(r) &= \ldots
\end{aligned}
\tag{L.6}
$$

Differentiating the volume V_n with respect to the radius r gives the surface S_n of the sphere in n dimensions

$$
S_n(r) = \frac{dV_n}{dr}(r) = n\, a_n\, r^{n-1} . \tag{L.7}
$$

Hence the circumference of a circle is

$$
S_2 = 2\pi r . \tag{L.8}
$$

The surface of a three-dimensional sphere is

$$
S_3 = 4\pi r^2 . \tag{L.9}
$$

L.2 Density of states of several particles

A particle in a "box" $[0, L]$ can be described by the Hamiltonian $\hat{H}$ such that

$$
\hat{H}\varphi(x) = -\frac{\hbar^2}{2\mu}\frac{\partial^2 \varphi}{\partial x^2}(x) . \tag{L.10}
$$

Its eigenfunctions obeying the strict boundary conditions $\varphi_k(0) = 0$ and $\varphi_k(L) = 0$ are

$$
\varphi_k(x) = \sin(kx) \tag{L.11}
$$

where k can take on the discret values

$$
k = n\frac{\pi}{L} , \qquad (n = 1, 2, 3, \ldots) \tag{L.12}
$$

The density of states in the k-space is

$$\rho_k = \frac{1}{\Delta k} = \frac{L}{\pi} . \tag{L.13}$$

This argumentation can be generalized to a Hamiltonian

$$\hat{H} = -\frac{\hbar^2}{2\mu} \sum_{i=1}^{n} \frac{\partial^2}{\partial x_i^2} \tag{L.14}$$

describing a particle in three dimensions ($n = 3$), or a system of particles. The coordinates x_i can be the particles' coordinates, or the Jacobi vectors.

The corresponding density of states is given by

$$\rho_k^{(n)} = \left(\frac{L}{\pi}\right)^n , \tag{L.15}$$

and the magnitude of the n-dimensional vector $(k_1, k_2, ..., k_n)$ is related to the energy E by

$$k(E) = \frac{1}{\hbar} \sqrt{2\mu E} . \tag{L.16}$$

The total number of states with energy less than E' is

$$\int_0^{E'} dE \, \rho_E^{(n)}(E) = \left(\frac{L}{\pi}\right)^n V_n^{(\text{sphere})}(k') \tag{L.17}$$

where

$$k' = k(E') . \tag{L.18}$$

Differentiation with respect to E' leads to

$$\rho_E^{(n)}(E) = \left(\frac{L}{\pi}\right)^n \left(\frac{dk}{dE}\right) \frac{d}{dk} V_n^{(\text{sphere})}(k) \tag{L.19}$$

Thus the density of states with respect to the energy is

$$\rho_E^{(n)}(E) = \left(\frac{L}{\pi}\right)^n \frac{1}{\hbar} \sqrt{\frac{\mu}{2E}} S_n^{(\text{sphere})}(k) \tag{L.20}$$

where $S_n^{(\text{sphere})}(k)$ is the surface of an n-dimensional sphere with radius k.

The density of states of the motion of one free particle is

$$\rho_E^{(3)}(E) = \left(\frac{L}{h}\right)^n 4\pi \, \mu^{3/2} (2E)^{1/2} . \tag{L.21}$$

It is the same as the density of states of the relative motion of two non-interacting free particles.

The density of states of the motion of two free particles is

$$\rho_E^{(6)}(E) = \left(\frac{L}{h}\right)^n \pi^3 \, \mu^3 (2E)^2 . \tag{L.22}$$

It is the same as the density of states of the relative motion of three non-interacting particles.

Appendix M

Spherical Bessel functions and related functions

Bessel functions and related functions are described in many books (see, for example, Refs. [3] and [116]).

Nevertheless, in order to facilitate my own work, I have assembled in this Appendix many important relations involving the Bessel functions, spherical Bessel functions, Riccati-Bessel functions and Riccati-Hankel functions.

M.1 Differential equation

The radial Schrödinger equation for the wavefunction $j_l(x)$ of a free particle can be written as

$$j_l''(x) + \left[1 - \frac{l(l+1)}{x^2} \right] j_l(x) = 0 . \tag{M.1}$$

The coordinate x is kr, where k is the wavenumber of the particle and r the radial distance. By definition, the solution $j_l(x)$ is regular in the origin ($x = 0$). It is called Riccati-Bessel function of the first kind [197].

The Riccati-Bessel function of the second kind, $n_l(x)$, is also called Riccati-Neumann function. Although it obeys the same differential equation (M.1) as the Riccati-Bessel function of the first kind, it is not a physically acceptable solution, because the corresponding three-dimensional wavefunction $(kr)^{-1} n_l(kr) Y_{lm}(\hat{r})$ does not solve the three-dimensional Laplace equation in the origin ($r = 0$).

The Riccati-Bessel functions $j_l(x)$ and $n_l(x)$ are given by

$$j_l(x) = \sqrt{\frac{\pi x}{2}} J_{l+\frac{1}{2}}(x) = (-x)^l \left(\frac{d}{dx} \frac{1}{x} \right)^l \sin x \tag{M.2}$$

$$n_l(x) = \sqrt{\frac{\pi x}{2}} N_{l+\frac{1}{2}}(x) = (-x)^l \left(\frac{d}{dx} \frac{1}{x} \right)^l (-\cos x) \tag{M.3}$$

where $J_\nu(x)$ and $N_\nu(x)$ are Bessel functions of the first and second kind, respectively. $N_\nu(x)$ is also called the Weber or Neumann function; many authors denote it $Y_\nu(x)$. We note the following relation:

$$N_{l+\frac{1}{2}}(x) \;=\; (-1)^{l+1}\, J_{-l-\frac{1}{2}}(x) \;. \tag{M.4}$$

In our notation, the spherical Bessel functions of the first and second kinds are $j_l(x)/x$ and $n_l(x)/x$, respectively.

M.2   Analytic continuation

It is convenient to define $j_l(x)$ and $n_l(x)$ on the open complex x-plane. Since they are real for real x, one can use the Schwartz reflection principle to deduce that

$$j_l(x^*) \;=\; j_l^*(x) \;, \tag{M.5}$$
$$n_l(x^*) \;=\; n_l^*(x) \;. \tag{M.6}$$

The ratio $j_l(x) \,/\, x^{l+1}$ and the product $x^l\, n_l(x)$ are entire functions of x. The irregular solution $n_l(x)$ has a pole of order l in $x = 0$: it is a meromorphic function.

The regular and irregular Riccati-Bessel functions have well-defined parities:

$$j_l(-x) \;=\; (-1)^{l+1}\, j_l(x) \tag{M.7}$$
$$n_l(-x) \;=\; (-1)^l\, n_l(x) \;. \tag{M.8}$$

M.3   Asymptotic behaviour

The asymptotic behaviour of the Riccati-Bessel functions for large x can be derived from the asymptotic expressions

$$\left(\frac{d}{dx}\frac{1}{x}\right)^l \sin x \;\approx\; x^{-l}\frac{d^l}{dx^l}\sin x \;,$$

$$\left(\frac{d}{dx}\frac{1}{x}\right)^l \cos x \;\approx\; x^{-l}\frac{d^l}{dx^l}\cos x \;.$$

The result is

$$j_l(x) \;\approx\; \sin\left(x - \frac{l\pi}{2}\right) \qquad (x \to \infty) \;, \tag{M.9}$$

$$n_l(x) \;\approx\; -\cos\left(x - \frac{l\pi}{2}\right) \qquad (x \to \infty) \;. \tag{M.10}$$

250

Eqs. (M.9) and (M.9) are useful approximations if x is somewhat larger than $\frac{1}{2}(l+1)/2$ [236].

In order to find the behaviour of $j_l(x)$ and $n_l(x)$ at short distances ($x \to 0$), we expand $\sin x$ and $\cos x$ in Taylor series and use the identities

$$\left(\frac{d}{dx}\frac{1}{x}\right)^l x^{2n+1} = \begin{cases} \frac{(2n)!!}{(2n-2l)!!} x^{2n-2l+1} & (l = 0, \ldots, n) \\ 0 & (l > n) \end{cases} \qquad \text{(M.11)}$$

$$\left(\frac{d}{dx}\frac{1}{x}\right)^l x^{2n} = \begin{cases} \frac{(2n-1)!!}{(2n-2l-1)!!} x^{2n-2l} & (l = 0, \ldots, n-1) \\ (2n-1)!! & (l = n) \\ (-1)^{l-n}(2n-1)!!(2n-2l-1)!!\, x^{2n-2l} & (l > n) \end{cases} \qquad \text{(M.12)}$$

The symbol $n!!$ is defined recursively:

$$\begin{aligned} 0!! &= 1 , \\ 1!! &= 1 , \\ n!! &= (n-2)!!\, n \qquad (n = 2, 3, 4, 5, \ldots) , \end{aligned}$$

so that

$$\begin{aligned} (2l)!! &= 2 \cdot 4 \cdot 6 \cdots (2l) , \\ (2l+1)!! &= 1 \cdot 3 \cdot 5 \cdots (2l+1) . \end{aligned}$$

We thus obtain the series

$$\frac{1}{x^{l+1}} j_l(x) = \sum_{n=0}^{\infty} (-1)^n \frac{1}{(2n+2l+1)!!} \frac{1}{(2n)!!} x^{2n} , \qquad \text{(M.13)}$$

$$\begin{aligned} x^l n_l(x) = &-\sum_{n=0}^{l-1} \frac{(2l-2n-1)!!}{(2n)!!} x^{2n} - \frac{1}{(2l)!!} x^{2l} \\ &- \sum_{n=l+1}^{\infty} (-1)^{l+n} \frac{1}{(2n)!!} \frac{1}{(2n-2l-1)!!} x^{2n} . \quad \text{(M.14)} \end{aligned}$$

Retaining only the lowest order terms ($n = 0$ in the above expressions), we obtain

$$j_l(x) = \frac{x^{l+1}}{(2l+1)!!} [1 + \mathcal{O}(x^2)] , \qquad \text{(M.15)}$$

$$n_l(x) = -\frac{(2l+1)!!}{2l+1} \frac{1}{x^l} [1 + \mathcal{O}(x^2)] . \qquad \text{(M.16)}$$

By comparing the second order terms [using the exact Eqs. (M.13) and (M.14)], one sees that Eqs. (M.15) and (M.16) are useful approximations for x^2 somewhat less than $4l+6$ and $4l+2$, respectively.

The function $j_l(x)/x$ is regular in the origin ($x = 0$), whereas $n_l(x)/x$ diverges when $x \to 0$. Therefore j_l and n_l are also referred to as the regular and irregular Riccati Bessel functions.

For real and positive x, they are bounded by the relations

$$|j_l(x)| \leq \text{const} \times \left(\frac{x}{1+x}\right)^{l+1} , \qquad \text{(M.17)}$$

$$|n_l(x)| \leq \text{const} \times \left(\frac{1+x}{x}\right)^{l} . \qquad \text{(M.18)}$$

M.4 Recursion relations

The derivative of the Riccati-Bessel function (M.2) is

$$j_l'(x) = \frac{l+1}{x} j_l(x) - j_{l+1}(x) . \qquad \text{(M.19)}$$

Deriving a second time and using the differential equation (M.1) yields the recursion relation

$$j_l(x) + j_{l+2}(x) = \frac{2l+3}{x} j_{l+1}(x) \qquad \text{(M.20)}$$
$$(l = 0, 1, 2, \ldots)$$

which is equivalent to that of the Bessel functions (see [39]):

$$J_{n-1}(x) + J_{n+1}(x) = \frac{2n}{x} J_n(x) \qquad \text{(M.21)}$$
$$(n = 1, 2, 3, \ldots) .$$

It is tempting to compute the Riccati-Bessel functions of higher orders numerically using the recursion relations. Formally, one may calculate $j_{l+1}(x)$ from $j_l(x)$ and $j_{l-1}(x)$, starting with $l = 1$. Unfortunately, this algorithm is *unstable* [187].

The Wronskian of $j_l(x)$ and $n_l(x)$ is

$$W[j_l, n_l] = j_l(x) n_l'(x) - j_l'(x) n_l(x) = 1 . \qquad \text{(M.22)}$$

This can be shown recursively starting with $W[j_0, n_0] = 1$. The Wronskians for the long-range asymptotic expressions (M.9) and (M.10) and for the short-range asymptotic expressions (M.15) and (M.16) also equal exactly 1.

M.5   Riccati-Hankel functions

Riccati-Hankel functions are defined as

$$
\begin{aligned}
h_l^{(1)}(x) &= j_l(x) + \mathrm{i}n_l(x) \;\rightarrow\; -\mathrm{i}e^{\mathrm{i}(x-l\pi/2)} &&(x \to \infty), &&\text{(M.23)}\\
h_l^{(2)}(x) &= j_l(x) - \mathrm{i}n_l(x) \;\rightarrow\; \mathrm{i}e^{-\mathrm{i}(x-l\pi/2)} &&(x \to \infty). &&\text{(M.24)}
\end{aligned}
$$

The Wronskian of $h_l^{(1)}$ and $h_l^{(2)}$ is

$$
W\left[h_l^{(1)}, h_l^{(2)}\right] = -2\mathrm{i} . \tag{M.25}
$$

The behaviour of $h_l^{(1)}(x)$ and $h_l^{(2)}(x)$ under $x \to -x$ is given by

$$
h_l^{(1)}(-x) = (-1)^{l+1} h_l^{(2)}(x) . \tag{M.26}
$$

The Riccati-Hankel functions are analytic in the whole open x-plane except for a pole of order l in $x = 0$. Using the definitions (M.23) and (M.24) and applying the Schwartz reflection prinicple on $j_l(x)$ and $n_l(x)$ one finds that

$$
h_l^{(1)}(x^*) = h_l^{(2)*}(x) . \tag{M.27}
$$

Bibliography

[1] http://www.daswillichwissen.de/Natrium, 2004.

[2] R. H. Bisseling, R. Kosloff and J. Manz. Dynamics of Hyperspherical and Local Mode Decay Studied by Time Dependent Wave Packet Propagation. *J. Chem. Phys.*, 83:993–1004, 1985.

[3] M. Abramowitz and I. A. E. Stegun. *Handbook of Mathematical Functions with Formulas, Graphs, and Mathematical Tables.* Dover, New York, 10th edition, 1972.

[4] R. Abrol and A. Kuppermann. An optimal adiabatic-to-diabatic transformation of the $1\,^2A'$ and $2\,^2A'$ states of H_3. *J. Chem. Phys.*, 116:1035, 2002.

[5] R. Abrol, A. Shaw, A. Kuppermann, and D. R. Yarkony. Accurate first-derivative nonadiabatic couplings for the H_3 system. *J. Chem. Phys.*, 115:4640, 2001.

[6] S. C. Althorpe. Time-dependent plane wave packet formulation of quantum scattering with application to $H + D_2 \rightarrow HD + D$. *J. Chem. Phys.*, 117(10):4623–4627, 2002.

[7] S. C. Althorpe. Plane wave packet study of direct and time-delayed mechanisms in the F + HD reaction. *Chem. Phys. Lett.*, 370:443, 2003.

[8] S. C. Althorpe. General time-dependent formulation of quantum scattering theory. *Phys. Rev. A*, 69(4):042702, 2004.

[9] S. C. Althorpe. Plane wave packet formulation of atom-plus-diatom quantum reactive scattering. *J. Chem. Phys.*, 121:1175, 2004.

[10] S. C. Althorpe, F. Fernndez-Alonso, B. D. Bean, J. D. Ayers, A. E. Pomerantz, R. N. Zare, and E. Wrede. Observation and interpretation of a time-delayed mechanism in the hydrogen exchange reaction. *Nature*, 416:67, 2002.

[11] Y. Andersson and H. Rydberg. Dispersion Coefficients for van der Waals Complexes, Including C_{60}-C_{60}. *Physica Scripta*, 60:211, 1999.

[12] F. J. Aoiz, L. Bañares, J. F. Castillo, M. Brouard, W. Denzer, C. Vallance, P. Honvault, J.-M. Launay, A. J. Dobbyn, and P. J. Knowles. Insertion and Abstraction Pathways in the Reaction $O(D_2)$ + H_2 → OH + H. *Phys. Rev. Lett.*, 86(9):1729–1732, 2001.

[13] F. J. Aoiz, L. Bañares, J. F. Castillo, V. J. Herrero, B. Martinez-Haya, P. Honvault, J. M. Launay, X. Liu, J. J. Lin, S. A. Harich, C. C. Wang, and X. Yang. The $O(^1D)$ + H_2 reaction at 56 meV collision energy: A comparison between quantum mechanical, quasiclassical trajectory, and crossed beam results. *J. Chem. Phys.*, 116(24):10692–10703, 2002.

[14] A. M. Arthurs and A. Dalgarno. The theory of scattering by a rigid rotator. *Proc. R. Soc. Lond. A*, 256:540, 1960.

[15] B. M. Axilrod and E. Teller. Interaction of the van der Waals type among three atoms. *J. Chem. Phys.*, 11:299–300, 1943.

[16] M. Aymar, C. H. Greene, and E. Luc-Koenig. Multichannel Rydberg spectroscopy of complex atoms. *Rev. Mod. Phys.*, 68:1015, 1996.

[17] L. Bañares, F. J. Aoiz, P. Honvault, B. Bussery-Honvault, and J.-M. Launay. Quantum mechanical and quasi-classical trajectory study of the $C(^1D)$ + H_2 reaction dynamics. *J. Chem. Phys.*, 118(2):565–568, 2003.

[18] N. Balakrishnan. On the role of van der Waals interaction in chemical reactions at low temperatures. *J. Chem. Phys.*, 121(12):5563–5566, 2004.

[19] N. Balakrishnan, A. Dalgarno, and R. C. Forrey. Vibrational relaxation of CO by collisions with ^{4}He at ultracold temperatures. *J. Chem. Phys.*, 113(2):621–627, 2000.

[20] N. Balakrishnan, R. C. Forrey, and A. Dalgarno. Quenching of H_2 Vibrations in Ultracold ^{3}He and ^{4}He Collisions. *Phys. Rev. Lett.*, 80:3224, 1998.

[21] N. Balucani, G. Capozza, L. Cartechini, A. Bergeat, R. Bobbenkamp, P. Casavecchia, F. J. Aoiz, L. Bañares, P. Honvault, B. Bussery-Honvault, and J.-M. Launay. Dynamics of the insertion reaction $C(1D)$+ H_2: A comparison of crossed molecular beam experiments with quasiclassical trajectory and quantum mechanical scattering calculations. *Phys. Chem. Chem. Phys.*, 6(21):4957, 2004.

[22] N. Balucani, L. Cartechini, G. Capozza, E. Segoloni, P. Casavecchia, G. G.Volpi, F. J. Aoiz, L. Bañares, P. Honvault, and J.-M. Launay. Quantum Effects in the Differential Cross Sections for the Insertion Reaction N(D) + H$_2$. *Phys. Rev. Lett.*, 89(1):013201, 2002.

[23] L. Bañares, F. J. Aoiz, P. Honvault, and J.-M. Launay. Dynamics of the S(^1D) + H$_2$ Insertion Reaction: A Combined Quantum Mechanical and Quasiclassical Trajectory Study. *J. Phys. Chem. A*, 108:1616, 2004.

[24] Z. Bačić and J. Z. H. Zhang. A new D_{3h} symmetry-adapted method for highly excited vibrational levels of floppy triatomics: the H$_3^+$ molecule. *Chem. Phys. Lett.*, 184:513, 1991.

[25] Z. Bačić and J. Z. H. Zhang. High-lying rovibrational states of floppy X$_3$ triatomics by a new D_3h symmetry adapted method: Application to the H$_3^+$ molecule. *J. Chem. Phys.*, 96(5):3707–3713, 1992.

[26] D. Baye, M. Hesse, and M. Vincke. The unexplained accuracy of the Lagrange-mesh method. *Phys. Rev. E*, 65:026701, 2002.

[27] R. J. Bell. Multipolar expansion for the non-additive third-order interaction energy of three atoms. *J. Phys. B: Atomic Molecular and Optical Physics*, 3(6):751–762, 1970.

[28] H. L. Bethlem, G. Berden, F. M. H. Crompvoets, R. T. Jongma, A. J. A. van Roij, and G. Meijer. Electrostatic trapping of ammonia molecules. *Nature*, 406:491–94, 2000.

[29] H. L. Bethlem, G. Berden, A. J. A. van Roij, F. M. H. Crompvoets, and G. Meijer. Trapping neutral molecules in a traveling potential well. *Phys. Rev. Lett.*, 84:5744–47, 2000.

[30] H. L. Bethlem, F. M. H. Crompvoets, R. T. Jongma, S. Y. T. van de Meerakker, and G. Meijer. Deceleration and trapping of ammonia using time-varying electric fields. *Phys. Rev. A*, 65:053416, 2002.

[31] D. Blume, C. H. Greene, and B. D. Esry. Comparative study of He$_3$, Ne$_3$, and Ar$_3$ using hyperspherical coordinates. *J. Chem. Phys.*, 113(6):2145–2158, 2000.

[32] R. K. Bock and W. Krischer. *Accelerator Physics - The Data Analysis BriefBook*. Springer, Berlin, 1998.

[33] E. Bodo, F. A. Gianturco, F. Sebastianelli, E. Yurtsever, and M. Yurtsever. Rotational cooling of Li$_2$ ($^1\Sigma_g+$) molecules by ultracold collisions with a helium gas buffer. *Theor. Chim. Acta*, 112:263, 2004.

[34] J. L. Bohn, B. D. Esry, and C. H. Green. Effective potentials for dilute Bose-Einstein condensates. *Phys. Rev. A*, 58:584, 1998.

[35] A. G. Borisov. Solution of the radial Schrödinger equation in cylindrical and spherical coordinates by mapped Fourier transform algorithms. *J. Chem. Phys.*, 114(18):7770, 2001.

[36] J. P. Boyd. A fast algorithm for Chebyshev, Fourier, and sinc interpolation onto an irregular grid. *J. Comp. Phys.*, 103:243, 1992.

[37] J. P. Boyd, C. Rangan, and P. H. Bucksbaum. Pseudospectral methods on a semi-infinite interval with application to the hydrogen atom: a comparison of the mapped Fourier-sine method with Laguerre series and rational Chebyshev expansions. *J. Comp. Phys.*, 188:56, 2003.

[38] S. E. Branchett, S. B. Padkjaer, and J.-M. Launay. Quantum dynamical study of the H + HCl → H_2 + Cl reaction. *Chem. Phys. Lett.*, 208:523, 1993.

[39] I. N. Bronstein, K. A. Semendyaev, G. Musiol, and H. Mühlig. *Taschenbuch der Mathematik*. Verlag Harri Deutsch, Thun, Frankfurt am Main, 2nd edition, 1995.

[40] D. A. Brue, X. Li, and G. A. Parker. Conical intersection between the lowest spin-aligned Li_3 ($^4A'$)) potential-energy surfaces. *J. Chem. Phys.*, 123(9):091101, 2005.

[41] N. Buck, L. C. Biedenharn, and R. Y. Cusson. Collective variables for the description of rotational motion in many particle systems. *Nucl. Phys. A*, 317:205, 1979.

[42] A. D. Buckingham, P. W. Fowler, and J. M. Hutson. Theoretical studies of van der Waals molecules and intermolecular forces. *Chem. Rev.*, 88:963, 1988.

[43] P. R. Bunker and P. Jensen. *Fundamentals of Molecular Symmetry*. Institute of Physics Publishing, 2004.

[44] J. P. Burke, C. H. Greene, and J. L. Bohn. Multichannel Cold Collisions: Simple Dependences on Energy and Magnetic Field. *Phys. Rev. Lett.*, 81(16):3355, 1998.

[45] B. Bussery-Honvault, P. Honvault, and J.-M. Launay. A study of the C(^1D) + H_2 → CH + H reaction: Global potential energy surface and quantum dynamics. *J. Chem. Phys.*, 115(23):10701–10708, 2001.

[46] F. Calogero. *Variable phase approach to potential scattering.* Academic Press, New York, 1967.

[47] T. Carrington. The advantage of writing kinetic energy operators in polyspherical curvilinear coordinates in terms of $z_i = \cos\phi_i$. *J. Chem. Phys.*, 112:4413, 2000.

[48] H. B. G. Casimir and D. Polder. The Influence of Retardation on the London-van der Waals Forces. *Phys. Rev.*, 73:360, 1948.

[49] G. Chalasinski and M. Gutowski. Weak interactions between small systems. Models for studying the nature of intermolecular forces and challenging problems for ab initio calculations. *Chem. Rev.*, 88:943, 1988.

[50] X. Chapuisat, A. Nauts, and G. Durand. A method to obtain the Eckart hamiltonian and the equations of motion of a highly deformable polyatomic system in tems of generalized coordinates. *Chem. Phys.*, 56:91, 1981.

[51] N. R. Claussen, E. A. Donley, S. T. Thompson, and C. E. Wieman. Microscopic Dynamics in a Strongly Interacting Bose-Einstein Condensate. *Phys. Rev. Lett.*, 89(1):010401, 2002.

[52] F. Cocchini, T. H. Upton, and W. Andreoni. Excited states and Jahn–Teller interactions in the sodium trimer. *J. Chem. Phys.*, 88(10):6068–6077, 1988.

[53] F. D. Colavecchia, J. P. Burke, Jr., W. J. Stevens, M. R. Salazar, G. A. Parker, and R. T. Pack. The potential energy surface for spin-aligned $Li_3(1\,^4A')$ and the potential energy curve for spin-aligned $Li_2(a\,^3\Sigma_u^+)$. *J. Chem. Phys.*, 118(12):5484–5495, 2003.

[54] F. D. Colavecchia, F. Mrugala, G. A. Parker, and R. T. Pack. Accurate quantum calculations on three-body collisions in recombination and collision-induced dissociation. II. The smooth variable discretization enhanced renormalized Numerov propagator. *J. Chem. Phys.*, 118:10387, 2003.

[55] D. T. Colbert and W. H. Miller. A novel discrete variable representation for quantum mechanical reactive scattering via the S-matrix Kohn method. *J. Chem. Phys.*, 96:1982, 1992.

[56] A. R. Cooper, S. Jain, and J. M. Hutson. Methods for calculating the bound state energies of van der Waals trimers: Applications to Ar_3. *J. Chem. Phys.*, 98:2160, 1993.

[57] A. Crubellier, O. Dulieu, F. Masnou-Seeuws, M. Elbs, H. Knöckel, and E. Tiemann. Simple determination of Na$_2$ scattering lengths using observed bound levels at the ground state asymptote. *Eur. Phys. J. D*, 6:211, 1999.

[58] J. Cubizolles, T. Bourdel, S. J. J. M. F. Kokkelmans, G. V. Shlyapnikov, and C. Salomon. Production of Long-Lived Ultracold Li$_2$ Molecules from a Fermi Gas. *Phys. Rev. Lett.*, 91(24):240401, 2003.

[59] M. T. Cvitaš, P. Soldàn, J. M. Hutson, P. Honvault, and J.-M. Launay. Ultracold Li + Li$_2$ Collisions: Bosonic and Fermionic Cases. *Phys. Rev. Lett.*, 94(3):033201, 2005.

[60] A. Dalgarno and W. D. Davison. The Calculation of Van der Waals Interactions. *Adv. At. Mol. Phys.*, 2:1, 1966.

[61] A. S. Davydov. *Quantum mechanics*. Pergamon press, 2nd edition, 1991.

[62] L. E. E. de Araujo, J. D. Weinstein, S. D. Gensemer, F. K. Fatemi, K. M. Jones, P. D. Lett, and E. Tiesinga. Two-color photoassociation spectroscopy of the lowest triplet potential of Na$_2$. *J. Chem. Phys.*, 119:2062, 2003.

[63] R. de Vogelaere. A method for the numerical integration of differential equations of second order without explicit first derivatives. *J. Res. Nat. Bur. Standards*, 54:119–125, 1955.

[64] A. Derevianko, W. R. Johnson, M. S. Safronova, and J. F. Babb. High-Precision Calculations of Dispersion Coefficients, Static Dipole Polarizabilities, and Atom-Wall Interaction Constants for Alkali-Metal Atoms. *Phys. Rev. Lett.*, 82:3589, 1999.

[65] E. A. Donley, N. R. Claussen, S. T. Thompson, and C. E. Wieman. Atom-molecule coherence in a Bose-Einstein condensate. *Nature*, 417:529, 2002.

[66] M. B. Doran and I. J. Zucker. Higher order multipole three-body van der Waals interactions and stability of rare gas solids. *J. Phys. C: Solid State Phys.*, 4(3):307–312, 1971.

[67] K. M. Dunseath, J.-M. Launay, M. Terao-Dunseath, and L. Mouret. Schwartz interpolation for problems involving the Coulomb potential. *J. Phys. B: Atomic Molecular and Optical Physics*, 35:3539, 2002.

[68] S. Dürr, T. Volz, A. Marte, and G. Rempe. Observation of Molecules Produced from a Bose-Einstein Condensate. *Phys. Rev. Lett.*, 92(2):020406, 2004.

[69] E. Nielsen and H. Suno and B. D. Esry. Efimov resonances in atom-diatom scattering. *Phys. Rev. A*, 66:012705, 2003.

[70] A. R. Edmonds. *Angular Momentum in Quantum Mechanics*. Princeton University Press, 2nd edition, 1960.

[71] V. Efimov. Energy levels arising from resonant two-body forces in a three-body system. *Phys. Lett. B*, 33:563, 1970.

[72] F. O. Ellison. A Method of Diatomics in Molecules. I. General Theory and Application to H_2O. *J. Am. Chem. Soc.*, 85:3540, 1963.

[73] F. O. Ellison, N. T. Huff, and J. C. Patel. A Method of Diatomics in Molecules. II. H_3 and H_3^+. *J. Am. Chem. Soc.*, 85:3544, 1963.

[74] B. D. Esry, C. H. Greene, and J. James P. Burke. Recombination of Three Atoms in the Ultracold Limit. *Phys. Rev. Lett.*, 83:1751, 1999.

[75] B. D. Esry, C. D. Lin, and C. H. Greene. Adiabatic hyperspherical study of the helium trimer. *Phys. Rev. A*, 54:394, 1996.

[76] B. D. Esry and H. R. Sadeghpour. Split diabatic representation. *Phys. Rev. A*, 68(4):042706, 2003.

[77] H. Essén. Quantization and independent coordinates. *Am. J. Phys.*, 46:983, 1978.

[78] A. Färbert and W. Demtröder. Fine and hyperfine structure of the triplet states $1^3\Sigma_u^+$ and $1^3\Sigma_g^+$ of the Na_2 molecule. *Chem. Phys. Lett.*, 264:225, 1997.

[79] A. Färbert, J. Koch, T. Platz, and W. Demtröder. Vibrationally resolved resonant two-photon ionization spectroscopy of the $1\ ^3\Sigma_g^+ g(b) \rightarrow 1^3\Sigma_u^+(X)$ transition of Na_2 . *Chem. Phys. Lett.*, 223:546, 1994.

[80] F. K. Fatemi, K. M. Jones, P. D. Lett, and E. Tiesinga. Ultracold ground-state molecule production in sodium. *Phys. Rev. A*, 66(5):053401, 2002.

[81] E. Fattal, R. Baer, and R. Kosloff. Phase space approach for optimizing grid representations: The mapped Fourier method. *Phys. Rev. E*, 53:1217, 1996.

[82] D. Field and L. B. Madsen. Time delays in cold elastic scattering. *J. Chem. Phys.*, 118:1679, 2003.

[83] A. Fioretti, D. Comparat, A. Crubellier, O. Dulieu, F. Masnou-Seeuws, and P. Pillet. Formation of cold Cs_2 molecules through photoassociation. *Phys. Rev. Lett.*, 80:4402–4405, 1998.

[84] A. Fioretti, J. Lozeille, C. Massa, M. Mazzoni, and C. Gabbanini. An optical trap for cold rubidium molecules. *Opt. Comm.*, 243:203, 2004.

[85] D. R. Flower, G. Bourhis, and J.-M. Launay. Molcol: A program for solving atomic and molecular collision problems. *Comp. Phys. Comm.*, 131:187, 2000.

[86] V. Fock. On the Schrödinger equation of the helium atom. *D. Kon. Nors. Vidensk. Selsk. Forh.*, 31:138, 1958.

[87] I. Fourré and M. Raoult. Application of generalized quantum defect theory to van der Waals complex bound state calculations. *J. Chem. Phys.*, 101(10):8709, 1994.

[88] J. H. Frederick and C. Woywod. General formulation of the vibrational kinetic energy operator in internal bond-angle coordinates. *J. Chem. Phys.*, 111:7255, 1999.

[89] J. G. Frey and B. J. Howard. The calculation of the ground state energy of weakly bound van der waals trimers using the method of hyperspherical harmonics I. The Born-Oppenheimer and adiabatic approximations. *Chem. Phys.*, 99:415, 1985.

[90] E. J. Friedman-Hill and R. W. Field. A reexamination of the Rydberg–Klein–Rees potential of the $a\ ^3\Sigma_u^+$ state of Na_2. *J. Chem. Phys.*, 96(4):2444–2448, 1992.

[91] C. Gabbanini, A. Fioretti, A. Lucchesini, S. Gozzini, and M. Mazzoni. Observation of translationally cold ground state rubidium molecules. *Phys. Rev. Lett.*, 84:2814–2817, 2000.

[92] S. M. Gatica, M. M. Calbi, M. W. Cole, and D. Velegol. Three-body interactions involving clusters and films. *Phys. Rev. B*, 68(20):205409, 2003.

[93] J. P. Gauyacq. Time delay for resonant vibrational excitation in electron–molecule collisions. *J. Chem. Phys.*, 93(1):384–392, 1990.

[94] D. Gottlieb and S. A. Orszag. *Numerical analysis of spectral methods: Theory and applications.* CBMS-NSF Regional Conference Series in Applied Mathematics, No. 26. Society for Industrial and Applied Mathematics, Philadelphia, Pa., 1977.

[95] E. Guarini, G. Casanova, U. Bafile, F. Formisano, R. Magli, and F. Barocchi. Direct determination of long-range dipolar interactions in Kr by neutron diffraction. *Europhys. Lett.*, 49:62, 2000.

[96] M. Gutowski. Highly accurate *ab initio* calculation of the interaction potential for two sodium atoms with parallel spins. *J. Chem. Phys.*, 110:4695, 1999.

[97] J. Herbig, T. Kraemer, M. Mark, T. Weber, C. Chin, H.-C. Nagerl, and R. Grimm. Preparation of a Pure Molecular Quantum Gas. *Science*, 301(5639):1510–1513, 2003.

[98] J. Higgins, C. Callegari, J. Reho, F. Stienkemeier, W. E. Ernst, M. Gutowski, and G. Scoles. Helium Cluster Isolation Spectroscopy of Alkali Dimers in the Triplet Manifold. *J. Phys. Chem. A*, 102:4952, 1998.

[99] J. Higgins, W. E. Ernst, C. Callegari, J. Reho, K. K. Lehmann, and G. Scoles. Spin Polarized Alkali Clusters: Observation of Quartet States of the Sodium Trimer. *Phys. Rev. Lett.*, 22:4532, 1996.

[100] J. Higgins, T. Hollebeek, J. Reho, T.-S. Ho, K. K. Lehmann, H. Rabitz, G. Scoles, and M. Gutowski. On the importance of exchange effects in three-body interactions: The lowest quartet state of Na_3. *J. Chem. Phys.*, 112(13):5751, 2000.

[101] T.-S. Ho, H. Rabitz, and G. Scoles. Reproducing kernel technique for extracting accurate potentials from spectral data: Potential curves of the lowest states $X^1\Sigma_g^+$ and $a^3\Sigma_u^+$ of the sodium dimer. *J. Chem. Phys.*, 112:6218, 2000.

[102] P. Hobza and R. Zahradník. Intermolecular interactions between medium-sized systems. Nonempirical and empirical calculations of interaction energies. Successes and failures. *Chem. Rev.*, 88:871, 1988.

[103] P. Honvault and J.-M. Launay. Quantum mechanical study of the F + $D_2 \rightarrow$ DF + D reaction. *Chem. Phys. Lett.*, 287:270, 1998.

[104] P. Honvault and J.-M. Launay. A quantum-mechanical study of the dynamics of the $N(^2D)$ + $H_2 \rightarrow$ NH + H reaction. *J. Chem. Phys.*, 111(15):6665–6667, 1999.

[105] P. Honvault and J.-M. Launay. Effect of spin-orbit corrections on the F + $D_2 \rightarrow$ DF + D reaction. *Chem. Phys. Lett.*, 303:657, 1999.

[106] P. Honvault and J.-M. Launay. Quantum chaos in atom-diatom reactive collisions. *Chem. Phys. Lett.*, 329:233, 2000.

[107] P. Honvault and J.-M. Launay. A quantum-mechanical study of the dynamics of the $O(^1D)$ + $H_2 \rightarrow$ OH + H insertion reaction. *J. Chem. Phys.*, 114(3):1057–1059, 2001.

[108] P. Honvault and J.-M. Launay. Dynamics of the $S(^1D)$ + $H_2 \rightarrow$ SH + H reaction: a quantitative description using an accurate quantum method. *Chem. Phys. Lett.*, 370:371, 2003.

[109] P. Honvault, J.-M. Launay, P. Soldàn, M. T. Cvitaš, and J. Hutson. Quantum dynamics of ultracold alkali + alkali dimer collisions. In *Interactions of Cold Atoms and Molecules*, page 20. CCP6, Daresbury, 2002.

[110] R. E. Howard, R. E. Roberts, and M. J. DelleDonne. Three-body effects in the exchange and dissociation encounters for $Ar+Ar_2$. *J. Chem. Phys.*, 65(8):3067–3074, 1976.

[111] F. Huarte-Larrañaga, X. Gimnez, J. M. Lucas, A. Aguilar, and J.-M. Launay. Exact quantum 3D cross sections for the Ne + $H_2^+ \rightarrow$ NeH^+ + H reaction by the hyperspherical method. Comparison with approximate quantum mechanical and classical results. *Phys. Chem. Chem. Phys.*, 1:1125, 1999.

[112] F. Huarte-Larrañaga, X. Gimnez, J. M. Lucas, A. Aguilar, and J.-M. Launay. Detailed Energy Dependences of Cross Sections and Rotational Distributions for the Ne + $H_2^+ \rightarrow$ NeH^+ + H Reaction. *J. Phys. Chem. A*, 104:10227, 2000.

[113] J. J. Hudson, B. E. Sauer, M. R. Tarbutt, and E. A. Hinds. Measurement of the electron dipole moment using YbF molecules. *Phys. Rev. Lett.*, 89:023003, 2002.

[114] J. M. Hutson and S. Jain. On the coupled-channel calculation of bound states for trimeric systems using hyperspherical coordinates. *J. Chem. Phys.*, 91:4197, 1989.

[115] I. A. Ivanov. Reconstruction of phase shifts as functions of energy using bound-state energies and low-energy scattering data. *Phys. Rev. A*, 67(3):032704, 2003.

[116] J. D. Jackson. *Classical Electrodynamics.* John Wiley & Sons, Inc., 3rd edition, 1998.

[117] A. S. Jensen, K. Riisager, D. V. Fedorov, and E. Garrido. Structure and reactions of quantum halos. *Rev. Mod. Phys.*, 76(1):215, 2004.

[118] B. Jeziorski, R. Moszynski, and K. Szalewicz. Perturbation Theory Approach to Intermolecular Potential Energy Surfaces of van der Waals Complexes. *Chem. Rev.*, 93:1887, 1993.

[119] S. Jochim, M. Bartenstein, A. Altmeyer, G. Hendl, C. Chin, J. H. Denschlag, and R. Grimm. Pure Gas of Optically Trapped Molecules Created from Fermionic Atoms. *Phys. Rev. Lett.*, 91(24):240402, 2003.

[120] S. Jochim, M. Bartenstein, A. Altmeyer, G. Hendl, S. Riedl, C. Chin, J. Hecker Denschlag, and R. Grimm. Bose-Einstein Condensation of Molecules. *Science*, 302(5653):2101–2103, 2003.

[121] B. R. Johnson. The multichannel log-derivative method for scattering calculations. *J. Comp. Phys.*, 14:445, 1973.

[122] B. R. Johnson. On hyperspherical coordinates and mapping the internal configurations of a three-body system. *J. Chem. Phys.*, 73:5051, 1980.

[123] B. R. Johnson. The classical dynamics of three particles in hyperspherical coordinates. *J. Chem. Phys.*, 79:1906, 1983.

[124] B. R. Johnson. The quantum dynamics of three particles in hyperspherical coordinates. *J. Chem. Phys.*, 79:1916, 1983.

[125] J. C. Juanes-Marcos and S. C. Althorpe. On the role of the conical intersection in H + H_2 reactive scattering. *Chem. Phys. Lett.*, 381:743, 2003.

[126] C. Jungen and F. Texier. On the construction of basis functions for quantum defect theory in arbitrary fields. *J. Phys. B: Atomic Molecular and Optical Physics*, 33:2495, 2000.

[127] G. Katz, K. Yamashita, Y. Zeiri, and R. Kosloff. The Fourier method for tri-atomic systems in the search for the optimal coordinate system. *J. Chem. Phys.*, 116(11):4403, 2002.

[128] A. J. Kerman, J. M. Sage, S. Sainis, T. Bergeman, and D. DeMille. Production and State-Selective Detection of Ultracold RbCs Molecules. *Phys. Rev. Lett.*, 92(15):153001, 2004.

[129] A. J. Kerman, J. M. Sage, S. Sainis, T. Bergeman, and D. DeMille. Production of Ultracold, Polar RbCs* Molecules via Photoassociation. *Phys. Rev. Lett.*, 92(3):033004, 2004.

[130] C. P. Koch, F. Masnou-Seeuws, and R. Kosloff. Creating Ground State Molecules with Optical Feshbach Resonances in Tight Traps. *Phys. Rev. Lett.*, 94(19):193001, 2005.

[131] C. P. Koch, J. P. Palao, R. Kosloff, and F. Masnou-Seeuws. Stabilization of ultracold molecules using optimal control theory. *Phys. Rev. A*, 70(1):013402, 2004.

[132] T. Koehler. Production of three-body Efimov molecules in an optical lattice, 12 2004. Talk at Laboratoire Aimé-Cotton.

[133] V. Kokoouline. private communication, 2005.

[134] V. Kokoouline, C. Drag, P. Pillet, and F. Masnou-Seeuws. Lu-Fano plot for interpretation of the photoassociation spectra. *Phys. Rev. A*, 65(6):062710, 2002.

[135] V. Kokoouline, O. Dulieu, R. Kosloff, and F. Masnou-Seeuws. Mapped Fourier methods for long range molecules: Application to perturbations in the $Rb_2(0_u^+)$ spectrum. *J. Chem. Phys.*, 110:9865, 1999.

[136] V. Kokoouline, O. Dulieu, R. Kosloff, and F. Masnou-Seeuws. Theoretical treatment of channel mixing in excited Rb_2 and Cs_2 ultra-cold molecules: determination of predissociation lifetimes with coordinate mapping. *Phys. Rev. A*, 62:032716, 2000.

[137] V. Kokoouline, O. Dulieu, and F. Masnou-Seeuws. Theoretical treatment of channel mixing in excited Rb_2 and Cs_2 ultra-cold molecules. perturbations in 0_u^+ photoassociation and fluorescence spectra. *Phys. Rev. A*, 62:022504, 2000.

[138] V. Kokoouline and C. H. Greene. Unified theoretical treatment of dissociative recombination of D_{3h} triatomic ions: Application to H_3^+ and D_3^+. *Phys. Rev. A*, 68:012703, 2003.

[139] V. Kokoouline, C. H. Greene, and E. B. D. Mechanism for the destruction of H_3^+ ions by electron impact. *Nature*, 412:891, 2001.

[140] D. D. Konowalow and M. E. Rosenkrantz. Long-range Interactions of $Na(3s\ ^2S)$ with $Na(3s\ ^2S)$ or $Na(3p\ ^2P)$. *J. Phys. Chem.*, 86:1099, 1982.

[141] R. Kosloff. Time Dependent Methods in Molecular Dynamics. *J. Phys. Chem.*, 92:2087–2100, 1988.

[142] R. Kosloff. Quantum molecular Dynamics on Grids. In R. H. Wyatt and J. Z. H. Zhang, editor, *Dynamics of Molecules and Chemical Reactions*, page 185. Marcel Dekker, New York, 1996.

[143] M. A. Kostin, O. L. Polyansky, and J. Tennyson. Calculations of rotation-vibration states with the z axis perpendicular to the plane: High accuracy results for H_3^+. *J. Chem. Phys.*, 116(17):7564–7573, 2002.

[144] V. V. Kresin, G. Tikhonov, V. Kasperovich, K. Wong, and P. Brockhaus. Long-range van der Waals forces between alkali clusters and atoms. *J. Chem. Phys.*, 108:6660, 1998.

[145] R. d. L. Kronig and I. I. Rabi. The Symmetrical Top in the Undulatory Mechanics. *Phys. Rev.*, 29:262, 1927.

[146] C. Kubach and N. Rougeau. On the use of a Born-Oppenheimer type separation in the treatment of the dynamics of molecular collisions. *J. Mol. Struct.*, 424:171, 1998.

[147] A. Kuppermann and G. C. Schatz. Quantum mechanical reactive scattering: An accurate three-dimensional calculation. *J. Chem. Phys.*, 62(6):2502–2504, 1975.

[148] A. Kuppermann, G. C. Schatz, and M. Baer. Coplanar and collinear quantum mechanical reactive scattering: The importance of virtual vibrational channels in the H + H_2 exchange reaction. *J. Chem. Phys.*, 61(10):4362–4363, 1974.

[149] A. Kuppermann and Y.-S. M. Wu. Sensitivity of the geometric phase effect to resonances, the potential energy surface, the partial wave sum, and the energy. *Chem. Phys. Lett.*, 349:537, 2001.

[150] L. Landau and E. Lifchitz. *Mécanique quantique*. Éditions Mir, Moscow, 3rd edition, 1974.

[151] L. Landau and E. Lifchitz. *Théorie des Champs*. Éditions Mir, Moscow, 5th edition, 1994.

[152] J.-M. Launay. Body-fixed formulation of rotational excitation: exact and centrifugal decoupling results for CO-He. *J. Phys. B: Atomic Molecular and Optical Physics*, 9:1823, 1976.

[153] J.-M. Launay. Computation of cross sections for the atomic fluorine + hydrogen($v = 0, j = 0$) → hydrogen fluoride($v'j$) + atomic hydrogen reaction by the hyperspherical method. *Theor. Chim. Acta*, 79:183, 1991.

[154] J.-M. Launay. Introduction to the quantum theory of reactive scattering. In *Dynamical Processes in Molecular Physics: Lectures from the first EPS Southern European School of Physics, Avila, September 1991*, pages 97–120. G. Delgado-Barrio (IOP Publishing Company), 1993.

[155] J.-M. Launay. Private communication, 2004.

[156] J.-M. Launay and M. Le Dourneuf. Hyperspherical description of collinear reactive scattering. *J. Phys. B: Atomic Molecular and Optical Physics*, 15(13):L455, 1982.

[157] J.-M. Launay and M. Le Dourneuf. Hyperspherical close-coupling equations of integral cross sections for the reaction H + H$_2$ → H$_2$ + H. *Chem. Phys. Lett.*, 163:178, 1989.

[158] J.-M. Launay and M. Le Dourneuf. Quantum-mechanical calculation of integral cross sections for the reaction F + H$_2$($v = 0, j = 0$) → FH($v'j'$) + H by the hyperspherical method. *Chem. Phys. Lett.*, 169:473, 1990.

[159] J.-M. Launay and S. B. Padkjr. Quantum-dynamical study of the Cl + H$_2$ → ClH + H reaction. *Chem. Phys. Lett.*, 181:95, 1991.

[160] M. Leduc, M. Portier, J. Lonard, M. Walhout, F. Masnou-Seeuws, K. Willner, and A. Mosk. Photoassociation spectroscopy of ultracold metastable helium atoms: numerical analysis. In *Laser Spectroscopy. Proceedings of the XVIth International Conference, Palm Cove, Far North Queensland, Australia 13 - 18 July 2003*. World Scientific, New Jersey, 2004.

[161] D. Lemoine. Optimized grid representations in curvilinear coordinates: the mapped sine Fourier method. *Chem. Phys. Lett.*, 210:492, 2000.

[162] J. Léonard, A. P. Mosk, M. Walhout, P. van der Straten, M. Leduc, and C. Cohen-Tannoudji. Analysis of photoassociation spectra for giant helium dimers. *Phys. Rev. A*, 69(3):032702, 2004.

[163] J. Léonard, M. Walhout, A. P. Mosk, T. Müller, M. Leduc, and C. Cohen-Tannoudji. Giant Helium Dimers Produced by Photoassociation of Ultracold Metastable Atoms. *Phys. Rev. Lett.*, 91:073203, 2003.

[164] B. Lepetit and J.-M. Launay. Quantum mechanical study of the reaction $He + H_2^+ \rightarrow HeH^+ + H$. *J. Chem. Phys.*, 95:5159, 1991.

[165] B. Lepetit, J.-M. Launay, and M. Le Dourneuf. Quantum study of electronically non-adiabatic collinear reactions. I. Hyperspherical description of the electronuclear dynamics. *Chem. Phys.*, 106:103, 1986.

[166] B. Lepetit, J.-M. Launay, and M. Le Dourneuf. Quantum study of electronically non-adiabatic collinear reactions. II. Influence of spin-orbit transitions on the F + HH reaction. *Chem. Phys.*, 106:111, 1986.

[167] D. L. Levier. *Etude de la collision réactive $Li+H_2 \rightarrow LiH+H$* . Phd thesis, Université Paris-Sud, Centre d'Orsay, 1995.

[168] B. R. Levy and J. B. Keller. Low-Energy Expansion of Scattering Phase Shifts for Long-Range Potentials. *J. Math. Phys.*, 4:54, 1963.

[169] L. Li, S. F. Rice, and R. W. Field. The Na_2 $a^3\Sigma_u^+$ state. Rotationally resolved OODR $3\Pi_g$ - $a^3\Sigma_u^+$ fluorescence spectroscopy. *J. Chem. Phys.*, 82:1178, 1985.

[170] F. J. Lin and J. T. Muckerman. Solution of the time-dependent Schrdinger equation employing a basis of explicit discrete-coordinate eigenfunctions: spherical and azimuthal symmetry, adiabaticity, and multiphoton excitation of a rotating Morse oscillator. *Comp. Phys. Comm.*, 63:538, 1990.

[171] B. Lindberg. A new efficient method for calculation of energy eigenvalues and eigenstates of the one-dimensional Schrödinger equation. *J. Chem. Phys.*, 88:3805, 1988.

[172] R. G. Littlejohn and M. Reinsch. Gauge fields in the separation of rotations and internal motions in the n-body problem. *Rev. Mod. Phys.*, 69:213, 1997.

[173] F. London-Berlin. Quantenmechanische Deutung des Vorgangs der Aktivierung. *Zeitschrift für Elektrochemie*, 35(9):552, 1929.

[174] V. F. Lotrich and K. Szalewicz. Three-Body Contribution to Binding Energy of Solid Argon and Analysis of Crystal Structure. *Phys. Rev. Lett.*, 79:1301, 1997.

[175] E. Luc-Koenig, R. Kosloff, F. Masnou-Seeuws, and M. Vatasescu. Photoassociation of cold atoms with chirped laser pulses: Time-dependent calculations and analysis of the adiabatic transfer within a two-state model. *Phys. Rev. A*, 70(3):033414, 2004.

[176] E. Luc-Koenig, M. Vatasescu, and F. Masnou-Seeuws. Optimizing the photoassociation of cold atoms by use of chirped laser pulses. *Eur. Phys. J. D*, 31:239, 2004.

[177] T. J. Lukka. A simple method for the derivation of exact quantum-mechanical vibration–rotation Hamiltonians in terms of internal coordinates. *J. Chem. Phys.*, 102:3945, 1995.

[178] S. Magnier. *Détermination des états électroniques excités des molécules Na₂ et Ka₂*. Phd thesis, Université Paris-Sud, Centre d'Orsay, 1993.

[179] S. Magnier, P. Millié, O. Dulieu, and F. Masnou-Seeuws. Potential curves for the ground and excited states of the Na_2 molecule up to the $(3s + 5p)$ dissociation limit: Results of two different effective potential calculations. *J. Chem. Phys.*, 98:7113, 1993.

[180] S. Mahapatra and N. Sathyamurthy. Correlation function approach to transition state resonances in collinear (He,H) collisions. *J. Chem. Phys.*, 102:6057, 1995.

[181] M. Mancini, G. Telles, A. Caires, V. Bagnato, and L. Marcassa. Observation of ultracold ground-state heteronuclear molecules. *Phys. Rev. Lett.*, 92:133203, 2004.

[182] D. E. Manolopoulos. An improved log derivative method for inelastic scattering. *J. Chem. Phys.*, 85(11):6425, 1986.

[183] H. Margenau. Van der Waals forces. *Rev. Mod. Phys.*, 11:1, 1939.

[184] M. Marinescu, H. R. Sadeghpour, and A. Dalgarno. Dispersion coefficients for alkali-metal dimers. *Phys. Rev. A*, 49:982, 1994.

[185] R. Martinazzo, E. Bodo, and F. A. Gianturco. A modified Variable-Phase algorithm for multichannel scattering with long-range potentials. *Comp. Phys. Comm.*, 151:187, 2003.

[186] B. Martínez-Haya, F. J. Aoiz, L. Bañares, P. Honvault, and J. M. Launay. Quantum mechanical and quasiclassical trajectory study of state-to-state differential cross sections for the F + D_2 → DF + D reaction in the center-of-mass and laboratory frames. *Phys. Chem. Chem. Phys.*, 1:3415, 1999.

[187] J. Mathews and R. L. Walker. *Mathematical Methods of Physics*. W. A. Benjamin, Inc., New York, 2nd edition, 1970.

[188] H. Mayer. Construction of the hyperspherical functions for the quantum mechanics of three particles. *J. Phys. A: Math. Gen.*, 8:1562, 1975.

[189] C. A. Mead. The geometric phase in molecular systems. *Rev. Mod. Phys.*, 64:51, 1992.

[190] A. V. Meremianin. Body frames in the separation of collective angles in quantum N-body problems. *Chem. Phys. Lett.*, 120:7861, 2004.

[191] R. Meyer. Trigonometric interpolation method for one-dimensional quantum mechanical problems. *J. Chem. Phys.*, 52:2053, 1970.

[192] F. H. Mies and M. Raoult. Analysis of threshold effects in ultracold atomic collisions. *Phys. Rev. A*, 62:012708, 2000.

[193] W. H. Miller. Coupled Equations and the Minimum Principle for Collisions of an Atom and a Diatomic Molecule, Including Rearrangements. *J. Chem. Phys.*, 50(1):407–418, 1969.

[194] W. E. Milne. The numerical determination of characteristic numbers. *Phys. Rev.*, 35:863, 1930.

[195] Y. Muto. *Proceedings of the Physico-Mathematical Society of Japan*, 17:629, 1943.

[196] M. Nest and P. Saalfrank. Open-system quantum dynamics for gas-surface scattering: Nonlinear dissipation and mapped Fourier grid methods. *J. Chem. Phys.*, 113:8753, 2000.

[197] R. G. Newton. *Scattering Theory of Waves and Particles*. Dover, Mineola, 2nd edition, 1982.

[198] E. E. Nikitin and S. Y. Umanskii. *Theory of Slow Atomic Collisions*. Springer-Verlag, Berlin, 1994.

[199] A. N. Nikolov, J. R. Ensher, E. E. Eyler, H. Wang, W. C. Stwalley, and P. Gould. Efficient production of ground-state potassium molecules at sub-mk temperatures by two-step photoassociation. *Phys. Rev. Lett.*, 84:246–249, 2000.

[200] N. Nikolov, E. E. Eyler, X. Wang, J. Li, H. Wang, W. C. Stwalley, and P. Gould. Observation of translationally ultracold ground state potassium molecules. *Phys. Rev. Lett.*, 82:703–6, 1999.

[201] S. W. O. I. Tolstikhin and M. Matsuzawa. 'Slow' variable discretization: a novel approach for Hamiltonians allowing adiabatic separation of variables. *J. Phys. B: Atomic Molecular and Optical Physics*, 29:L389, 1996.

[202] V. N. Ostrovsky, V. Kokoouline, E. Luc-Koenig, and F. Masnou-Seeuws. Lu-Fano plots for potentials with non-Coulomb tail: application to vibrational spectra of long-range diatomic molecules. *J. Phys. B: Atomic Molecular and Optical Physics*, 34:L27–L38, 2001.

[203] P. Pellegrini and O. Dulieu and F. Masnou-Seeuws . Formation of Cs_2 molecules via Feshbach resonances stabilized by spontaneous emission: theoretical treatment with the Fourier grid method. *Eur. Phys. J. D*, 20:77, 2002.

[204] R. T. Pack. Space-fixed vs body-fixed axes in atom-diatomic molecule scattering. Sudden Approximations. *J. Chem. Phys.*, 60(2):633, 1974.

[205] R. T. Pack. Coordinates for an optimum CS approximation in reactive scattering. *Chem. Phys. Lett.*, 108:333, 1984.

[206] R. T. Pack. Conformally Euclidean internal coordinate space in the quantum three-body problem. *Chem. Phys. Lett.*, 230:223, 1994.

[207] R. T. Pack and G. A. Parker. Quantum reactive scattering in three dimensions using hyperspherical (APH) coordinates. Theory. *J. Chem. Phys.*, 87:3888, 1987.

[208] R. T. Pack and R. B. Walker. Some symmetry-induced isotope effects in the kinetics of recombination reactions. *J. Chem. Phys.*, 121(2):800–812, 2004.

[209] A. N. Panda and N. Sathyamurthy. Bound and Quasibound States of He_2H^+ and He_2D^+. *J. Phys. Chem. A*, 107:7125, 2003.

[210] G. A. Parker, F. D. Colavecchia, and R. T. Pack. Theoretical treatment of three-body collisions in recombination and collision-induced dissociation. In *Interactions of Cold Atoms and Molecules*. CCP6, Daresbury, 2002.

[211] G. A. Parker, M. Keil, M. A. Morrison, and S. Crocchianti. Quantum reactive scattering in three dimensions: Using tangent-sphere coordinates to smoothly transform from hyperspherical to Jacobi regions. *J. Chem. Phys.*, 113(3):957–970, 2000.

[212] L. Pauling and E. B. Wilson. *Introduction to Quantum Mechanics*. McGraw-Hill, Inc., New York, 1935.

[213] T. Peng and J. Z. H. Zhang. A reactant-product decoupling method for state-to-state reactive scattering. *J. Chem. Phys.*, 105(14):6072–6074, 1996.

[214] H. M. Pickett. Vibration-Rotation Interactions and the Choice of Rotating Axes for Polyatomic Molecules. *J. Chem. Phys.*, 56(4):1715–1723, 1972.

[215] P. Pillet and F. Masnou-Seeuws. Jeu de photons pour chimie froide. *La Recherche*, 318:44–47, 1999.

[216] B. Podolsky. Quantum-mechanically correct form of Hamiltonian function for conservative systems. *Phys. Rev.*, 32:812, 1928.

[217] W. H. Press, S. A. Teukolksy, W. T. Vetterling, and B. P. Flannery. *Numerical Recipes in Fortran.* Cambridge University Press, 2nd edition, 1992.

[218] S. R. Procter, Y. Yamakita, F. Merkt, and T. Softley. Phase space manipulation of cold free radical OH molecules. *Chem. Phys. Lett.*, 374:667, 2003.

[219] G. Quéméner, P. Honvault, and J.-M. Launay. Sensitivity of the dynamics of Na + Na$_2$ collisions on the three-body interaction at ultralow energies. *Eur. Phys. J. D*, 30, 2004.

[220] G. Quéméner, P. Honvault, J.-M. Launay, P. Soldán, D. E. Potter, and J. M. Hutson. Ultracold quantum dynamics: Spin-polarized K + K$_2$ collisions with three identical bosons or fermions. *Phys. Rev. A*, 71:032722, 2005.

[221] M. Raoult and G. G. Balint-Kurti. Frame transformation theory for heavy particle scattering: Application to the rotational predissociation of Ar-H$_2$. *J. Chem. Phys.*, 93(9):6508–6519, 1990.

[222] M. Raoult and F. H. Mies. Feshbach resonance in atomic binary collisions in the Wigner threshold law regime. *Rev. Phys. Appl.*, 70:012710, 2004.

[223] A. E. Reed, L. A. Curtiss, and F. Weinhold. Intermolecular interactions from a natural bond orbital, donor-acceptor viewpoint. *Chem. Rev.*, 88:899, 1988.

[224] C. A. Regal, M. Greiner, and D. S. Jin. Observation of Resonance Condensation of Fermionic Atom Pairs. *Phys. Rev. Lett.*, 92(4):040403, 2004.

[225] C. A. Regal, C. Ticknor, J. L. Bohn, and D. S. Jin. Creation of ultracold molecules from a Fermi gas of atoms. *Nature*, 424:47, 2003.

[226] J. H. Reho, J. Higgins, M. Nooijen, K. K. Lehmann, G. Scoles, and M. Gutowoski. Photoinduced nonadiabatic dynamics in quartet Na_3 and K_3 formed using helium nanodroplet isolation. *J. Chem. Phys.*, 115:10265, 2001.

[227] R. Remmert. *Funktionentheorie 1*. Springer-Verlag Berlin Heidelberg, 4th edition, 1995.

[228] M. Rérat and B. Bussery-Honvault. Intramolecular dependence of the frequency dependent polarizabilities of $Li_2(a^3\Sigma_u^+)$ and $Na_2(a^3\Sigma_u^+)$ and van der Waals dispersion coefficients for atom-diatom and diatom-diatom alkali dimers. *Mol. Phys.*, 101:373, 2003.

[229] S. Rutz, H. Ruppe, E. Schreiber, and L. Wöste. Femtosecond Wave Packet Dynamics in Alkali Trimers. *Z. Phys. D*, 40:25, 1997.

[230] H. R. Sadeghpour, J. L. Bohn, M. J. Cavagnero, B. D. Esry, I. I. Fabrikant, J. H. Macek, and A. R. P. Rau. Collisions near threshold in atomic and molecular physics. *J. Phys. B: Atomic Molecular and Optical Physics*, 33(5):R93–R140, 2000.

[231] J. M. Sage, S. Sainis, T. Bergeman, and D. DeMille. Optical production of ultracold polar molecules. *Phys. Rev. Lett.*, 94:203001, 2005.

[232] M. Salci, S. B. Levin, and N. Elander. Search for bound and quasi-bound states in the spin-polarized atomic tritium trimer. *Phys. Rev. A*, 69(4):044501, 2004.

[233] C. Samuelis, E. Tiesinga, T. Laue, M. Elbs, H. Knöckel, and E. Tiemann. Cold atomic collisions studied by molecular spectroscopy. *Phys. Rev. A*, 63(1):012710, 2001.

[234] L. J. Schaad and J. Hu. The Schrödinger equation in generalized coordinates. *J. Mol. Struct.*, 185:203, 1989.

[235] G. C. Schatz and A. Kuppermann. Dynamical resonances in Collinear, Coplanar, and Three-Dimensional Quantum Mechanical Reactive Scattering. *Phys. Rev. Lett.*, 35:1266, 1975.

[236] L. I. Schiff. *Quantum Mechanics*. McGraw-Hill, Inc., New York, 3rd edition, 1968.

[237] R. Schmied and K. K. Lehmann. Computer-generated character tables and nuclear spin statistical weights: application to benzene dimer and methane dimer. *J. Mol. Spect.*, 226:201–202, 2004.

[238] E. Schreiber and S. Rutz. Wave Packet Propagation Phenomena in Na_2 and K_3 Molecules. In M. Chergui, editor, *Femtochemistry - Ultrafast Chemical and Physical Processes in Molecular Systems*, page 217. World Scientific, Singapore, 1996.

[239] D. W. Schwenke and D. G. Truhlar. The effect of Wigner singularities on low-temperature vibrational relaxation rates. *J. Chem. Phys.*, 83(7):3454–3461, 1985.

[240] M. J. Seaton. Quantum defect theory. *Rept. Prog. Phys.*, 46(2):167–257, 1983.

[241] Y. Shi and D. J. Tannor. Symmetry adapted Fourier solution of the time-dependent Schrödinger equation. *J. Chem. Phys.*, 92(4):2517–2525, 1990.

[242] R. T. Skodje, R. Sadeghi, H. Kppel, and J. L. Krause. Spectral quantization of transition state dynamics for the three-dimensional $H+H_2$ reaction. *J. Chem. Phys.*, 101:1725, 1994.

[243] D. Skouteris, J. F. Castillo, and D. E. Manolopoulos. ABC: a quantum reactive scattering program. *Comp. Phys. Comm.*, 133:128, 2000.

[244] B. M. Smirnov and M. I. Chibisov. Electron exchange and changes in the hyperfine state of colliding alkaline metal atoms. *Sov. Phys. JETP*, 21:624, 1965.

[245] F. T. Smith. Lifetime Matrix in Collision Theory. *Phys. Rev.*, 118:349, 1960.

[246] F. T. Smith. A Symmetric Representation for Three-Body Problems. I. Motion in a plane. *J. Math. Phys.*, 3(4):735, 1962.

[247] P. Soldàn, M. T. Cvitaš, and J. M. Hutson. Three-body nonadditive forces between spin-polarized alkali-metal atoms. *Phys. Rev. A*, 67:054702, 2003.

[248] P. Soldán, M. T. Cvitaš, J. M. Hutson, P. Honvault, and J.-M. Launay. Quantum Dynamics of Ultracold $Na + Na_2$ Collisions. *Phys. Rev. Lett.*, 89:153201, 2002.

[249] O. Sorensen, D. V. Fedorov, and A. S. Jensen. Two-body correlations in N-body boson systems. *Phys. Rev. A*, 66(3):032507, 2002.

[250] D. Spelsberg, T. Lorenz, and W. Meyer. Dynamic multipole polarizabilities and long range interaction coefficients for the systems H, Li, Na, K, He, H^-, H_2, Li_2, Na_2, and K_2. *J. Chem. Phys.*, 99:7845, 1993.

[251] J. M. Standard and P. R. Certain. Bounds to two- and three-body long-range interaction coefficients for S-state atoms. *J. Chem. Phys.*, 83(6):3002–3008, 1985.

[252] F. Stienkemeier, W. E. Ernst, J. Higgins, and G. Scoles. On the use of liquid helium cluster beams for the preparation and spectroscopy of the triplet states of alkali dimers and other weakly bound complexes. *J. Chem. Phys.*, 102:615, 1994.

[253] K. E. Strecker, G. B. Partridge, and R. G. Hulet. Conversion of an Atomic Fermi Gas to a Long-Lived Molecular Bose Gas. *Phys. Rev. Lett.*, 91(8):080406, 2003.

[254] K. T. Tang, J. M. Norbeck, and P. R. Certain. Upper and lower bounds of two- and three-body dipole, quadrupole, and octupole van der Waals coefficients for hydrogen, noble gas, and alkali atom interactions. *J. Chem. Phys.*, 64:3063, 1976.

[255] M. R. Tarbutt, H. L. Bethlem, J. J. Hudson, V. L. Ryabov, V. A. Ryzhov, B. E. Sauer, G. Meijer, and E. A. Hinds. Slowing heavy, ground-state molecules using an alternative gradient declerator. *Phys. Rev. Lett.*, 92:173002, 2004.

[256] J. Tennyson and J. R. Henderson. Highly excited rovibrational states using a discrete variable representation: The H_3^+ molecular ion. *J. Chem. Phys.*, 91(7):3815–3825, 1989.

[257] J. Tennyson, M. A. Kostin, P. Barletta, G. J. Harris, O. L. Polyansky, J. Ramanlal, and N. F. Zobov. DVR3D: a program suite for the calculation of rotation-vibration spectra of triatomic molecules. *Comp. Phys. Comm.*, 163:85, 2004.

[258] The National Institute of Standards and Technology (NIST). `http://physics.nist.gov`, 2005.

[259] T. C. Thompson, G. Izmirlian, Jr., S. J. Lemon, D. G. Truhlar, and C. A. Mead. Consistent analytic representation of the two lowest potential energy surfaces for Li_3, Na_3, and K_3. *J. Chem. Phys.*, 82(12):5597–5603, 1985.

[260] T. C. Thompson, D. G. Truhlar, and C. A. Mead. On the form of the adiabatic and diabatic representation and the validity of the adiabatic approximation for X_3 Jahn–Teller systems. *J. Chem. Phys.*, 82(5):2392–2407, 1985.

[261] T. V. Tscherbul and A. A. Buchachenko. Quantum scattering equations for non-adiabatic transitions in collisions between a Hund case (c) diatomic molecule and a structureless atom with application to $I_2($ E 0_g^+) + Ar. *Journal of Physics B: Atomic, Molecular and Optical Physics*, 37(8):1605–1619, 2004.

[262] I. Tuvi and Y. B. Band. Hermiticity of the Hamiltonian matrix in a discrete variable representation. *J. Chem. Phys.*, 107:9079, 1997.

[263] N. Uudus, S. Magaki, and N. Balakrishnan. Quantum mechanical investigation of rovibrational relaxation of H_2 and D_2 by collisions with Ar atoms. *J. Chem. Phys.*, 122(2):024304, 2005.

[264] A. van der Avoird, P. E. S. Wormer, and R. Moszynski. From Intermolecular Potentials to the Spectra of van der Waals Molecules, and Vice Versa. *Chem. Rev.*, 93:1931, 1993.

[265] N. Vanhaecke, D. Comparat, and P. Pillet. Rydberg decelerator using a travelling electric-field gradient. *J. Phys. B*, 38:s409, 2005.

[266] N. Vanhaecke, W. de Souza Melo, Laburthe Tolra, B., D. Comparat, and P. Pillet. Accumulation of cold cesium molecules via photoassociation in a mixed atomic and molecular trap. *Phys. Rev. Lett.*, 89:063001, 2002.

[267] F. Visser, P. E. S. Wormer, and P. Stam. Time-dependent coupled Hartree-Fock calculations of multipole polarizabilities and dispersion interactions in van der Waals dimers consisting of He, H_2, Ne, and N_2. *J. Chem. Phys.*, 79:4973, 1983.

[268] E. Vliegen, H. J. Woerner, T. Softley, and F. Merkt. Nonhydrogenic effects in the deceleration of Rydberg atoms in inhomogeneous electric fields. *Phys. Rev. Lett.*, 374:667, 2004.

[269] H. von Busch, V. Dev, H.-A. Eckel, S. Kasahara, J. Wang, W. Demtröder, P. Sebald, and W. Meyer. Unambiguous Proof for Berry's Phase in the Sodium Trimer: Analysis of the Transition $A\ ^2E'' \leftarrow X\ ^2E'$. *Phys. Rev. Lett.*, 81:4584, 1998.

[270] D. Wang, J. Qi, M. F. Stone, O. Nikolayeva, B. Hattaway, S. D. Gensemer, H. Wang, W. T. Zemke, P. L. Gould, E. E. Eyler, and W. C.

Stwalley. The photoassociative spectroscopy, photoassociative molecule formation, and trapping of ultracold $^{39}K^{85}Rb$. *Eur. Phys. J. D*, 31:165, 2004.

[271] D. Wang, J. Qi, M. F. Stone, O. Nikolayeva, H. Wang, B. Hattaway, S. D. Gensemer, P. L. Gould, E. E. Eyler, and W. C. Stwalley. Photoassociative production and trapping of ultracold KRb molecules. *Phys. Rev. Lett.*, 93:243005, 2004.

[272] H. Wei. Ghost levels and near-variational forms of the discrete variable representation: Application to H_2O. *J. Chem. Phys.*, 106(17):6885, 1997.

[273] J. D. Weinstein, R. deCarvalho, T. Guillet, B. Friedrich, and J. M. Doyle. Magnetic trapping of calcium monohydride molecules at millikelvin temperatures. *Nature*, 395:148, 1998.

[274] R. C. Whitten and F. T. Smith. Symmetric Representation for Three-Body Problems. II. Motion in Space. *J. Math. Phys.*, 9(7):1103, 1968.

[275] K. Willner. Low-energy scattering by a long-range potential. Poster, June 2005. EPIC conference, San Martino al Cimino, Viterbo.

[276] K. Willner, O. Dulieu, and F. Masnou-Seeuws. Mapped grid methods for long-range molecules and cold collisions. *J. Chem. Phys.*, 120(2):548–561, 2004.

[277] E. B. Wilson, J. C. Decius, and P. C. Cross. *Molecular Vibrations*. McGraw-Hill, Inc., New York, 1955.

[278] N. J. Wright and J. M. Hutson. Regular and irregular vibrational states: Localized anharmonic modes and transition-state spectroscopy of Na_3. *J. Chem. Phys.*, 112:3214, 2000.

[279] Y.-S. M. Wu and A. Kuppermann. The importance of the geometric phase effect for the $H + D_2 \rightarrow HD + D$ reaction. *Chem. Phys. Lett.*, 235:105, 1995.

[280] K. Xu, T. Mukaiyama, J. R. Abo-Shaeer, J. K. Chin, D. E. Miller, and W. Ketterle. Formation of Quantum-Degenerate Sodium Molecules. *Phys. Rev. Lett.*, 91(21):210402, 2003.

[281] T. Yanao and K. Takatsuka. Collective coordinates and an accompanying metric force in structural isomerization dynamics of molecules. *Phys. Rev. A*, 68(3):032714, 2003.

278

[282] D. R. Yarkony. Diabolical conical intersections. *Rev. Mod. Phys.*, 68:985, 1996.

[283] W. T. Zemke and W. C. Stwalley. Analysis of exchange energy at long range for states of alkali diatomic molecules correlating to two ground state atoms. *J. Chem. Phys.*, 111:4962, 1999.

[284] J. Z. H. Zhang. Progress of basis optimization techniques in variational calculation of quantum reactive scattering. *J. Chem. Phys.*, 94(9):6047–6054, 1991.

[285] J. Z. H. Zhang and W. H. Miller. New method for quantum reactive scattering, with applications to the 3-D H + H_2 reaction. *Chem. Phys. Lett.*, 140:329, 1987.

[286] J. Z. H. Zhang and W. H. Miller. Quantum reactive scattering via the S-matrix version of the Kohn variational principle: Differential and integral cross sections for $D + H_2 \rightarrow HD + H$. *J. Chem. Phys.*, 91(3):1528–1547, 1989.

[287] J. Z. H. Zhang and W. H. Miller. Quasi-adiabatic basis functions for the S-matrix Kohn variational approach to quantum reactive scattering. *J. Phys. Chem.*, 94:7785, 1990.

[288] W. Zhu, T. Peng, and J. Z. H. Zhang. Reactant-product decoupling method for state-to-state reactive scattering: A case study for 3D H + H_2 exchange reaction (J = 0). *J. Chem. Phys.*, 106:1742, 1997.

[289] M. W. Zwierlein, C. A. Stan, C. H. Schunck, S. M. F. Raupach, S. Gupta, Z. Hadzibabic, and W. Ketterle. Observation of Bose-Einstein Condensation of Molecules. *Phys. Rev. Lett.*, 91(25):250401, 2003.

Kai Willner

Dipartimento di Chimica
Università di Roma "La Sapienza"
Piazzale Aldo Moro 5
I - 00185 Roma
Italy
E-mail: `k.willner@caspur.it`

Born on 17 January 1975 at Freiburg im Breisgau (Germany)
German citizen

1985 - 1995	Student at Friedrich-Schiller-Gymnasium Ludwigsburg *Abitur*
1992 - 1993	Student at The Settlers High School Bellville (South Africa)
1995 - 1996	Military service at Albersdorf
1996 - 1999	Studies at Universität Karlsruhe (TH) *Vordiplom Meteorologie*
1999 - 2001	Studies at Université Paris VI - Pierre et Marie Curie *Maîtrise de Physique* *Diplôme d'Etudes Approfondies "Lasers et Matière"*
2001 - 2005	Graduate studies at Université Paris-Sud XI Preparation of the present thesis in the group "Atomes et Molécules Froids" at Laboratoire Aimé Cotton (Orsay)
since March 2005	Post-doctoral fellow at the Chemistry Department of Università di Roma "La Sapienza"

Publications:

K. Willner, O. Dulieu, and F. Masnou-Seeuws. Mapped grid methods for long-range molecules and cold collisions. *J. Chem. Phys.* **120** 548 (2004)

M. Leduc, M. Portier, J. Léonard, M. Walhout, F. Masnou-Seeuws, K. Willner, and A. Mosk. Photoassociation spectroscopy of ultracold metastable helium atoms: numerical analysis. In *Laser Spectroscopy. Proceedings of the XVIth International Conference, Palm Cove, Far North Queensland, Australia 13 - 18 July 2003.* World Scientific, New Jersey, 2004.

Theoretische Untersuchung von schwach gebundenen Vibrationszuständen des Natriumtrimers: numerische Methoden; Aussichten für die Bildung von Na$_3$ in einem ultrakalten Gas

- Eine numerische Methode des Typs "Fouriergitter mit variabler Schrittweite" wurde verbessert. Mit Hilfe von diskreten Sinus- und Kosinustransformationen wurde eine Matrixdarstellung des Hamiltonoperators berechnet; es wurde beobachtet, dass das Spektrum dieser Matrix frei von sogenannten "Geisterlösungen" ist.

- Die Energiewerte der höchsten, sehr schwach gebundenen Vibrationszustände des van-der-Waals-Komplexes Na-Na$_2$ wurden mittels einer hypersphärischen sektordiabatischen Methode berechnet. Die berechneten Vibrationsniveaus wurden mit Hilfe der Quantendefekttheorie interpretiert.

Theoretical study of weakly bound vibrational states of the sodium trimer: numerical methods; prospects for the formation of Na_3 in an ultracold gas

- A Mapped Fourier Grid method for solving the radial Schrödinger equation is improved. It is observed that a discrete sine and cosine transform algorithm allows to compute a Hamiltonian matrix the spectrum of which is free of spurious eigenvalues.

- The energies of the highest, very weakly bound vibrational states of the Na-Na_2 van der Waals complex are computed using a hyperspherical diabatic-by-sector method. The computed levels are analyzed using quantum defect theory.

Etude théorique d'états vibrationnels faiblement liés du trimère de sodium: méthodes numériques; perspectives pour la formation de Na$_3$ dans un gaz ultra-froid

- Une méthode numérique de type "grille de Fourier à pas variable" pour résoudre l'équation de Schrödinger radiale est améliorée. Il est observé qu'un algorithme de transformations sinus et cosinus discrètes permet de représenter l'hamiltonien par une matrice dont le spectre ne contient pas de niveaux parasites.

- Les énergies des états vibrationnels les plus faiblement liés du complexe van der Waals Na-Na$_2$ sont calculées par une méthode hypersphérique diabatique-par-secteur. Les niveaux calculés sont analysés par théorie du défaut quantique.